Novel multi-mechanism neuroprotective coumarin conjugates as disease-modifying therapies for Alzheimer's disease

BP Repsold
12534005

Thesis submitted for the degree *Doctor Philosophiae* in Pharmaceutical Chemistry at the Potchefstroom Campus of the North-West University

Promoter: Prof SF Malan
Co-Promoter: Prof DW Oliver

May 2016

Abstract

Alzheimer's Disease (AD) is the most prominent of all the types of dementias. It's a neurodegenerative disease that affects the central nervous system (CNS) and general symptoms includes a decline in cognitive abilities (memory, problem-solving, and paying attention) and non-cognitive side effects such as anxiety, depression, apathy and psychosis. AD can be divided into early-onset familial AD (EOFAD) and late-onset AD (LOAD), caused by gene mutations and with CNS changes during aging respectively. The latter route cause is found to be the most prevalent. In 2013, an estimated 5.2 million Americans of all ages were diagnosed with AD. The number of AD cases is rapidly escalating and it's approximated that by the mid-21st century, an individual in the United States will develop AD every 33 seconds.

On a cellular level, AD is characterised by the presence of extracellular plaques containing the beta-amyloid protein (Aβ), intracellular neurofibrillary tangles (NFTs) of hyper-phosphorylated tau protein and microgliosis (neuro-inflammation). The most dominant neuronal loss is in the cholinergic system but dysfunctions of the dopaminergic systems have been found to be contributing factors. The current clinically available medicinal agents for the treatment of AD include the three acetylcholinesterase (AChE) inhibitors (donepezil, rivastigmine, galanthamine) and one non-competitive N-methyl D-aspartate (NMDA) antagonist (memantine). However, because of the existence of compensating parallel pathways in such a complex disease, these drugs don't address the underlying mechanisms and thus only provide symptomatic relief of AD.

This study focused on a strategy based on the rationale that a single compound may have the ability to interact with multiple disease contributing targets, also known as multi-target-directed ligands (MTDLs). This may deliver desired synergistic/potentiating effects, of which AChE and monoamine oxidase-B (MAO-B) inhibition are fundamental in this study.

Coumarin analogues (4- and 7-substituted) were conjugated to selected structures (morpholine, piperidine, erucic acid) *via* etherification and esterification using conventional and microwave-assisted methods. The microwave-assisted method proved more feasible in both yield and reaction time. The final products were obtained as amorphous waxes or solids through chromatographic and/or crystallisation procedures using appropriate organic solvents.

NMR and MS spectroscopic methods were implemented to confirm the correctness of the final newly synthesized structures.

The synthesised derivatives were evaluated for their *in vitro* activities as MAO-B and AChE inhibitors. A fluorometric assay using kynuramine as substrate was used to determine the MAO-B activities of the compounds. Recombinant hMAO-B was used as the enzyme source and the results of the enzyme inhibition were expressed as IC_{50}-values. The acetylcholinesterase from *Electrophorus electricus* / electric eel hydrolysis (EE AChE) of DTNB [5,5'di thiobis(2-nitrobenzoic acid] was utilised to test compounds for AChE activity. The EE AChE enzyme inhibition results were expressed as percentage at both 1 µM and 100 µM concentrations.

Computer aided molecular modelling studies were conducted using Accelrys® Discovery Studios® V3.1.1 software utilising the published hMAO-B (2V61) and hAChE (4EY7) crystal structures. The prepared proteins were typed with the CHARMm forcefield, ionised, protonated (pH 0 – 14) and energy minimised. The structures of the test compounds were docked in the active sites of the enzymes using the CDOCKER® module.

The coumarin-morpholine ether conjugate, **BPR 10** (4-[2-(morpholin-4-yl)ethoxy]-2H-chromen-2-one) proved to be the most promising hMAO-B inhibitor with an IC_{50} of 0.372 µM. The coumarin-piperidine conjugates, **BPR13** (4-methyl-7-[2-(piperidin-1-yl)ethoxy]-2H-chromen-2-one) and **BPR12** [(7-[2-(piperidin-1-yl)ethoxy]-2H-chromen-2-one)] were the most potent inhibitors of EE AChE with an inhibitory activity of 57.43 % at 100 µM and 30.90 % at 1 µM respectively.

The docking studies, showed that the morpholino-coumarin compound, **BPR 10** was able to occupy both the entrance and substrate cavities of the active site of MAO-B. The results demonstrated that the coumarin moiety occupies the substrate cavity while the morpholine moiety is present in the entrance cavity. **BPR10** shows Pi-interactions with residues CYS172, LEU171 and ILE198, and a relatively strong H-bond is present between the pyrone ring and CYS172. The coumarin entity of the compound is positioned in the "aromatic cage" of the substrate cavity. **BPR13** occupied both the peripheral anionic site (PAS) and the catalytic anionic site (CAS) of hAChE, with the coumarin positioned in the PAS region, the linker in the gorge (between the PAS and CAS regions) and the piperdine entity in the CAS region. **BPR13** formed Pi-interactions with TRP286 and TYR341, and a H-bond with TYR72 in the PAS.

It is concluded that the coumarin structure serves as an effective pharmacophoric multi-target-directed ligand scaffold and that conjugated compounds of coumarin has the potential to exhibit both MAO-B and AChE inhibition. This multi-target-directed approach may have the potential to delay the incidence and/or the progression of AD and serves as a basis for further studies, amongst others, *in vivo* investigations.

Opsomming

Alzheimer se siekte (AD) is die algemeenste van al die tipes van dementia. Dit is ‘n neurodegeneratiewe siekte wat die sentrale senuweestelsel (CNS) aantas. Algemene simptome van AD sluit in ‘n afname in kognitiewe vermoë (geheue, probleemoplossing en konsentrasie) asook nie-kognitiewe effekte byvoorbeeld angs, depressie, apatie en psigose. AD kan verdeel word as vroeë-manifisterende-familiële AD (EOFAD) en laat-manifisterende AD (LOAD). Dit word veroorsaak deur mutasies van gene en veranderinge in die CNS met ouderdom. Laasgenoemde wyse van AD ontwikkeling kom die meeste voor by pasiente. In 2013 was daar na raming ongeveer 5.2 miljoen Amerikaners van alle ouderdomme met AD gediagnoseer. Die insidensie van AD styg voordurend en daar word voorspel dat teen die middel van die 21ste eeu, die aantal AD pasiënte in die VSA elke 33 sekondes met een sal toeneem.

Op sellulêre vlak word AD gekarakteriseer deur die teenwoordigheid van: ekstrasellulêre plaatjies bestaande uit Beta-amyloïde proteïen; intrasellulêlere neurofibrillêre knope (NFTs) saamgestel uit hiper-gefosforileerde tau en mikrogliosis (neuro-inflammasie). Die verlies van neurone vind hoofsaaklik in die cholinergiese sisteem plaas, maar daar is bevind dat bydraende faktore ontwikkel agv disfunksies vanuit die dopaminergiese stelsel. Huidige beskikbare geneesmiddels vir die behandeling van AD behels die drie asetielcholienesterase (AChE) inhibeerders (donepisiel, rivastigmien en galantamien) asook ‘n nie-kompeterende N-metiel-D-aspartaat (NMDA) antagonis (memantien). In komplekse siektetoestande is daar egter kompenserende, parallelle weë teenwoordig met die gevolg dat die bogenoemde geneesmiddels slegs simptomatiese verligting verskaf en nie die onderliggende meganismes behandel nie.

Hierdie studie is gebasseer op die beginsel dat n enkele verbinding oor die vermoë kan beskik om met meer as een teiken kan reageer wat tot die patologie van die siekte bydra. Hierdie ligandbenadering staan bekend as “meervoudige teikengerigte ligande” (MTGLe) “(multi-target-directed ligands (MTDLs)”. Hierdie benadering hou die potensiaal in dat gewenste sinergistiese effekte moontlik is waarvan AChE en monoamienoksidase-B (MAO-B) inhibisie fundamenteel is tot hierdie studie.

Kumarienanaloë (gesubsidieerd op posisies 4 en 7) is gekonjugeer met geselekteerde, strukture (morfolien, piperidien en erusiek suur) deur veretering en verestering deur gebruik te maak van konvensionele asook mikrogolfmetodes. Hierdie studie het aan getoon dat die mikrogolfmetode meer voordele inhou in terme van verhoogde opbrengs en verminderde reaksietyd as die standaard metode. Die finale produkte is deur chromatografie prosedures as wasse of amorfe vaste stowwe verkry of deur kristallisasie prosedures deur die gepaste organiese oplosmiddels te gebruik. KMR- en MS-spektrofotometriese tegnieke is gebruik om die strukture van die gesintetiseerde verbindings te bevestig en te karakteriseer.

Die gesintetiseerde verbindings is *in vitro* as inhibeerders van MAO-B en AChE getoets. MAO-B aktiwiteit van die verbindings is fluorometries bepaal deur gebruik te maak van kynuramien as substraat. Rekombinante hMAO-B is as bron van die ensiem gebruik en die resultate van MAO-B ensiem inhibisie is as IC_{50}-waardes uitgedruk. AChE-inhibisie is ook spektrofotometries bepaal gebasseer op die beginsel van die hidrolise van DTNB [5,5 di-tiobis (2-nitrobensoësuur)] deur EE AChE (Asetielcholienesterase afkomstig van ‘n elektriese paling). Die resultate van EE AChE ensiem inhibisie is weergegee as persentasie van beide 1 µM en 100 µM konsentrasies.

Rekenaar gebaseerde molekulêre modellering is uitgevoer deur gebruik te maak van Accelrys® Discovery Studios® V3.1.1 sagteware met die gepubliseerde hMAO-B (2V61) en hAChe (4EY7) kristalstrukture. Die voorbereide proteine is geprogrameer met die CHARM® elektoniese kragveld, geïnosieer, geprotoneer (pH 0 - 14) en energieminimaliseringssiklus. Passing van die strukture van die gesintetiseerde inhibeerders is in die aktiewe setels van die ensieme is met behulp van die CDOCKER® module gedoen. Hierdeur is die sleutel ligand-ensieminteraksies geïdentifiseer.

In vitro studies het getoon dat die kumarien-morfolien eterkonjugaat **BPR10** (4[2-(morfien-4-iel)etoksie] 2*H*-chromeen) die mees belowendste inhibeerder van hMAO-B was met ‘n IC_{50}-waarde van 0.372 µM. Die kumarien-piperidien eterkonjugaat, **BPR13** (4-metiel-7-[2-(piperidien-1-iel)etoksie]-2*H*-chromeen) en **BPR12** [(7-[2-(piperidien-1-iel)etoksie]-2*H*-chromeen)] was die mees belowendste inhibeerders van EE AChE met inhibisie van 57.43 % by 100 µM en 30.90 % by 1 µM onderskeidelik.

Die molekulêre modelleringstudies het aan getoon dat die morfolieno-kumarien, **BPR10** het beide die ingangs- en substraatsetels beset, met die kumarien teenwoordig in die substraatsetel terwyl die morfolien in die ingang van die aktiewe setel van hMAO-B beset. **BPR10** toon Pi-interaksies met CYS172, LEU171 en ILE198 asook ‘n sterk H-binding tussen

die piroon ring van die kumarien en CYS172. Die kumarienfarmakofoor is ook geleë in die “aromatiese hok” van die substraatholte. **BPR13** beset beide die perifere anioniese gebied (PAS) en die katalitiese anioniese gebied (CAS) van die aktiewe setel van hAChE. Die kumarien is teenwoordig in die PAS, die verbindingketting in die kloof (area tussen die PAS abd CAS areas) en die piperdien in die CAS area. **BPR13** vorm Pi-interaksies met TRP286 en TYR341 asook ‘n H-binding met TYR72 in die PAS area.

Die resultate toon dat die kumarien struktuur kan dien as ‘n effektiewe farmakoforiese “meervoudige teikengerigte ligand (“multi-target-directed ligand”) bousteen en dat die gekonjugeerde kumarienverbindings oor die potensiaal beskik om beide MAO-B en AChE ensieme te inhibeer. Hierdie “meervoudige teikengerigte ligand” benadering het die moontlike potensiaal om AD se ontwikkeling en progressiewe patologie te voorkom of te vertraag. Die resultate van hierdie studie dien as ‘n grondslag vir verdere navorsing, wat *in vivo* studies insluit.

Aknowledgements

First and foremost, I thank my creator for giving me the talent, opportunity and perseverance to overcome the obstacles during this study and endow me with the passion for my reasearch.

To my supervisor and mentor, Prof. S.F Malan and co-supervisor, Prof D.W. Oliver, my greatest appreciation for your guidance, support and valuable insights.

My family: my dad, J.H. Repsold, my mother, F. Repsold and my grandmother, Liza van Zyl for their continuously inspiration and motivation. You were all a pillar of strength to me.

My brother and sister in-law: Johann and Zelda Repsold for always reassuring and believing in me.

To my friend and colleague, Prof Jacques Joubert for his endless support and assistance.

Prof. Jaques Petzer and his wife, Prof Anel Petzer for all their assistance and wisdom.

To my dearest friends: S.G. van Rooy, Gerhard Schalkwyk (aka Morph) and Marnitz Verwey for their motivation during hard times.
My friends and parents away from home; Leone and Meyer van Rooyen – for their advice, reassurance and hospitality.

To Prof Jeanetta du Plessis for her humanity and comprehension during difficult times.
My physician, Dr. Nel Roodt, for his vigilance regarding my health difficulties.

The North West University (Potchefstroom Campus) for the use of their facilities.
The National Research Foundation (NRF) for funding.

Table of Contents

List of Figures

List of Tables

List of Spectra

List of Graphs

List of Schemes

List of Abbreviations

A

Aβ: β-amyloid protein or amyloid-β protein
$Aβ_{40}$: Aβ that ends in residue 40
$Aβ_{42}$: Aβ that ends in residue 42
ACE: Angiotensin-converting enzyme
ACh: Acetylcholine
AChE: Acetylcholinesterase
AChEI: Acetylcholinesterase inhibitor
AD: Alzheimer's Disease
ADL: Assessment of activities of daily living
ADME: Absorption, distribution, metabolism and excretion
ADRDA: Alzheimer's Disease and Related Disorders Association
AGE: Advanced glycooxidation end products
AICD: APP intracellular domain
APP: Amyloid precursor protein
APOE: Apolipoprotein E
AAPH: 2,2'-azobis(2-amidinopropane)dihydrochloride
APP- βCTFs: APP-β carboxyl terminal fragments
APH-1: Anterior pharynx defective 1 homolog A

D

DAPT: (N-[*N*-(3,5-difluorophenacetyl)-L-alanyl]-*S*-phenylglycine *t*-butyl ester)
DCM: Dichloromethane
DLBD: Diffuse Lewy body disease
DPPH: Di-(phenyl)-2,4,6-trinitrophenyl) iminoazanium
DPPH: 2,2-Diphenyl-1-picrylhydrazyl

B

BACE 1: Beta-site amyloid precursor protein cleavage enzyme
b.d.: twice daily
BDNF: Brain-derived neurotrophic factor
BH4: Tetrahydrobiopterin
BPSD: Behavioural and psychological symptoms of dementia
BuChE: Butyrylcholinesterase
BuChEI: Butyrylcholinesterase inhibitor
Bzl: Benzyl

C

CA: Carbonic Anhydrase
cAMP: Cyclic adenosine monophosphate
Cdk5: Cyclin dependent kinase-5
ChEIs: Cholinesterase inhibitors
CNS: Central nervous system
COX-2: Cyclooxygenase-2
CREB: cAMP response element
CSDD: Cornell scale for depression in dementia
CSF: Cerebrospinal fluid
CTF: C-terminal fragment
CTFs: C-terminal fragments
CTGF: Connective tissue growth factor

E

EEG: Electroencephalography
EGF: Epidermal growth factor
ELISA: Enzyme-linked immunosorbent assay
eNOS/NOS2: Endothelial Nitric Oxide Synthase
EOFAD: Early-onset familial Alzheimer's Disease

F

FAD: Flavin adenine dinucleotide
FDA: Food and Drug Administration
FDG-PET: Fluorodeoxy-glucose-Positron emission tomography
FLAIR: Fluid attenuated inversion recovery
FMN: Flavin mononucleotide

I

IDE: Insulin-degrading enzyme
iNOS/NOS2: Inducible Nitric Oxide Synthase
IL-6: Interleukin-6

L

LOAD: Late-onset Alzheimer's Disease
LPS: Lipopolysaccharide
LRP: Low-density lipoprotein receptor
LTP: Long-term potentiation

N

nAChRs: Nicotinic acetylcholine receptors
NADPH: Nicotinamide adenine dinucleotide phosphate
***N*-Boc**: *Tert*-butyloxycarbonyl protecting group
Nct: Nicastrin
NEP: Neprilysin
NFTs: Neurofibrillary tangles
NF-κB: Nuclear factor kappa-light-chain-enhancer of activated-B cells
NINCDS: National Institute of Neurological and Communicative Disorders and Stroke
NMDA: N-methyl-D-aspartate
nNOS/NOS1: Neuronal nitric oxide synthase
NOS: Nitric Oxide Synthase
NO: Nitric oxide
NSAIDs: Non-steroidal anti-inflammatory drugs
NTF: N-terminal fragment

G

GSK-3: Glycogen synthase kinase-3

H

H_2O_2: Hydrogen peroxide
hAChE: Recombinant human Acethylcholine Esterase
HAT: Histone acetyltransferase
HDAC: Histone deacetylase
HDACi's: Histone deacetylase inhibitors
hMAO-A: Recombinant human monoamine oxidase-A
hMAO-B: Recombinant human monoamine oxidase-B

M

MAO: Monoamine oxidase
MAO-A: Monoamine oxidase-A
MAO-B: Monoamine oxidase-B
MEC: Mecamulaminn
MMSE: Mini-Mental State Examination
MRI: Magnetic resonance imaging
MTDL: Multi-targeted drug ligand
MTs: Microtubules

O

$O^{2\cdot-}$: Superoxide
$OH^{\cdot}$: Hydroxyl radicals
$ONOO^{\cdot}$: Peroxynitrite

P

PD: Parkinson's Disease
PAI-1: Plasmin activation inhibitor-1
PAS: Peripheral anionic site
P-CREB: cAMP response element-binding protein

R

RA: Rheumatoid arthritis

RAGE: Receptor for advanced glycation end products

RAVLT: Rey Auditory Verbal Learning Test

RCS: Reactive chlorine species

RNAi: RNA interference

RNS: Reactive nitrogen species

ROO$^{\cdot}$: Peroxyl radicals

ROS: Reactive oxygen species

RTK: Tyrosine Kinase receptor

S

SAR: Structure activity relationships

SCT: Scopolamine

SPECT: Single photon emission computed tomography

#

ε2, ε3 and ε4: Alleles occur at the APOE locus

5-HT$_4$: 5-Hydroxytryptamine receptor subtype 4

5-HT: 5-Hydroxytryptamine / Serotonin

PHFs: Paired helical filaments

PI3-K: Phosphatidylinositol-3-kinase

PKA: Protein kinase A

PKC: Protein kinase C

PL: Plasma lipids

PLCγ: Phospholipase C

PNS: Peripheral nervous system

PSEN1: Presenilin-1

PSEN2: Presenilin-2

T

TACE: TNF-alpha Converting Enzyme

TC: Total cholesterol

TG: Total triglyceride

TGF-β1: Transforming growth factor

TNF: Tumour necrosis factor

TNF-α: Tumour necrosis factor-alpha

TrkB: BDNF receptor

VW

VDCCs: Voltage-dependent calcium channels

WCST: Wisconsin card sorting test

WMH: White matter hyperintensities

Chapter 1 Introduction

1.1 OVERVIEW.

Alzheimer's Disease (AD) is a neurodegenerative disease that affects the central nervous system (CNS) of the elderly population. It's associated with a decline in cognitive abilities (learning and memory) and non-cognitive (e.g. anxiety, depression, apathy and psychosis). Risk factors are mainly aging, but also include cardiovascular diseases, obesity, diabetes and genetic factors.

1.1.1 Prevalence.

In 2013, an estimated 5.2 million Americans of all ages had AD. This includes an estimated 5 million people age 65 and older (late-onset AD abbreviated LOAD; Hebert *et al.,* 2013), and 200,000 individuals under the age 65 (early-onset AD / EOAD). Once afflicted with AD, the average lifespan is about 8 – 10 years (Small *et al.,* 1997).

The prevalence of AD in the USA is one in nine people age 65 and older (11 %); about one-third of age 85 and older (32 %), 13 % of ages 65 – 74, 44 % in the age group 75 – 84 and 4 % under 65 (Hebert *et al.,* 2013). This implies that one person in the United States develops AD every 68 seconds. It's estimated that by the mid 21st century someone in the United States will develop AD every 33 seconds (Alzheimer's Association, facts and figures, 2013).

In 2015, 46.8 million people are living with dementia worldwide (http://www.worldalzreport2015.org/). Statistics predicts that in 2050, someone in the world could develops this neureodegenarive disorder every 3 seconds (**Table 2.2, Figure 2.4**).

1.1.2. Classification.

AD exists in both familial and sporadic forms (**Chapter 2; section 2.1.2**). Familial forms are caused by mutations in single genes that are inherited and this accounts for approximately 5% of the AD cases. On the contrary, sporadic forms consists of multifactorial etiology and are significantly more prevalent (Serretti *et al.,* 2007).

1.1.3. Pathogenesis and Pathology.

AD progresses to affect limbic structures, subcortical nuclei and cortical regions, thus influencing multiple neurotransmitter systems. The most dominant neuronal loss is in the cholinergic system (Perry, 1986; Fibiger, 1991), where cholinergic neurons and the number of nicotinic acetylcholine receptors (nAChRs) declines in the hippocampus and cortex (Paterson and Nordberg, 2000; Perry *et al.,* 2000). This atrophy of the hippocampus can spread to the amygdala. (Mott *et al*., 2005). Non-cognitive behavioral and neuropsychiatric symptoms often accompany AD (Assal & Cummings, 2002) and usually arise from the dysfunction of the serotonergic and dopaminergic systems (Assal *et al*., 2002; Erkinjuntti, 2002). The pathogenesis of AD can grossly be categorised into: the amyloid pathology, the tau pathology and microgliosis (neuro-inflammation) with neuronal loss.

The characteristics of AD include the accumulation extracellular plaques containing the beta-amyloid protein (Aβ) and intracellular neurofibrillary tangles (NFTs) of hyperphosphorylated tau protein (**Figure 1.1** and **Figure 1.2**). A direct relationship between neuronal synapse degeneration and Aβ deposition (Saido T.C. 2003) have been demonstrated.

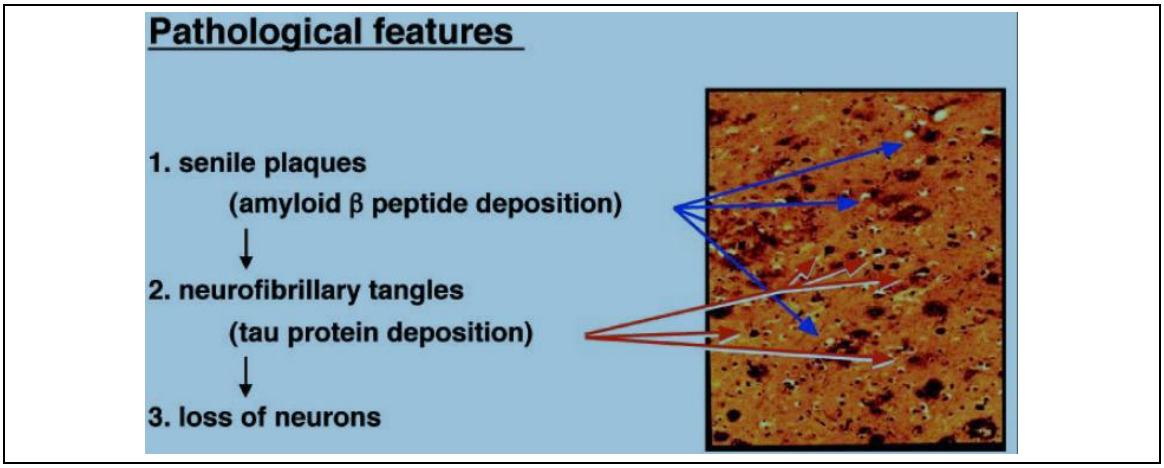

Figure 1.1: Chronology of the major AD pathological events; senile plaques and neurofibrillary tangles (Saido T.C. 2003).

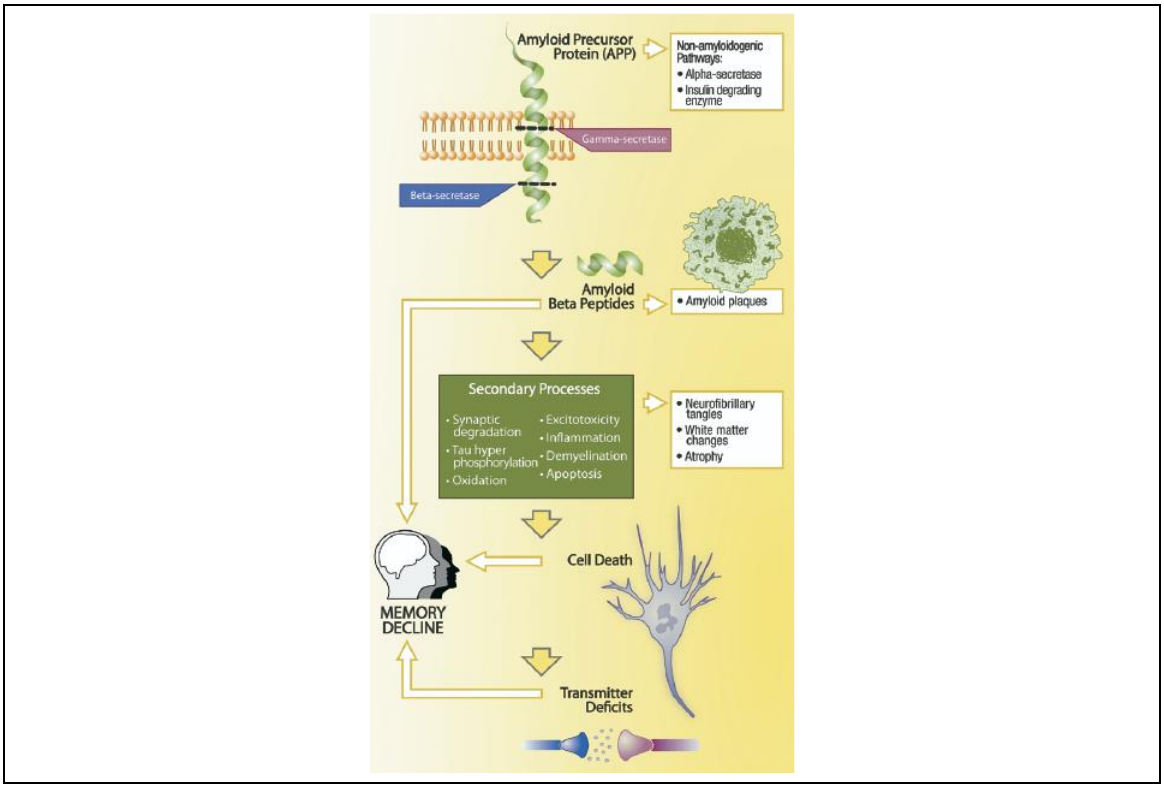

Figure 1.2: The cascade of events currently hypothesised to comprise the pathophysiology of AD (Salloway *et al.,* 2008).

1.1.4. Current Treatment Regime

No single ''magic bullet'' to prevent or cure AD exists and current treatment only provide symptomatic relieve that doesn't significantly address the underlying neurodegeneration and pathophysiology of the disease (Kasa *et al*., 1997; Gualtieri *et al*., 1996).

The U.S. Food and Drug Administration (FDA) has approved four drugs for AD treatment; three acetylcholinesterase (AChE) inhibitors and one non-competitive N-methyl D-aspartate (NMDA) antagonist. For mild to severe AD, Donepezil, Rivastigmine or Galantamine temporarily maintains cognitive abilities and behavioural symptoms. Memantine has been implemented for symptomatic treatment of AD patients (Mobius, 2008; Winblad *et al*., 2003; Rogawski *et al*., 2003; Reisberg *et al*., 2003).

1.1.4.1. Donepezil.

Donepezil (**Figure 1.3**) is a selective, reversible acetylcholinesterase inhibitor (AChEI), available in 5 and 10 mg dosages. Treatment is usually initiated at 5 mg/day and gradually increased to 10 mg/day. An extended release formulation (23 mg/day) is available (Burns *et al*., 1999; Anand *et al*., 2000; Farlow *et al*., 2010).

1.1.4.2. Rivastigmine.

Rivastigmine (**Figure 1.3**) is an AChEI and buturylcholinesterase (BChEI) inhibitor. Treatment is initiated at 1.5 mg twice daily (b.d.) and gradually increased 6 mg b.d. (Birks, 2006; Raina *et al*., 2008).

1.1.4.3. Galanthamine.

Except for its AChE inhibitory effect, galanthamine (**Figure 1.3**) is a nicotinic acetylcholine receptor agonist. (Lanctôt *et al*., 2009). Treatment is initiated at 4 mg b.d. and increased gradually to 12 mg b.d.

1.1.4.4. Memantine.

In the U.S. and Europa, Memantine (**Figure 1.3**), an N-methyl D-aspartate (NMDA) antagonist is used to block the toxic effects (Ca^{2+} influx and excess glutamate) of moderate to severe AD. Treatment is initiated at 5 mg once daily, but may be increased to 10 – 20 mg/day and gradually increased to 28 mg/day (Reisberg *et al*., 2003).

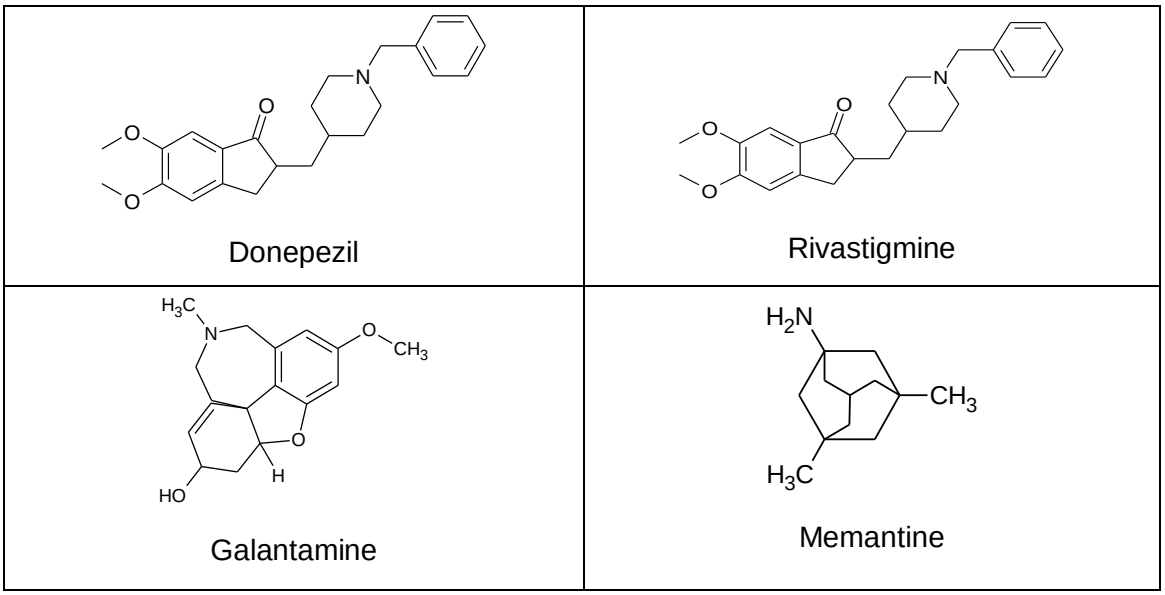

Figure 1.3: Current treatment regime for AD.

1.2. THE MULTI-TARGET-DIRECTED LIGAND (MTDL) AND DISEASE MODIFYING THERAPY APPROACH.

Drug discovery research have for many decades followed the approach that a primary single mode of pathophysiology is key to the development of a disorder, requiring highly specific and selective compounds for single target interaction. This one-molecule, one-target paradigm have been utilised reasonably successful for disorders where a single target has been identified.

However, it became increasingly evident with the introduction of molecular biology, pharmacogenomics and other biochemical fields that the underlying mechanisms of disease are significantly more complex. Additionally, cells can compensate during drug intervention, by amongst others, the existence of parallel pathways (Frant *et al.,* 2005; Mencher *et al.,* 2005), adding to the complexities and leading to failures in therapy. Thus, drugs interacting with a single target may therefore be ineffective for the treatment of diseases such as neurodegenerative and other complex diseases which involve multiple pathogenic factors. A new strategy is emerging based on the rationale that a single compound might be able to interact with multiple targets (**Figure 1.4**) for the treatment of neurodegenerative diseases.

For AD disease-modifying therapies there are three guiding issues: firstly, the disease arises not from a single cause but from multiple potential targets resulting in the cumulative effects in the pathiophysiological outcome of the disease; secondly, the disease is continuous, presenting with gradual progression affecting more biological systems; and thirdly, that as the population ages, the public health burden posed by AD will increase worldwide (Duara *et al.,* 2009).

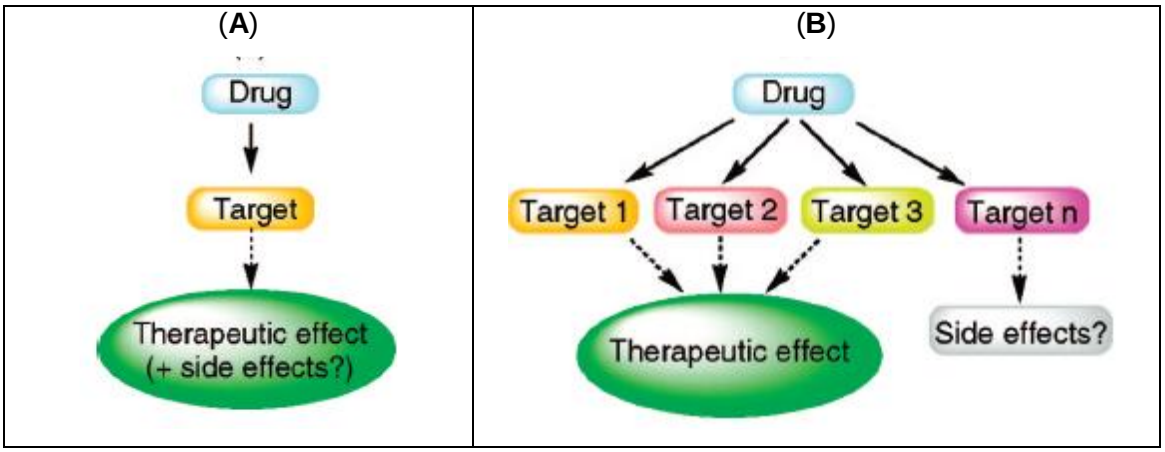

Figure 1.4: The one-molecule, one-target paradigm (**A**) *versus* the MTDL (**B**) approach.

1.3. MEDICINAL CHEMISTRY RATIONALE.

The medicinal chemistry of the structures being studied in this field presented opportunities to design novel structures with multiple modes of interaction at multiple targets. Below are presented some of the rational approaches to supports the current study.

Table 1.1: Selected moieties in this study utilising highhroug put *in silico* screening.

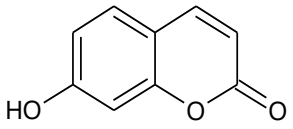 7C (7-Hydroxycoumarin)		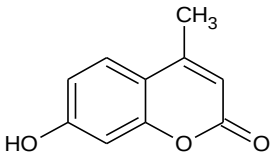 4MC (7-Hydroxy-4-methyl coumarin)		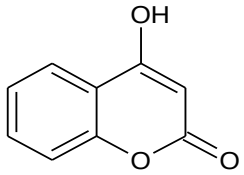 4C (4-Hydroxycoumarin)
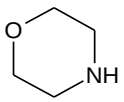 Morpholine	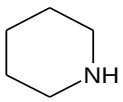 Piperidine	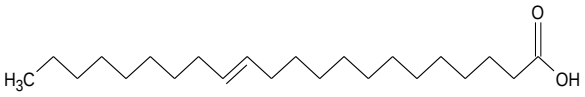 Erucic Acid		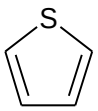 Thiophene

1.3.1 Coumarin.

Dimmerisation has proven to be a promising approach with numerous advantageous properties like *bis*(7)tacrine, also known as *bis*(7)cognitin (Pang *et al.,* 1996), with selective inhibiton of AChE (Rakonczay 2003), a 1000-fold increase in AChE inhibition potency and with double interaction with both the active and peripheral sites of AChE. It thus has the ability to inhibit AChE-induced Aβ aggregation as well (Inestrosa *et al.,* 1996). It also has neuroprotective effects related to the interaction with β-secretase enzyme (BACE-1), NMDA and $GABA_A$ receptors. (Fang *et al.;* 2010; Fu *et al.;* 2009; Li *et al.,* 2009). Its numerous additional neuroprotective properties include protection against Aβ induced neuronal apoptosis, the regulation of L-type voltage-dependent calcium channels (VDCCs), which in turn causes a decrease of intracellular Ca^{2+}concentration (Fu *et al.,* 2006), and counteracting oxidative stress induced by H_2O_2. All the above advantages prompted us to investigate the effects of certain dimer coumarin analogues.

1.3.2 Piperidine

Some piperdine acts as γ-secretase modulators, which also exhibits high *in vitro* and *in vivo* potency against $Aβ_{42}$ peptide (Oehlrich *et al.,* 2013; Close *et al.,* 2012; McBriar *et al.,* 2008; Li *et al.,* 2007; Josien 2007) and inhibitory activities against $Aβ_{42}$ aggregation and AChE-induced Aβ aggregation (Kwon *et al.,* 2007). Some piperidine hybrids also exhibits moderate to good AChE inhibitory activity (Kumar *et al.,* 2013; Meng *et al.,* 2012; Girisha *et al.,* 2009), while other have the advantage of good metal-chelating ability (Meng *et al.,* 2012). Another piperidine compound, 1-((3-bzl-3-methyl-2,3-dihydro-1-benzofuran-6-yl) carbonyl) piperidine (MDA7) proved to promote Aβ clearance and restore synaptic plasticity, cognition and memory (Wu *et al.,* 2013).

1.3.3. Morpholine

Morpholine conjugates revealed the ability to decrease metal-induced (Fe and Cu) Aβ aggregation (Jones *et al.,* 2012)**.** While some compounds e.g. [(G3)-Mor] significantly reduced the Aβ toxicity (Klajnert *et al.,* 2012), other morpholine hybrids act as muscarinic receptor 1 agonists, enhance memory function in animal models of Alzheimer's presenile dementia and also modulate APP secretion (Malviya *et al.;* 2009; Kumar *et al.,* 2008).

1.3.4 Thiophene

Some thiopene compounds are endowed with AChE inhibitory activity (Jeyachandran *et al*., 2013; Bharate *et al.,* 2009; Pietsch *et al.,* 2005).

1.3.5. Eruric acid

Erucic acid (cis-13-docosenoic acid), is a monounsaturated omega-9 fatty acid which is present in wallflower seed, rapeseed oil and canola (20 - 54 %) (Sahasrabudhe, M. R. 1977), and in mustard oil (42 %).

Erucic acid deficiency was detected in the early phase of neurodegeneration and this strongly supported it as supplement to counteract AD progression (Iuliano *et al*., 2013).

Rapeseed were tested for inhibitory effects on $A\beta_{25-35}$ – induced cell death and proved to offer protection against Aβ-mediated cell death (Okada *et al*., 2013). Erucic acid is also described to reduce AD and dementias and serves as nutrient for the structure and function of the brain which determines visual, cerebral and intellectual abilities (Bourre, J.M. 2005).

1.4. AIMS AND OBJECTIVES OF THE STUDY.

Considering the increase in AD worldwide incidence, mortality and the burden on the economy, together with current treatments available which only provides partial symptomatically relieve, designing novel drugs using a MTDL approach is of vital importance.

In view of the multiple underlying pathology and the effects of the multi-modal mechanisms (**Chapter 2**) of AD – it was hypothesised that the coumarin chemical scaffold could serve as a suitable nucleus for the design of novel structures to interact with multiple targets relevant in AD.

The coumarin structure with substitution in positions 7 and 4 allows for unique chemical modifications resulting in novel structures with the potential to address the multiple target

approach of the AD. Additionally, these modifications could effectively be implemented to ensure that the physical properties of the newly designed structures meet the required properties for successful ADME (absorption, distribution, metabolism, excretion) outcomes.

The aims and objectives of the current study was therefor to successfully design novel structures that could meet the criteteria of multiple target interactions involved in AD and that could serve as potential therapeutic agents or novel leads for further design and discovery studies.

The study design included the critical elements of a medicinal chemistry investigation as outlined below:

i. Utilise molecular modeling and computational chemistry to design novel structures and investigate the interactions at the molecular level (target site directed) using amongst others protein crystallographic data. Gain insight into the mode of interaction at these sites;
ii. successfully synthesise the designed structures;
iii. determine their structures using acceptable structure elucidation techniques;
iv. Determine the pharmacological activities at the proposed targets using *in vitro* studies i.e. at the multifunctional targets (i.e. AChE and MAO-B);
v. Present new opportunities for drug discovery in the field of AD.

Chapter 2 Literature Overview

2.1 INTRODUCTION.

Dr. Alois Alzheimer observed specific lesions in and around neurons in one of his patients, Auguste D., a 51 year old female admitted for presenile dementia. More than a century ago he argued these specific lesions he described (**Figure 2.1**) were accountable for this dementia disorder (Alzheimer, 1911), which would later be known as Alzheimer's Disease (AD). AD is a neurodegenerative disorder accompanied with a decline in cognitive abilities (learning and memory), and non-cognitive symptoms (anxiety, depression, apathy and psychosis) which impairs patients' quality of daily life.

Figure 2.1: Neurofibrillary tangles as drawn by Alois Alzheimer (Alzheimer, 1911).

2.1.1. Pathology.

The β-amyloid protein (Aβ) in plaques and the tau protein in tangles comprise the hallmarks of AD. Thus, the accumulation of these extracellular plaques containing the Aβ protein and intracellular neurofibrillary tangles of hyperphosphorylated tau protein in the brain indicates presence of AD (**Figure 2.2**).

Aβ plays a role in modifying synaptic transmission; and the beta-site amyloid precursor protein [APP] cleavage enzyme (BACE1) contributes to learning and memory development (Laird *et al*., 2005). AD progresses to affect limbic structures, subcortical nuclei and cortical regions, thus influencing multiple neurotransmitter systems with the most prominent neuronal loss in the cholinergic system (Perry, 1986; Fibiger, 1991), where cholinergic neurons are progressively degraded causing a quantitative decline of nicotinic acetylcholine receptors

(nAChRs) in the hippocampus and cortex (Paterson *et al*., 2000; Perry *et al*., 2000). This hippocampal atrophy can extend to the amygdala (Mott *et al*., 2005). Non cognitive behavioural and neuropsychiatric symptoms often accompany AD (Assal *et al*., 2002) and usually arise from the dysfunction of the serotonergic and dopaminergic systems rather than the cholinergic systems (Assal *et al*., 2002; Erkinjuntti, 2002).

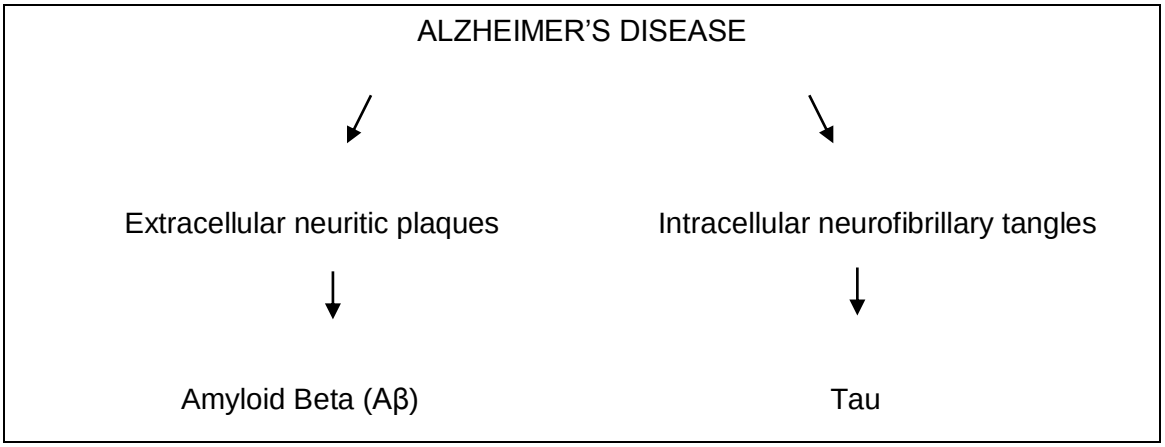

Figure 2.2: The hallmarks of AD.

2.1.2. Classification.

A feature of in AD is the presence of familial (rare) and non-familial (common), the latter also frequently described as sporadic or idiopathic. Familial forms are caused by mutations and inherited. Only 5 % (or less) of all AD cases are due to early-onset familial AD / EOFAD (Ott *et al*., 1998; Tanzi 1999). The common, sporadic form on the other hand consists of a multifactorial etiology, in which some genetic polymorphisms are known to act as predisposing factors (Serretti *et al*., 2007).

Early-onset familial AD (EOFAD) is often transmitted as an autosomal dominant trait with onset ages below 65 years and is caused by exceptional, but highly penetrant mutations in genes namely Amyloid precursor protein (APP), Presenilin-1 (PSEN1) and Presenilin-2 (PSEN2). The majority of AD occurs after the age of 65, also known as late-onset AD (LOAD). LOAD is characterised by a more complicated and interlinked pattern of genetic and non-genetic factors (**Figure 2.3**).

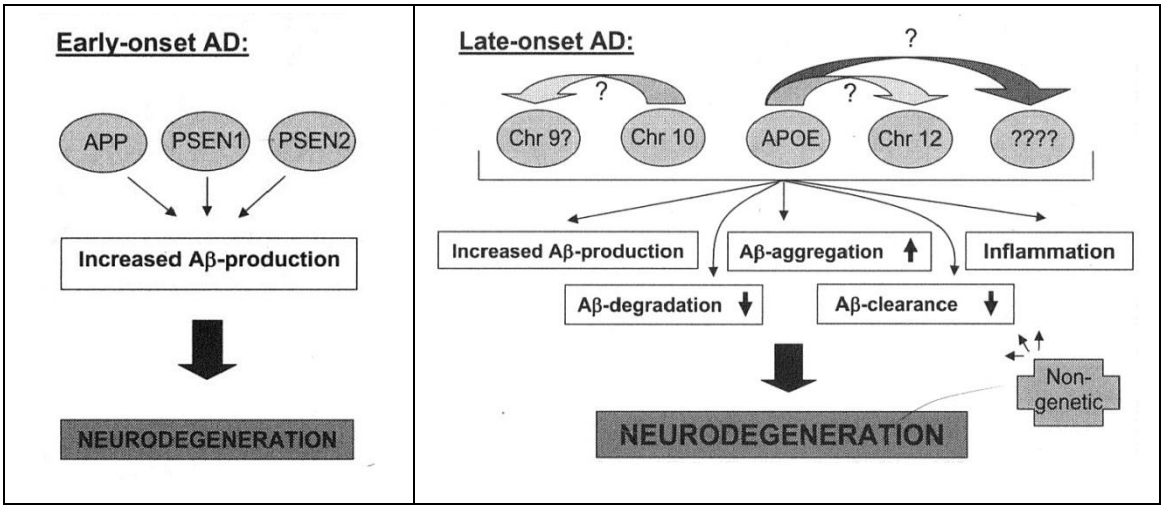

Figure 2.3: Pattern of known and proposed AD genes. **Left Panel**: Mutations of the EOFAD genes (APP, PSEN1, PSEN2) which causes Aβ-production and neurodegeneration and AD. **Right Panel**: The proposed LOAD genes. These risk-factor genes and interwoven mechanisms leading to AD neurodegeneration (Sisodi, 2007).

2.1.3. Prevalence.

In 2006, 26.6 million cases of AD were reported worldwide (**Table 2.1;** range, 11.4 – 59.4 million) and it is further predicted that by the year 2050, the worldwide AD prevalence will increase fourfold, up to 106.8 million (range, 47.2 – 221.2 million). The reason for this increase is the increase in the general age of the world's population (Brookmeyer *et al*., 2007). Whereas other major causes of death have been on the decrease, deaths attributable to AD increased 47 %. Today, the disability weight of AD on individuals older than 60 years of age is larger than that of stroke, musculoskeletal disorders, cardiovascular disease, and cancer (World Health Report 2012). An estimated 5.3 million Americans of all ages have AD. This figure includes 5.1 million people aged 65 years and older, and 200,000 individuals under age 65 years with EOAD (Alzheimer's Association, 2006).

According to the Alzheimer's Association, one in eight persons aged 65 years and older (13 %) has AD and every 70 seconds, someone in America develops AD (Alzheimer's Association, 2009). By the middle of the 21st century, someone will develop AD every 33 seconds (Alzheimer's Association, 2009). Although AD and mortality from AD can occur in people under age 65, its primary occurrence is amongst the elderly. As shown in **Table 2.1**, mortality rates from AD increase dramatically between the age groups of 65 to 74, 75 to 84, and 85 years and older.

Table 2.1.: United States AD death rates (per 100,000) by age, for 2000, 2004, and 2005 (Kung *et al.*, 2008).

AGE (YEARS)	2000	2004	2005
45-54	0.2	0.2	0.2
55-64	2.0	1.9	2.1
65-74	18.7	19.7	20.5
75-84	139.6	168.7	177.3
85+	667.7	818.8	861.6

Considering the worldwide population, 46.8 million people are living with dementia in 2015. It's predicted in 2050, someone in the world could develops this neureodegenarive disorder every 3 seconds (**Table 2.2, Figure 2.4**).

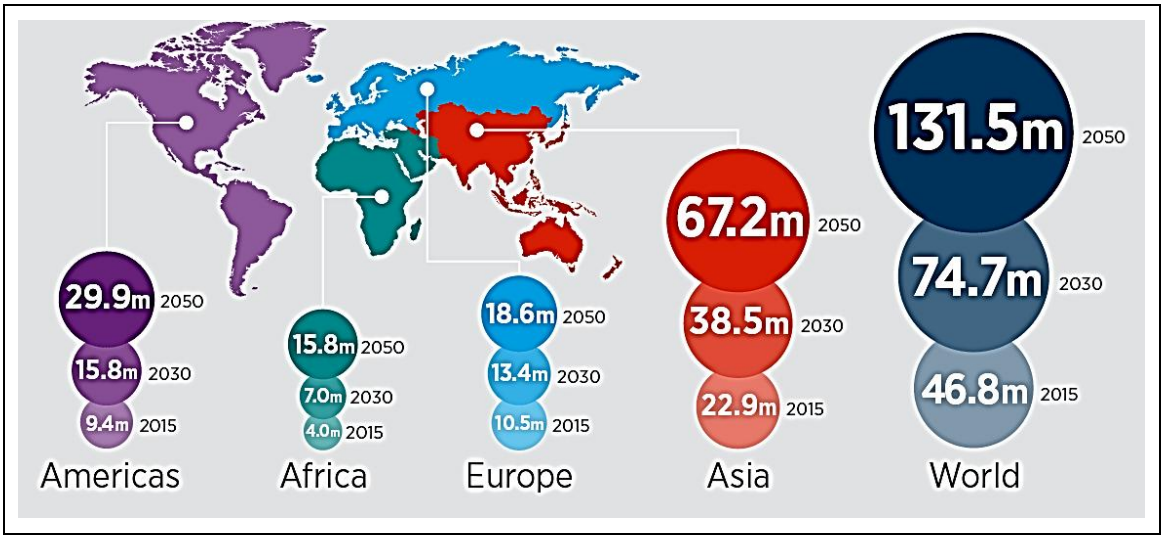

Figure 2.4: Predicted worldwide prevalence of dementia from 2105 until 2050 (http://www.worldalzreport2015.org/).

Table 2.2.: Region coverage, with respect to the size of the elderly population in 2015 (http://www.worldalzreport2015.org/).

Region	Over 60 year old population (millions)	Number of eligible dementia prevalence studies (additional since WAR 2009)	Number of studies / 10 million population	Total population studied	Total population studied / million population
ASIA	485.83	144 (71)	3.0	420 143	865
Australasia	5.80	4 (0)	6.9	2 223	383
Asia Pacific, High Income	52.21	30 (8)	5.7	46 843	897
Asia, Central	7.43	0 (0)	0	0	0
Asia, East	218.18	89 (55)	4.1	342 231	1 569
Asia, South	139.85	14 (7)	1.0	19 673	141
Asia, Southeast	61.72	6 (1)	1.0	7 144	116
Oceania	0.64	1 (0)	15.6	2 029	3 170
EUROPE	176.61	78 (17)	4.4	106 909	605
Europe, Western	107.89	71 (15)	6.6	104 447	968
Europe, Central	26.92	6 (2)	2.2	2 462	91
Europe, Eastern	41.80	1 (0)	0.2	Not Available	Couldn't be calculated
AMERICAS	145.51	34 (6)	2.3	94 875	643
North America	74.88	15 (2)	2.0	42 361	548
Caribbean	5.78	5 (1)	8.7	24 625	4 260
LA, Andean	5.51	3 (0)	5.4	3 465	629
LA, Central	24.64	6 (2)	2.4	12 665	514
LA, Southern	9.88	1 (0)	1.0	4 689	475
LA, Tropical	24.82	4 (1)	1.6	7 070	285
AFRICA	87.19	17 (12)	1.9	18 126	208
North Africa /Middle east	39.83	6 (4)	1.5	8 371	215
SSA, Central	4.78	4 (4)	8.4	3 020	632
SSA, East	19.86	1 (1)	0.5	1 198	60
SSA, Southern	6.06	1 (0)	1.7	150	25
SSA, West	17.56	5 (3)	2.8	5 387	307
WORLD	895.14	273 (106)	3.0	640 053	715

2.1.4. Current Treatment Regime.

Four cholinesterase inhibitors (ChEIs), tacrine, donepezil, rivastrigmine, and galantamine, have been approved by the Food and Drug Administration (FDA) for the treatment of AD. Tacrine is available, however no longer marketed due to safety and tolerability concerns. Memantine, an N-methyl-D-aspartate (NMDA) receptor antagonist, is also approved in the United States and Europe for the treatment of moderate to severe AD (**Figure 2.5**).

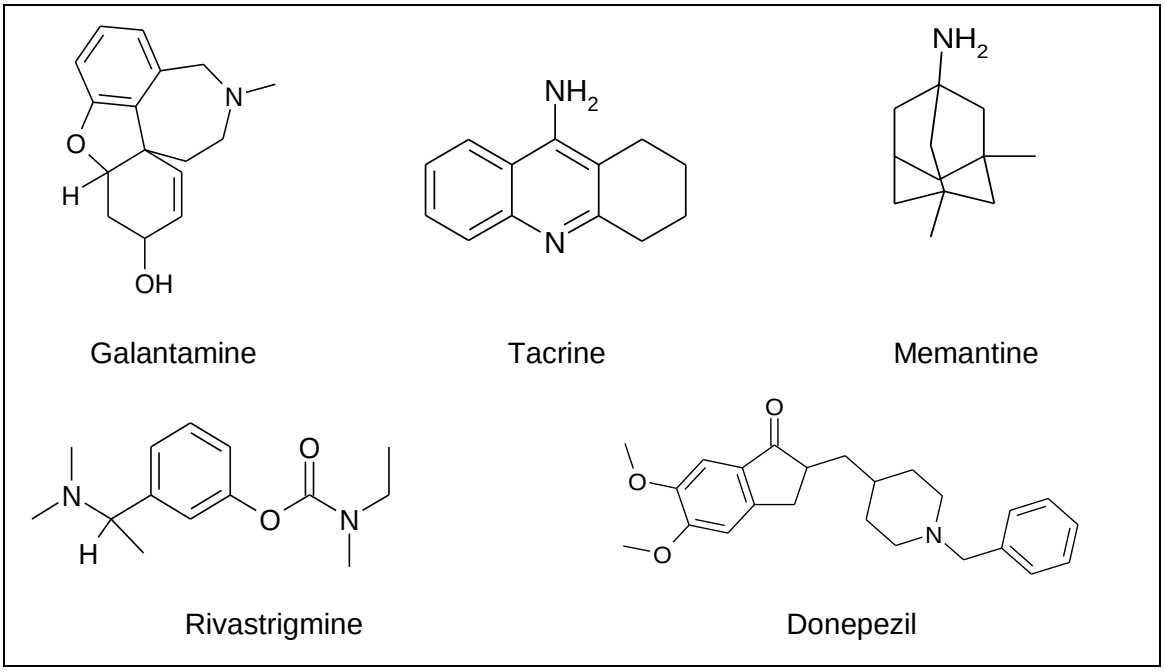

Figure 2.5: Current treatment regime for AD.

2.1.5. Diagnosis.

Typically, AD is noticeable by cognitive debility, with deficits in episodic memory, for example recalling recent events, losing items around the house, and recurrencing questioning. As the disease advances, aphasia, apraxia, agnosia, and visuospatial difficulties and executive dysfunction arises. Clinical diagnosis uses criteria of which the McKhann criteria published in 1984 (McKhann *et al*., 1984) are the most widely implemented (**Table 2.3**).

Table 2.3: Criteria for probable Alzheimer's disease according to the Alzheimer's Association (McKhann *et al*., 1984).

1.	Dementia established by clinical examination and confirmed by neuropsychological tests.
2.	Deficits in two or more areas of cognition, including memory impairment.
3.	Progressive worsening of memory and other cognitive functions.
4.	No disturbances of consciousness.
5.	Onset between ages 40 and 90.
6.	Absence of systemic disorders or other brain disease that in and of themselves could account for the progressive deficits in memory and cognition.

2.1.5.1. Medical history.

Past medical history, co-morbidities, family and educational history are taken into account.

2.1.5.2. Assessment of cognitive functions.

Screening tests are employed both to assess cognitive functions and to detect patients who require more detailed investigation. A number of neuropsychological tests which calculate memory, executive functions, language, praxis and visual-spatial abilities are employed. The Mini-Mental State Examination (MMSE) are most commoly used which compensates for (Sikkes *et al*., 2009) higher and lower educated individuals (O'Bryan *et al*., 2008).

2.1.5.2.1. Memory functions

Episodic memory is impaired in early AD and is caused by atrophy of the entorhinal cortex in the hippocampus while retrieval of memory depends on the frontal lobe and subcortical structures. The California Verbal Learning Test (Lange *et al*., 2002) or Buschke Free and Cued Selective Reminding test are employed (Salmon *et al*. 2002). The 'Logical Memory' test or in the '5 word' test (Dubois *et al*., 2002) are implemented to distinguish between free and delayed recall, with high specifity and sensitivity.

2.1.5.2.2. Executive functions.

Decreased verbal fluency can be determined through the Wisconsin card sorting test (WCST) (Nagahama *et al*., 2005); reduced speed of processing rate with the Trail Making test (Zakzanis *et al*., 2005) and defects in automatic responses *via* the Stroop test (Kramer *et al*., 2002).

2.1.5.2.3. Language.

The type and stage of dementia affects speech comprehension and production, reading and writing praxis and visual-spatial abilities. The clock-drawing test can be performed in the case of AD (**Figure 2.6**).

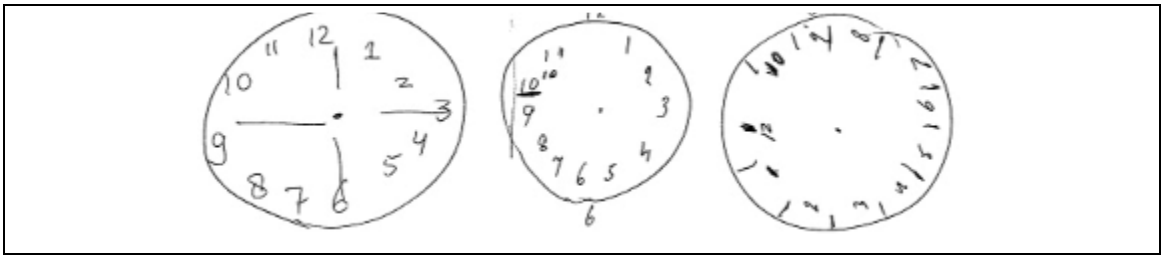

Figure 2.6: Different images of clock drawings by patients with AD (Scheltens *et al*., 2009).

The patient is requested to draw a clock with the time of 10 past 11 (Adapted from Cheltens *et al*., 2009). The Boston Naming test (Coen *et al*., 1999) or the Graded Naming test (Ahmed *et al*., 2008) are also frequently used (Kawas *et al*., 2003).

2.1.5.3. Assessment of activities of daily living (ADL).

The Disability Assessment for Dementia and the Bristol ADL are most useful informant-based questionnaires, however their complete psychometric properties are of moderate quality (Sikkes *et al*., 2009). The Blessed Roth Dementia Scale and the Informant Questionnaire on Cognitive Decline in the Elderly can alternatively be used (Waldemar *et al*., 2007).

2.1.5.4. Assessment of behavioural and psychological symptoms.

''Behavioural and psychological symptoms of Dementia'' (BPSD) is used to describe the non-cognitive symptoms (apathy, psychosis, affective and hyperactive behaviours) of dementia (Aalten *et al*., 2008). The Cornell scale for depression in dementia (CSDD) is sensitive and specific for detecting depression freely of the severity of dementia (Müller et al., 2005).

2.1.5.5. Neuroimaging.

The purpose of structural imaging in AD excludes other, potentially surgically treatable diseases and include specific findings for AD. Hippocampal atrophy is best viewed on magnetic resonance imaging (MRI) and more modern type CT scanner (Wattjes *et al*., 2009) with sensitivity and specificity of 80 - 90 % (Scheltens *et al*. 2009; Wattjes *et al*. 2009; Scheltens *et al*.; 2002).

Medial temporal lobe atrophy is prominent (**Figure 2.7**), but the atrophy pattern of the entire brain should be taken into consideration, rather than a secluded medial temporal lobe.

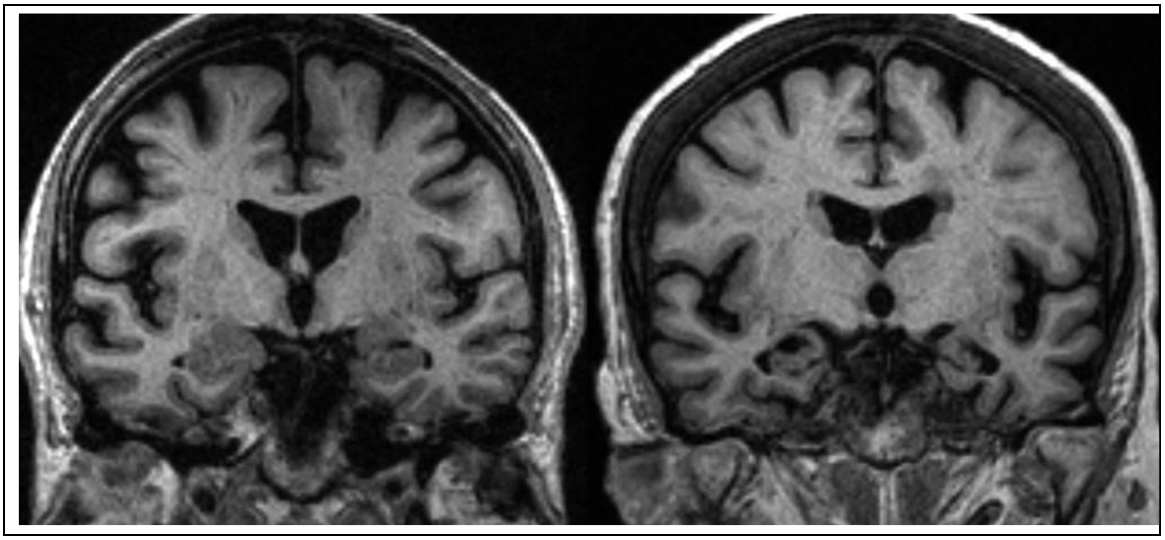

Figure 2.7: Coronal T1-weighted MRI scans of control (**left**) and AD patient (**right**), with both 75 of age. The AD patient shows clear atrophy of the hippocampus (Scheltens *et al*., 2009).

Universal atrophy and prominent medial temporal lobe athropy usually charachterises AD. But, atypical forms of AD, especially prevalent among younger AD patients have been described with prominent posterior atrophy, (**Figure 2.8**).

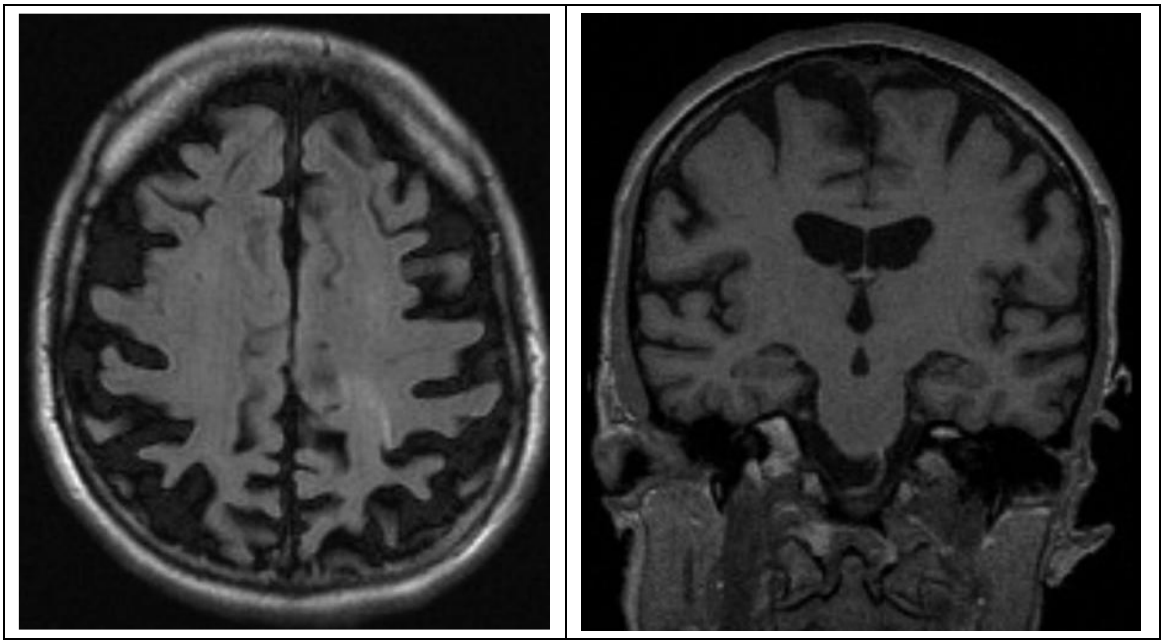

Figure 2.8: EOFAD (age 51). **Left**: Parietal and posterior cingulate atrophy is pronounced. **Right**: An intact medial temporal lobe (Scheltens *et al*., 2009).

In AD, signs of small-vessel disease can be detected on MRI, called white matter hyperintensities (WMH) and lacunar infarcts (lacunes) (**Figures 2.9 A** and **2.9 B**) and microbleeds (**Figure 2.10**).

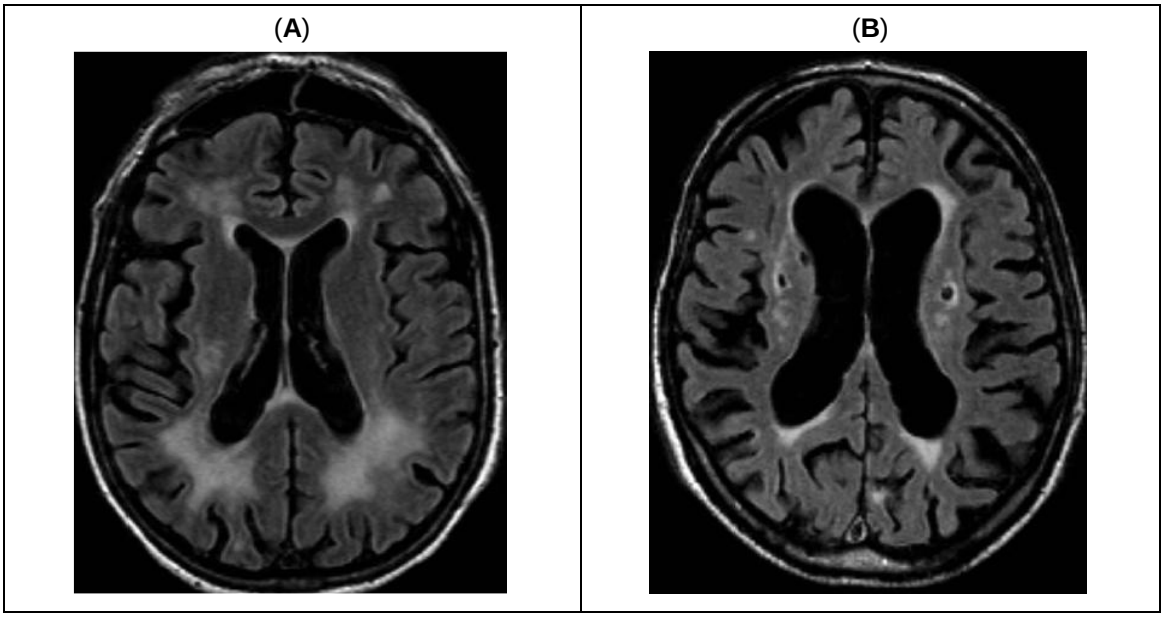

Figure 2.9: (A): Cerebrovascular pathology on axial fluid attenuated inversion recovery (FLAIR) MRI scans. Confluent white matter changes (Fazekas scale 3). **(B):** Cerebrovascular pathology on axial fluid attenuated inversion recovery (FLAIR) MRI scans. Lacunar infarcts in basal ganglia on both sides (Scheltens *et al*., 2009).

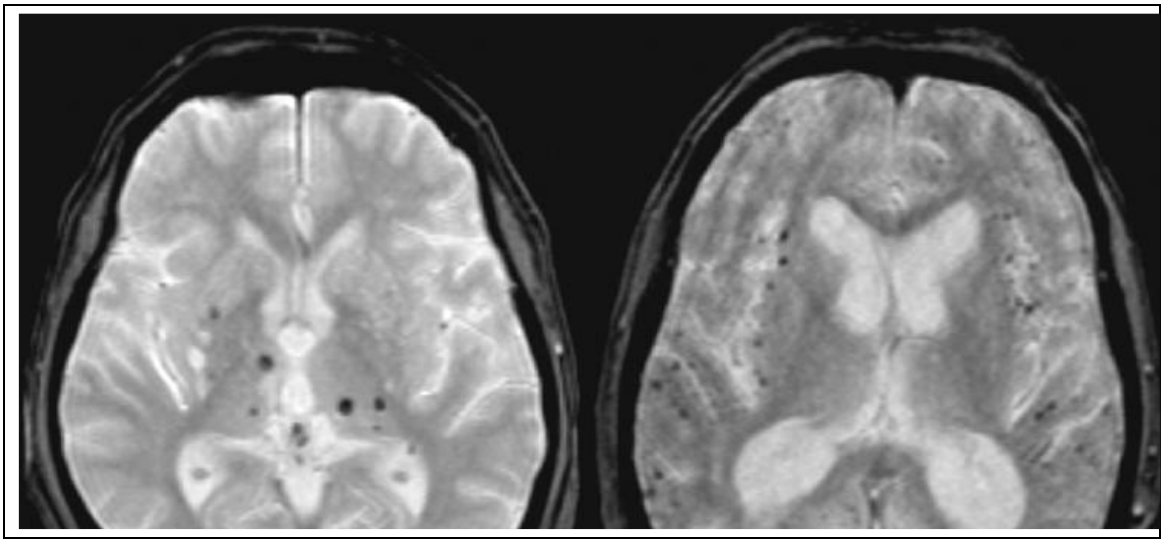

Figure 2.10: Microbleeds on Flash/T2*/2D axial MRI scan. **Left**: mainly in the basal ganglia. **Right**: predominantly located cortically (Scheltens *et al*., 2009).

The use of functional neuroimaging [i.e., fluorodeoxy-glucose- (FDG-) PET and single photon emission computed tomography (SPECT)] increases dementia diagnosis. A positive perfusion SPECT scan raised the likelihood of AD detection to 92 %, whereas a negative SPECT scan lowered the detection to 70 %.

18FDG-PET revealed both sensitivity of 93 % and specificity of 63 % in the diagnosis of AD (Silverman *et al*., 2005) while FDG-PET is particularly useful in the differential diagnosis of AD from other dementias with specificity greater than 95 % (Panegyres *et al*., 2009).

2.1.5.6. Electroencephalography (EEG).

A low alpha frequency, elevated theta frequency and lower mean frequency according to EEG are characteristic for AD patients, (Jelic *et al*., 2009).

2.1.5.7. Cerebrospinal fluid (CSF) analysis.

The elevation of the 14-3-3 protein reveals neuronal loss and supports diagnosis of CJD (WHO manual for surveillance of human transmissible spongiform encephalopathies, (WHO 2011; Otto *et al*., 2002; Sanchez-Juan *et al*., 2006). In the CSF of AD patients, decreased $A\beta_{42}$ levels and elevated total-tau are present. It has a recorded sensitivity and specificity of 86 % and 90 % respectively (Blennow *et al*., 2003).

2.1.5.8. Genetic testing.

APP, PS1 and PS2 gene mutations elucidate 50 % of EOFAD (Chen *et al*., 2002). The ApoE Ɛ4 allele is the only genetic factor consistently implicated in LOAD (Brouwers *et al*., 2008).

2.2. ENZYMES INVOLVED IN AD.

Although AD neuronal loss is prominent in the cholinergic system, the dopaminergic and serotonergic systems are also affected (review section 2.1.1). Therefore, in this section, multiple targets of importance in the AD neurodegeneration cascade will be briefly discussed followed by a summary and structure activity relationships (SAR) of derivatives containing the coumarin pharmacophore which are active on these systems. Emphasis are placed on monoamine oxidase B (MAO-B) and acetylcholinesterase (AChE), but numerous other targets will also be considered.

2.2.1. Secretases.

2.2.1.1. Amyloid Precursor Protein (APP) secretases.

APP is the precursor protein to the amyloid-β-protein (Aβ), the 40-42 amino acid residues component of senile plaques in AD patients which forms the amyloid hypothesis of AD. APPs infusion into animal brain resulted in increased synaptic density and enhanced memory function (Roch *et al*., 1994; Meziane *et al*., 1998), and stimulated neurite outgrowth This phenotype is compatible with the up regulation of APP expression during neuronal maturation (Hung *et al*., 1992). Injection of APP antibodies directly into the brain caused impairment in behavioural tasks in adult rat (Meziane *et al*., 1998). Binding sites for APPs in epidermal growth factor (EGF)-responsive neural stem cells is located in the subventricular zone (Caille *et al*., 2004). The reduction in APP levels in CSF of AD patients, together with a decrease of other growth factors in the brain, are of importance.

APP is a type I membrane protein with two sites of cleavages, one in the extracellular domain (β-secretase cleavage) and the other in the transmembrane region (γ-secretase cleavage), which are pivotal for Aβ release (**Figure 2.11**). Amyloidogenic processing (β-secretase cleavage) is the preferred pathway of APP metabolism in neurons due to the greater abundance of beta-site amyloid presurcor protein cleavage enzyme (BACE1), while the non-amyloidogenic pathway (γ-secretase cleavage) is present in all other cell types. APP can be modulated by the activation of cell-surface receptors e.g. serotonin 5-hydroxytryptamine (5-HT_4) receptor, matabotropic glutamate receptor, muscarinic acetylcholine receptors and platelet-derived growth factor receptor. In turn, downstream signalling regulates Aβ secretion by intermediates such as protein kinase C (PKC), protein kinase A (PKA), phosphatidylinositol 3 kinase, mitogen-activated protein kinase, extracellular signal-regulated kinase, Src tyrosine kinase, small GTPase Rac, inositol 1,4,5-triphosphate, cyclic adenosine monophosphate (cAMP) and calcium.

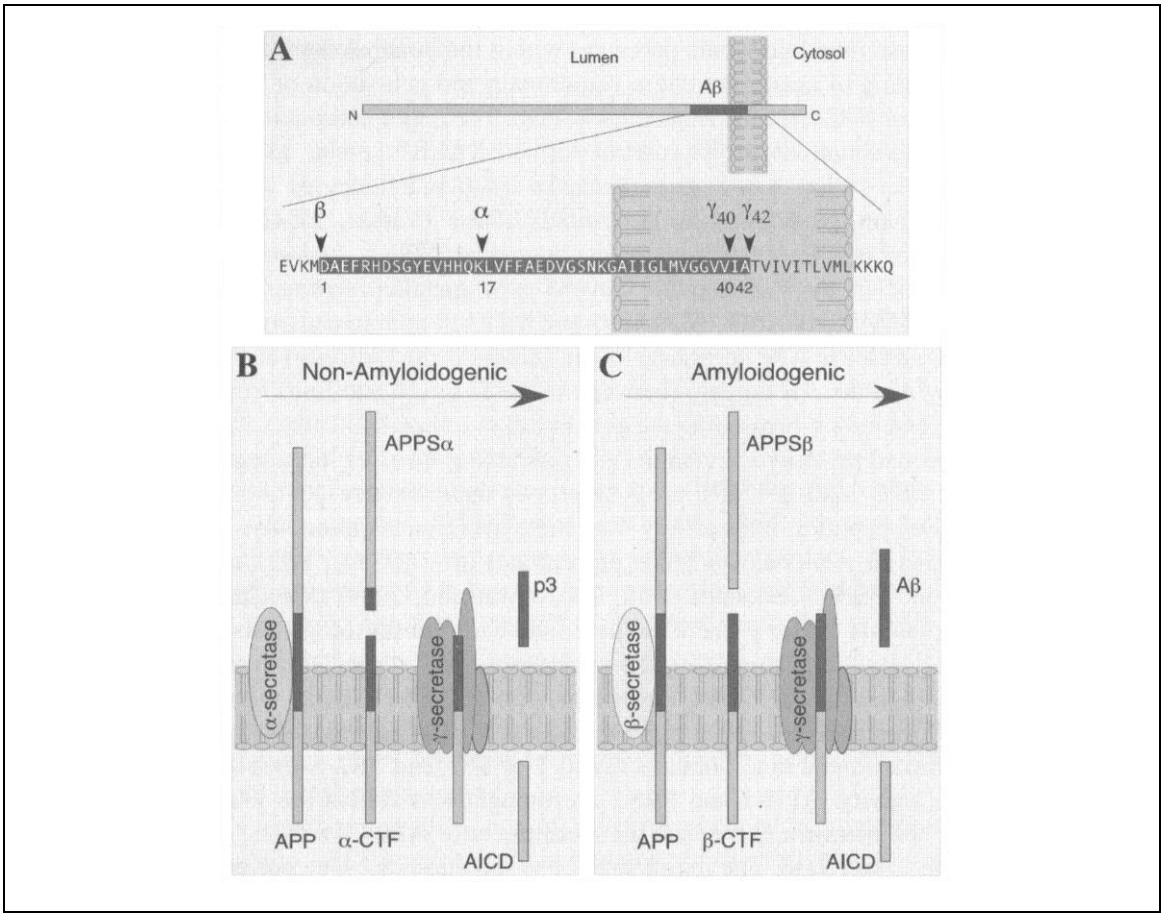

Figure 2. 11: Proteolytic processing of APP. (**A**) Schematic structure of APP shown with Aβ domain. The major sites of cleavage by α-, β-, and γ-secretases are indicated along with Aβ numbering from the N-terminus of Aβ (Asp1). (**B**) Non-amyloidogenic processing of APP refers to sequential processing of APP by membrane-bound α- and γ-secretases. α-secretases cleaves within the Aβ domain, thus precluding generation of intact Aβ peptide. The fates of N-terminally truncated Aβ (p3) and APP intracellular domain (AICD) are not fully resolved. (**C**) Amyloidogenic processing of APP is carried out by sequential action of membrane-bound β- and γ-secretases (Adapted from Sisodia, 2007).

APP is rapidly anterogradely transported in axons of both the peripheral nervous system (PNS) and central nervous system (CNS) (Kamal *et al*., 2001; Lazarov *et al*., 2002; Sheng *et al*., 2002, Sheng *et al*., 2003). In the CNS, β- and γ-sectretase releases of Aβ peptides at axon terminals, modulate synaptic activity *via* NMDA receptor interactions (Kamanetz *et al*., 2003). Thus, A*β* might be involved in NMDA receptor trafficking and can cause synaptic dysfunction (Snyder *et al*., 2005).

2.2.1.2. β-secretase (BACE).

Two vital enzymes β-secretase (BACE1 and BACE2) and γ-secretase have been identified as possible objects for therapeutic intervention (Vassar *et al*., 1999; De Strooper *et al*., 2003). A very attractive approach in lowering Aβ is to inhibit β-secretase, generally referred to as beta-site amyloid precursor protein [APP] cleavage enzyme (BACE1), a transmembrane aspartyl

protease responsible for N-terminal cleavage of the APP leading to the production of the Aβ peptide (Selkoe, 2002).

Full- length APP undergoes consecutive proteolytic processing **Figure 2.10**:

1. First, APP is cleaved *via* α-secretase (non-amyloidogenic pathway) or β-secretase (amyloidogentic pathway) within the luminal domain and liberates membrane-tethered α- or β-C terminal fragments (CTFs). The dominant neuronal β-secretase is BACE1 (β-site APP cleaving enzyme or Asp-2 or memapsin). BACE1 cleaves APP within the ectodomain, generating the N-terminus of Aβ (Vassar, 2004). Numerous zinc metalloproteinases includes TACE/ADAM17, ADAM9, ADAM10, MDC-9 and BACE2 (Allinson *et al*., 2003). This is located between residues Lys16 and Leu17 of the Aβ peptide.
2. The second proteolytic event in APP processing is the intramembranous cleavage of α- and β-CTFs *via* γ-secretases, to yield p3 (3 kDa) and Aβ (4 kDa) peptides. The minimum components of γ-secretase includes presenilin-1 or -2 (PS1 or PS2), nicastrin, anterior pharynx defective 1 homolog A (APH-1) and presenilin enhancer 2 homolog (PEN-2) (Edbauer *et al*., 2003; Iwatsubo, 2004). APP levels in concert with levels and activities of BACE1 plays a critical role in the susceptibility and pathogenesis of AD (Wong *et al*., 2002). In the CNS, Aβ peptides are produced by two enzymes: BACE1 which generates APP-β carboxyl terminal fragments (APP- βCTFs) (Hussain *et al*., 1999; Sinha *et al*., 1999; Vassar *et al*., 1999; Yan *et al*., 1999; Lin *et al*., 2000) and cleavage of APP-βCTFs *via* the γ-secretase complex (Francis *et al*., 2002; De Strooper, 2003; Selkoe *et al*., 2003; Tagasuki *et al*., 2003) and ultimately causes Aβ peptide secretion. APP also has the ability to be cleaved endoproteolytically through an non-amyloidogenic pathway involving an α-secretase *via* TNF-alpha Converting Enzyme (TACE) (Allinson *et al*., 2003), or BACE2 (Farzan *et al*., 2000; Yan *et al*., 2001). p3 Fragments are formed by γ-secretase cleavage of APP-αCTFs. These α-secretase and BACE2 cleavagespreclude the formation of Aβ peptides and are hypothesised to protect organs from Aβ amyloidosis.

The APP-βCTFs or αCTF that are cleaved by γ-sectretase causes the release APP intracellular domain (AICD), which in turn forms a multimeric complex with the nuclear adaptor protein, Fe65, and the histone acetyltransferase, Tip60 (Cao *et al*., 2001; Baek *et al*., 2002). This complex formed between APP and Fe65 has also been implicated in neurite growth and synapse modification (Sabo *et al*., 2003).

Then why do neurons form amyloid in the CNS while this occurrence is absent in other cells? The distributions and levels of BACE1 and BACE2/TACE, are the key determinants for CNS Aβ amyloidosis (Wong *et al*., 2001). To support this, firstly, with the exception of the relatively

higher levels of BACE1 in the olfactory bulb, the levels of BACE1 in most regions of the brain appear to be uniform (Laird *et al*., 2005). Secondly, neurons enriched in BACE1 and APP are conspicuous in presynaptic terminals in the hippocampus (Laird *et al*., 2005), a region critical for learning and memory and one that is vulnerable in AD. APP is anterogradely transported in the CNS (Buxbaum *et al*., 1998; Lazarov *et al*., 2002; Sheng *et al*., 2002) and initial reports indicated that BACE1's anterogradely transported to a greater extent than in the PNS (Kamal *et al*., 2001; Sheng *et al*., 2003). Thirdly, physiologically high levels of BACE1 in neurons are coupled with low levels of α-sectretase and BACE2 activities. In contrast, non-neuronal cells exhibit low levels of active BACE1 and high levels of BACE2 and/or α-sectretase activities (Laird *et al*., 2005).

2.2.2.1. Deletion of BACE1 and Aβ amyloidosis

Studies with BACE1 ablation in APP*swe*; PS1ΔE9 mice were subjected to the Morris water maze task (Laird *et al*., 2005) and it was concluded that BACE1 ablation prevents cognitive abnormalities, thus suggesting BACE1 – inhibitors as potential treatment to addres AD.

2.2.2.2. BACE1 and APP processing in cognition and emotion

Recent studies demonstrated that isoform-specific deletion of *Fe*65 is associated with memory deficits (Wang *et al*., 2004) and that interactions of the APP intracellular domain (AICD) with Fe65-dependent pathways are crucial for normal cognitive function.

2.2.2.3. Relevance to coumarin

Garino and co-workers (2006), reported a series of coumarin analogues conjugated with phenyl-piperazine moieties (**Figures 2.12** and **2.13**), which demonstrated improved BACE1 inhibitory activities (Garino *et al*., 2006).

Index:	R =	X =	
1	H	*N*-Boc	
2	H	*N*-Bzl	
3	H	NH TFA	
4	OMe	*N*-Boc	
5	OMe	*N*-Bzl	
6	OMe	NH TFA	**(1 - 6)**

Figure 2.12: 3,8-Substituted coumarin derivatives with BACE1 inhibitory activity (Garino *et al*., 2006).

Index:	X =
7	*N*-Boc
8	NH TFA
9	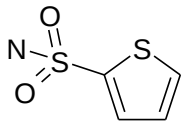

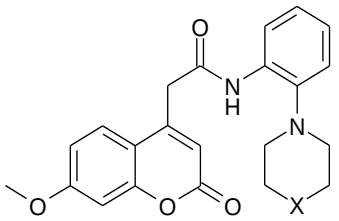

(7 - 9)

Figure 2.13: BACE1 inhibitory activities of 4,7-Substituted coumarin derivatives (Garino *et al*., 2006).

The coumarinyl compounds **2** and **3** revealed IC_{50} of 0.76 µM and 0.67 µM respectively, with the most potent inhibitor, compound **7** (IC_{50} = 0.093 µM). Compound **7**, (linked to the amide function *via* a methylene spacer) is of interest in the design of analogues with various lengths of linkers introduced between the heterocycles and the carbonyl of the amide group. Coumarins substituted in position 3 and containing the *N*-Boc group on the piperazine ring (**1** and **4**) (IC_{50} = 1 µM and 2.4 µM respectively) has slightly decreased BACE1 inhibitory activity.

2.2.2.3. γ-Secretase.

$A\beta_{40}$ and $A\beta_{42}$ are the main sites of γ-secretase cleavage. More than 90 % of Aβ secreted is $A\beta_{40}$, while $A\beta_{42}$ is less than 10 %. In addition, γ-secretase cleavage also liberates APP intracellular domain (AICD).

2.2.2. Presenilin (PS).

Presenilins (PS1 and PS2) are highly hydrophobic proteins, consist of 467 and 448 amino acid residues, respectively (Sherrington *et al*., 1995). Apart from its essential role in the proteolytic function of the γ-secretase, also participate in calcium homeostasis, neuronal signalling and trafficking, protein degradation, neurite outgrowth, apoptosis, memory and synaptic plasticity (Sisodia *et al*., 1999; Koo *et al*., 2004; Thinakaran *et al*., 2004). Support that PS were catalytically active proteases originated from studies revealing that several γ-secretase inhibitors bound to PS (Esler *et al*., 2000; Li *et al*., 2000; Seiffert *et al*., 2000).

Labelled inhibitors of γ-secretase specifically bound to the N-terminal fragment (NTF) and C-terminal fragment (CTF) of presenilins, while full-length PS was not labelled, further suggesting that full length PS is an inactive precursor for the active dimeric form of PS (**Figure 2.14**). Thus, the catalytic centre of γ-secretase resides at the heterodimeric interface of PS fragments (Tomita *et al*., 2001; Wang *et al*., 2004). Down regulation of Nicastrin (Nct) resulted in a loss of γ-secretase activity (Edbauer *et al*., 2000; Francis *et al*., 2002). Nct comprises in Notch signalling pathway and Aβ generation in both fly and mouse (Chung *et al*., 2001; Edbauer *et al*., 2002; Hu *et al*., 2002; Li *et al*., 2003; Lopez-Schier *et al*., 2002). Downregulation of Aph-1 or Pen-2 levels causes a decrease in γ-secretase activity.(Francis *et al*., 2002; Lee *et al*., 2002; Tagasuki *et al*., 2003). Thus, PS, Nct, Aph-1 and Pen-2 are the

essential components that constitute the γ-secretase complex and are vital for APP and Notch processing.

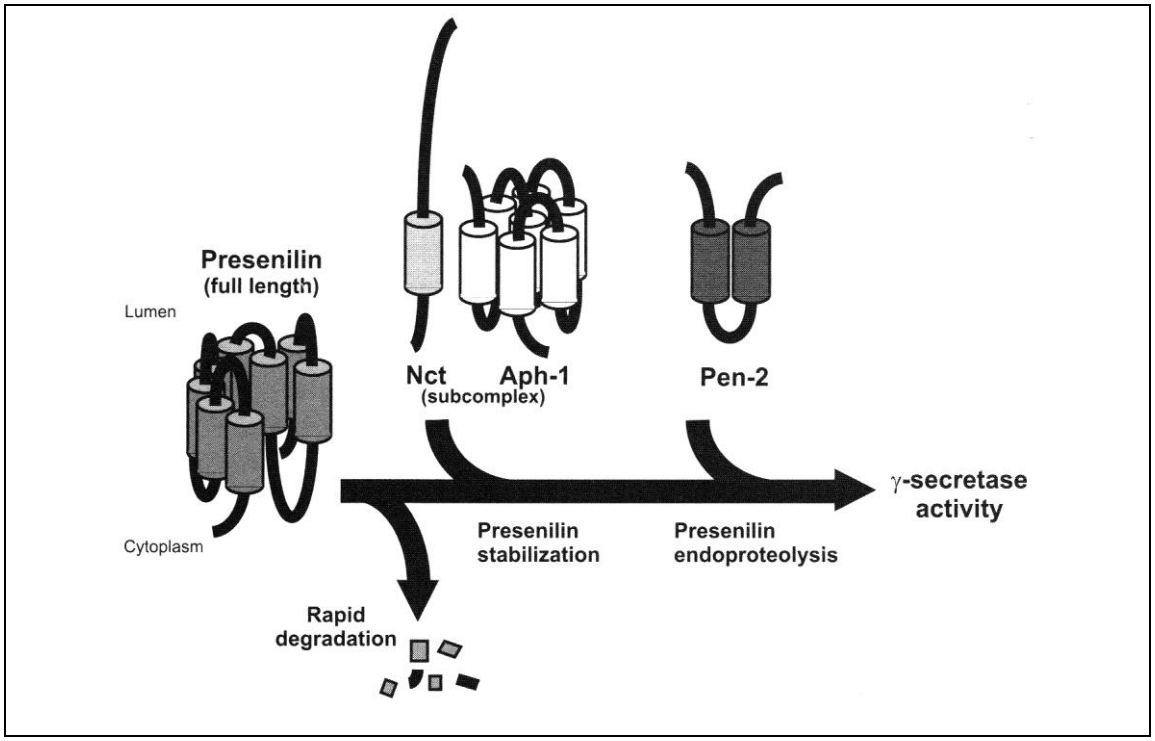

Figure 2.14: Components of γ-Secretase, the assembly and activation of the γ-secretase complex. Presenilin holoprotein (full-length) is rapidly degraded, whereas a fraction of presenilin is stabilised by binding to Nicastrin and Aph-1 (subcomplex). Subsequent binding of Pen-2 to the ternary complex induces the endoproteolysis of presenilin and confers γ-secretase activity. Cylindrical colums represent the putative transmembrane domains of each component (Adapted from Sisodia, 2007).

The dipeptide type γ-secretase inhibitor, DAPT (N-[*N*-(3,5-difluorophenacetyl)-L-alanyl]-S-phenylglycine *t*-butyl ester) (Dovey et al., 2001) revealed decreases in cortical Aβ after acute administration of DAPT in mutant APP transgenic mice.

2.2.3. Inflammatory enzymes.

Cell-based studies have demonstrated that non-steroidal anti-inflammatory drugs (NSAIDs) can alter γ-secretase (Weggen *et al*., 2001). Some commonly used NSAIDs selectively inhibit $A\beta_{42}$ generation, and consequently increase $A\beta_{38}$ production (a less fibrillogenic species). Based on epidemiological evidence in arthritis patients, NSAID treatment reduced incidence and slowed AD progression, thus making NSAIDs prospective anti-AD candidates. It is postulated that $A\beta_{42}$-lowering NSAIDs bind to PS, changing its conformation and method of binding to APP (Lleó *et al*., 2004).

2.2.3.1. Relevance to coumarin.

7-hydroxycoumarin derivatives (**Figure 2.15**) were synthesised and investigated for their anti-inflammatory effects on the expression of inflammatory enzymes, inducible nitric oxide synthase (iNOS) and cyclooxygenase-2 (COX-2) (Timonen *et al*., 2011).

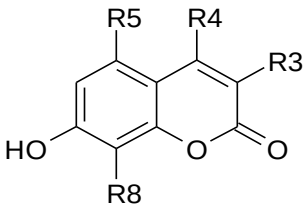

(10 - 17)

Index:	R3=	R4=	R5=	R8=
10	Et	Me	H	Me
11	H	Pr	Me	H
12	Me	Me	H	OMe
13	F	Me	H	OMe
14	H	Ph	H	OMe
15	H	Ph	H	H
16	H	2-F-C_6H_4	H	H
17	H	Ph	H	OMe

Figure 2.15: Derivatives of 7-hydroxycoumarin evaluated for effects on inflammatory enzymes (Timonen *et al*., 2011).

The 7-hydroxycoumarins were exposed to the inflammatory stimulus lipopolysaccharide (LPS), which induced production of the pro inflammatory cytokine interleukin-6 (IL-6) that was monitored *via* concentration measurement in the cell culture medium by immunoassay. In resting cells the IL-6 production was low, but this was significantly enhanced when cells were activated by LPS addition. At a 100 µM concentration, compounds **10,** and **16** inhibited IL-6 production by more than 80 %, while compound **15** had an inhibitory effect of less than 30 %. Sandhya and co-workers (2011) synthesised coumarin derivatives using various aromatic and heterocyclic amines (**Figure 2.16**) and assayed these compound for anti-inflammatory COX-2 inhibition (Sanhya *et al*., 2011).

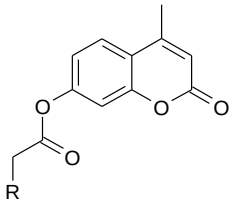

(18 - 31)

Index:	R =	Index:	R =
18	C_6H_5NH	**25**	*p*-OCH_3-C_6H_5NH
19	*o*-NO_2-C_6H_5NH	**26**	*o*-CH_3-C_6H_5NH
20	*m*-NO_2-C_6H_5NH	**27**	*m*-CH_3-C_6H_5NH
21	*p*-NO_2-C_6H_5NH	**28**	*p*-CH_3-C_6H_5NH
22	*o*-Cl-C_6H_5NH	**29**	1,5-dihydro-4*H*-1,2,4-triazol-4-amino
23	*p*-Cl-C_6H_5NH	**30**	1,3-benzothiazol-2-amino
24	*o*-OCH_3-C_6H_5NH	**31**	1,3-thiazol-2-amino

Figure 2.16: Coumarin derivatives with anti-inflammatory activity (Sandhya *et al*., 2011).

Compounds **29** to **31** revealed moderate anti-inflammatory and analgesic activities. The activity of compound **30** started to decrease after 1 h, (probably due to metabolic instability), while compounds **21** and **26** revealed moderate activity and a decrease in activity after 3 h. Compound **31** was the most active among the series with good anti-inflammatory and analgesic activity that could be ascribed to the presence of heterocyclic substituent. This SAR was confirmed by replacement of the heterocyclic ring with a substituted phenyl group, which resulted in a decrease in activity (Sandhya *et al*., 2011).

A set of novel biscoumarin–chalcone hybrids was synthesised and evaluated for both their anti-inflammatory and anti-oxidant activity (**Figure 2.17**). The tested compounds exhibited significant scavenging activities, thus revealing a template for the design of new anti-inflammatory agents (Sashidhara *et al*., 2011).

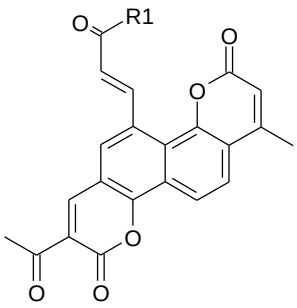

(32 - 37)

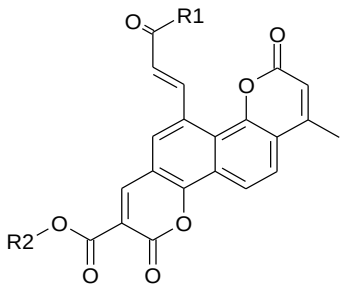

(32 - 37)

Index:	R_1 =	R_2 =	Index:	R_1 =	R_2 =
32	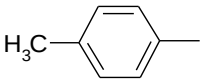	H	**35**	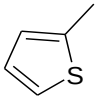	CH_3
33	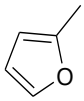	H	**36**	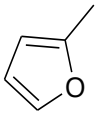	C_2H_5
34	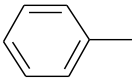	CH_3	**37**	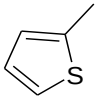	C_2H_3

Figure 2.17: Biscoumarin–chalcone hybrids as anti-oxidants (Sashidhara *et al*., 2011).

At 100 mg/kg, compounds **32, 33** and **34** (**Figure 2.17**) demonstrated 29 %, 26 %, and 33 % anti-inflammatory activity respectively, in comparison with 59.5 % with Ibuprofen as reference drug at the equivalent dose (Sashidhara *et al*., 2011).

Compounds **37**, **35** and **36** (**Figure 2.17**) illustrated weak anti-inflammatory activities of 8.77 %, 3.5 % and 13 % respectively. Compounds **37, 36** and **34** showed mild anti-oxidant activity and significant superoxide anion inhibition of 24 %, 30 % and 29 %, hydroxyl radical inhibition by 26 %, 21 % and 27 % and microsomal lipid peroxidation inhibition by 27 %, 24 % and 23 %, respectively, (in contrast with Allupurinol as reference drug with 42 % inhibition in superoxide anions at 20 µg/mL, Manitol and *α*-Tocopherol with 40 % and 41 % inhibition of hydroxyl ions and microsomal lipid peroxidation at 100 µg/mL, respectively). The most active anti-inflammatory agent was compound **37,** which in addition had potent antioxidant activity, suggesting that the anti-inflammatory property of the compound might be partly due to its radical scavenging activity (Sashidhara *et al*., 2011).

Tumour necrosis factor-alpha (TNF-α) and IL-6 are two major multifunctional pro-inflammatory mediators involved in a variety of autoimmune conditions such as pain and joint destruction, characteristics of rheumatoid arthritis (RA) (Josef *et al*., 2003). TNF-α and IL-6 inhibitors may thus be of interest in AD (**Figure 2.18**), psychiatric disorders, cancer, diabetes, and depression (Handraskar *et al*., 2005; Rosler *et al*., 2001; Jahromi *et al*., 2000).

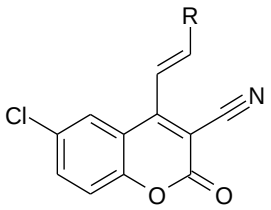

(38 - 59)

Index:	R =	Index:	R =
38	Phenyl	**49**	4-OHC_3 Phenyl
39	4-F Phenyl	**50**	3,4-$DiOCH_3$ Phenyl
40	2-Cl Phenyl	**51**	3,4,5- $TriOCH_3$ Phenyl
41	3-Cl Phenyl	**52**	3-OC_6H_5 Phenyl
42	4-Cl Phenyl	**53**	4-SCH_3 Phenyl
43	3-Br Phenyl	**54**	2-Ethenyl phenyl
44	2-NO_2 Phenyl	**55**	9-Anthracyl
45	3-NO_2 Phenyl	**56**	2-Furyl
46	3-OH Phenyl	**57**	3-Indolyl
47	4-OH Phenyl	**58**	4-*N,N*-$DiCH_3$ amine phenyl
48	2-OCH_3 Phenyl	**59**	3-OCH_3 Phenyl

Figure 2.18: 4-styrylcoumarin derivatives as inhibitors of TNF-α and IL-6 with anti-tubercular activity (Upadhyay *et al*., 2011).

A methoxy group on phenyl ring at *m*-position (e.g. compound **59**) revealed promising TNF-α inhibitory activity, while substitution with a phenyl ring containing an electron withdrawing group resulted in molecules devoid of activity (compound **39** - **45**). An unsubstituted phenyl group (compound **38**) retains good inhibitory activity of IL-6, while substitution weakens the inhibitory activity. Compound **47,** which contains a hydroxyl group at the *p*-position of the phenyl ring, had increased potency while bulky moieties results in inactive molecules (Upadhyay *et al*., 2011). In contrast, molecules having bulky groups revealed good anti-tubercular activity, as observed for compound **51** and **55** and electron withdrawing groups at the *m*-position of the phenyl ring (compounds **41** - **45**) demonstrated increased activity.

Promising activity against IL-6 was noted with compounds **38**, **45** and **47** (72–87 % inhibition) while compound **59** exhibited significant TNF-α inhibitory activity (73 % inhibition at 10 µM). Compounds **51**, **52**, **55** and **58**, on the other hand revealed 87 %, 72 %, 81 % and 79 % inhibition respectively against M. Tuberculosis H37Rv strain at <6.25 µM. These SAR might provide a potentially suitable tool for designing new molecules having selectivity and inhibitory activity towards TNF-α and IL-6. Furthermore, the 4-styrylcoumarin moiety can be altered as a lead compound for anti-inflammatory or anti-tubercular agents (Upadhyay *et al*., 2011).

Eclipta alba Hassk (Asteraceae) have in important role in traditional Ayurvedic (native to India) and Unani (the middle-east and south-asia) systems of holistic health and herbal medicine. Its main constituents are wedelolactone and demethylwedelolactone (**Figure 2.19**). Both these coumarins analogues reported to possess anti-inflammatory activities (Leal *et al*., 2000).

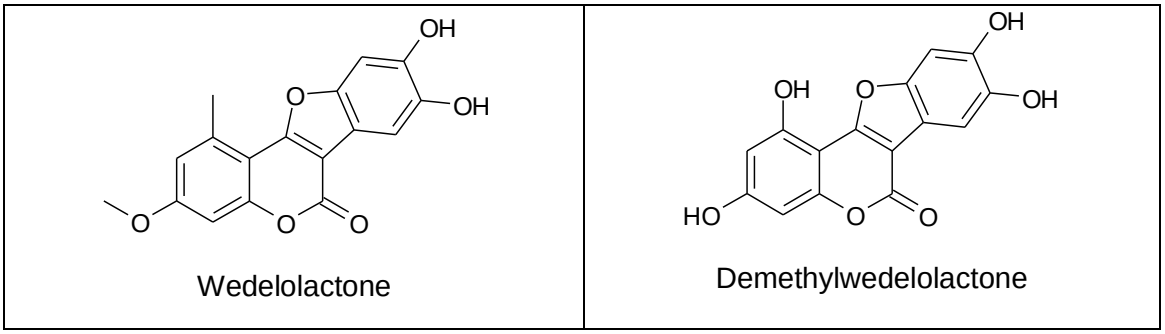

Figure 2.19: Structures of Wedelolactone and Demethylwedelolactone (Leal *et al*., 2000).

2.2.4. Protein kinases.

Several systems have been observed to be abnormal in AD such as calpains which cleave p35 to p25 and could promote increased activity of kinases such as cyclin dependent kinase-5 (cdk5) and glycogen synthase kinase 3 (GSK-3) (Grynspan *et al*., 1997; Grynspan *et al*., 1997). As mentioned earlier, one of the hallmarks of AD is the neurofibrillary tangles that consist of tau (see section 2.2.4.2). Tau serve as a substrate for several kinases *in vivo* and *in vitro* and a large quantity of kinases have been reported to be associated with neurofibrillarly tangles in AD brains (Buee *et al*., 2001). In cultured neurons or in normal animal brain, the two major kinases involved in abnormal tau phosphorylation appear to be GSK3 and cdk5 (Planel *et al*., 2002; Maccioni *et al*., 2001).

2.2.4.1. Glycogen synthase kinase 3 (GSK-3).

Glycogen synthase kinase 3 (GSK-3) is a serine/threonine protein kinase that mediates the incorporation of phosphate molecules onto serine and threonine amino acid residues. In mammals, GSK-3 is encoded by two known genes, namely GSK-3α and GSK-3β. The importance of GSK on tauopathy has also been supported following the observation that PS1 can activate P13K/Akt signalling leading to inactivation of GSK-3, and that pathogenetic PS1 mutations inhibit the PS1-dependent PI3K/Akt activation (Baki *et al*., 2004). GSK-3 plays a pivotal role in AD, because it has been evident that it can be activated by Aβ and hyperphosphorylated tau protein (Avila *et al*., 2007).

It's hypothesised that altered ionic homeostasis and oxidative stress following Aβ accumulation change the balance between the phosphatases and kinases that regulate the level of phosphorylation of tau protein, leading to its hyperphosphorylation, separation from microtubules, abnormal accumulation and polymerisation with tangle formation, thus

ultimately causing synaptic dysfunction and axonal loss (Brion *et al*., 1998; Sorrentino *et al*., 2007).

Frost *et al*., (2009) confirmed that extracellular tau aggregates are absorbed by cultured cells. Internalised tau aggregates displace tubulin, induce fibrillisation of intracellular full-length tau and the ability to increase fibril formation of recombinant tau monomer *in vitro*. Newly aggregated intracellular tau transfers between co-cultured cells and that tau aggregates can propagate a fibrillar, misfolded state (**Figure 2.20**) from the outside to the inside of a cell (Frost *et al*., 2009).

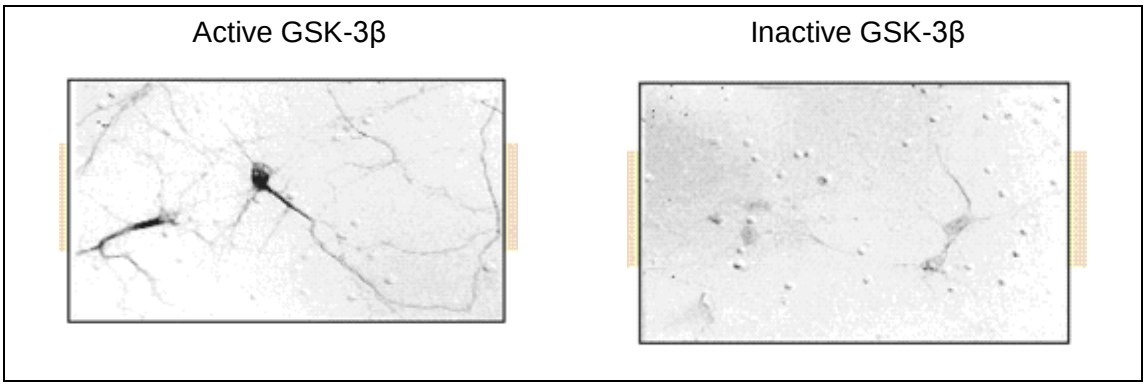

Figure 2.20: The effect of active and inactive GSK-3β on neurons (Frost *et al*., 2009).

Relevance of GSK-3β in AD can be summarised as follows:

1. Studies in rodent revealed that memory impairments in AD might be the consequence from increased GSK-3 signalling, which in turn impairs hippocampal memory formation and blocks synaptic long-term potentiation (LTP).
2. Increased GSK-3 signalling contributes to the formation of neurofibrillary tangles (NFTs) and amyloid plaques.
3. Increased GSK-3 signalling in AD mice caused abnormal APP processing, thus Aβ production is increased and neurotoxicity is induced (Giese, 2009).

Notably, in addition to potentiating α-secretase, some muscarinic agonists seem to inhibit GSK-3 (Forlenza *et al*., 2000). Limited information exists about the degradation of tau *in vivo*, but it is evident that inhibition of proteasome activity through injection of Epoxomicin negates the clearance of tau, supporting the concept that tau is, in part, cleared by proteasome (Oddo *et al*., 2004).

Lithium has been illustrated to reduce tau hyperphosphorylation *via* inhibiting GSK-3β in cell culture (Lovestone *et al*., 1999) and in transgenic mice (Noble *et al*., 2005). Through its inhibitory GSK-3α actions, lithium additionally prevents Aβ peptide accumulation in the brains of mice that overproduce APP (Phiel *et al*., 2003) thus providing beneficial neuroprotection from both NFTs and amyloid plaque formation. Valproatic acid acts in a similar way. Application of GSK-3 inhibitors stimulates axon formation and elongation of mature neurons whether in presence or absence of inhibitory substrates (Dill *et al*, 2008).

2.2.4.2. Cyclin dependent kinase-5 (Cdk5).

Neurodegeneration has been strongly associated with cdk5 activity through elevation of its activator, p25 (Patrick *et al*., 1999; Patrick *et al*., 2001). Cell based studies have suggested a link between Aβ, cdk4 and tau (Town *et al*., 2002; Rank *et al*., 2002; Otth *et al*., 2002). Cdk5 - induced tau hyperphosphorylation has been illustrated in APP transgenic mouse models while increased tau phosphorylation by cdk5 is sufficient to directly destabilise microtubules (MTs) and contribute to Aβ toxicity (Evans *et al*., 2000).

2.2.5. Acetylcholineterase (AChE).

Cholinesterase inhibitors (ChEIs) reduces the acetylcholinesterase (AChE)-induced metabolism of acetylcholine (ACh) in the synaptic cleft, increases the intrasynaptic residence time of ACh and facilitates interaction between ACh and the postsynaptic cholinergic receptor. ChEIs have been reported to be effective on cognitive performance in both AD and diffuse Lewy body disease (DLBD) as well as on cognitive and behavioural symptoms in PD (Parkinson's Disease) associated dementia (Weber *et al*., 2001; Aarsland *et al*., 2002, 2003; Giladi *et al*., 2003; Pakrasi *et al*., 2003; Leroi *et al*., 2004; Emre *et al*., 2004). Studies also suggest that ChEIs might reduce APP processing and provide some degree of neuroprotection (Francis *et al*., 2005; Mori *et al*., 2006; Sabbagh *et al*., 2006; Nordberg *et al*., 2006).

Three inhibitors of cholinesterase are currently available for treatment of AD, namely galantamine, donepezil, and rivastigmine (**Figure 2.5**). Galantamine and donepezil selectively inhibit AChE, while rivastigmine additionally inhibits butyrylcholinesterase (BuChe) (Rogers *et al*., 1998; Rosler *et al*., 1999; Raskind *et al*., 2000).

Aβ aggregation can be induced by AChE through the direct interaction of its peripheral anionic site (PAS) with fibrils of the peptide (Alvarez *et al*., 1995). Ligands having affinity for both the catalytic site and PAS of AChE would inhibit this process. Antagonism of the M_2 autoreceptors in combination with AChE inhibition, facilitate the release of Ach and prevent ACh breakdown and AChE mediated Aβ fibrils formation (Melchiorre *et al*., 1993; Melchiorre *et al*., 2003). AP 2238 (**Figure 2.21**) is one such compound that illustrated AChE inhibition and suppression of Aβ aggregation (Piazzi *et al*., 2003).

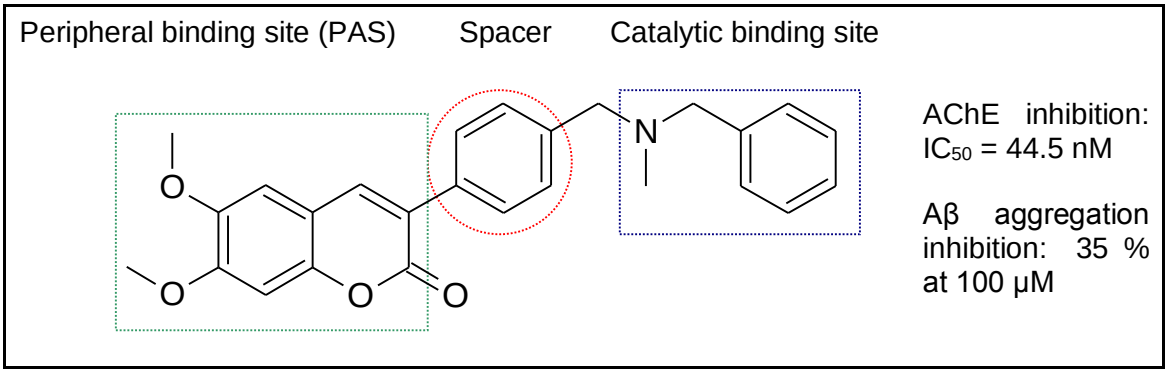

Figure 2.21: Structure of AP 2238 designed to bind both the AChE peripheral catalytic site (green dashed line) and the catalytic binding site (blue dashed line) in order to counteract AChE induced Aβ aggregation as well as increasing ACh concentration (Piazzi *et al*., 2003).

2.2.5.1. Relevance to coumarin.

Index:	R =	
60	Me (AP2238)	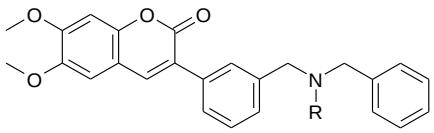
61	Et (AP2243)	
62	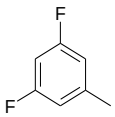	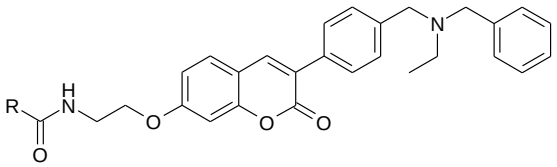 **(62 - 65)**
63	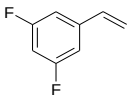	
64	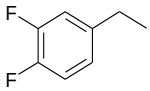	
65	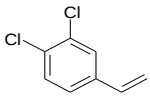	
66	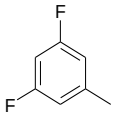	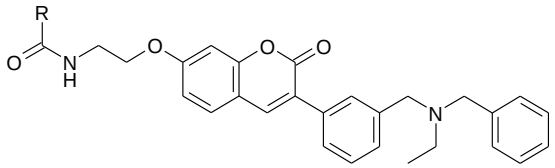 **(66 - 69)**
67	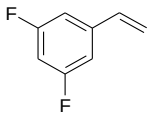	
68	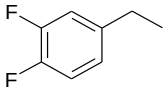	
69	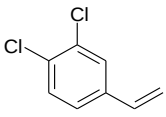	

Figure 2.22: Coumarins with both hAChE and BACE1 inhibitory activities (Piazzi *et al*., 2007).

Due to the multifactorial nature of AD, molecules that modulate the activity of a single protein target are unable to significantly modify the progression of the disease. Following a MTDL

(multi-targeted drug ligand) paradigm, authors reported the first dual AChE/BACE1 inhibitors (Piazzi *et al*., 2007). The designed MTDLs coumarin derivatives (inhibitors of both hAChE and BACE1), with substitution on both the 6 and 7 position of the coumarin moiety (**Figure 2.21**) were synthesised and biologically evaluated. Although 10-fold less potent than compound **61** (Piazzi *et al*., 2007), compounds **62**, **66** and **68** still maintained a fairly good activity. Compound **65** (IC_{50} = 267 µM), with a trans-3,4-dichlorocinnamic substituent revealed a decrease in activity, leading to the conclusion that molecules containing bulky groups are not favourable to penetrate the hAChE gorge to establish proper interactions (as the substituent in that position might detrimentally interact with the surrounding hAChE PAS residues).

All compounds showed activity toward BACE1, while activity does not seemed be influenced either by the position of the substituent on the coumarin nucleus, or by the different electron withdrawing group on the phenyl ring. Compound **63** (IC_{50} = 99 nM) was the most potent inhibitor of the series, while compounds **62, 66** and **68** seemed to be promising hits and are able to inhibit both enzymes with sub-micromolar affinity, an essential characteristic for MTDLs candidates (Piazzi *et al*., 2007).

DCM (dichloromethane) extracts of *Ferulago campestris* roots were used in a bioassay-guided fractionation in the search of AChE inhibitors. Three coumarin derivatives (umbelliprenin, coladonin and coladin), were isolated (**Figure 2.23**) and were shown to inhibit AChE (Dall'Acqua *et al*., 2010). e

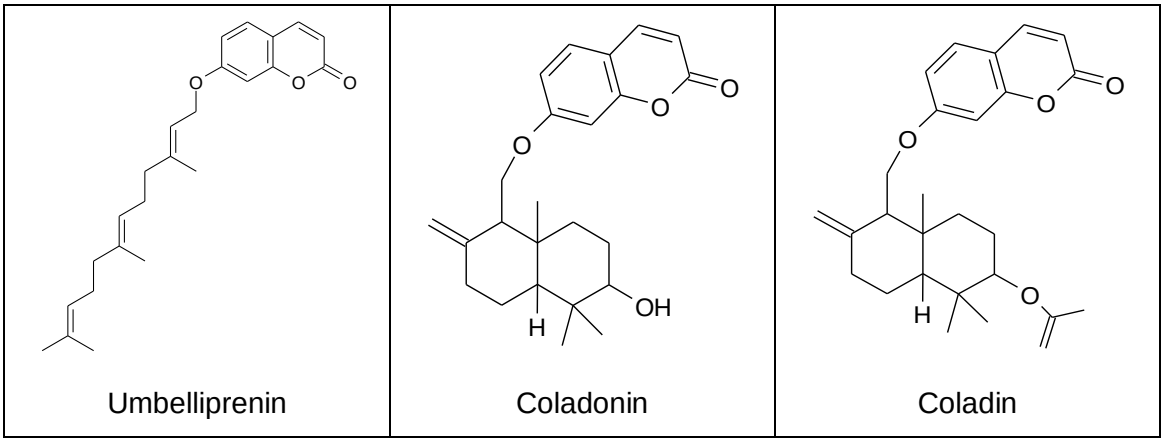

Figure 2.23: Structures of coumarins isolated from *Ferulago campestris* roots (Dall'Acqua *et al*., 2010).

Coumarins have also been isolated from the rhizomes of *Peucedanum ostruthium* (**Figures 2.24** and **2.25**) and that may potentially inhibit AChE (Joa *et al*., 2011).

Index:	R_1 =	R_2 =	
70	H	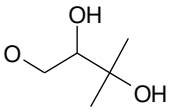	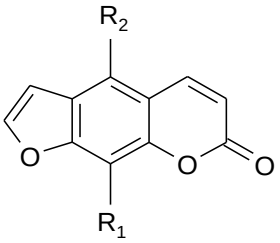 **(70 - 74)**
71	H	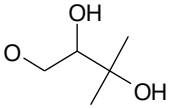	
72	H	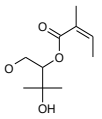	
73	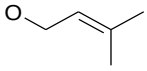	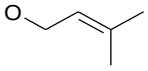	
74	H	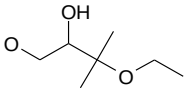	

Figure 2.24: Isolated furanocoumarin from the rhizomes of *Peucedanum ostruthium* (Joa *et al.*, 2011).

Index:	R_1 =	R_2 =	R_3 =	
75	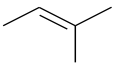	OMe	H	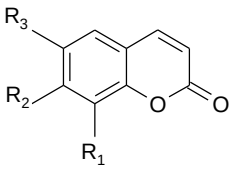 **(75 - 76)**
76	H	OH	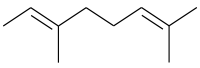	

Figure 2.25: Simple coumarin analogues isolated from the rhizomes of *Peucedanum ostruthium* (Joa *et al*., 2011).

Three similar coumarin derivates (**Figure 2.26**) were isolated from the roots and stem bark of *Clausena pentaphylla* and analysis of their spectral data confirmed their structures as 3, 10-bis (1, 1-dimethyl prop-2-en-1-yl)-5, 6, 7-trihydroxy-8, 8-dimethyl-7, 8-dihydro pyranochromen-2- one, bergapten and xanthotoxin (Intekhab *et al*., 2008).

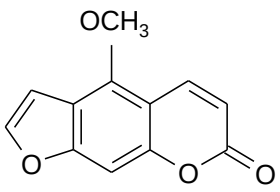	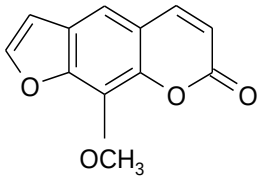	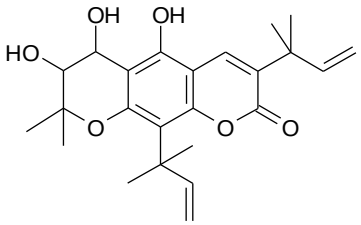
Bergapten	Xanthotoxin	3, 10-bis (1, 1-dimethyl prop-2-en-1-yl) - 5, 6, 7-trihydroxy-8, 8-dimethyl-7, 8-dihydro pyranochromen-2- one

Figure 2.26: Structures of coumarins isolated from the roots and stem bark of *Clausena pentaphylla* (Intekhab *et al*., 2008).

Fallarero and co-workers (2012) tested natural and synthesised coumarins against AChE (**Figures 2.27 - 2.28**).

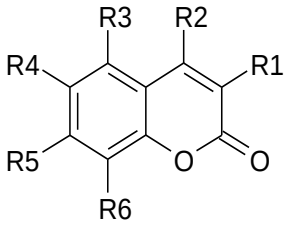

(77 - 98)

Index:	R_1 =	R_2 =	R_3 =	R_4 =	R_5 =	R_6 =
77	H	CH_3	H	H	OH	H
78	H	H	H	OCH_3	OCH_3	H
79	H	H	H	OH	OCH_3	H
80	H	H	H	OCH_3	OH	OH
81	H	H	H	OCH_3	OCH_3	OH
82	H	H	H	H	OH	OH
83	H	H	H	H	OCH_3	OH
84	H	H	H	OCH_3	OH	H
85	H	H	H	H	OH	H
86	H	H	H	CH_3	H	H
87	H	OH	H	H	H	H
88	Acetonylbzl	OH	H	H	H	H
89	H	CH_3	H	OCH_3	H	H
90	H	CH_3	H	H	OCH_3	H
91	H	H	H	H	H	H
92	H	CH_3	OH	H	OH	H
93	H	CH_3	H	OH	OH	H

Figure 2.27: Simple coumarins with AChE inhibitory activity (Fallarero *et al*., 2012).

94	H	CH_3	H	H	OH	OH
95	H	H	H	H	OCH_3	H
96	COOH	H	H	Br	Br	H
97	H	H	H	$C_6H_{12}0_6$	OH	H
98	H	H	H	OH	OH	H

Figure 2.27: Simple coumarins with AChE inhibitory activity - continue (Fallarero *et al*., 2012).

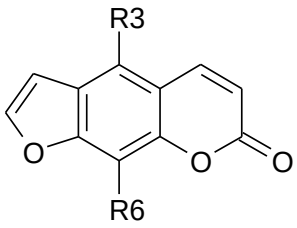

(99 - 100)

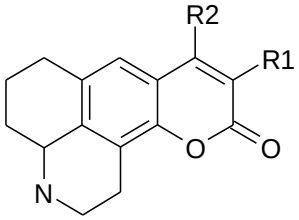

(101 -102)

Index:	R_3 =	R_6 =	Index:	R_1 =	R_2 =
99	OCH3	H	**101**	H	CF3
100	H	OCH3	**102**	H	CH3

Figure 2.28: Fused coumarins anti-AChE activity (Fallarero *et al*., 2012).

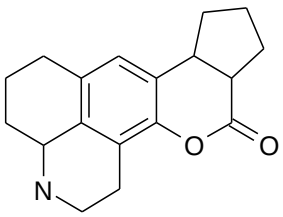

103

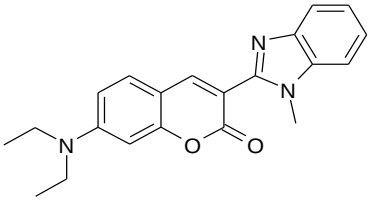

104

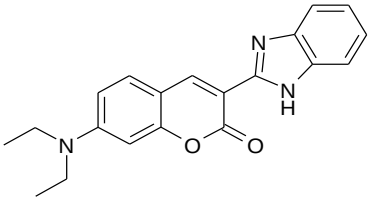

105

Figure 2.29: Coumarins that inhibits AChE (Fallarero *et al*., 2012).

Compound **103** revealed the highest activity (*K*i = 2.36 ± 0.17 µM) and the occurrence of a mixed-type ChE (cholinesterase) inhibition. Activity was also detected in compounds **101**, **102**, **104** and **105** (the only tetracyclic coumarin derivatives present in the library). Compounds **89** and **90** (6 - and 7-methoxy derivatives of the 4-methylated coumarin, respectively) displayed slight AChE inhibition (4.7 % and 4.9 % respectively) while none of the other 4-methylated coumarins substituted with hydroxyl groups in positions 5, 6 or 7 (compounds **92 - 94**) were found active. Compounds **101 - 105** showed a concentration-dependent inhibitory effect. In *silico* studies reveals H-bondi interaction between the carbonyl group of compound **103** and the hydroxyl group of Ser 200, together with π–π stacking interaction between compound **103** and Phe 330. These interactions are proposed to occur as the primary binding to the active site while a secondary interaction within the PAS is possible.

Interaction seems to occur between the carbonyl group of compound **103** and the amide group of Arg 289 (Fallarero *et al*., 2012). Various authors have previously described that some coumarins, particularly those derived from umbelliferone, can act as AChEI and reported IC_{50} values of moderate to low activity, e.g. 29 µM for Umbelliferone (**85**) (Kang *et al*., 2001) and 168 µM for Scopoletin (**84**) (Rollinger *et al*., 2004). To confirm the effect of substituents on the coumarin pharmacophore, Brühlmann and authors (Brühlmann *et al*., 2001), have established that substitutions in position C-7 of the coumarin nucleus by small groups (e.g. hydroxyl, methoxy) revealed IC_{50} values ranging from 28 to100 µM and generally have a lower inhibiting effect when compared to substitutions at C-7 with larger groups (e.g. bzloxy, O–CH_2–C_6H_5) where IC_{50} values ranging from 3.4 to 31 µM were observed (Fallarero *et al*., 2012).

The presence of a cyclised isoprenoid moiety at C-6 favour AChE inhibition for example in the case of the furano or pyranocoumarins *vs.* simple coumarins, without a cyclised unit at C-6 (Kang *et al*., 2001). The inclusion of the furano moiety however does not necessary increase the AChE inhibitory activity in furanocoumarins when compared to simple coumarins, as can be seen from the results obtained in screening with Bergapten (**99**) or Xanthotoxin (**101**) which only displayed inhibitory activity at 30 µM.

IC_{50} values registered for furanocoumarins show moderate to low activity in the micromolar range, e.g. xanthotoxin with IC_{50} ranging from 54 to 580 µM (Kang *et al*., 2001; Miyazawa *et al*., 2004). The inhibitory activity of natural furanocoumarins can be significantly increased when larger substituents in positions 5 or 8 are present (Di Giovanni *et al*. 2008).
These authors reported a high AChE inhibitory activity (IC_{50} = 15.8 and 9.3 µM) in furanocoumarins containing O–CH_2–CH=C–$(CH_3)_2$ substitutions on positions 5 and 8, respectively, instead of OCH_3, as in compound **99** and **100**. The calculated pIC_{50} for compound **103** is in the same range of values determined for other active synthetic coumarins (pIC_{50} = 4.83–4.96 µM) (Di Giovanni *et al*., 2008).

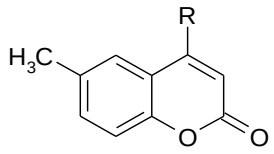 **(106 - 110)**		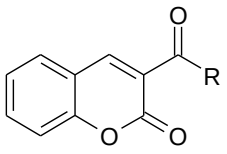 **(111 - 115)**	
Index	R =	Index	R =
106	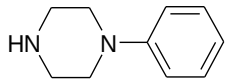	**111**	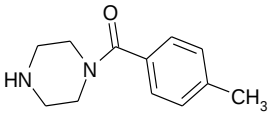
107	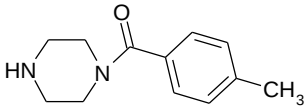	**112**	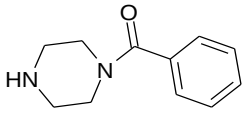
108	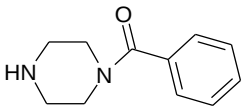	**113**	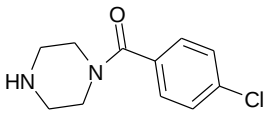
109	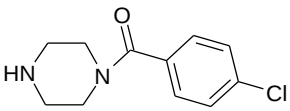	**114**	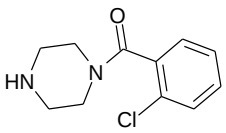
110	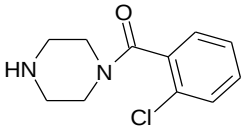	**115**	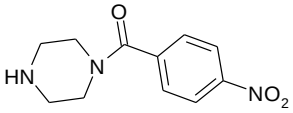

Figure 2.30: Coumarin-derivatives with AChE inhibition (Zhou *et al*., 2008).

Compounds with phenylpiperazine moieties on positions 3 and/or 4 of the coumarin ring revealed better AChE inhibition than that of the 6-substituted coumarins while most of the 6-substituted coumarins did not reveal any inhibition. The 4-phenylpiperazine substituted coumarins **106** and **107** (**Figure 2.30**) showed significant activities with IC_{50} values of 4.5 µmol/L and 5.3 µmol/L, respectively. In agreement with donepezil, (which has two carbons between the carbonyl-carbon atom and piperazine ring) this suggests that the distance between carbonyl-carbon atom and nitrogen atom of piperazine ring is important for the AChE inhibitory activities. Compounds with benzoylpiperazine groups as substitutions, **110 - 115** and **107 - 110** (**Figure 2.30**), revealed some AChE inhibitory activity, which concludes that benzoylpiperazine groups support AChE inhibitory activity.

2.2.6. Carbonic Anhydrase (CA) and Zn^{2+} homeostasis.

The early stages of AD that is characterised by memory abnormalities involves multiple neurotransmitter deficits in the hippocampal formation (Hyman *et al*., 1984). Changes in the synaptic spine as well as dendrite loss during aging significantly decreases brain carbonic

anhydrase (CA) (Meier-Ruge *et al*., 1980) and is more noticeable in AD patients (Meier-Ruge *et al*., 1984).

CA is inactive without zinc (co-factor in its active site), causing it and other zinc-containing proteins to function abnormally in dementia associated with AD and aging. At 1 μm or lower, zinc induces immediate aggregation of the N-terminal fragment of $A\beta_{40}$ (Huang *et al*., 2000), and in AD plaques, Zn^{2+} it's concentrated to ~ 1 mM (Lovell *et al*., 1998; Racchi *et al*., 1999). Aβ binds to zinc and deposits at sites that contain high concentrations of zinc (Racchi *et al*., 1999; Bush *et al*., 1994; Brown *et al*., 1997; Cuajungco *et al*., 2000). The hippocampus contains the highest concentration of Zn^{2+} in the brain, which plays an essential role Aβ formation and might clarify why Aβ deposits are often concentrated in the hippocampus region (Suh *et al*., 2000).

Decreasing Aβ formation reduces behavioural impairment in transgenic mice (Schenk *et al*., 1999; Janus *et al*., 2000; Morgan *et al*., 2000) and copper-zinc chelators solubilise Aβ plaques (Cherny *et al*., 1999) and reduce Aβ accumulation in AD transgenic mice (Cherny *et al*., 2001; Gouras *et al*., 2001).

Two findings suggest that Aβ deposition might produce a functional zinc deficiency. Firstly, in the hippocampal culture neurons, low zinc concentration significantly protect against Aβ toxicity (Lovell *et al*., 1999). Secondly, several groups report that zinc supplements either preserve cognitive functions significantly or slow the cognitive decline in AD patients (Huang *et al*., 2000).

If zinc deficiency does contribute to AD, not only CA but numerous proteins would be affected (McCall *et al*., 2000) and Zn^{2+} supplements, although reported to protect cognition significantly in AD patients (Huang *et al*., 2000), might also controversially destabilise soluble Aβ, thereby worsening cognition. Modulation or attenuation of the zinc-Aβ interaction and protection of zinc-containing proteins still remains an interesting therapeutic strategy.

2.2.6.1. Relevance to coumarin.

A natural derivative of coumarin: 6-(1*S*-hydroxy-3-methylbutyl)-7-methoxy-2*H*-chromen-2-one (**Figure 2.31**), isolated from *Leionemaellipticum*, was proven to possess significant CA inhibitory activity (Vu *et al*., 2009).

For the isomeric 7,8-disubstituted - and 6,7-disubstituted coumarins (**Figure 2.31**), only the first substitution pattern resulted in highly effective CA IX/XII inhibitors, whereas the corresponding isomers (6-7-disubstituted coumarins) were ineffective as CA I,II and XII inhibitors (Maresca *et al*., 2010).

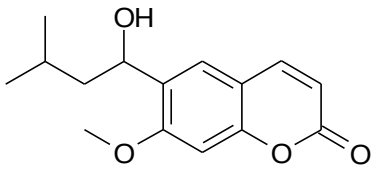

6-(1*S*-hydroxy-3-methylbutyl)-7-methoxy-2*H*-chromen-2-one

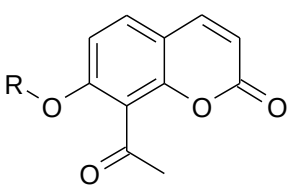

7,8-disubstituted coumarin

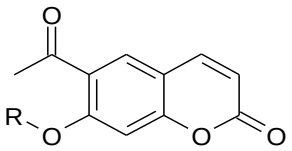

6-7-disubstituted coumarin

Figure 2.31: Structure of 6-(1S-hydroxy-3-methylbutyl)-7-methoxy-2H-chromen-2-one, 7,8-disubstituted coumarin and 6-7-disubstituted coumarin (Maresca *et al*., 2010; Vu *et al*., 2010).

Carta and authors (2012), synthesised a series of coumarins incorporating *tert*-butyl-dimethylsilyloxy - or allyoxy- moieties on positions 4,6 or 7 of the heterocyclic ring and converted it to their corresponding 2-thioxo-coumarins.

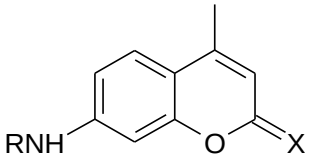

(116 - 119)

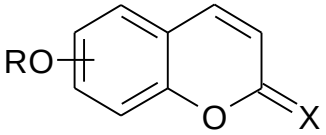

(120 - 137)

Index:	R =	X =	Index:	R =	X =
116	Ac	O	**127**	*t*-Bu(Me_2)Si	S
117	3,5-$Me_2C_6H_3NHCO$	O	**128**	H	S
118	*t*-Bu-OCO	O	**129**	CH_2=CH-CH_2	O
119	H	O	**130**	CH_2=CH-CH_2	O
120	H	O	**131**	CH_2=CH-CH_2	O
121	H	O	**132**	CH_2=CH-CH_2	S
122	H	O	**133**	CH_2=CH-CH_2	S
123	*t*-Bu(Me_2)Si	O	**134**	CH_2=CH-CH_2	S
124	*t*-Bu(Me_2)Si	S	**135**	$OHCH_2CH_2$	O
125	H	S	**136**	Ts-OCH_2CH_2	O
1126	*t*-Bu(Me_2)Si	O	**137**	FCH_2CH_2	O

Figure 2.32: Coumarins with hCA inhibitory activity (Carta *et al*., 2012).

Other derivatives incorporating hydroxyethyloxy-, tosylethoxy- and 2 fluro-ethyloxy-moieties in position 7 were synthesised together with derivatives of 4-methyl-7-amino coumarin incorporating acetamido, 3,5-dimethylphenylureido- and *tert*-butyloxycarbonylamido functionalities (**Figure 2.32**). These compounds were assayed against human carbonic anhydrase (hCA I,II,IX,XII) (Carta *et al*., 2012).

2.2.7. Monoamine oxidase B (MAO-B).

Monoamine oxidase (MAO) is a ~ 60-kDa outer mitochondrial membrane flavin adenine dinucleotide (FAD) co-factor containing the class of enzymes that's located in neuronal, glial and other cells (Bach *et al*., 1988; Hubálek *et al*., 2005). According to substrate and inhibitor specificities, and structural differnces, it exists as two isoforms, namely MAO-A and MAO-B (Grimsby *et al*., 1990).

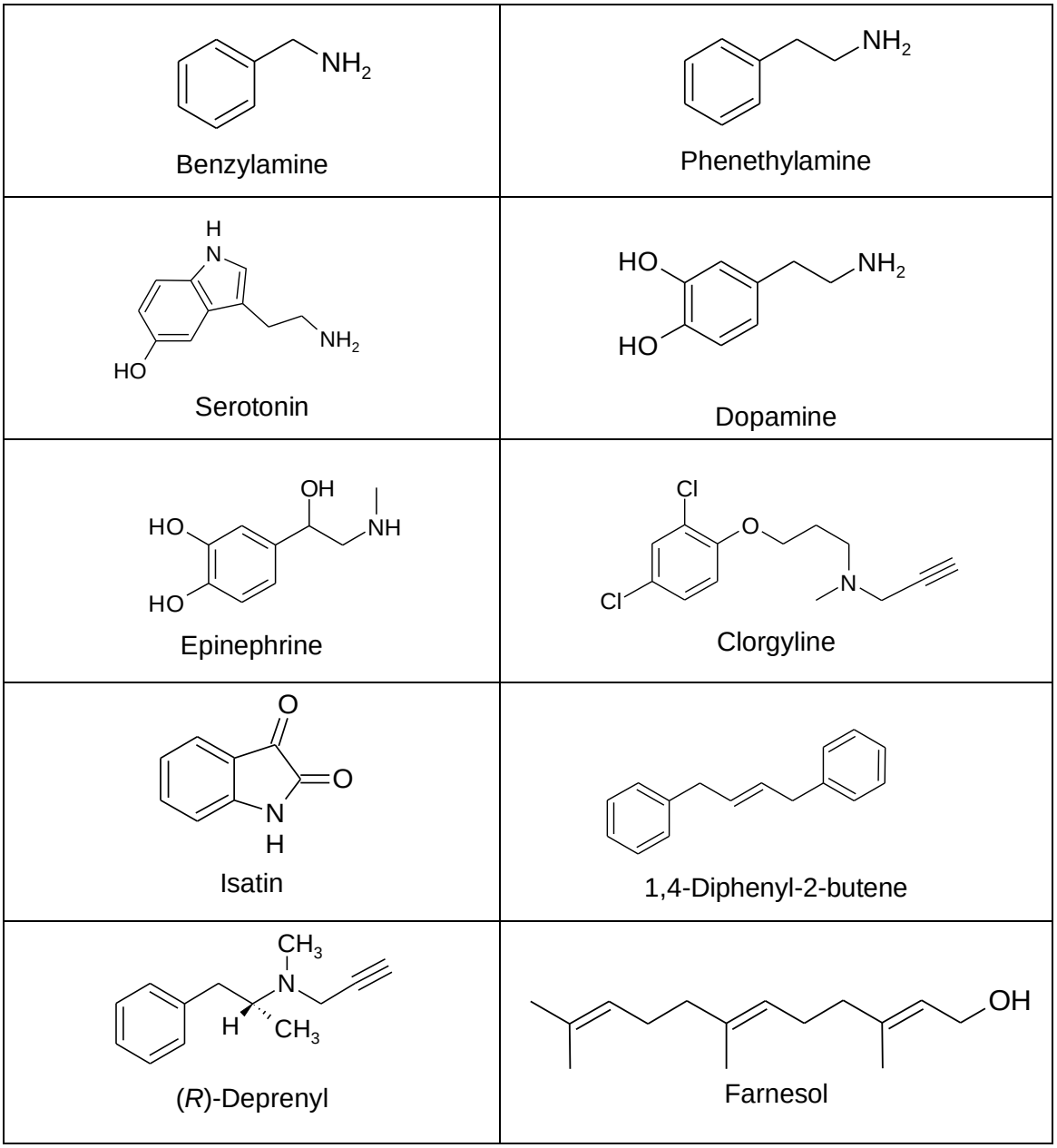

Figure 2.33: Chemical structures of MAO substrates and inhibitors.

MAO-A catalyses the deamination of serotonin (5-HT), norephinephrine and epinephrine (**Figure 2.33**) and inhibition (e.g. by Clorgyline) of this enzyme results in an anti-depressant and anti-anxiety effect. MAO-B catalyses the deamination of Dopamine, ß-phenylethylamine and benzylamine (**Figure 2.33**) and irreversible inhibition (e.g. by (*R*)-Deprenyl) results in anti-

Parkinson's and anti-Alzheimer's effects, thus emphasising its relevance in neuroprotective studies (Ooms *et al*., 2003).

Although MAO-A and MAO-B are different with regards to substrate specifities, they are similar in that both have the same type of covalent flavin (8α-S-cysteinyl FAD) and share a ~ 70 % sequence identity (Edmondson *et al*., 2004). A common characteristic of MAO's not found in other outer membrane mitochondrial proteins is the presence of a C terminal non-cleavable targeting signal sequence which is inserted in the membrane without proteolitic maturation (Binda *et al*., 2004).

MAO-B is a FAD co-factor containing enzyme, consisting of 520 amino acids and is located in the outer mitochondrial membranes of neuronal, glial and other cells. It exists as a dimer in its membrane bound form and the membrane binding site of each monomer faces the membrane surface (**Figure 2.34**) and partly interacts with it (Binda *et al*., 2004). MAO-B constitutes about 80 % of the total MAO activity in the human brain (Riederer *et al*., 1978; Sonsalla *et al*., 1988) and is the predominant form of the enzyme in the striatum (Riederer *et al*., 1989). The crystal structure of human MAO-B at 3 Å reveals that this dimeric enzyme has a C-terminal transmembrane helix protruding from each monomer that anchors it to the membrane (Binda *et al*., 2004).

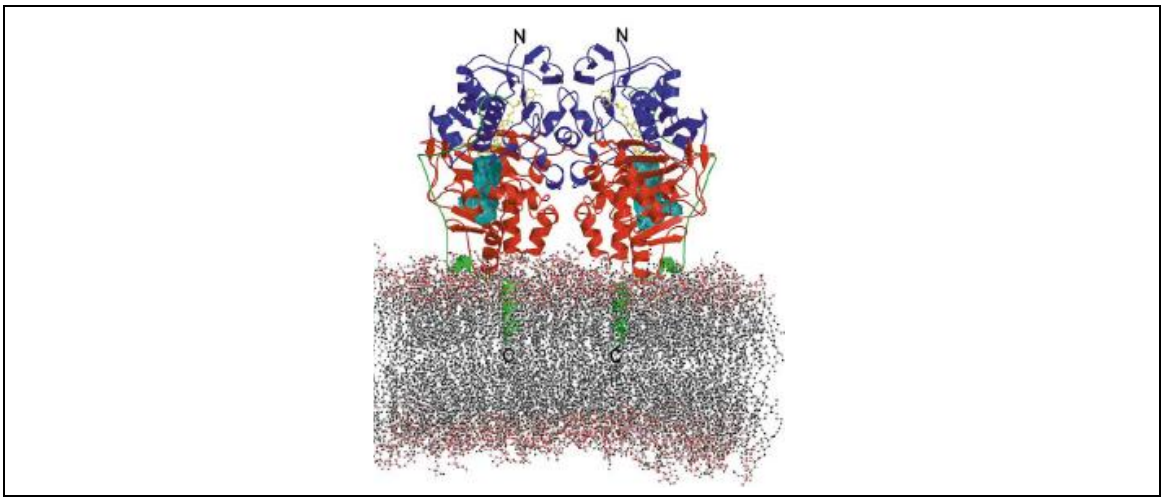

Figure 2.34: Three-dimensional structure of human MAO-B with the dimer bound to the phospholipid bilayer. Each monomer has a two-domain overall topology, consisting of the FAD binding domain in blue and the substrate-binding domain in red. The amino and carboxy termini of each monomer are highlighted as N and C, respectively. The FAD co-factor is represented in yellow ball-and-stick. The C-terminal membrane-binding region is depicted in green. In each monomer the active site cavity is coloured in light blue (Binda *et al*., 2004).

The entrance from the surface to the active site of the enzyme consists of two cavities (**Figures 2.34** and **2.35**) namely the entrance cavity and the substrate cavity (Hubálek *et al*., 2005). The entrance cavity occupies a volume of 290 Å^3 whilst the hydrophobic substrate cavity is larger and a have a volume of 420 Å^3 (Edmonson *et al*., 2004). The combined 700 Å^3 large cavity originates from one side of the protein surface and stretch deep into the protein till it

reaches the FAD co-factor. It is this entity that forms the active site of the enzyme (Binda *et al*., 2004).

The Connolly channel surface in translucent yellow (**Figure 2.35**) illustrates these two distinct cavities inside the binding site; the entrance cavity, which is connected to the outside of the protein, and the substrate cavity, located in the vicinity of the FAD. Ile199 and Tyr326 (**Figure 2.35**; carbon atoms in magenta) separates these two cavities (Novaroli *et al*., 2006).

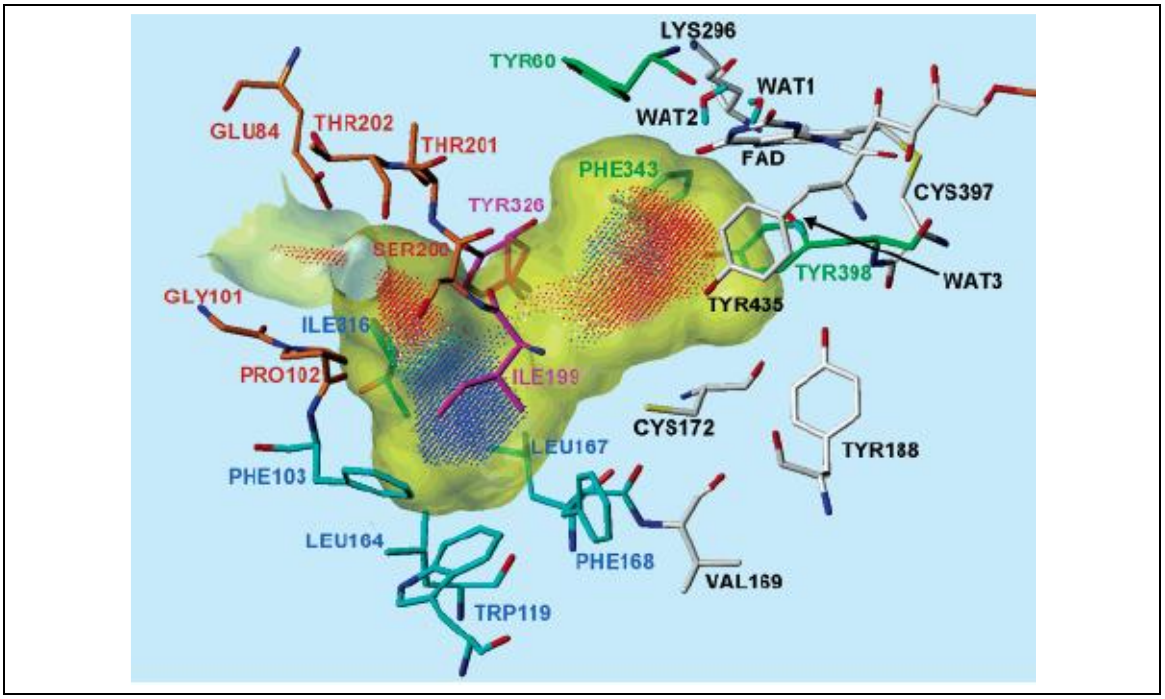

Figure 2.35: Binding site of MAO-B. The Connolly channel surface of the cavities is displayed in translucent yellow. The coloured dots describing the lipophilicity inside the pockets are colour-coded according to their MLP (polar values in red, magenta, orange, and yellow; hydrophobic values in blue, cyan, green-blue and green). The amino acids potentially interacting with the ligands are color-coded following their localisation around the binding site. The FAD co-factor and the three selected water molecules (WATX) are represented as an integral part of the MAO-B structure model (Novaroli *et al*., 2006).

The substrate cavity is mainly polar and is evident by a number of polar side chains (**Figure 2.35**) and accessible H-bonding groups as well as the presence of the flavin nucleus and the three buried water molecules in the vicinity of this cavity. The substrate cavity is also more sterically constrained than the entrance cavity (Novaroli *et al*., 2006). It is shaped like a flat, elongated disc with the longer axis perpendicular to the flavin ring (Edmondson *et al*., 2004). The active site cavity gating loop, residues 99-112, is believed to be partly embedded in the membrane, suggesting that the membrane have a controlling function over this gating loop.

An inhibitor must traverse the entrance cavity in order to gain access to the substrate cavity (**Figure 2.35**). This is true for small molecule inhibitors such as isatin (**Figure 2.33**) that has been shown to bind within the substrate cavity of the enzyme (Binda *et al*., 2003). Larger inhibitors, such as 1,4-diphenyl-2-butene and *trans*, *trans*-farnesol (**Figure 2.33**), appears to exhibit a dual binding mode that involves traversing both the entrance and substrate cavities

(Binda *et al*., 2003). When larger inhibitors occupy the active site, Ile199 is rotated (**Figures 2.35** and **2.36**) out of its normal conformation (Edmondson *et al*., 2004). Ile199 therefore serves as a 'gating switch/guard', separating the two cavities in order to accommodate these larger inhibitors (Hubálek *et al*., 2005).

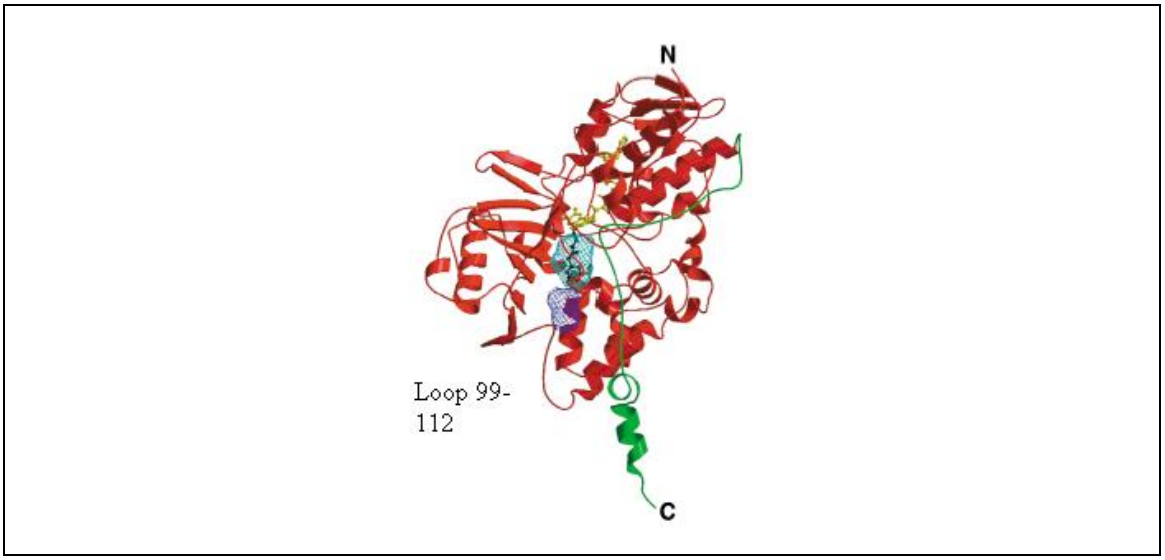

Figure 2.36: The substrate path from the protein surface to the FAD in the MAO-B monomer. Adjacent to the active site cavity (cyan) is the entrance cavity (blue), which is underneath loop 99-112. The FAD is in yellow and the covalent pargyline is in black (Binda *et al*., 2001).

MAO-B oxidises exogenous amines, whereas MAO-A carries out the degradation of bulkier endogenous amine neurotransmitters, such as serotonin (Binda *et al*., 2001). Both enzymes' active site consists of covalent FAD as well as two tyrosines constituting the aromatic cage (Binda *et al*., 2002), thus, revealing the same catalytic mechanism (Edmonson *et al*., 2004). In contrast, the surface area of the active sites opposite to the FAD shows major differences (**Figure 2.37**).

The differences between human MAO-B and MAO-A in respect to substrate cavity residues include Leu171 (MAO-B)/Ile180 (MAO-A), Cys172/Asn181, Ile199/Phe208 and Tyr326/Ile335 (**Table 2.4**). These amino acids are located in the substrate cavity [**Figure 2.37 (A)**] and are in Van der Waals contact with the phenyl ring of Chlorgyline. Three residues (Leu171/Ile199 and Tyr326) separate the substrate cavity from the entrance cavity. Side chain changes affect accommodation of the substrate but seperates these two cavities (Wu *et al*., 1993; Geha *et al*., 2001; Binda *et al*., 2001).

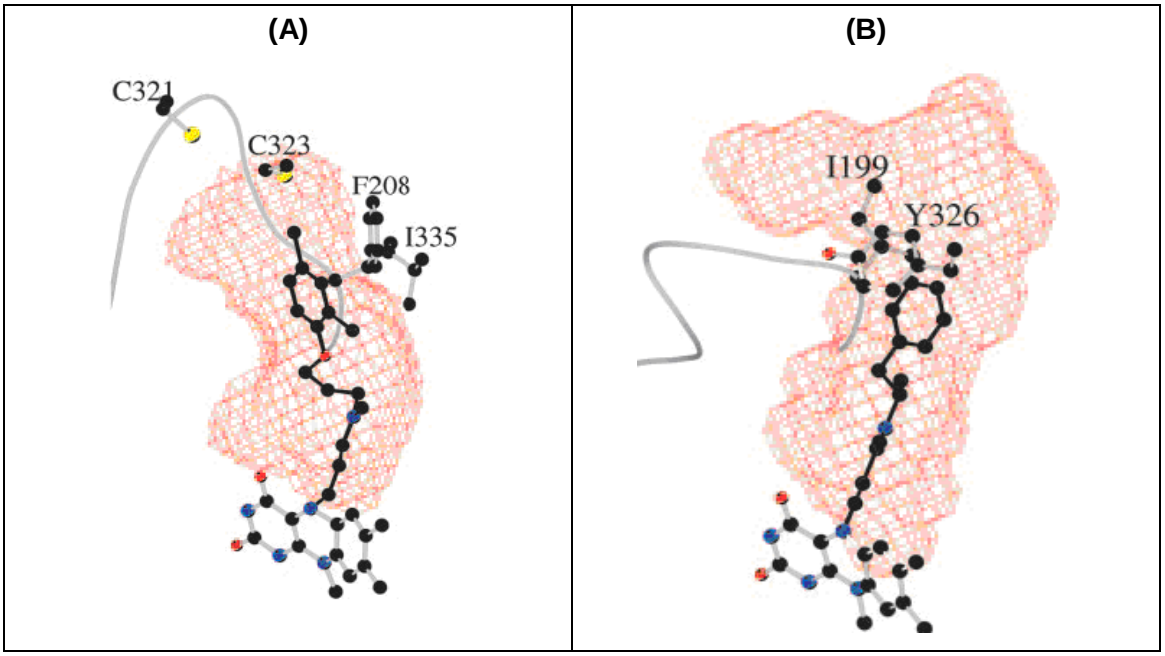

Figure 2.37: The active site cavities in hMAO-A (A) and hMAO-B (B) in complex with clorgyline and (*R*) deprenyl respectively. Active site comparison of hMAO-A and hMAO-B with the crucial Phe208 and Ile335 (A) residues of hMAO-A superimposed to the corresponding Ile199 and Tyr326 (B) residues of hMAO-B (DeColibus *et al*., 2005).

Table 2.4: Comparison of the active site residues in hMAO-A and hMAO-B (deColibus *et al*., 2005).

hMAO A	hMAO B	hMAO A	hMAO B
Tyr-69	Tyr-60	Gln-74	Gln-65
Val-91	Val-82	Val-93	Glu-84
Leu-97	Leu-88	Ile-180	Leu-171
Asn-181	Cys-172	Ile-207	Ile-198
Phe-208	Ile-199	Ser-209	Ser-200
Val-210	Thr-201	Glu-216	Glu-207
Cys-323	Thr-314	Ile-325	Ile-316
Ile-335	Tyr-326	Leu-337	Leu-328
Met-350	Met-341	Phe-352	Phe-343
Tyr-407	Tyr-398	Tyr-444	Tyr-435

The active site cavities of the enzymes (**Figure 2.37**) are thus different with regards to shape and size. hMAO-A's active site consist of a single hydrophobic cavity of ~ 550 Å^3, much shorter in length and wider than that of the longer and narrower ~700 Å^3 hMAO-B site (deColibus *et al*., 2005). hMAO-B substrate entry therefore requires the entrance and substrate cavities fused for certain inhibitors, where hMAO-A lacks this particular characteristic.

Catecholamines, (dopamine in particular), are either metabolised by MAO-B or spontaneously degraded by auto oxidation to yield hydrogen peroxide (H_2O_2) and dopamine–quinones

(Sulzer & Xecca, 2000; Graham *et al*., 1978). The H_2O_2 is fed into the reactive oxygen species (ROS) cycle (**Figure 2.38**) and the dopamine–quinone can modify protein sulfhydryl groups *via* nucleophilic additions. This leads to exacerbation of inflammation and tissue damage (Graham *et al*., 1978; Stokes *et al*., 1999; Tse *et al*., 1976).

Reversibly inhibiting MAO-B increases dopamine levels (reduction of dopamine catabolism) and in turn the generation of ROS (Knoll & Magyar, 1972; Laux *et al*., 1995). The ideal would be to develop safer inhibitors, designed to be reversible while retaining selectivity towards MAO-B and exhibiting a dual mechanism of action (AChE inhibition in this study) for AD neuroprotection.

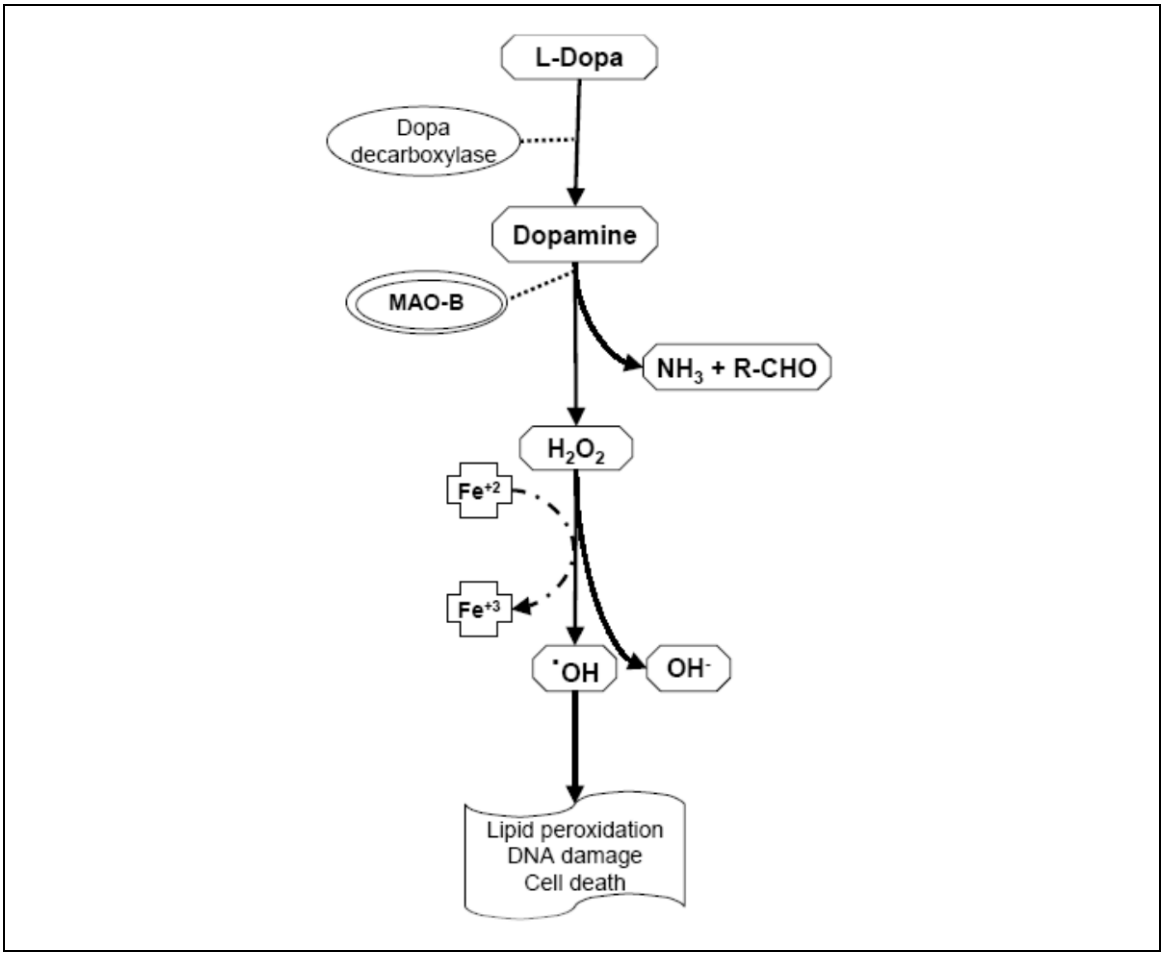

Figure 2.38: MAO-B biochemistry and production of free radicals causing oxidative stress (Riederer *et. al*., 2004).

2.2.7.1. Relevance to coumarin.

A series of 6-substituted: 3-aryl,3-carbonyl, 3-acyl and 3-carboxyhydrazido coumarins (**Figures 2.39** and **2.40**) with several alkyl, hydroxyl, halogen, and alkoxy groups in the two benzene rings were synthesised and evaluated *in vitro* against human monoamine oxidase B (hMAO-B) (Matos *et al*., 2011; Secci *et al*., 2011).

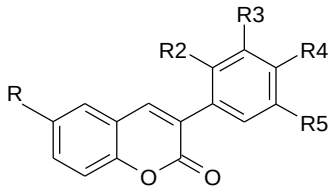

(138 - 159)

Index:	R =	R_2 =	R_3 =	R_4 =	R_5 =
138	OCH_3	H	CH_3	H	H
139	OCH_3	H	H	CH_3	H
140	OH	H	H	CH_3	H
141	$C_3H_5O_2$	H	H	CH_3	H
142	C_5H_9O	H	H	CH_3	H
143	CH_3	H	H	H	H
144	CH_3	H	H	CH_3	H
145	CH_3	H	CH_3	H	H
146	CH_3	H	H	OCH_3	H
147	CH_3	H	OCH_3	H	H
148	CH_3	OCH_3	H	H	H
149	CH_3	H	OCH_3	H	OCH_3
150	CH_3	H	OCH_3	OCH_3	H
151	CH_3	H	OCH_3	OCH_3	OCH_3
152	CH_3	H	Br	OCH_3	H
153	CH_3	H	OCH_3	Br	H
154	CH_3	Br	OCH_3	H	OCH_3
155	CH_3	Br	OCH_3	OCH_3	OCH_3
156	CH_3	H	H	OH	H
157	CH_3	H	OH	H	H
158	CH_3	OH	H	H	H
159	CH_3	H	$C_3H_5O_2$	H	H

Figure 2.39: Structure of 6-substituted-3-arylcoumarin derivatives (Matos *et al*., 2011).

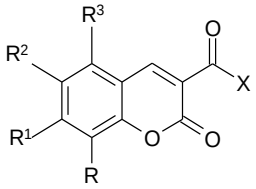

(160 - 217)

Index:	X =	R =	R_1 =	R_2 =	R_3 =
160	CH_3	H	H	H	H
161	CH_3	OH	H	H	H
162	CH_3	H	OH	H	H
163	CH_3	H	H	OH	H
164	CH_3	H	OCH_3	H	H
165	CH_3	H	$N(Et)_2$	H	H
166	CH_3	H	H	CH_3	H
167	CH_3	H	H	Cl	H
168	CH_3	H	H	Br	H
169	CH_3	H	H	-CH=CH-CH=CH-	H
170	CH_3	Br	H	Cl	H
171	CH_3	Br	H	Br	H
172	CH_3	I	H	I	H
173	Ph	H	H	H	H
174	Ph	OH	H	H	H
175	Ph	H	OH	H	H
176	Ph	H	H	OH	H
177	Ph	H	OCH_3	H	H
178	Ph	H	$N(Et)_2$	H	H
179	Ph	H	H	CH_3	H
180	Ph	H	H	Cl	H
181	Ph	H	H	Br	H
182	Ph	H	H	-CH=CH-CH=CH-	H
183	Ph	Br	H	Cl	H
184	Ph	Br	H	Br	H
185	Ph	I	H	I	H
186	OEt	OH	H	H	H
187	OEt	H	OH	H	H
188	OEt	H	H	OH	H

Figure 2.40: Structures of 3-carbonyl, 3-acyl, and 3-carboxyhydrazido coumarin conjugates inhibiting hMAO-B (Secci *et al*., 2011).

189	OEt	H	OCH_3	H	H
190	OEt	H	H	OCH_3	H
191	OEt	H	$N(Et)_2$	H	H
192	OEt	Br	H	Cl	H
193	OEt	Br	H	Br	H
194	OEt	I	H	I	H
195	OEt	H	OCH_2(3-Cl-Ph)	H	H
196	OEt	H	OCH_2(4-t-butil-Ph)	H	H
197	OEt	H	OCH_2(3,4-Cl-Ph)	H	H
198	OEt	H	O-cyclophenyl	H	H
199	OEt	H	H	H	H
200	OH	OH	H	H	H
201	OH	H	OCH_3	OH	H
202	OH	H	H	H	H
203	OH	H	$N(Et)_2$	OCH_3	H
204	OH	H	H	H	H
205	OH	Br	H	Cl	H
206	OH	Br	H	Br	H
207	OH	I	OCH_2(3-Cl-Ph)	I	H
208	OH	H	OCH_2(4-t-butil-Ph)	H	H
209	OH	H	OCH_2(3,4-Cl-Ph)	H	H
210	OH	H	O-cyclophenyl	H	H
211	OH	H	H	H	H
212	$NHNH_2$	H	H	H	H
213	NHNH-Ph	H	H	H	H
214	NHNH-(2-NO_2-Ph)	H	H	H	H
215	NHNH-(4-CH_3-Ph)	H	H	H	H
216	NHNH-(4-Cl-Ph)	H	H	H	H
217	NHNH-(2,4-NO_2-Ph)	H	H	H	H

Figure 2.40: Structures of 3-carbonyl, 3-acyl, and 3-carboxyhydrazido coumarin conjugates inhibiting hMAO-B - continue (Secci *et al*., 2011)

Compounds **160 - 172** (3-methylketone coumarin derivatives) revealed an increase in both inhibitory activity and selectivity towards hMAO-B compared to their corresponding arylketones (**173 - 185**). The presence of hydroxyl groups at position R, R_1, or R_2 (**161 - 163**) slightly reduced activity compared to OCH_3 and $N(Et)_2$ at position R_1 (**164** and **165**). Hydroxyl groups at R_2 resulted in poor inhibition of both MAO-A and MAO-B, while a fused ring at R_2-

R_3 (**169**) increased the activity. Dihalo-substitution (compounds **170** and **171**), displayed the best IC_{50} values in the nanomolar range. Substitution with an arylketone (compounds **173 - 185**) limited the biological activity, probably due to the steric hindrance of the aromatic ring. On the contrary, a COOEt moiety at C3 position (compounds **186 - 199**), improved the inhibitory activity and selectivity towards hMAO-B, especially with the presence of a bzloxy group (compounds **195 - 197**), e.g. compounds **195** (IC_{50} hMAO-B = 7.01 ± 0.21 nM; Ratio > 14,265) and **197**, bearing two chlorine atoms on the aryl ring (IC_{50} hMAO-B = 9.47 ± 0.39 nM; ratio >10,560). Both the selectivity and hMAO-B inhibition was decreased with the hydrolysis of ethyl esters to their corresponding carboxylic acids, except for compound **210** (R_1 **=** 3',4'-dichloro-bzleoxy group), which is still active in the nanomolar range. Compounds that contain a hydrazido moiety (**213 - 217**) revealed promising results in terms of inhibitory activity and selectivity towards hMAO-B (Secci *et al*., 2011).

3-Aryl4-hydroxycoumarin substituted derivatives with methoxy and/or substituents introduced in the 3-phenyl ring, with position 6 in the coumarin moiety unsubstituted or substituted with a methyl/chloro moiety (**Figure 2.41**) were synthesised and evaluated for MAO-B inhibitory activity. The presence of a methyl group slighty improved activity (**218** *vs*. **219**), whereas a chloro atom as a substituent (**220** and **221**) considerably improves both MAO-B inhibition and selectivity (Serra *et al*., 2012).

Index:	R_1 =	R_2 =	R_3 =	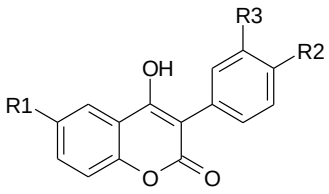 **(218 - 221)**
218	H	OMe	H	
219	Me	OMe	H	
220	H	OMe	Cl	
221	Cl	OMe	Cl	

Figure 2.41: Structures of 3-aryl-4-hydroxycoumarin derivatives inhibiting hMAO-B (Serra *et al*., 2012).

2.2.8. Nitric Oxide Synthase (NOS).

Nitric oxide synthase (NOS) catalyses the conversion of L-arginine to yield L-citrulline and nitric oxide (NO) (Knowles *et al*., 1994). Co-factors involved are NADPH, FMN and tetrahydrobiopterin (BH4) (Knowles *et al*., 1994). Three isoforms of NOS exist (named by the tissue they were first cloned from) namely: neuronal NOS (nNOS/NOS1); inducible NOS (iNOS/NOS2) and endothelial NOS (eNOS/NOS2) (Knowles *et al*., 1994). *Via* a Ca^{2+} dependent manner in neurons, nNOS are activated to produce NO (Knowles *et al*., 1994), while in a Ca^{2+}-independent manner, NOS in glial cells (iNOS) produce NO (Bolaiños *et al*., 1994).

Total and serum NO levels were found to be elevated in AD patients compared to controls (Vural *et al*., 2009). In addition, an increase in leukocyte NOS activity in AD patients were also observed (De Servi *et al*., 1999). Excessive NO production (Klinge *et al*., 2008) together with upregulated expression of iNOS (Wang *et al*., 2004) was also noted in AD patients.
eNOS gene expression and eNOS protein phosphorylation are stimulated through resveratol leading to a neuroprotective, vasorelaxent effect (Klinge *et al*., 2008; Li *et al*., 2009). Additionally, resveratol demonstrated to suppress iNOS activity (through inhibiting NF-kβ), thus protect neurons from Aβ-induced neurotoxicity (Chen *et al*., 2005). As mentioned, chronic inflammatory and oxidative stress processes are present in AD patients (Galimberti *et al*., 2011). The toxicity of $A\beta_{32}$, the toxic domain of $A\beta_{42}$ (Maurice *et al*., 1996; Delobbette *et al*., 1997), could be due to NO production *via* iNOS that consequently produce spatial memory deficits (Diaz *et al*., 2011).

The liberation of NO through the stimulation of the iNOS cascade, together with the the synthesis of pro-inflammatory cytokines (eg. IL-1β and TNF-α) was shown to play a crucial role in Aβ35 cell death and spatial memory neurotoxity and accelerated cell death (Akama *et al*., 1998; Diaz *et al*., 2012).

Thus, it would be functional to inhibit the iNOS blockade which may subsequently prevent:

1. $A\beta_{32}$ nitrosative stress and an inflammatory response, and
2. Neurodegeneration coupled with cognitive decline.

2.2.8.1. Relevance to coumarin.

Various coumarins have been reported to inhibit NO production (Motai *et al*., 2004; Kontogiorgis *et al*., 2006). Further studies revealed some plant derived coumarins to inhibit the activation of NF-κB (Pande *et al*., 2005), which is known to bind to the promoter region of iNOS gene and plays a pivotal role in LPS mediated iNOS expression in macrophages and other cells. Various 7-methoxycoumarins have also been reported to inhibit the iNOS–NO pathway (Nakamura *et al*., 2009).

The Sesquiterpene coumarin derivatives, fukanemarin B, fukanefuromarin E, fukanefuromarin F and fukanefuromarin G (**Figure 2.42**) was isolated from the roots of *Ferula fukanensis* and exhibited NO production inhibition and iNOS gene expression (Motai *et al*., 2010).

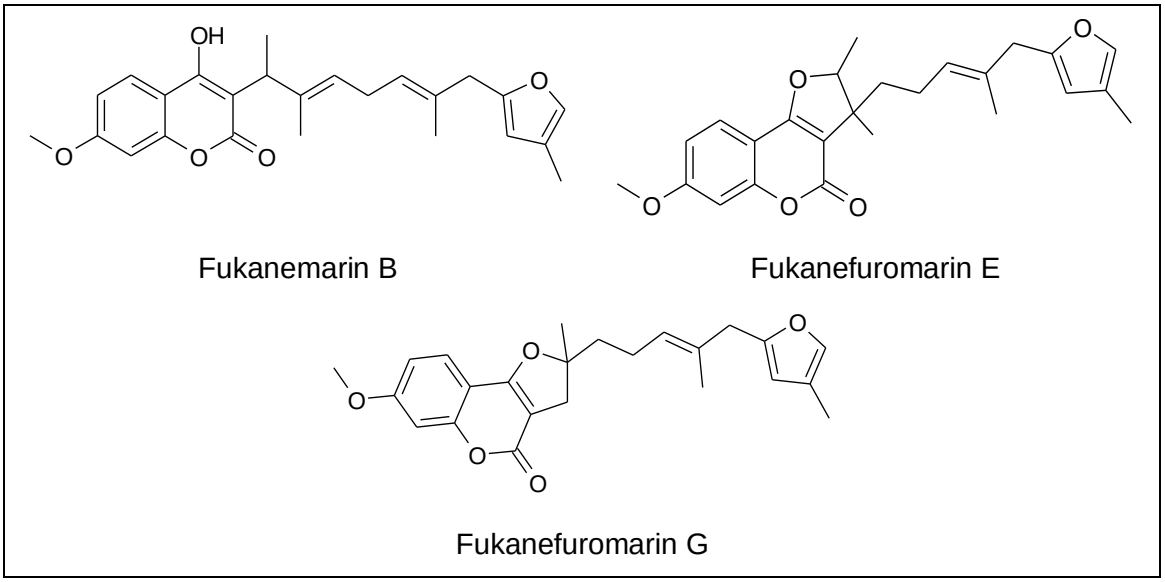

Figure 2.42: Structure of sesquiterpene coumarin derivatives (Motai *et al*., 2010).

7-Hydroxycoumarin derivatives (**Figure 2.43**) were investigated for their anti-inflammatory effects on the expression of inflammatory enzymes iNOS and COX-2 (Timonen *et al*., 2011).

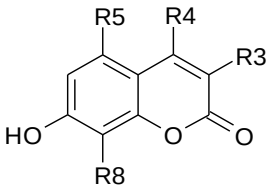

(222 - 229)

Index:	R_3=	R_4=	R_5=	R_8=
222	Et	Me	H	Me
223	H	Pr	Me	H
224	Me	Me	H	OMe
225	F	Me	H	OMe
226	H	Pr	H	OMe
227	H	Ph	H	H
228	H	2-F C_6H_4	H	H
229	H	Ph	H	OMe

Figure 2.43: 7-hydroxycoumarin derivatives endowed with NOS inhibitory activity (Timonen *et al*., 2011).

All three compounds containing a phenyl ring at position 4 were highly active in inhibiting NO production and iNOS expression. Only compound **225** (7-hydroxy-8-methoxy-3,4-dimethylcoumarin) lacked high iNOS, NO and IL-6 inhibition activity. 3-Alkyl substitution is a requirement as indicated by high activities (Timonen *et al*., 2011).

At 100 µM concentrations, compounds **222**, **226 - 229** significantly inhibited LPS-induced NO production by more than 80 % as compared to cells treated with LPS alone, while compounds

226 - 228, also inhibited LPS-induced NO production by more than 50 % at 10 µM. Compounds **223**, **225**, **227 - 229** inhibited iNOS protein expression by more than 80 % at 100 µM concentration and compounds **227 - 229** inhibited iNOS expression by more than 45 % at a 10 µM concentration (Timinonen *et al*., 2011).

2.2.9. Histone acetyltransferase (HAT) and Histone deacetylase (HDAC).

Histone acetyltransferase (HATs) catalyses the acetylation of lysine residues of histone proteins, relaxing chromatin structure and promotes gene transcription (Berger, 2007; Jenuwein *et al*., 2001; Kouzarides, 2007). This post-translational modification is reversed by histone deacetylases (HDACs) (Levenson *et al*., 2004) and reducing the levels of histone acetylation by preventing HAT activity promotes amnesia and interferes with the association of hippocampus-dependent memories (Alarcon *et al*., 2004; Korzus *et al*., 2004; Wood *et al*., 2006). Inhibiting HDACs, will increase the acetylation and gene transcription and consequently enhance hippocampus-dependent memory formation (Guan *et al*., 2009; Levenson *et al*., 2004; Vecsey *et al*., 2007; Wood *et al*., 2006). Inhibitors of histone deacetylases (HDACi's) revealed to repair cognitive function in an inducible model of neurodegeneration (Fischer *et al*., 2007).

2.2.9.1. Relevance to coumarin.

Huang and co-workers synthesised and evaluated coumarin based compounds (**Figure 2.44**) against histone deacetylase. All compounds (230 – 233) revealed relative HDAC inhibitory activity, with 232 as the most potent compound (Huang *et al*., 2011).

Index:	n =	
230	4	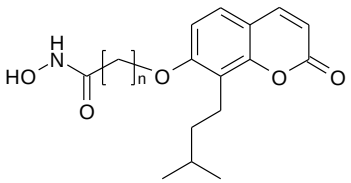 **(230 - 233)**
231	5	
232	6	
233	7	

Figure 2.44: Coumarin compounds with activity against HDAC (Huang *et al*., 2011).

2.2.10. Oxidative stress.

There's evidence of the presence of oxidative stress in both AD and amyloid-bearing transgenic mice (Smith *et al*., 1996; Smith *et al*., 1998). The neurotoxicity of Aβ has been linked to H_2O_2 liberation in cell cultures by a mechanism that is likely to be ascribed to Aβ coordinating redox active metal ions (Barnham *et al*., 2004).

Spectrophotometry revealed that the Aβ reduced Fe^{3+} to Fe^{2+} and Cu^{2+} to Cu^{+} while molecular oxygen was then trapped by Aβ and reduced to H_2O_2 (Huang *et al*., 1999; Huang *et al*., 1999). In the presence of Cu^{2+} or Fe^{3+}, Aβ produced a thiobarbituric-reactive substance that in turn generates the hydroxyl radical. Tabner (2002), used spin-trapping to identify the radical produced by Aβ in the presence of Fe^{2+}, concluding that it was OH (Tabner *et al*., 2002).

Free radicals include ROS [e.g. superoxide (O^{2-}), hydroxyl radicals (OH^{-}), peroxyl radicals (ROO^{-}) and hydrogen peroxide (H_2O_2)], and reactive nitrogen species (RNS) [e.g. nitric oxide (NO) and peroxynitrite ($ONOO^{-}$)]. Reactive chlorine species (RCS), such as hypochlorous acid (**Figure 2.38**) can also be included (Wallace, 1999; Vertuani *et al*., 2004; Ischiropoulos & Beckman 2003; Klebanoff *et al*., 2005).

2.2.10.1. Relevance to coumarin.

Index:	R =	R' =	R_1 =	R_2 =	R_3 =
234	H	H	H	OCH_3	OCH_3
235	CH_3	Cl	H	OCH_3	OCH_3
236	CH_3	H	H	OCH_3	OCH_3
237	CH_3	H	H	H	OCH_3
238	CH_3	H	H	H	NO_2
239	CH_3	H	H	H	OH
240	CH_3	H	H	H	Br
241	CH_3	H	H	H	H
242	CH_3	H	Br	H	H
243	CH_3	Br	H	OCH_3	OCH_3
244	H	H	H	OH	OH
245	CH_3	Cl	H	OH	OH

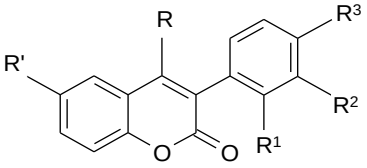

(234 - 245)

Figure 2.45: 3-Aryl coumarins with antioxidant and lipoxygenase inhibitory activity (Roussaki *et al*., 2010).

A series of coumarin derivatives substituted with a phenyl ring on position 3 were synthesised (**Figure 2.45**) and *in vitro* antioxidant activity was evaluated using two different antioxidant assays namely radical scavenging ability *via* di-(phenyl)-2,4,6-trinitrophenyl) iminoazanium (DPPH) stable free radical and inhibition of lipid peroxidation induced by the thermal free radical 2,2'-azobis(2-amidinopropane)dihydrochloride (AAPH)]. Moreover, the compounds' ability to inhibit soybean lipoxygenase was determined as an indication of potential anti-inflammatory activity (Roussaki *et al*., 2010).

The antioxidant activity of the coumarin derivatives xanthotoxol and methyl substituted xanthol (**Figure 2.46**) has also been reported (Xiao *et al*., 2010).

Index:		R_1 =	R_2 =	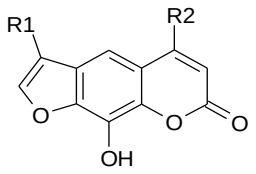
246	Xanthotoxol	H	H	
247	8-hydroxy-4methylsporan	H	CH_3	
248	8-hydroxy-4,9-dimethylsporan	CH_3	CH_3	

Figure 2.46: Xanthotoxol and methyl substituted xanthotoxol conjugates (Xiao *et al*., 2010).

Apart from similar biological activities as coumarins, 4-methylated coumarins are known to be less toxic and have been studied as novel antioxidants (Natella *et al*., 2010; Pandaey *et al*., 2007; Tyagi *et al*., 2005; Yu *et al*., 1999; Raj *et al*., 1998). A series of 4-methylated coumarin derivatives containing the 4, 5-dihydropyrazole moiety (**Figure 2.47**) were examined for their antioxidant activities (Xiao *et al*., 2012).

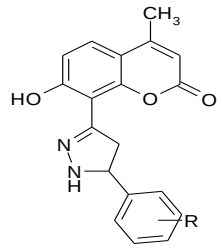

(249 - 250)

Index:	R =
249	3-nitro
250	3-methoxy-4-hydroxy

Index:	R =
251	3-nitro
252	3-methoxy-4-hydroxy
253	3,4-dihydroxy
254	2,4-dihydroxy
255	2-hydroxy

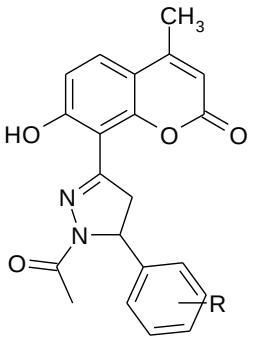

(251 - 255)

Figure 2.47: Structures of 4-methylated coumarin derivatives containing 4,5-dihydropyrazole moiety (Xiao *et al*., 2012).

Novel 4-hydroxy-bis-coumarins (**Figure 2.48**) were synthesised and evaluated as antioxidants. It was discovered that substitution in the aromatic nucleus of the 4-hydroxy-biscoumarins contributed to antioxidant activity (Kancheva *et al*., 2010).

Index:	R_1 =	R_2 =	R_3 =	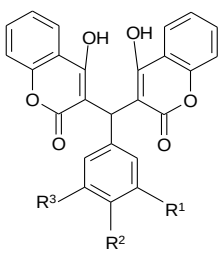
256	OH	OH	H	
257	OCH_3	OCH_3	H	
258	OCH_3	OH	OCH_3	
259	OCH_3	OCH_3	OCH_3	
260	OCH_3	OH	N_2O	

(256 - 260)

Figure 2.48: 4-Hydroxy bis-coumarins as radical scavengers and antioxidants (Kancheva *et al*., 2010).

Derivatives of 4-Schiff base-7-bzloxy-coumarins (**Figure 2.49**) were synthesised based on the 7-bzloxy-coumarin structure as novel antioxidants (Zhang *et al*., 2011).

In vitro antioxidant results revealed that 2,2-diphenyl-1-picrylhydrazyl (DPPH) radical scavenging activities of some compounds' antioxidant activity are superior to that of ascorbic acid, therefore making 4-Schiff base-7-bzloxy-coumarin derivatives efficient as antioxidants (Zhang *et al*., 2011).

Index:	R_1 =	R_2 =
261	H	NH_2
262	OCH_2Ph	NH_2
263	H	C_6H_5NH
264	OCH_2Ph	C_6H_5NH
265	H	*p*-NO_2-C_6H_4NH
266	OCH_2Ph	*p*-NO_2-C_6H_4NH
267	H	*o*-NO_2-*p*-NO_2-C_6H_3NH
268	H	*o*-NH_2-C_6H_4
269	OCH_2Ph	*o*-NH_2-C_6H_4
270	H	*p*-OH- C_6H_4
271	OCH_2Ph	*p*-OH- C_6H_4
272	H	*o*-OH- C_6H_4
273	OCH_2Ph	*o*-OH- C_6H_4
274	H	OH
275	OCH_2Ph	OH

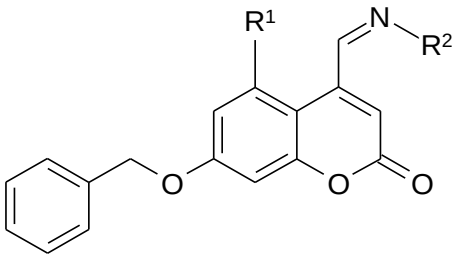

(261 - 275)

Figure 2.49: Novel 4-Schiff base-7-bzloxy-coumarin derivatives as antioxidant (*Zhang et al*., 2011).

2.3. TAU.

The purpose of tau is to bind to, stabilise, and promote the polymerisation of microtubules (MTs), the support structure that allows the flow of nutrients through the neurons (Cleveland *et al*., 1997; Weingarten *et al*., 1975). However, during the pathogenic cascade that leads to tauopathy, tau detaches from these MTs, becomes hyperphosphorylated and aggregates in filaments that eventually accumulate and bundles into the large somatodendritic neurofibrillarly tangles that represent the histological hallmarks of this group of diseases, also known as tauopathies. Neurofibrillary tangles (NFTs) are thus the damaged remains of these nerve cell MTs. It's assumed that this change in properties leads to two major consequences, the destabilisation of transport tracks and the pathological aggregation of tau in the cytosol (Braak *et al*., 1991). This is due to its anomalous aggregation in the form of AD neurofibrillary

tangles and neurophil threads which consists of filaments of polymerised tau protein named paired helical filaments (PHFs) and a minority of straight filaments (Crowther *et al*., 2000).

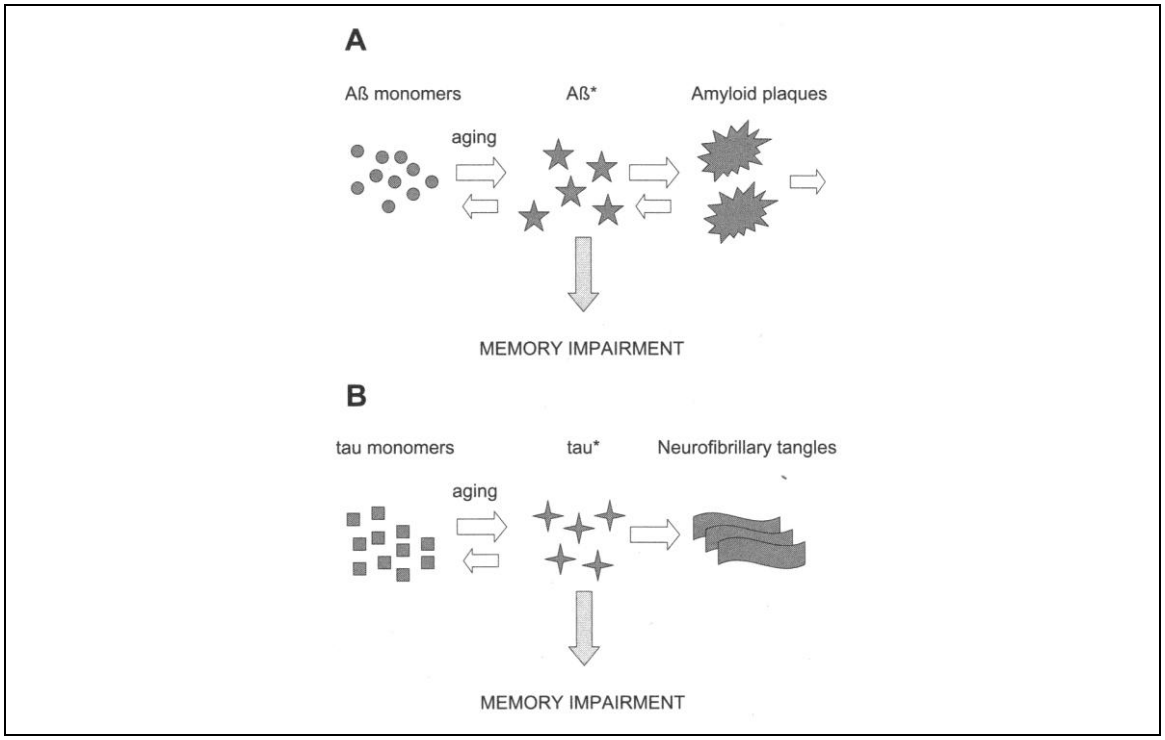

Figure 2.50: The Aβ and tau hypotheses of memory impairment in AD. Models summarising the relationship between memory impairment and Aβ in plaque-forming APP transgenic mice and tangle-forming transgenic mice. (**A**) The hypothetical amyloid cascade involves the conversion of monomeric Aβ (Circles) to Aβ*, which are as yet unidentified soluble Aβ assemblies in the brain that disrupt cognitive function independently of amyloidosis or neurodegeneration. There may be a dynamic equilibrium between Aβ*, Aβ monomers and amyloid plaques. Amyloid plaques have not been shown to induce cognitive dysfunction directly and may be cleared by cells and molecules involved in the inflammatory system. (**B**) The hypothetical NFTs cascade entails the conversion of monomeric tau (squares) to tau*, which are as yet unidentified tau species in the brain that disrupt cognitive function independently of tangle formation or neurodegeneration. NTs contain a form of tau that appears to be a stable protein fate, as it accumulates even when tau protein production is greatly reduced. NFTs do not appear to impair memory function (Adapted from Sisodia, 2007).

This anomalous tau is highly phosphorylated, is redistributed into the “incorrect” compartment (from axonal to somatodendritic), and it is in part truncated by caspases and other proteases (**Figure 2.50**). Tau phosphorylation is a normal physiological process which decreases tau’s binding affinity for MTs and regulates MTs polymerisation (Biernat *et al*., 1993; Bramblett *et al*., 1993; Drechsel *et al*., 1992; Yoshiba *et al*., 1993). Thus phosphorylation sites can be sub-divided into two groups according to the manner in which residues are phosphorylated: proline-directed kinases and non-prolinedirected kinases (Billlingsley *et al*., 1997; Buee *et al*., 2000). Tau serves as the substrate for several kinases *in vivo* and *in vitro* while a large number of kinases have been reported to be associated with NFTs in AD brains (Buee *et al*., 2001).

In cultured neurons and in normal animal brain, the two major kinases involved in abnormal tau phosphorylation is GSK-3 specifically GSK3-β and cdk5 (Planel *et al*., 2002; Maccioni *et al*., 2001).

Schachter and authors (2007), evaluated the relative roles of cdk5 and GSK3β in regulating the phosphorylation of tau at various sites in cellular and neuronal systems and concluded that GSK-3 plays more dominant role than cdk5 in the regulation of tau phosphorylation (refer to **section 2.2.4.1**). The imbalance of the kinases and phosphatases that regulate tau phosphorylation is evident in the lithium-induced inhibition of GSK-3 and resulting reduction in phosphorylation, aggregation of tau and tauopathy, and thus neurodegeneration (Noble *et al*., 2005).

Lithium has been illustrated to reduce hyperphosphorylation of tau proteins *via* inhibiting GSK-3β in both cell culture (Lovestone *et al*., 1999) and in transgenic mice (Noble *et al*., 2005). Through its inhibitory actions on GSK-3α, lithium additionally prevents Aβ plaque accumulation in the brains of mice that overproduce APP (Phiel *et al*., 2003) thus providing beneficial neuroptotection *via* both NFTs and Aβ plaques formation. Another such agent is valproic acid. Dill, (2008) investigated the role of GSK-3 inactivation on neurite and axon growth from adult concluded that GSK-3β inhibitors stimulates axon formation and elongation of mature neurons (Dill *et al*, 2008).

2.4. SIGNALLING MECHANISMS (RECEPTORS).

In AD, cognitive decline appears to precede Aβ plaque deposition and neurodegeneration (Morris *et al*., 1996; Hsia *et al*., 1999; Lue *et al*., 1999; Naslund *et al*., 2000) thus, not only Aβ contributes to brain dysfunction but, additional mechanisms comprises neuronal function. Aβ adopts diverse aggregated conformations *in vivo* (e.g. oligomers, protofibrils and fibrils which alters neuronal homeostasis (Kayed *et al*., 2003; Lacor *et al*., 2004).

Aβ may affect critical signal transduction processes that facilitates plastic neuronal learning and memory and utilises two prominent signalling pathways:

i. NMDA receptor activation and regulation of downstream signal transduction pathways, and
ii. Brain-derived neurotrophic factor (BDNF) signalling, BDNF receptor (TrkB) activation and the regulation of downstream pathways.

2.4.1. N-methyl-Daspartate (NMDA).

NMDA antagonists blocks the induction LTP while defects in NMDA receptor activation compromise these defects. (Balazs, 2005).

Mice deficient in BDNF or TrkB, exhibited impaired dendritic and axonal arborisation, synaptic activity and neuronal plasticity, impairment in LTP and learning and memory (Korte *et al*., 1995; Patterson *et al*., 1996; Causing *et al*., 1997; Martinez *et al*., 1998; Minichiello *et al*., 1999).

CREB, [which regulates expression of cAMP response element (CRE)-containing genes], plays a pivotal part in cognitive processes (Bourtchuladze *et al*., 1994; Yin *et al*., 1994; Tully 1997; Abel *et al*., 1998). NMDA induced a marked increase in cAMP response element-binding protein (P-CREB) levels, while this effect was suppressed to approximately one half by sub lethal concentrations of $A\beta_{42}$. Depolarisation-induced promotion of P-CREB was also suppressed *via* a high K_i 40 ± 2.0 μM compared to untreated controls after $A\beta_{42}$ (Tong *et al*., 2001).

2.4.2. Brain-Derived neurotrophic factor (BDNF).

BDNF signals cells *via* a receptor Tyrosine kinase (RTK, TrkB), which in turn triggers (either directly or through binding of adapter proteins) the activation of signal transduction pathways e.g. the Ras/MAPK, akt/PI 3-K and phospholipase C (PLCγ) pathways, thereby delivering the pleiotropic effects of BDNF (**Figure 2.51**).

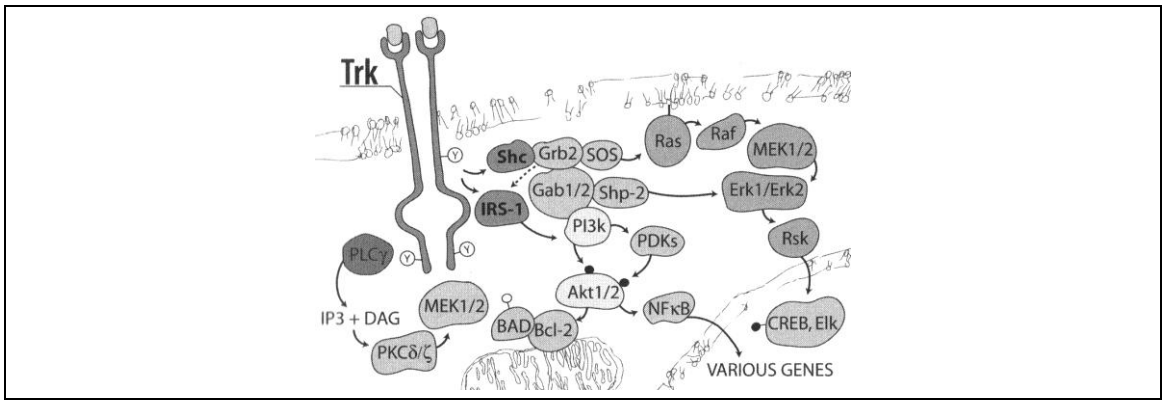

Figure 2.51: The receptor tyrosine kinase (TrkB) activates three major transduction pathways: phosphatidylinositol-3-kinase (PI3-K)/AKT, Ras/MAPK and PLCγ/PKC pathways (Sisodia, 2007).

Neuronal protection is one of the important purposes of BDNF and abstraction of trophic support results in significant cell loss. This protective effect of BDNF is severely compromised by sub-lethal concentrations of $A\beta_{42}$. Camptothecin (an DNA topoiomerase-1 inhibitor that causes DNA damage) treatment causes massive cell loss and was noticeably reduced by BDNF treatment. This was also observed in cortical neurons where BDNF provided protection from apoptosis induced by Camptothecin, (Morris *et al*., 1996).

2.4.3. Nicotinic Acetylcholine receptors.

Scopolamine (SCT) was earlier identified as an inhibitor of AChE while Ensaculin, a synthetically modified derivative (**Figure 2.52**), also showed anti-dementia activity (Hoer *et al*., 2002).

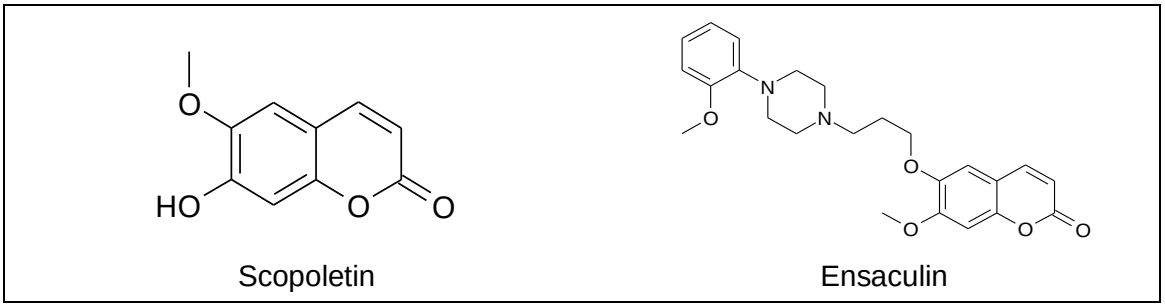

Scopoletin Ensaculin

Figure 2.52: Structures of Scopoletin and Ensaculin (Hoer *et al*., 2002).

SCT potentiated the K^+-evoked release of ACh from superfused frontal cortex synaptosomes while this effect was abolished by mecamulaminn (MEC), a nAChR antagonist and mimicked by galantamine. It could be concluded that SCT amplifies presynaptic activity-dependent ACh release, enhances LTP in the hippocampal CA1 area of the hippocampus, and exerts cognition-improving properties in cholinergically and in age-impaired mice. It's assumed that SCT's main mechanism of action is the agonism of the nAChRs while additionally enhancing NMDA-dependent LTP, thus ameliorating memory impairments (Hornick *et al*., 2011).

2.5. Aβ GENERATION.

2.5.1. Cholesterol.

The CNS accounts for only ~2 % of whole body mass but contains ~ 25 % of the total cholesterol. The average cholesterol concentration of fresh tissue is ~2.2 mg/g but in the brain it ranges between 15-20 mg/g (Dietschy *et al*., 2001; Dietschy *et al*., 2004). About 70-80 % of cholesterol in the adult brain is located in glial cells' specialised membranes while neurons contain only a small fraction (Vance *et al*., 2005). Because of cholesterol's central role in determining the physical properties of cellular membranes, even small changes in cholesterol homeostasis will consequently affect numerous cellular events. Research indicates that the rate of CNS sterol flux is elevated and proportional to the stage of dementia (Lutjohann *et al*., 2000).

Cholesterol depletion by Lovastatin treatment and Methyl-B-cyclodextrin extraction inhibits APP processing *via* BACE1 and lowers Aβ production (Simons *et al*., 1998; Ehehalt *et al*., 2003). This treatment also stimulate non-amyloidogenic processing of APP *via* α-secretase ADAM10 (Kojro *et al*., 2001).

Amyloidogenic processing of APP depends on cholesterol rich membrane domains whereas non-amyloidogenic α-cleavage in the phospholipid-rich domain of plasma membrane (Ehehalt *et al*., 2003). Localisation of APP to the the plasma membrane might directly regulate APP processing (non-amyloidgenic or amyloidgenic) (Abad-Rodriguez *et al*., 2004).

2.5.2. Neprilysin (NEP).

Reduced levels of NEP mRNA and protein have been observed in brain regions vulnerable to Aβ deposition (Carpentier *et al*., 2002; Iwata *et al*., 2002; Iwata *et al*., 2004; Mohajeri *et al*., 2004; Caccamo *et al*., 2005), and in AD patients (Yasojima *et al*., 2001). Additionally, NEP levels consistently declines with aging (Yasojima *et al*., 2001; Carpentier *et al*., 2002; Iwata *et al*., 2002; Caccamo *et al*., 2005; Hama *et al*., 2005; Saito *et al*., 2005), which support the notion that reduction of NEP activity play a role in the development of idiopathic AD.
It has also been reported that NEP has also been shown to both induce local reductions in steady-state Aβ levels and delay plaque deposition (Marr *et al*., 2003; Iwata *et al*., 2004).

2.6. Aβ AGGREGATION.

2.6.1. Metal ions.

Both non-metal Aβ and metal-associated Aβ aggregates are present in AD patients and Aβ has been described to form aggregates through two types of reactions:

i. A non-metal dependent association (“apo-Aβ) where non-metallated aggregates of apo-Aβ form amyloid fibrils and soluble oligomers (*via* intermolecular H-bonding and hydrophobic interactions).
ii. A metal dependent association where metalleted Aβ (usually binding Cu^{2+}, Zn^{2+} or Fe^{3+}) forms ionically bridged aggregates, covalently crosslinked oligomers (when bound to Cu^{2+}).

In vitro studies revealed that Zn^{2+}, Cu^{2+} and Fe^{3+} have the cability of Aβ aggregation and precipitation (Bush *et al*., 1994; Huang *et al*., 1997; Atwood *et al*., 1998; Atwood *et al*., 2000). The ionic assembly of Aβ aggregates (*via* Cu^{2+} and Zn^{2+}) is reversible with chelation (Huang *et al*., 1997; Atwood *et al*., 1998; Atwood *et al*., 2000) (Cherny *et al*., 1999; Cherny *et al*., 2001; Ritchie *et al*., 2003).
Metals are present in relative high concentrations in the neocortical regions (the brain region most susceptible to AD). During neurotransmission, high concentrations of Zn (300 μM) (Frederickson, 1989) and Cu (30 μM) are released (Schlief *et al*., 2005), which may elucidate why Aβ precipitation accumulates in the synapses (Terri *et al*., 1991).

Figure 2.53: The primary amino acid sequence of Aβ. The key residues involved in transition metal binding are indicated in bold. The 42 residue form is enriched in plaque pathology. The rat sequence is the same as the mouse sequence, with two of the substitutions involving metal coordinates. The sole methionine at residue 35, which plays important roles in membrane insertion, redox activity and toxicity is highlighted (Adapted from Sisodia, 2007).

The histidine residues of Aβ (position 6, 13 and 14; **Figure 2.53**) in the N-terminus enables Aβ to coordinate up to 3.5 moles of Cu or Zn (Atwood *et al*., 2000).

2.6.2. Apolipoprotein E (APOE).

After the finding that Aβ was able to bind apolipoprotein E (APOE) the functional involvement of APOE in AD, a common polymorphism in APOE that maps near the 19q linkage region, was confirmed to be associated with an increased risk of AD (Saunders *et al*., 1993; Strittmatter *et al*., 1993).

Three major alleles occur at the APOE locus – ε2, ε3 and ε4. The ε4 allele has been revealed to increase the risk for AD, while ε2 has been associated with a decreased risk for AD (Corder *et al*., 1994).

The most widely used hypothesis assumes that the different polymorphic variants of APOE directly influence Aβ-accumulation (Strittmatter *et al*., 1993), and supported by several facts:

i. Elevated quantities of Aβ plaques in the brain of ε4-alelle carriers *vs.* non-carriers;
ii. The presence or absence of human APOE markedly effects the Aβ deposition, and
iii. APOE ε4 decreases the onset age in EOFAD (**section 2.1.2**) caused by PSEN1 mutations (Nacmias *et al*., 1995).

Aβ clearance *via* low-density lipoprotein receptor (LRP), or *via* a systematic dysfunction in lipid transport indicated that high plasma cholesterol levels are associated with increased Aβ plaques (Poirrier 2000). When lipid-free and lipid-associated APOE are in conjuction, it can bind Aβ (Strittmatter *et al*., 1993; LaDu *et al*., 1994; LaDu *et al*., 1995; Aleshkov *et al*., 1997; Yang *et al*., 1997; Morikawa *et al*., 2005).

APOE is involved in the γ-secretase cleavage of APP (Irizarry *et al*., 2004). It was observed that in a control population, the ε4 allele had a frequency of ~0.15, but ~0.50 in LOAD (section 2.1.2) patients (Strittmatter *et al*., 1993). Numerous reports confirmed that the ε4 allele was an AD risk factor while the ε2 allele seems to be protective. (Corder *et al*., 1993; Mayeux *et al*., 1993; Corder *et al*., 1994; Poirer, 1994; Strittmatter *et al*., 1996).

2.6.2.3. Relevance to coumarin.

Novel benzocoumarin derivatives were synthesised and evaluated for their *in vivo* antidyslipidemic activity (**Figures 2.54** and **2.55**). These compounds inhibited cholesterol biosynthesis and additionally potentiated the activity of lipolytic enzymes to promote early clearance of circulated lipids (Sasidhara *et al*., 2010).

Index:	R =	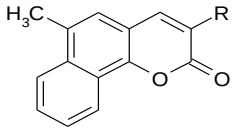
276	$COCH_3$	
277	Cl	
278	CN	**(276 - 278)**

Figure 2.54: Novel coumarin derivatives as potential antidyslipidemic agents (Sasidhara *et al*., 2010).

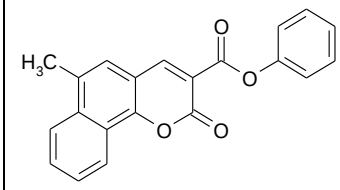

279

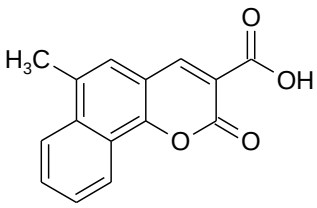

280

Index:	R =
281	C_2H_5
282	CH_3
283	Propyl
284	Iso-propyl
285	Butyl

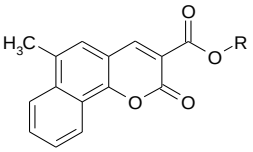

(281 - 285)

Figure 2.55: Novel antidyslipidemic coumarin derivatives (Sasidhara *et al*., 2010).

Compound **282**, was the most potent with 27 %, 26 % and 26 % lowering in TC (total cholesterol), PL (plasma lipids) and TG (total triglyceride), respectively, while compounds **276**, **277**, **281 - 285** revealed mild activity (comparable with standard drug 100 mg/kg Gemfibrozil which decreased levels of TC, PL and TG in plasma by 34 %, 38 % and 35%, respectively). Compound **278** revealed significant reversal of plasma PHLA in hyperlipidemic rats by 25 % (comparable to Gemfibrozil, with 28 % reversal of activity).

At 200 µg/mL, compound **278** showed significant superoxide anions inhibition (32 %), hydroxyl radical inhibition (49 %) and microsomal lipid peroxidation inhibition (38 %) (comparable to the standard drug, 20 µg/mL Alloperinol with 80 % inhibition in superoxide anions and 100 µg/mL Manitol and α-Tocopherol with 52 % and 47 % inhibition of hydroxyl ions and microsomal lipid peroxidation, respectively).

Regarding SAR, the minimum structural requirement for binding of the derivatives to the target includes an aromatic or heteroaromatic ring at the 7th and 8th position, which is hypothesised to participate in π–π stacking with aromatic amino acid residues of the receptor. In the lactam ring either an acid or ester group at position 3 is required for *in vivo* dyslipidemic activity.

Although an electron withdrawing entity at position 3 is desired, the lack of activity for compound **278** (containing a –CN group) might be ascribed to its reversible conversion to –C

≡N. Increased activity and selectivity may also be due to substitution of Cl for CN (Sasidhara *et al*., 2010).

2.6.3. Inhibition of nucleation (Aβ aggregation inhibitors).

Researchers identified analogues of naturally occurring coumarin (**Figure 2.56**) as novel inhibitors of Aβ aggregation (Soto-Ortega *et al.,* 2011).

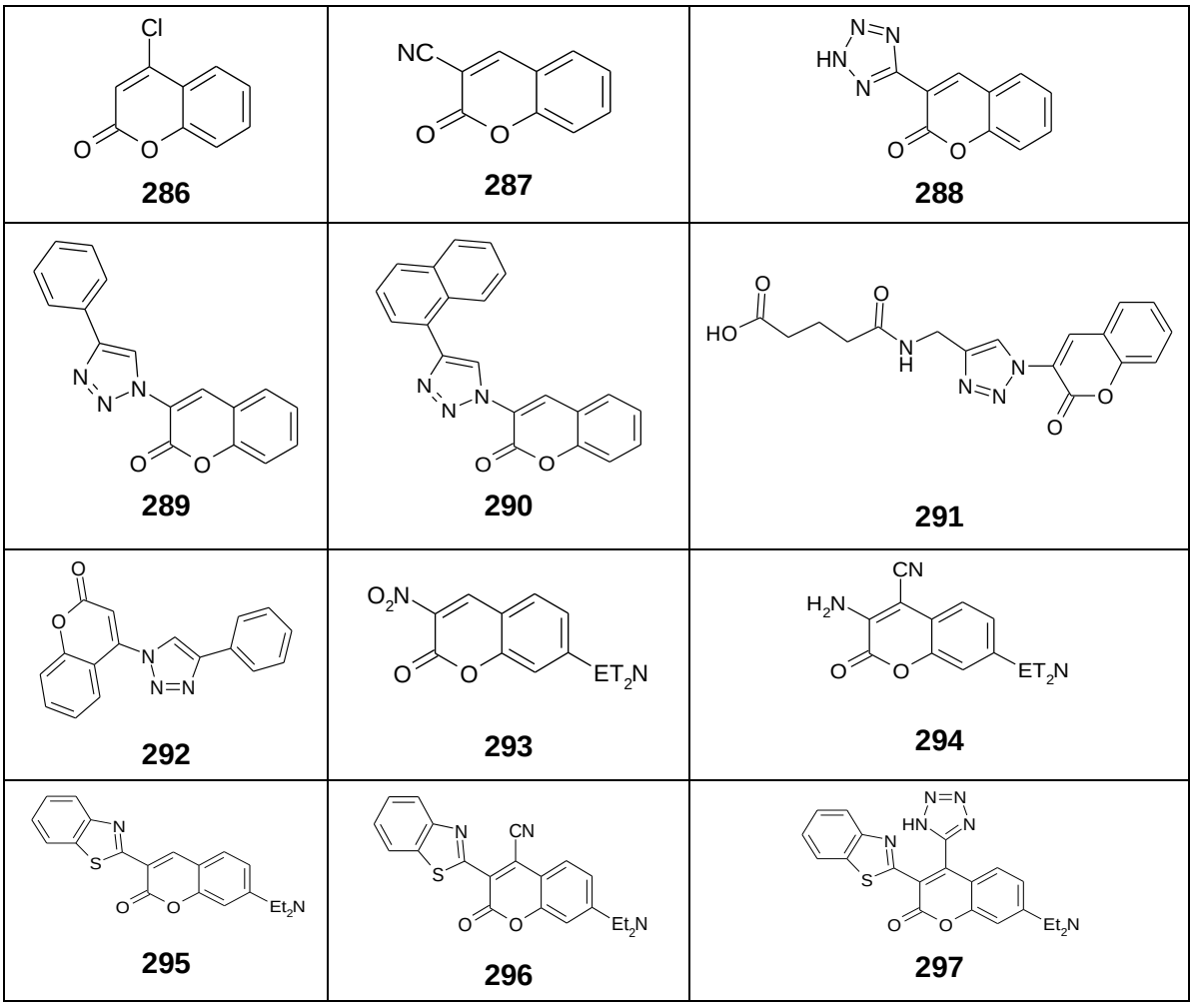

Figure 2.56: Coumarin analogues with Aβ aggregation inhibitory activity (Soto-Ortego *et al*., 2011).

Derivatisation of the coumarin nucleus (**Figure 2.56**) resulted in inhibitory capabilities and where an inhibitor intervenes within the nucleation dependent Aβ aggregation pathway (Soto-Ortega *et al.,* 2011).

2.7. Aβ DEGREDATION.

Aβ production is normally eliminated *via* numerous processes, which includes:

i. proteolytic degradation,

ii. cell-mediated clearance,

iii. active transport out of the brain, and

iv. deposition into insoluble aggregates.

2.7.1. Angiotensin-converting enzyme (ACE).

Angiotensin-converting enzyme (ACE) is a metalloprotease that degrades Aβ *in vitro* (Hu *et al*., 2001). An association between ACE and the risk of LOAD exists, therefore making ACE is an interesting target for AD drug design (Kehoe *et al*., 2004).

2.7.1.1. Relevance to coumarin.

In order to create some novel antihypertensive candidates, authors prepared hybrids of the coumarin moiety and pyrimidine ring scaffold (**Figures 2.57 - 2.59**) with known potential cardiovascular activity. The result indicated that an increase in aqueous solubility and a hydrophobic character is the main stay for high relaxation activity (Kamilia *et al*., 2011). These compounds could prove beneficial in Aβ degradation.

Index	R_1 =	R_2 =	R_3 =
298	Cl	H	CH_3
299	$-N(C_2H_2)_2$	H	CH_3
300	CH_3	H	CH_3
301	$-C_6H_5$	H	CH_3
302	Cl	H	Cl
303	Cl	$-CH_2CH_2Cl$	CH_3
304	NH_2	CN	C_6H_5
305	NH_2	$-C(NH_2)=N-OH$	C_6H_5

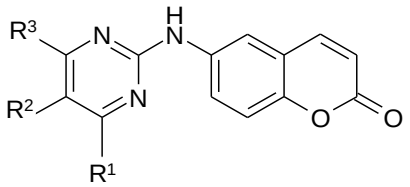

(298 - 305)

Figure 2.57: Vasorelaxant novel coumarin - pyrimidine hybrids (Kamilia *et al*., 2011).

Index	R_1 =	R_2 =
306	H	CH_3
307	H	OH
308	CN	C_6H_5
309	$-C(NH_2)=N-OH$	C_6H_5
310	CN	$4-N(C_2H_5)_2C_6H_4$

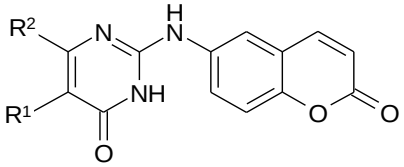

(306 - 310)

Figure 2.58: Coumarin–pyrimidine hybrids with vasorelaxant activity (Kamilia *et al*., 2011).

Index	Ar =
311 (a, b)	5-CH_3-C_4H_2O
312 (a, b)	C_4H_3S
313 (a, b)	C_6H_5
314 (a, b)	4-CH_3-C_6H_4
315 (a, b)	4-CF_3-C_6H_4
316 (a, b)	4-SCH_3-C_6H_4
317 (a, b)	4-NO_2-C_6H_4

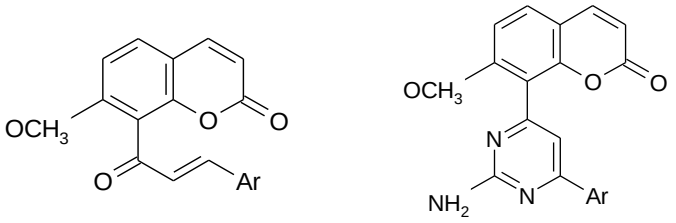

(a) **(b)**

(311 - 317)

Figure 2.59: Novel coumarin - pyrimidine vasorelaxant hybrids (Kamilia *et al*., 2011).

2.7.2. Receptor for advanced glycation end products (RAGE).

RAGE binds a broad repertoire of ligands including products of non-enzymatic such as AGE, Aβ, the S100/calgranulin family of pro-inflammatory cytokines-like mediators, and group 1 DNA binding protein Ampotherin (Hori *et al*., 1995; Yan *et al*., 1996; Hoffman *et al*., 1999; Kislinger *et al*., 1999; Stern *et al*., 2002). RAGE biology is dictated through the accumulation of its ligands, thus deposition of ligands activates receptor expression (Stern *et al*., 2002). It has also been evident that treatment with sRAGE significantly reduces Aβ accumulation (Deane *et al*., 2003).

2.7.2.1. Relevance to coumarin.

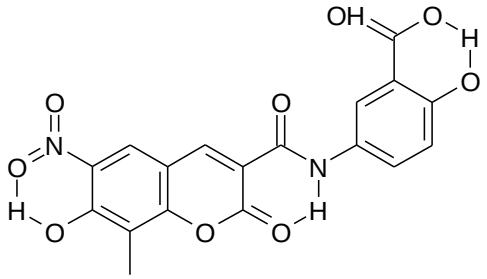

Nicousamide

Figure 2.60: Structure of Nicousamide.

Nicousamide, a novel coumarin - aspirin derivative (**Figure 2.60**), revealed to inhibit AGE-induced transforming growth factor (TGF-β1) and connective tissue growth factor (CTGF). Nicousamide blocked AGE-induced G1-arrest in mesangial cells and tubular epithelia while suppresses the AGE matrix metalloproteinase (Li *et al*., 2012).

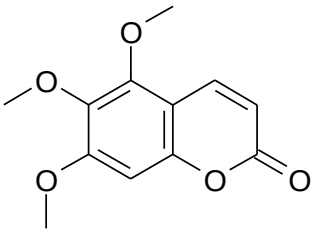

5,6,7-trimethoxy-coumarin

Figure 2.61: Structure of 5,6,7-trimethoxy-coumarin.

Eremurus persicus (Liliaceae) locally called "Serish", is traditionally used for the treatment of liver and stomach disorders, constipation and diabetes. Authors investigated the antiglycation activity of *E*. *persicus*. It was reported that 5,6,7-trimethoxy-coumarin (**Figure 2.61**) is the active compound responsible for the antiglycation property of this plant (Asgarpanah *et al*., 2011).

2.7.3. Insulin degrading enzyme (IDE).

Insulin-degrading enzyme (IDE) was shown to degrade Aβ within crude brain homogenates (Kurochkin *et al*., 1994), and was later independently identified capable of major Aβ-degrading activity (Qiu *et al*., 1997; Qiu *et al*., 1998). Neurons from IDE knockout mice revealed > 90 % reduction of extracellular Aβ degradation (Farris *et al*., 2003).

2.7.4. Plasmin.

Plasmin was identified to degrade and reduce the toxicity of both monomeric and fibrillar Aβ. This was fuelled by the discovery of genetic linkage between LOAD and a region of Chr.10 containing the gene for urokinase olasminogen (uPA), (Tucker *et al*., 2000; Bertram *et al*., 2000; Ertekin-Taner *et al*., 2000; Myers *et al*., 2000).

2.7.3.1. Relevance to coumarin.

Compounds (**Figure 2.62**) that activate plasmin could thus increase Aβ clearance. In this regard, administration of plasmin activation inhibitor-1 (PAI-1) to APP transgenic mice was reported to lower both plasma and brain Aβ levels (Pangalos *et al*., 2005).

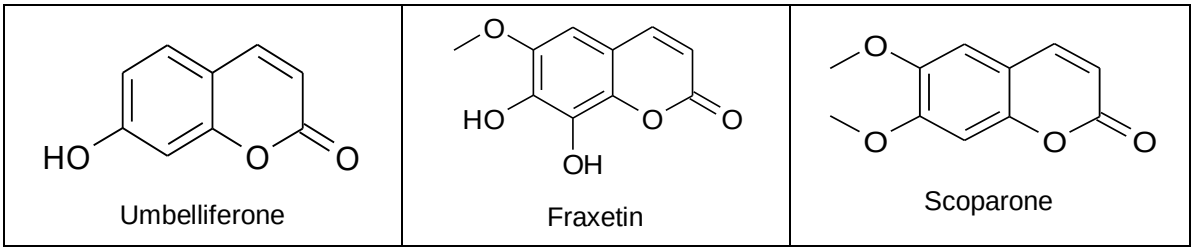

Figure 2.62: Structure of Umbelliferone, Fraxetin and Scoparone.

2.8. CONCLUSION.

Taken all the 'targets' of the pathogenesis in AD described in this chapter into account, it is clear that selective substitution on different positions of the coumarin moiety could result in compounds with pronounced activity and selectivity towards specific targets in the treatment of AD. Understanding and employing these SAR concepts is crucial in the design for novel MTDLs. The next chapter will discuss the synthesis of coumarin derivatives as MTDLs followed by biological evaluation results, focusing on AChE and MAO-B inhibition.

Chapter 3 Chemistry

3.1. INTRODUCTION.

Coumarins originated from 'Coumarou' which is the vernacular name of the tonka bean (*Dipteryx odorata* Willd., Fabaceae), and was first isolated in 1820 (Bruneton, 1999). They are widely available in nature (Egan *et al*., 1990; Egan *et al*., 1992; Fin *et al*., 2002; Lake *et al*., 1999) eg. in oils such as cinnamon bark oil (7,000 ppm), cassia leaf oil (up to 87,300 ppm) and even lavender oil. Coumarins are not restricted to oils, but are also found in fruits (bilberry, cloudberry), green tea and other foods such as chicory other foods (Lake *et al*., 1999).

It belongs to the benzopyrone compound family, consists of a benzene ring conjugated to a pyrone ring (Ojala, 2001) and includes α - benzopyrones (the coumarins) and the γ - benzopyrones (mainly the flavonoids; **Figure 3.1**).

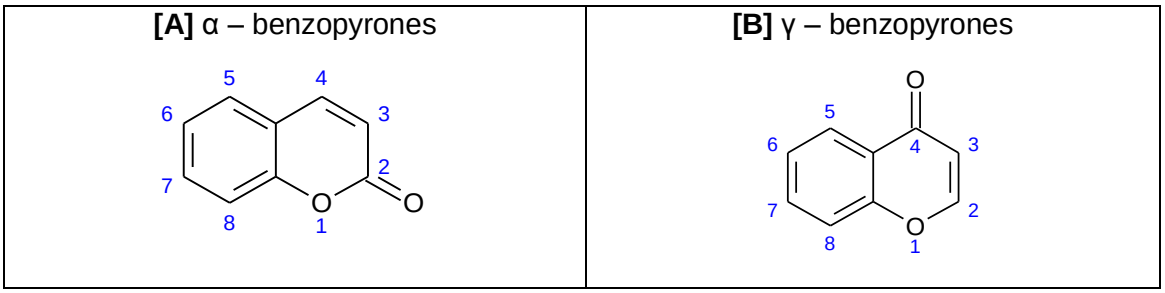

Figure 3.1: Benzopyrone subclasses, with the basic coumarin structure [(α - benzopyrone) (**A**)], as well as the flavonoid [(γ - benzopyrone) structure (**B**)].

The α-benzopyrones can further be sub-divided (**Table 3.1**) into four main coumarin types (according to the position and type of substition) namely: the simple coumarins, furanocoumarins, pyranocoumarins and the pyrone-substituted coumarins (Keating *et al*., 1997).

Table 3.1: The four main coumarin subtypes including structural features and examples.

Classification	Characteristics	Example(s)	
Simple Coumarins	Hydroxylated, aloxylated or alkylated benzene ring	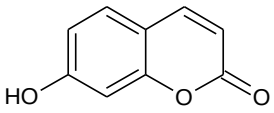 7-hydroxycoumarin	
Furanocoumarin	A 5 – membered furan ring attached to the benzene ring (Linear or Angular).	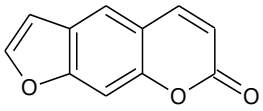 Psolaren	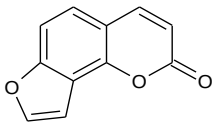 Angelicin
Pyranocoumarin	A 6 – membered Pyran ring attached to the benzene ring (Linear or Angular).	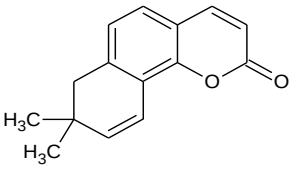 Seselin	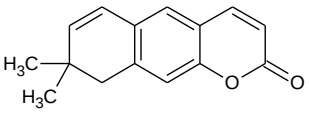 Xanthyletin
Pyrone – substituted coumarins.	Substition on the pyrone ring (often C3 or C4 position).	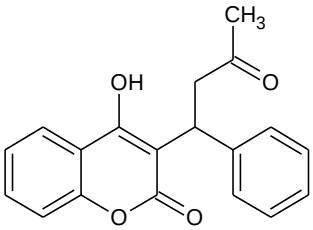 Warfarin	

3.2. Absorption and Distribution

Coumarin and the 7-hydroxycoumarin both have low water solubility (0.22 % and 0.031 %, respectively) resulting in low *in vivo* bioavailability and exhibits high partition coefficients, octanol/water (21.5 and 10.4 respectively), resulting in rapid absorption once they are in aqueous solution. Together with their non-polarity, this means that they should cross lipid bilayers easily by means of passive diffusion (Cooke, 1999).

3.3. Microwave-assisted synthesis

Microwave energy (radiation) is applicable in chemistry to accelerate charged particles (electrons and protons) to high energies thus causing them to collide and form covalent bonds (de la Hoz *et al*., 2005).

This radiation causes an abrupt increase in temperature known as a microwave-induced thermal effect (increase in temperature).

The microwave reactor is equipped with an integrated equilibrium system and as the temperature rises, the radiation will decrease to compensate for the selected settings. This microwave–induced thermal effect together with the contributing exothermal reaction, it is critical to keep the temperature as low as possible (which in turns means an increase in radiation)l. Cooling of the reaction mixture with nitrogen has its own benefits, but has a financial disadvantage. In this study we used an adapted cooling system with the microwave reactor (refer to **section 3.5** and **Figure 3.2**).

Advantages of microwave-assisted synthesis:

i. Extreme reaction rate acceleration that is associated with uncomplicated purification/isolation;
ii. Enhanced physicochemical properties;
iii. Yield improvement;
iv. Generation of new ‘’potential products’’ and
v. Financial benefits e.g. less solvent(s) is used, absence of expensive catalyst etc. (Cecilia *et al*., 2007).

Disadvantages of microwave-assisted synthesis:

i. Limitation of solvent (because of the microwave – induced thermal effect). Solvents with a low boiling point are excited much easier which makes cooling/reflux much more uncontrollable, therefore we only choose solvents with a boiling point of 60 °C and above;
ii. The generation of new product(s)/by - product(s) can complicate the isolation of the desired products;
iii. Temperature regulation (sometimes cooling with nitrogen is required) and
iv. High investment costs (Nuchter *et al*., 2004).

3.4. SYNTHESIS.

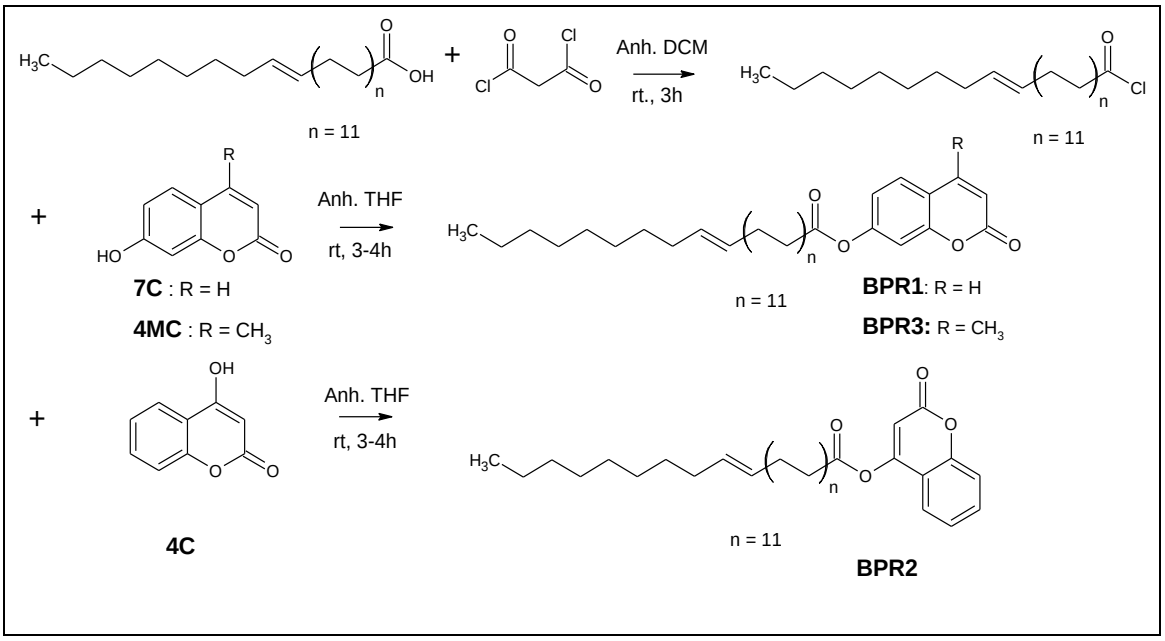

Scheme 3.1: The synthesis of erucic acid - coumarin conjugates synthesis (**BPR1, BPR2, BPR3**).

Erucic acid was first converted to its corresponding acyl chloride by means of oxacyl chloride in dry DCM to provide a more efficient nucleofillic attack on the respective coumarins (**Scheme 3.4 and section 3.5.1 – section 3.5.3**). Note that the resulting products are waxes with relative low melting points, which have numerous advantages such as possible pro drug benefits and transdermal properties.

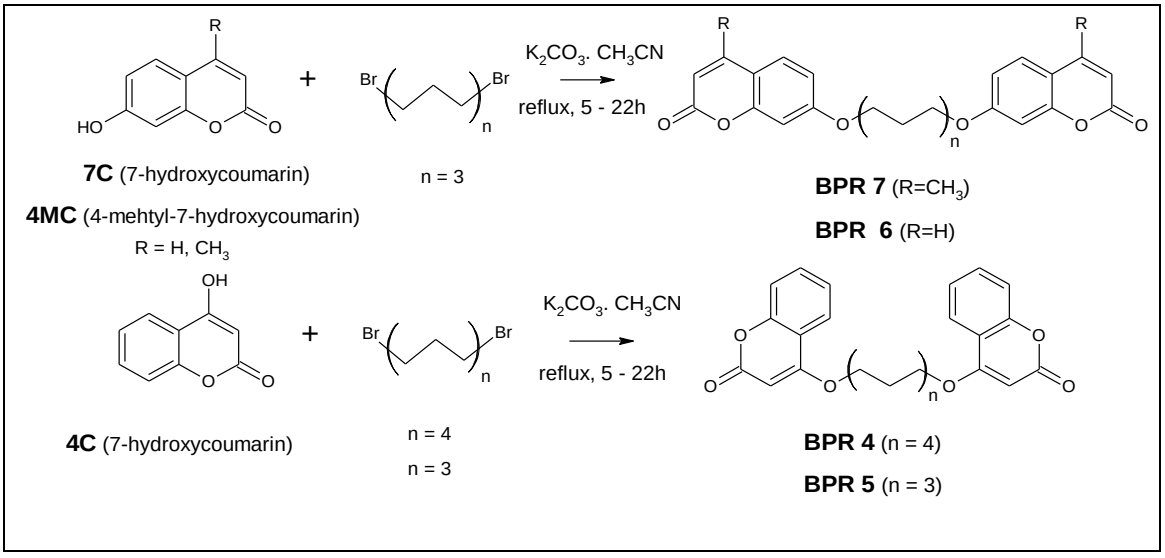

Scheme 3.2: Synthesis of coumarin dimer derivatives.

Synthesis of dimers invoked widespread attention (**Chapter 1 - section 1.2**). The classical Williamson etherfication was followed where the different coumarins **7C** (7-hydroxycoumarin); **4MC** (7-Hydroxy-4-methyl coumarin) and **4C** (4-hydroxycoumarin) behave as nucleophiles

and displace the appropiate halide (1,3 dibromo-propane and 1,4 dibromo-ethane) *via* an S_N2 reaction to produce the corresponding coumarin dimer. A basic salt (K_2CO_3) and a spatula point of KI where used as suitable ''catalysts'' in Acetonitrile (**scheme 3.1 and section 3.5.4 – 3.5.7**). With microwave-assisted synthesis an increase in product yield as well as a decrease in reaction time was achieved.

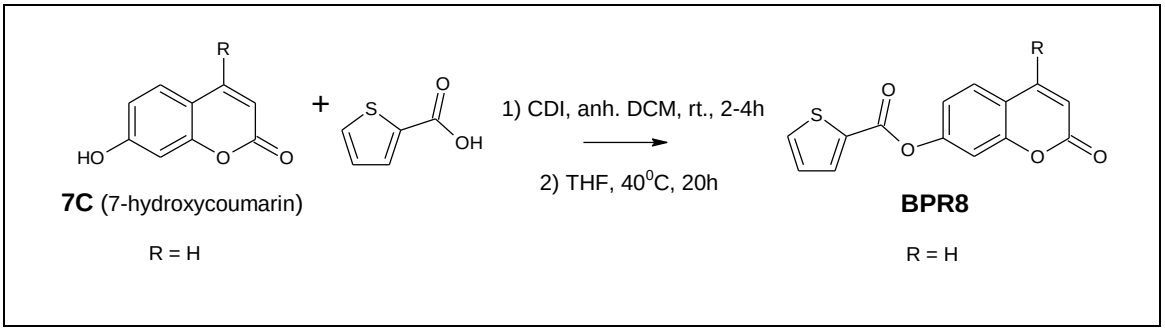

Scheme 3.3: Synthesis of coumarin - thiophene conjugate **(BPR8)**.

Activating die thiophene acid *in situ* using CDI in dry DCM provides the appropriate conditions for nucleophillic attack by the coumarin (7-hydroxycoumarin, 4-methylated-7hydroxycoumarin and 4-hydroxycoumarin) the produce the coumarin–thiophene conjugate (**Scheme 3.3 and section 3.5.8**).

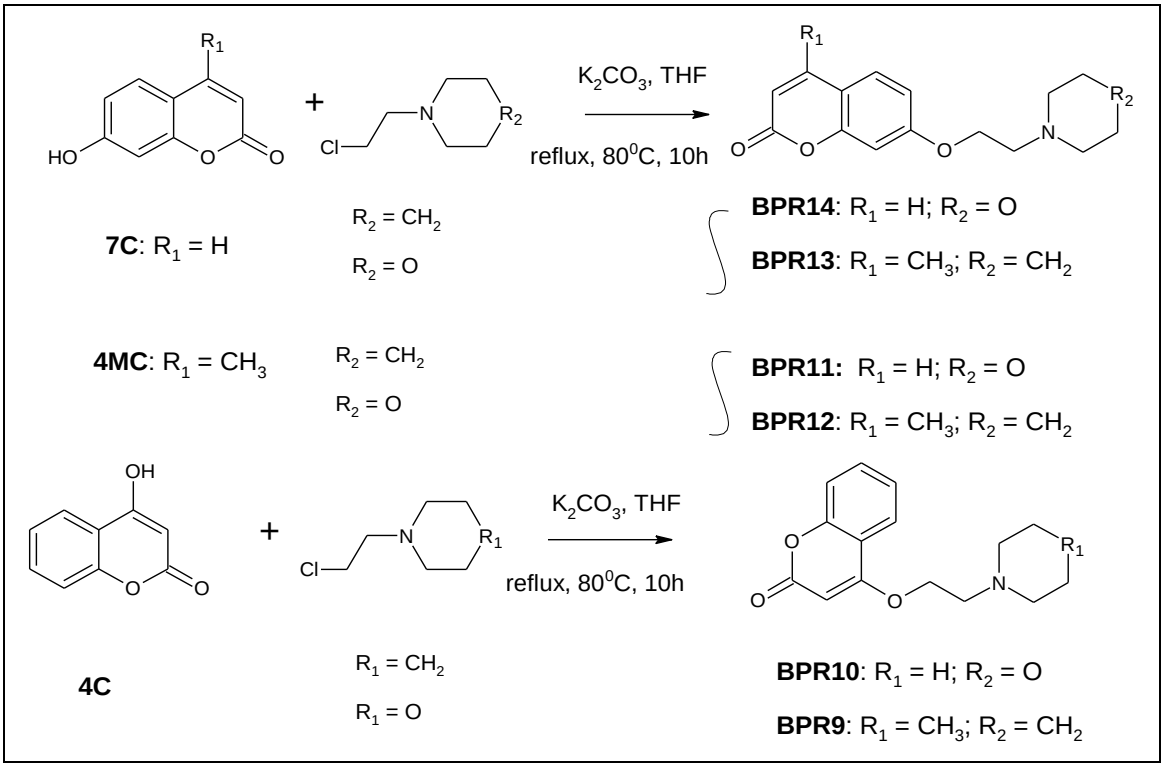

Scheme 3.4: Synthetic route of coumarin derivates conjugated with piperidine and morpholine **(BPR10**, **BPR11, BPR12, BPR13. BPR14).**

Following the aboved mentioned method, etherfication of the coumarin derivatives with chloro-ethanepiperidine and chloro-ethanemorpholine through conventional heating produced the respective coumarin conjugates (**Scheme 3.2 and sections 3.5.9 – 3.5.14).**

3.5. MATERIALS, METHODS AND INSTRUMENTATION.

Materials: Starting materials were obtained from Sigma-Aldrich and Merck and was used without further purification or converted to intermediate (more reactive) derivatives. All solvents used were anhydrous. Drying after extraction of the organig fractions was achieved using Magnesium sulphate ($MgSO_4$).

Thin layer chromatography (TLC): TLC was carried out to determine the completeness of the reaction. Silica gel 60 sheets (Merck) containing UV_{254} fluorescent indicator were employed with the appropriate mobile phase for each reaction. The developed TLC sheets were observed under an UV at a wavelength of 354 nm and the R*f* values noted.

Melting points (Mp): A Büchi B-545 melting point apparatus was used to measure the Mp of all synthesised compounds.

Mass spectra (MS): High resolution mass spectra (HRMS) and nominal mass spectra (MS) were obtained with a Bruker micrOTOF-Q II mass spectrometer in atmospheric-pressure chemical ionization (APCI) mode.

Nuclear magnetic resonance (NMR): A Bruker Avance III 600 spectrometer, at frequencies of 600 MHz and 150 MHz, were used to record proton (^1H) and carbon (^{13}C) NMR spectra, respectively. NMR experiments were conducted in $CDCl_3$ and the chemical shifts reported in parts per million (δ) downfield. Spin multiplicities are given as s (singlet), bs (broad singlet), d (doublet), dd (doublet of doublets), t (triplet), q (quartet) or m (multiplet). The coupling constants (J) of the molecule's atoms involved are given in H*z*.

Microwave-assisted synthesis: A CEM Discovery® microwave reactor fitted with a cooler, a 100 mL flask with the suitable volume solvent together with the adapted cooling system (as discussed below) was implemented. The air was cooled by using a length of silicon tube (inlet tube) that increases the surface flow area exposed to the cooler environment. The cooler environment was achieved by merely packing ice and salt layer upon layer in a 5L container which contains the above mentioned in lead tube in a spiral formation (**Figure 3.2**). This shifted the inlet temperature from room temperature up to -9 °C, causing the integrated system

to compensate for a cooler environment (although the reactions was exothermic) and consequently increasing radiation. Another technique applied was to radiate the reaction for a smaller period of time, cool it down and then repeat the reaction.

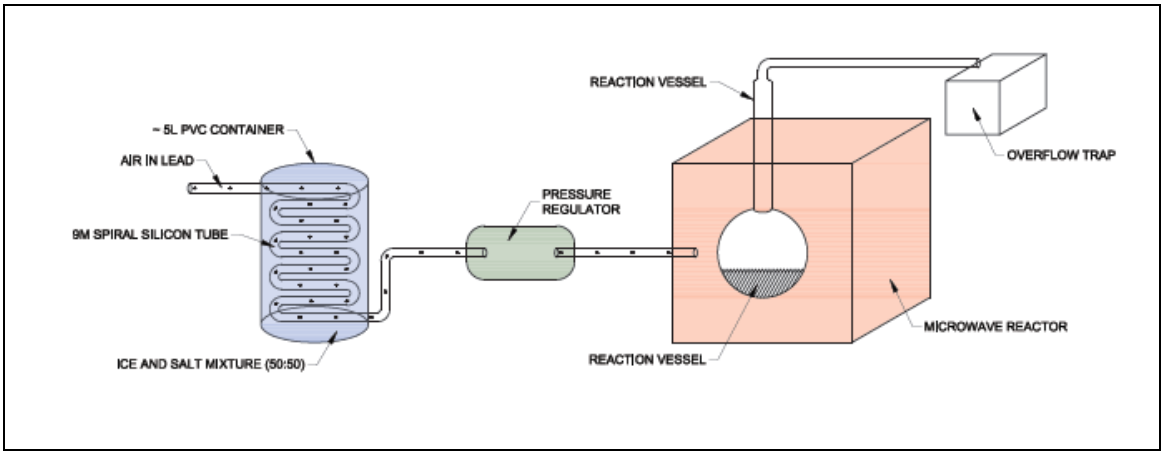

Figure 3.2: Schematic outlay of the modified microwave reactor used in this study.

3.5.1. 2-Oxo-2H-chromen-7-yl docos-24-enoate (BPR1).

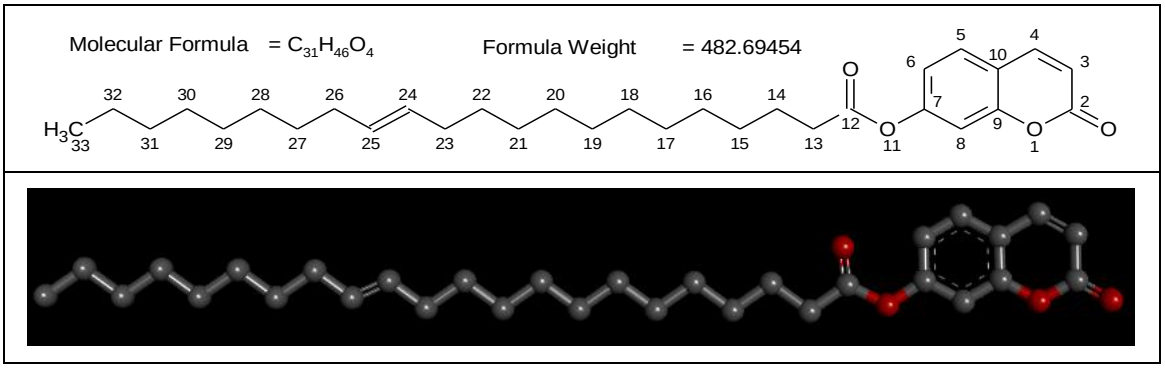

A mixture of 3.36 mmol, 1139 mg, 1 mol eqv. Erucic acid and 3.36 mmol, 427 mg. / 289 µL oxacyl chloride was suspended in 30 mL dry Dichloromethane (DCM) and stirred for 2 hours at room temperature (rt). The reaction turned yellowish and the corresponding erucyl chloride was formed. The excess oxacyl chloride as well as the DCM was removed under vacuum (60 °C). The remaining erucyl chloride was suspended in 30 mL Tetrahydrofuran (THF) and, on an ice bath, 3.70 mmol, 600 mg, 1.1 mol eqv. 7-hydroxycoumarin and 7.40 mmol, 1022 mg, 2.2 mol eqv. K_2CO_3 was added. The suspension was stirred for another 3 - 4 hours at room temperature (rt)., filtered and purified using column chromatography with DCM:Cyclohexane (3:1). It was dried, filtered and concentrated, a white wax with a sweet odour formed.

R*f*: 0.491. Mp: 53.8 - 54.5 °C. **^{1}H NMR** (600 MHz, $CDCl_3$, **Annexure A - Spectrum 1**): δ 7.67 (d, *J* = 9.5 Hz, 1H, H_4); 7.46 (d, *J* = 8.4 Hz, 1H, H_5); 7.08 (d, *J* = 2.1 Hz, 1H, H_6); 7.04 – 6.99 (m, 1H, H_8); 6.37 (d, *J* = 9.5 Hz, 1H, H_3); 5.32 (t, *J* = 4.7 Hz, 2H, $H_{24, 25}$); 2.56 (t, *J* = 7.5

Hz, 2H, H_{13}); 1.99 (m, 4H, $H_{23, 26}$); 1.77 – 1.70 (m, 4H, H_{14}); 1.35 – 1.19 (m, 28H, $H_{15 - 22, 27 - 32}$); 0.85 (t, *J* = 7.0 Hz, 3H, H_{33}). **^{13}C NMR** (151 MHz, $CDCl_3$. **Annexure A - Spectrum 2**): δ 171.61 (C_{12}); 160.35 (C_2); 154.68 (C_9); 153.29 (C_7); 142.84 (C_4); 129.91 (C_{24}); 129.85 (C_{25}); 118.43 (C_5); 116.56 (C_6); 116.00 (C_{10}); 110.43 (C_3); 34.32 (C_8); 31.89 (C_{13}); 30.92 (C_{31}); 29.75 - 29.05($C_{15 – 23, 26 - 29}$); 27.19(C_{30}); 24.77(C_{14}); 22.67(C_{32}); 14.18 (C_{33}). **MS**: EIMS 315; EI-HRMS *m*/*z*: calculated for **$C_{31}H_{46}O_4$**, 482.6945, found 481.3297 (**Annexure B - Spectrum 29**). Yield: 860 mg, 1.78 mmol, 48.11 %.

3.5.2. 2-Oxo-2H-chromen-4-yl docos-24-enoate (BPR 2).

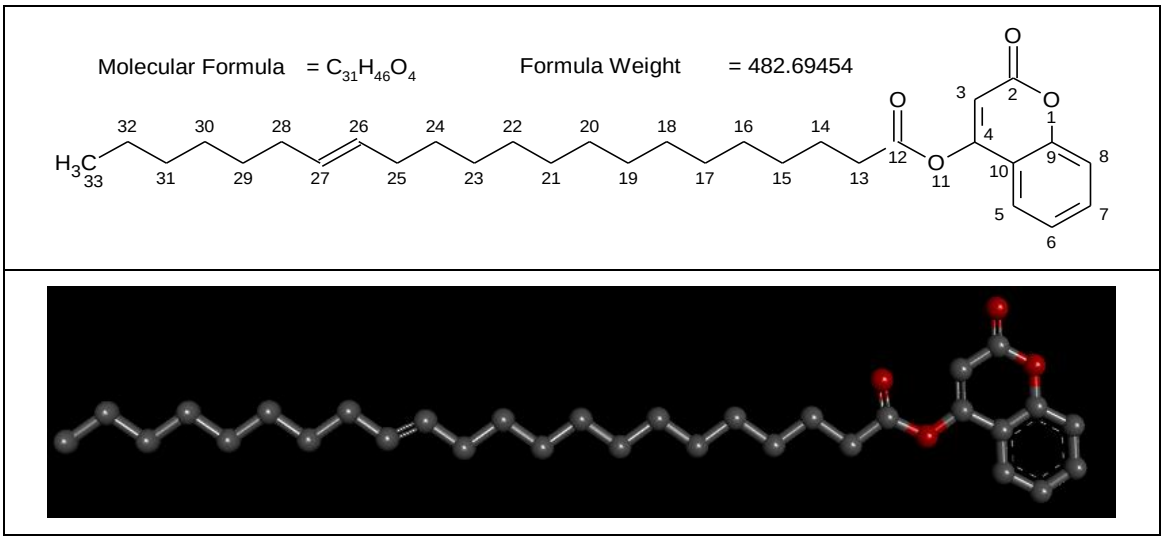

A mixture of 3.36 mmol, 1139 mg, 1 mol eqv. Erucic acid and 3.36 mmol, 427 mg. / 289 µL oxacyl chloride was suspended in 30 mL dry DCM and stirred for 2 hours at rt. to form the corresponding erucyl chloride. The reaction turned yellowish. The excess oxacyl chloride as well as the DCM were removed under vacuum (60 °C). The remaining residue was suspended in 30 mL THF and, on an ice bath, 3.70 mmol, 600 mg, 1.1 mol eqv. 4-hydroxycoumarin and 7.40 mmol, 1022 mg, 2.2 mol eqv. K_2CO_3 were added and stirred for another 3 - 4 hours at rt., then filtered. The filtrate was purified using column chromatography with DCM:Cyclohexane (8:2) and concentrated to yield a white wax with a sweet odour developed.

R*f*: 0.585. Mp: 77 – 79 °C. **^{1}H NMR** (600 MHz, $CDCl_3$, **Annexure A - Spectrum 3**): δ 7.60 (dd, *J* = 7.9, 1.5 Hz, 1H, H_5); 7.56 (m, 1H, H_7); 7.34 (dd, *J* = 1, 0.6 Hz, 1H, H_6); 7.30 – 7.26 (m, 1H, H_8); 6.50 (s, 1H, H_3), 5.33 (m, 2H, $H_{26,27}$); 2.68 (t, *J* = 7.5 Hz, 2H, H_{13}); 1.77 (m, 4H, $H_{25,28}$); 1.39 – 1.17 (m, 28H, $H_{15 - 24,29 - 32}$); 0.85 (t, *J* = 7.0 Hz, 3H, H_{33}). **^{13}C NMR** (151 MHz, $CDCl_3$, **Annexure A - Spectrum 4**): δ 169.53 (C_{12}); 161.50 (C_4); 158.34 (C_2); 153.65 (C_9); 132.71 (C_7); 129.92 (C_{26}); 129.83 (C_{27}); 124.26 (C_5); 122.66 (C_6); 117.09 (C_8); 115.53 (C_{10}); 105.06 (C_3); 34.55 (C_{13}); 30.92 (C_{31}); 29.75 - 29.16 ($C_{15 - 25}$); 29.00 (C_{28}); 27.19 (C_{29}); 26.89 (C_{30});

24.65 (C_{14}); 22.67 (C_{32}); 14.10 (C_{33}). **MS**: EIMS 315; EI-HRMS *m*/*z*: calculated for **$C_{31}H_{46}O_4$**, 482.6945, found 481.303 (**Annexure B - Spectrum 30**). Yield: 710 mg, 1.47 mmol, 39.73 %.

3.5.3. 4-Methyl-2-oxo-2H-chromen-7-yl docos-25-enoate (BPR 3).

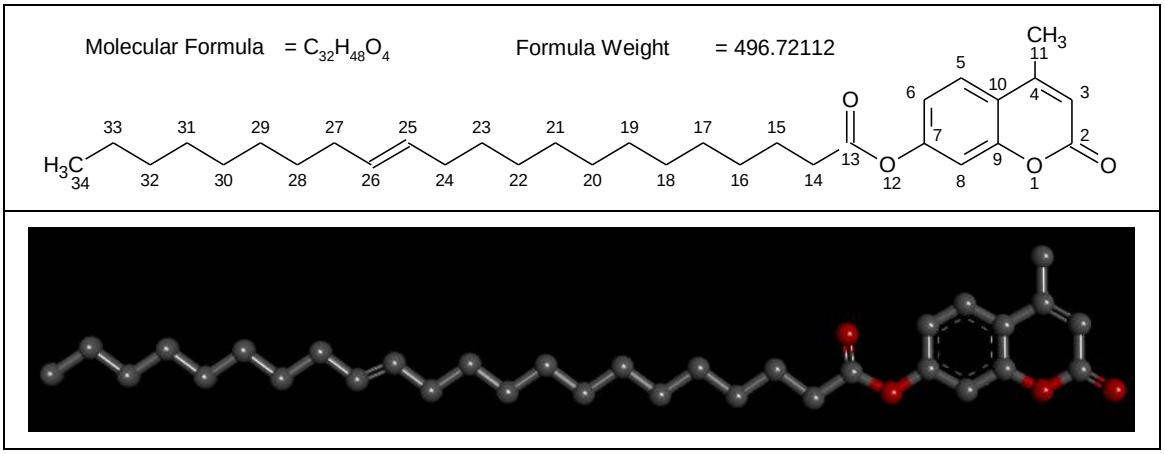

Erucic acid (3.78 mmol, 1281 mg, 1mol eqv) and 3.78 mmol, 482 mg. / 325 µL, 1 mol eqv. oxacyl chloride were suspended in 30 mL dry DCM and stirred for 2 hours at rt. The corresponding erucyl chloride was formed and the excess oxacyl chloride and DCM removed under vacuum (60 °C). To the above residue, on an ice bath, 3.40 mmol, 600 mg, 0.9 eqv. 4-methylated-7-hydroxycoumarin and 3.78 mmol, 1023 mg, 1.8 mol eqv. K_2CO_3. was added, stirred for 14 hours at rt. and filtered. The filtrate was purified using column chromatography with DCM:Cyclohexane (7:1) and then concentrated to leave a white wax with a sweet odour formed.

R*f*: 0.528. Mp: 49 - 51.2 °C. **^{1}H NMR** (600 MHz, $CDCl_3$, **Annexure A - Spectrum 5**): δ 7.58 (d, *J* = 8.6 Hz, 1H, H_5); 7.08 (d, *J* = 2.2 Hz, 1H, H_6); 7.04 (dd, *J* = 8.6, 2.3 Hz, 1H, H_8); 6.24 (s, 1H, H_3); 5.37 – 5.29 (m, 2H, $H_{25,26}$); 2.56 (t, *J* = 7.5 Hz, 2H, H_{14}); 2.41 (s, 3H, H_{11}); 2.03 – 1.95 (m, 4H, $H_{24,27}$); 1.77 – 1.70 (m, 2H, H_{15}); 1.33 - 1.21 (m, 28H, $H_{16-13,28-33}$); 0.85 (t, *J* = 7.0 Hz, 3H, H_{34}). **^{13}C NMR** (151 MHz, $CDCl_3$, **Annexure A - Spectrum 6**): δ 171.64 (C_{13}); 160.51 (C_2); 154.17 (C_7); 153.18 (C_9); 151.87 (C_4); 129.90 (C_{25}); 125.30 (C_{26}); 118.11 (C_5); 117.73 (C_6); 114.45 (C_{10}); 110.44 (C_3); 34.32 (C_8); 31.89 (C_{14}); 30.92 (C_{32}); 29.75 - 27.19 ($C_{27-31,16-24}$); 24.77 (C_{15}); 22.67 (C_{33}); 18.71 (C_{11}); 14.10 (C_{34}). **MS**: EIMS 315; EI-HRMS *m*/*z*: calculated for **$C_{32}H_{48}O_4$**, 496.721, found 497.3558 (**Annexure B - Spectrum 31**). Yield: 685 mg, 1.38 mmol, 40.59 %.

3.5.4. 4,4'-[Butane-1,4-diylbis(oxy)]bis(2*H*-chromen-2-one) (BPR4)

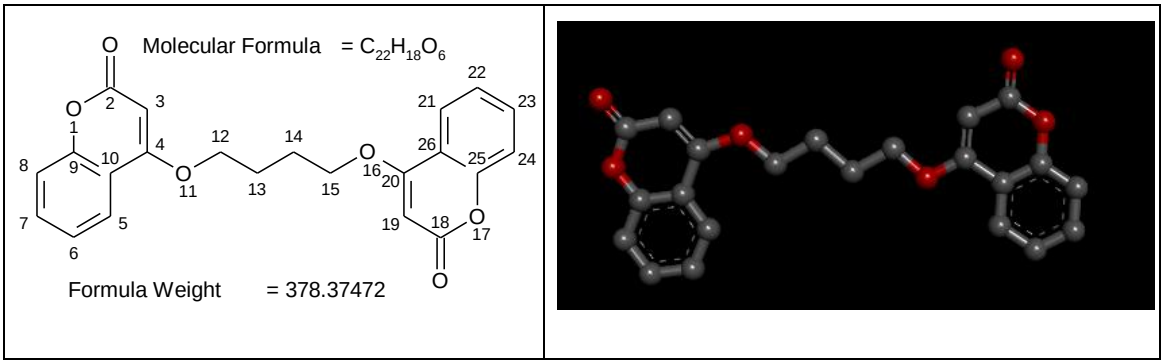

In a 50 mL flask, 3.08 mmol, 500 mg, 1 mol eqv. 4-hydroxycoumarin; 6.16 mmol, 852 mg, 2 mol eqv. K_2CO_3 and 3.08 mmol, 123 mg, 1 mol eqv. NaH (60 % dispersed in oil) were suspended in 6 - 8 mL DMF. It was stirred for 30 minutes at rt and to this stirred solution, 1.54 mmol, 333. mg / 184 µL, 0.5 mol eqv. 1,4-dibromobutane was slowly added and it was stirred for a further 20 hours at 50 °C (don't exceed 60 °C). The mixture was feiltrated and 40 - 50 mL water was added to the suspension until a white precipitate formed. It was washed with cyclohexane to dispose of the excess DMF. Yield: 195 mg, 0.52 mmol, 16.88 %.

Alternative method:

In a 50 mL flask, 3.08 mmol, 500 mg, 1 mol eqv. 4-hydroxycoumarin; 6.16 mmol, 852 mg, 2 mol eqv. K_2CO_3 and 3.08 mmol, 123 mg, 1 mol eqv. NaH (60 % dispersed in oil) were suspended in 30 mL anhydrous acetonitrile and stirred for 30 minutes at rt. 1.54 mmol, 333 mg. / 184 µL, 0.5 mol eqv. 1,4-dibromobutane was slowly added. Using the microwave reactor, the solution was irradiated according the following preferences: Open vessel with cooling on; Power 200 Watt; Temperature 45 °C; Run Time 1:30 min; Hold Time 1:30 min. It was cooled down between sessions and radiation repeated for another 3 times. The reaction mixture was filtered, concentrated and recrystallised to yield white crystals.

R*f*: 0.282. Mp: 173.2 - 175.2 °C. **^{1}H NMR** (600 MHz, $CDCl_3$, **Annexure A - Spectrum 7**): δ 7.77 (dd, *J* = 7.9, 1.4 Hz, 2H, $H_{5,21}$); 7.56 – 7.49 (m, 2H, $H_{7,23}$); 7.28 - 7.20 (m, 4H, $H_{8,24,6,22}$); 5.66 (s, 2H, $H_{3,19}$); 4.29 (bs, 2H, $H_{12,15}$); 2.23 (bs, 2H, $H_{13,14}$); 1.63 (s, 2H, H_2O; $CDCL_3$). **^{13}C NMR** (151 MHz, $CDCl_3$, **Annexure A - Spectrum 8**): δ 165.37 ($C_{4,20}$); 162.77 ($C_{2,18}$); 153.26 ($C_{9,25}$); 132.53 ($C_{7,23}$); 123.90 ($C_{5,21}$); 122.71 ($C_{6,22}$); 116.82 ($C_{8,24}$); 115.47 ($C_{10,26}$); 90.66 ($C_{3,19}$); 68.66 ($C_{12,15}$); 25.38 ($C_{13,14}$). **MS**: EIMS 315; EI-HRMS *m*/*z*: calculated for **$C_{22}H_{18}O_6$**, 378.3747, found 379.1206 (**Annexure B - Spectrum 32**). Yield: 418 mg, 1.10 mmol, 35.71 %. (211.552 % increase in yield).

3.5.5. 4,4'-[Propane-1,3-diylbis(oxy)]bis(2*H*-chromen-2-one) (BPR 5).

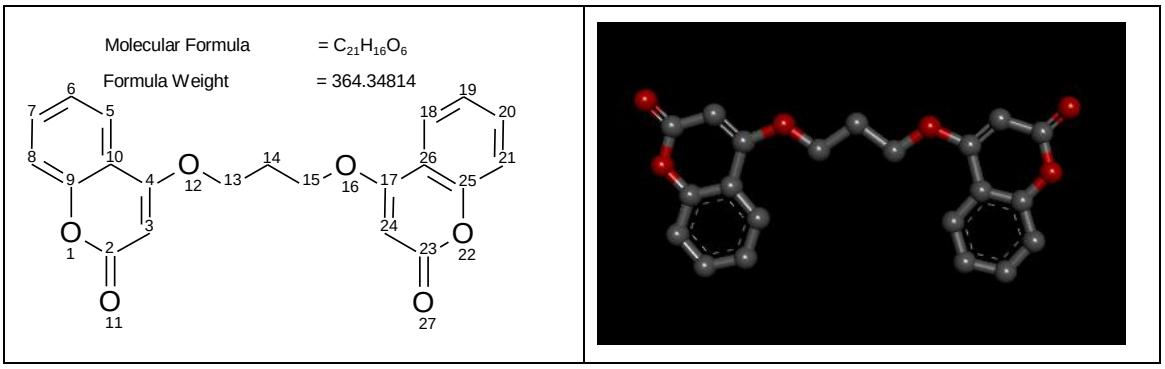

In a 50 mL flask, 3.08 mmol, 500 mg, 1 mol eqv. 4-hydroxycoumarin; 6.16 mmol, 852 mg, 2 mol eqv. K_2CO_3 and 3.08 mmol, 123 mg, 1 mol eqv. NaH (60 % dispersed in oil) were suspended in 6 - 8 mL DMF and stirred for 30 minutes at rt. Next, 1.54 mmol, 311 mg. / 157 µL, 0.5 mol eqv. 1,3-dibromopropane was slowly added and it was stirred for 18 hours at 50 °C. The solution was filtered and 25 mL water was added until a precipitate formed. The white precipitate was washed with cyclohexane to remove the excess DMF. Yield: 186 mg, 0.51 mmol, 16.56 %.

Alternative method:

In a 50 mL flask, 3.08 mmol, 500 mg, 1 mol eqv. 4-hydroxycoumarin; 6.16 mmol, 852 mg, 2 mol eqv. K_2CO_3 and 3.08 mmol, 123 mg, 1 mol eqv. NaH (60 % dispersed in oil) were combined in 30 mL anhydrous acetonitrile and stirred for 30 minutes at rt. To the solution, 1.54 mmol, 311 mg. / 157 µL, 0.5 mol eqv. 1,3-dibromopropane was slowly added. Using the microwave reactor, the mixture was irradiated with the following preferences: Open vessel with cooling on; Power 200 Watt; Temperature 45 °C; Run Time 1:30 min; Hold Time 1:30 min. The suspension was cooled down between sessions and radiation repeated for another 3 times. It was filtered, concentrated and recrystallised - white crystals formed.

R*f*: 0.378. Mp: 203.7 – 205 °C. **^{1}H NMR** (600 MHz, $CDCl_3$, **Annexure A - Spectrum 9**): δ 7.77 (dd, *J* = 7.9, 1.3 Hz, 2H, $H_{5,18}$); 7.56 – 7.48 (m, 2H, $H_{7,20}$); 7.30 (m, 2H, $H_{6,19}$), 7.25 (dd, *J* = 10.1, 5.0 Hz, 2H, $H_{8,21}$); 5.72 (s, 2H, $H_{3,24}$); 4.38 (t, *J* = 5.9 Hz, 2H, $H_{13,15}$); 2.54 (m, 1H, H_{14}); 1.63 (s, 2H, H_2O; $CDCL_3$). **^{13}C NMR** (151 MHz, $CDCl_3$, **Annexure A - Spectrum 10**): δ 165.22 ($C_{4,17}$); 162.66 ($C_{2,23}$); 153.29 ($C_{9,25}$); 132.62 ($C_{7,20}$); 124.03 ($C_{5,18}$); 122.73 ($C_{6,19}$); 116.89 ($C_{8,21}$); 115.37 ($C_{10,26}$); 90.87 ($C_{3,24}$); 65.34 ($C_{13,15}$); 27.95 (C_{14}). **MS**: EIMS 315; EI-HRMS *m*/*z*: calculated for **$C_{21}H_{16}O_6$**, 364.348, found 365.1034 (**Annexure B - Spectrum 33**). Yield: 510 mg, 1.40 mmol, 45.45 %. (274.456 % increase in yield).

3.5.6. 7,7'-[Propane-1,3-diylbis(oxy)]bis(2*H*-chromen-2-one) (BPR6).

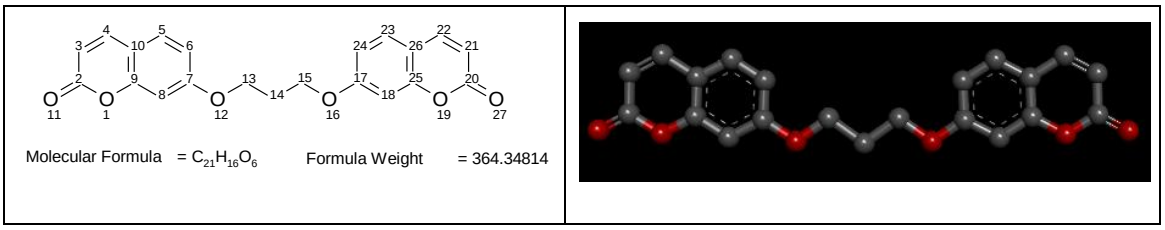

In a 50 mL flask, 3.08 mmol, 500 mg, 1 mol eqv. 7-hydroxycoumarin; 6.16 mmol, 852 mg, 2 mol eqv. K_2CO_3 and 3.08 mmol, 123 mg, 1 mol eqv. NaH (60 % dispersed in oil) was suspended in 6 – 8 mL DMF and stirred for 30 minutes at rt. Portion-wise, 1.54 mmol, 311 mg. / 157 µL, 0.5 mol eqv. 1,3-dibromopropane was added and stirred for 18 hours at 50 °C. The solution was filtered and 25 mL of water was added until a precipitate formed. The precipitate was washed with cyclohexane to dispose of the excess DMF. Yield: 186 mg, 0.52 mmol, 16.88 %.

Alternative method:

In a 50 mL flask, 3.08 mmol, 500 mg, 1 mol eqv. 7-hydroxycoumarin; 6.16 mmol, 852 mg, 2 mol eqv. K_2CO_3 and 3.08 mmol, 123 mg, 1mol eqv. NaH (60% dispersed in oil) in 30 mL anhydrous acetonitrile were combined and stirred for 30 minutes at rt. To this solution, 1.54 mmol, 311 mg. / 157 µL, 0.5 mol eqv. 1,3-dibromopropane was added. Implementing the microwave reactor, the suspension was irradiated according the following preferences: Open vessel with cooling on; Power 200 Watt; Temperature 45 °C; Run Time 1:30 min; Hold Time 1:30 min. The reaction was cooled down between sessions and radiation repeated for an additional 3 times. It was then filtered and concentrated - a white precipitate formed.

R*f*: 0.359. Mp: 177 – 180 °C. **^{1}H NMR** (600 MHz, $CDCl_3$, **Annexure A - Spectrum 11**): δ 7.61 (d, *J* = 9.5 Hz, 2H,$H_{4, 22}$); 7.35 (d, *J* = 8.6 Hz, 2H,$H_{5, 23}$); 6.88 (dd, J = 8.6, 2.4 Hz, 2H, $H_{6, 24}$); 6.73 (s, 2$H_{8, 18}$); 6.23 (d, *J* = 9.5 Hz, 2H,$H_{3, 21}$); 4.21 (t, *J* = 6.0 Hz, 4H, $H_{13, 15}$); 2.32 (m, 2H, H_{14}); 1.64 (s, 2H, H_2O; $CDCL_3$). **^{13}C NMR** (151 MHz, $CDCl_3$, **Annexure A - Spectrum 12**): δ 161.89 ($C_{7,17}$); 161.15 ($C_{2,20}$); 155.82 ($C_{9,25}$); 143.36 ($C_{4,22}$), 128.80 ($C_{5,23}$), 113.19 ($C_{6,21}$); 112.87 ($C_{3,24}$), 112.36 ($C_{10.26}$), 101.37 ($C_{8,18}$), 64.66 ($C_{13, 15}$), 28.77 (C_{14}). **MS**: EIMS 315; EI-HRMS *m*/*z*: calculated for **$C_{21}H_{16}O_6$**, 364.3481, found 365.1042 (**Annexure B - Spectrum 34**). Yield: 405 mg, 1.11 mmol, 36.04 % (213.351 % increase in yield).

3.5.7. 7,7'-[Propane-1,3-diylbis(oxy)]bis(4-methyl-2*H*-chromen-2-one) (BPR7).

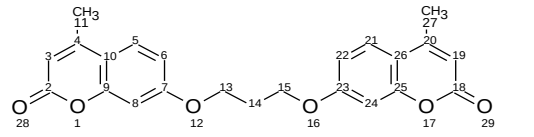

Formula Weight = 392.4013 Molecular Formula = $C_{23}H_{20}O_6$

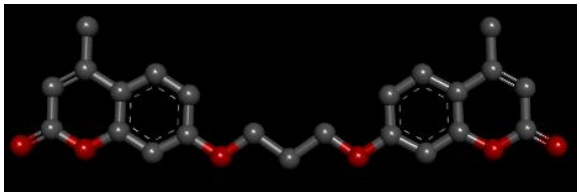

A mixture of 3.41 mmol, 600 mg, 1 mol eqv. 4-methylated-7-hydroxycoumarin; 6.82 mmol, 941 mg, 2 mol eqv. K_2CO_3 and 3.08 mmol, 136 mg, 1 mol eqv. NaH (60 % dispersed in oil) was suspended in 10 mL DMF and stirred for 30 min at rt. To the solution, 1.70 mmol, 344 mg. / 173 µL, 0.5 mol eqv. 1,3-dibromopropane was added and it was stirred for 20 hours at 50 °C. The reaction mixture was purified using column chromatography DCM:Cyclohexane (9:1). After completion, it was concentrate and recrystallised, a white crystalline solid formed.
Yield: 197 mg, 0.50 mmol, 14.66 %.

Alternative method:

In 30 mL anhydrous acetonitrile, 3.41 mmol, 600 mg, 1 mol eqv. 4-methylated-7-hydroxycoumarin; 6.82 mmol, 941 mg, 2 mol eqv. K_2CO_3 and 3.08 mmol, 136 mg, 1 mol eqv. NaH (60 % dispersed in oil) were suspended and stirred for 30 min at rt. Afterwards, 1.70 mmol, 344 mg. / 173 µL, 0.5 mol eqv. 1,3-dibromobutane was slowly added. The suspension was irradiated according the following preferences: Open vessel with cooling on; Power 200 Watt; Temperature 45 °C; Run Time 1:30 min; Hold Time 1:30 min. The reaction was cooled down between sessions and radiation repeated for an additional 3 times. It was then filtered, concentrated and recrystallised - white crystals formed.
R*f*: 0.208. Mp: 183.5 – 186 °C. **^{1}H NMR** (600 MHz, $CDCl_3$, **Annexure A - Spectrum 13**): δ 7.47 (d, *J* = 7.0 Hz, 2H, $H_{5, 21}$); 6.86 (dd, J = 8.8. 2.5 Hz, 2H, $H_{6,22}$); 6.80 (d, *J* = 2.5 Hz, 2H,$H_{8,24}$) 6.11 (s, 2H,$H_{3, 19}$); 4.58 (m, 4H, $H_{13,15}$); 5.42 (dd, *J* = 17.3, 1.4 Hz, 2H, H_{14}); 2.37 (s, 6H, $H_{11,27}$); 1.26 (s, 2H, H_2O; $CDCL_3$). **^{13}C NMR** (151 MHz, $CDCl_3$, **Annexure A - Spectrum 14**): δ 161.54 (C2, 18); 161.29 (C7, 23); 155.18 (C9, 25); 152.52 (C4, 20); 132.15 (C5, 21); 125.51 (C10, 26); 118.52 (C6, 22); 112.78 (C3, 19); 112.00 (C8, 24); 101.70 (C13, 15); 69.20 (C14); 18.67 (C11, 27). **MS**: EIMS 315; EI-HRMS *m*/*z*: calculated for **$C_{23}H_{20}O_6$**, 392.4013, found 391.2808 (**Annexure B - Spectrum 35**). Yield: 495 mg, 1.26 mmol, 36.95 % (252.046 % increase in yield).

3.5.8. 2-Oxo-2*H*-chromen-7-yl thiophene-2-carboxylate. (BPR8).

Formula Weight = 272.27592

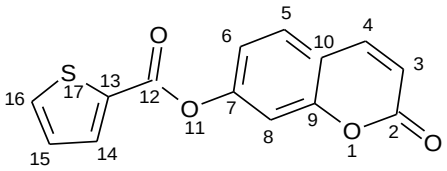

Molecular Formula = $C_{14}H_8O_4S$

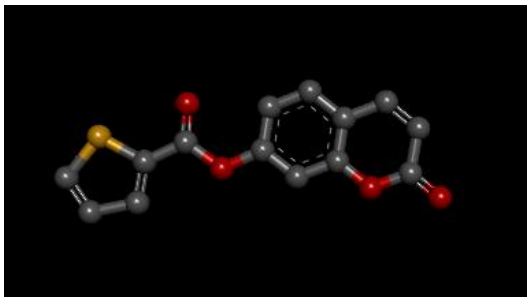

First off, activation chemistry was implemented by suspending 3.90 mmol, 500mg, 1 mol eqv 2-thiophenecarboxylic acid (TP) and 5.07 mmol, 822 mg, 1.3 mol eqv. N.N'-carbonyldiimidazole (CDI) in 30 mL dry DCM. The solution was stirred for 2 - 4 hours at rt. and the solvent removed *in vacuo*. To the residue obtained, 3.90 mmol, 632 mg, 1 mol eqv 7-hydroxycoumarin and 7.80 mmol 1078 mg, 2 mol eqv. K_2CO_3 in 40 mL THF was added and it was stirred for an additional 20 hours at 40 °C. The reaction was cooled down, extracted with 2 X 60 mL ethyl acetate and dried using magnesium sulphate. The solution was filtered, dried and purified with column chromatography using DCM:Cyclohexane (9:1). It was further concentrated and recrystallised – a white crystalline solid formed.

R*f*: 0.358. Mp: 145 - 146.2 °C. **^{1}H NMR** (600 MHz, Acetone; **Annexure A - Spectrum 15**): δ 8.04 (dd, *J* = 3.8, 1.2 Hz, 1H, H_{14}); 8.03 – 8.01 (m, 1H, H_4); 8.01 (d, *J* = 1.1 Hz, 1H, H_{16}); 7.78 (d, *J* = 6.6 Hz, 1H, H_5); 7.36 (m, 1H, H_{15}); 7.31 (dd, J = 3.4, 2.1 Hz, 1H, H_6); 7.30 (dd, *J* = 6.9, 1.4 Hz, 1H, H_8); 6.42 (dd, *J* = 9.6, 3.9 Hz, 1H, H_3); 2.12 – 1.96 (m, 2H, H_2O; Acetone). **^{13}C NMR** (151 MHz, DMSO, **Annexure A - Spectrum 16**): δ159.61 (C_2); 154.11 (C_7); 152.51 (C_{12}); 143.82 (C_9); 135.82 (C_4); 135.65 (C_{13}); 131.31 (C_{16}); 129.45 (C_5); 128.83 (C_{15}); 118.72 (C_6); 116.97 (C_{10}); 115.74 (C_3); 110.35 (C_8). **MS**: EIMS 315; EI-HRMS *m/z*: calculated for **$C_{16}H_{18}SO_4$**, 272.2759, found 273.0218 (**Annexure B - Spectrum 36**). Yield: 402 mg, 1.48 mmol, 37.95 %.

3.5.9. 4-[2-(Piperidin-1-yl)ethoxy]-2*H*-chromen-2-one. (BPR9)

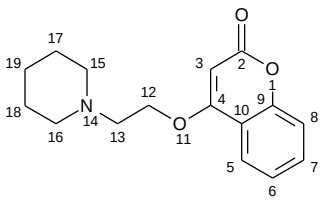

Formula Weight = 273.32696 Molecular Formula = $C_{16}H_{19}NO_3$

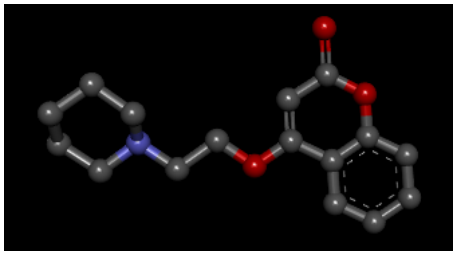

In a 100 mL flask equipped with a cooler, 7.40 mmol, 1362 mg, 1.2 mol eqv. 1-(2-chloroethyl) piperidine hydrochloride; 6.17 mmol, 1000 mg, 1 mol eqv. 4-hydroxycoumarin and 12.33 mmol, 1700 mg, 2 mol eqv. K_2CO_3 were suspended in 75 mL dry Acetonitrile. The reaction was refluxed for 10 hours at 80 °C, cooled down, filtered and evaporated under vacuum. The filtrate was then extracted with 100 mL water and 2 x 30 mL ethyl acetate. The combined organic fractions were collected, dried, filtered and concentrated to a volume of ~ 5 mL. Following recrystallision at rt., bulky, yellow crystals formed.

R*f*: 0.548. Mp: 117 – 118 °C. **^{1}H NMR** (600 MHz, $CDCl_3$, **Annexure A - Spectrum 17**): δ 7.78 (dd, *J* = 7.9, 1.5 Hz, 1H, H_5); 7.54 - 7.50 (m, 1H, H_7); 7.29 (dd, *J* = 8.3, 0.6 Hz, 1H, H_6); 7.24 (m, 1H, H_8); 5.66 (s, 1H, H_3); 4.23 (t, *J* = 5.8 Hz, 2H, H_{12}); 2.86 (t, *J* = 5.8 Hz, 2H, H_{13}); 2.51 (s, 4H, $H_{15,16}$); 1.61 - 1.55 (m, 4H, $H_{17,18}$); 1.46 – 1.39 (m, 2H, H_{19}). **^{13}C NMR** (151 MHz, $CDCl_3$, **Annexure A - Spectrum 18**): δ 165.51 (C_4); 162.88 (C_2); 153.30 (C_9); 132.34 (C_7); 123.84 (C_5); 123.04 (C_6); 116.74 (C_8); 115.69 (C_{10}); 90.57 (C_3); 67.70 (C_{12}); 57.01 (C_{13}); 55.01 ($C_{16,15}$); 25.95 ($C_{17,18}$); 24.01(C_{19}). **MS**: EIMS 315; EI-HRMS *m*/*z*: calculated for **$C_{16}H_{19}NO_3$**, 273.3270, found 274.1429 (**Annexure B - Spectrum 37**). Yield: 635 mg, 2.32 mmol, 31.35 %.

3.5.10. 4-[2-(Morpholin-4-yl)ethoxy]-2*H*-chromen-2-one. (BPR10).

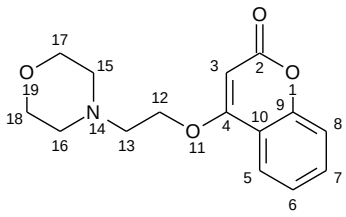

Molecular Formula = $C_{15}H_{17}NO_4$ Formula Weight = 275.29978

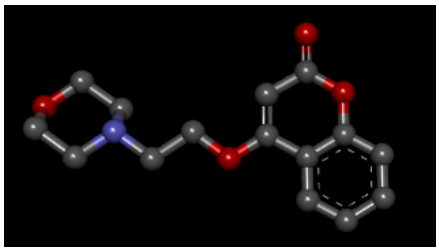

Using a 100 mL flask, 7.40 mmol, 1378 mg, 1.2 mol eqv. 4-(2-chloroethyl) morpholine hydrochloride; 6.17 mmol, 1000 mg, 1 mol eqv. 4-hydroxycoumarin and 12.33 mmol, 1.70 mg, 2 mol eqv. K_2CO_3 were combined with a mixture of 75 mL anhydrous acetonitrile and 5 mL acetone. The reaction was refluxed for at 80 °C for 5 hours, cooled down, filtered and evaporated to dryness. The filtrate was extracted with 100 mL water and 2 x 30 mL ethyl acetate. The organic fractions were combined, dried and filtered. The filtrate was concentrated and recrystallised at 5 °C. Dark, yellow needles formed.

R*f*: 0.622. Mp: 121.3 – 122 °C. **^{1}H NMR** (600 MHz, $CDCl_3$. **Annexure A - Spectrum 19**): δ 7.76 (dd, *J* = 7.9, 1.5 Hz, 1H, H_5); 7.54 – 7.50 (m, 1H, H_7); 7.29 (d, *J* = 8.3 Hz, 1H, H_6); 7.27 – 7.23 (m, 1H, H_8); 5.66 (s, 1H, H_3); 4.24 (t, *J* = 5.5 Hz, 2H, H_{12}); 3.72 – 3.69 (m, 4H, $H_{17,18}$); 2.89 (t, *J* = 5.5 Hz, 2H, H_{13}); 2.60 – 2.56 (m, 4H, $H_{15,16}$). **^{13}C NMR** (151 MHz, $CDCl_3$, **Annexure A - Spectrum 20**): δ 165.38 (C_4); 162.75 (C_2); 153.28 (C_9); 132.48 (C_7); 123.86 (C_5); 122.92

(C_6); 116.78 (C_8); 115.57 (C_{10}); 90.63 (C_3); 67.45 ($C_{17,18}$); 66.86 (C_{12}); 56.69 (C_{13}); 53.99 ($C_{15,16}$). **MS**: EIMS 315; EI-HRMS *m*/*z*: calculated for **$C_{15}H_{17}NO_4$**, 275.2998, found 278.1229 (**Annexure B - Spectrum 38**). Yield: 583 mg, 2.18 mmol, 29.46 %

3.5.11. 7-[2-(Morpholin-4-yl)ethoxy]-2*H*-chromen-2-one (BPR 11).

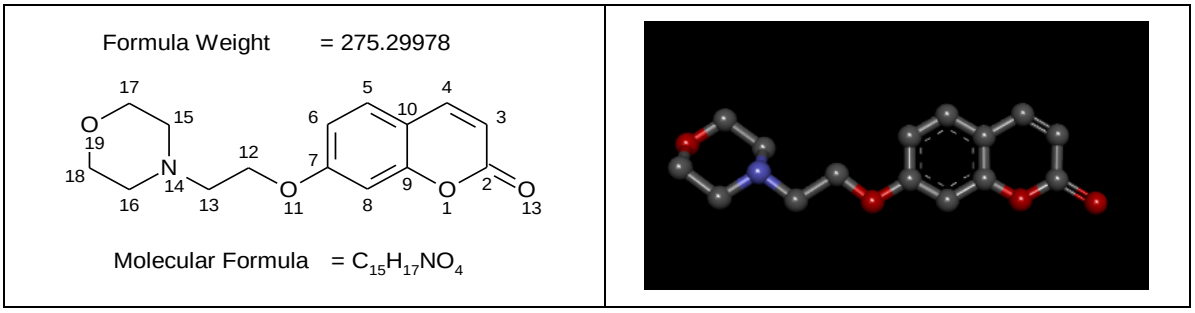

In a 100 mL flask, 6.16 mmol, 1705 mg, 1 mol eqv. 4-(2-chloroethyl) morpholine hydrochloride; 6.17 mmol, 1000 mg, 1 mol eqv. 7-hydroxycoumarin and 12.33 mmol, 1170 mg, 2 mol eqv. K_2CO_3 were suspended in 50 mL anhydrous acetonitrile. The solution was refluxed for 5 hours at 80 °C, cooled down, filtered and evaporated to dryness. The remaining emulsion was extracted with 100 mL brine and 2 x 30 mL ethyl acetate. The combined organic fractions were collected, dried, filtered, concentrated and recrystallised. Dark, yellow needles appeared.

R*f*: 0.216. Mp: 118.6 - 119.1 °C. **^{1}H NMR** (600 MHz, $CDCl_3$, **Annexure A - Spectrum 21**): δ 7.61 (d, *J* = 9.5 Hz, 1H, H_4); 7.34 (d, *J* = 8.6 Hz, 1H, H_5); 6.83 (dd, *J* = 8.6, 2.4 Hz, 1H, H_6); 6.79 (d, *J* = 2.4 Hz, 1H, H_8); 6.23 (d, *J* = 9.5 Hz, 1H, H_3); 4.13 (t, *J* = 5.6 Hz, 2H, H_{12}); 3.74 – 3.68 (m, 4H, $H_{17,18}$); 2.81 (t, *J* = 5.6 Hz, 2H, H_{13}); 2.56 (s, 4H, $H_{15,16}$). **^{13}C NMR** (151 MHz, $CDCl_3$, **Annexure A - Spectrum 22**): δ 161.87 (C_7); 161.14 (C_2); 155.81 (C_9); 143.34 (C_4); 128.74 (C_5); 113.19 (C_{10}); 112.97 (C_6); 112.63 (C_3); 101.43 (C_8); 66.85 ($C_{17,18}$); 66.40 (C_{12}); 57.28 (C_{13}); 54.07 ($C_{15,16}$). **MS**: EIMS 315; EI-HRMS *m*/*z*: calculated for **$C_{15}H_{17}NO_4$**, 275.2999, found 276.1217 (**Annexure B - Spectrum 39**). Yield: 709 mg, 2.58 mmol, 41.88 %.

3.5.12. 7-[2-(Piperidin-1-yl)ethoxy]-2*H*-chromen-2-one (BPR 12).

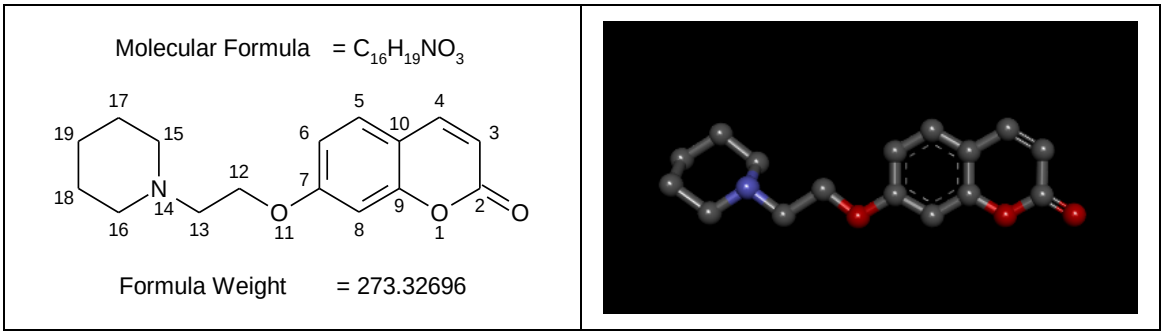

In a 100 mL flask equipped with a cooler, 6.17 mmol, 1135 mg, 1 mol eqv. 1-(2-chloroethyl) piperidine hydrochloride; 6.17 mmol, 1000 mg, 1 mol eqv. 7-hydroxycoumarin and 12.33 mmol, 1705 mg, 2 mol eqv. K_2CO_3 were suspended in 50 mL anhydrous acetonitrile. The reaction was refluxed at 80 °C for 3 hours, cooled down, filtered and evaporated to dryness. The remaining residue was extracted with 100 mL brine and 2 x 30 mL ethyl acetate. The collected combined organic fractions were dried, filtered and concentrated to a volume of ~ 5 mL. It was recrystallised and bulky, yellow crystals were produced.

R*f*: 0.164. Mp: 89.4 - 90.5 °C. **^{1}H NMR** (600 MHz, $CDCl_3$, **Annexure A - Spectrum 23**): δ 7.60 (d, *J* = 9.5 Hz, 1H, H_4); 7.33 (d, *J* = 8.6 Hz, 1H, H_5); 6.82 (dd, *J* = 8.6, 2.4 Hz, 1H, H_6); 6.79 (d, *J* = 2.4 Hz, 1H, H_8); 6.21 (d, *J* = 9.5 Hz, 1H, H_3); 4.12 (t, *J* = 6.0 Hz, 2H, H_{12}); 2.76 (t, *J* = 6.0 Hz, 2H, H_{13}); 2.47 (bs, 4H, $H_{15,16}$); 1.60 – 1.55 (m, 4H, $H_{17,18}$); 1.42 (bs, 2H, H_{19}). **^{13}C NMR** (151 MHz, $CDCl_3$, **Annexure A - Spectrum 24**): δ 162.05 (C_7); 161.21 (C_2); 155.81 (C_9); 143.38 (C_4); 128.67 (C_5); 113.03 (C_3); 112.98 (C_6); 112.50 (C_{10}); 101.48 (C_8); 66.63 (C_{12}); 57.58 (C_{13}); 55.06 ($C_{15,\ 16}$); 25.88 ($C_{17,\ 18}$); 24.09 (C_{19}). **MS**: EIMS 315; EI-HRMS *m*/*z*: calculated for **$C_{16}H_{19}NO_3$**, 273.3267, found 274.1434 (**Anneture B - Spectrum 40**). Yield: 307 mg, 1.12 mmol, 18.15 %.

3.5.13. 4-Methyl-7-[2-(Piperidin-1-yl)ethoxy]-2*H*-chromen-2-one (BPR 13).

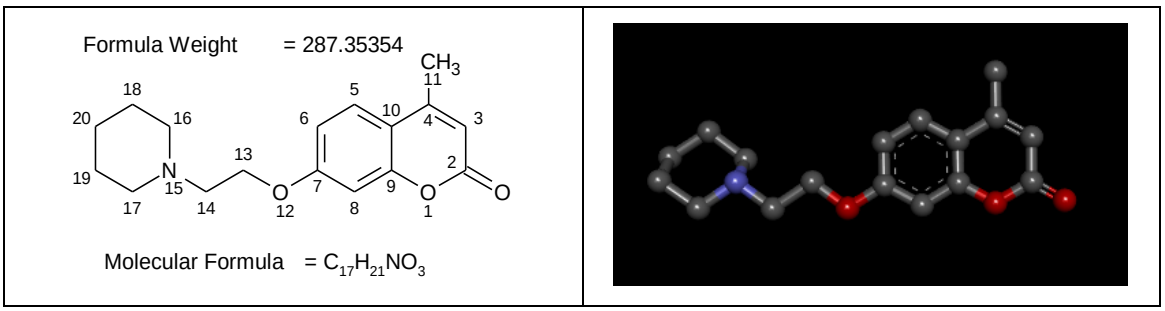

A combination of 3.41 mmol, 1600 mg, 1 mol eqv. 4-methylated-7-hydroxycoumarin and 6.81 mmol, 941 mg, 2 mol eqv. K_2CO_3 was suspended in 30 mL Acetonitrile in a 50 mL flask equipped with a cooler, and stirred for 30 minutes at rt. To this solution, 4.09 mmol, 752 mg, 1.2 mol eqv. 1-(2-chloroethyl) piperidine hydrochloride; was added portion-wise. Next, it was refluxed for 3 hours at 80 °C, cooled down, filtered and evaporated to dryness. The remaining residue was extracted with 100 mL brine and 2 x 30 mL ethyl acetate. The combined organic fractions were dried, filtered, concentrated and recrystallised. Yellow crystals formed.

R*f*: 0.315. Mp: 102 – 104 °C. **^{1}H NMR** (600 MHz, $CDCl_3$, **Annexure A - Spectrum 25**): δ 7.44 (d, *J* = 8.8 Hz, 1H, H_5), 6.82 (dd, *J* = 8.8, 2.4 Hz, 1H, H_6), 6.76 (d, *J* = 2.4 Hz, 1H, H_8), 6.08 (d, *J* = 0.9 Hz, 1H, H_3), 4.12 (t, *J* = 5.9 Hz, 2H, H_{13}), 2.76 (t, *J* = 5.9 Hz, 2H, H_{14}), 2.48

(bs, 4H, $H_{16,17}$), 2.35 (d, *J* = 1.0 Hz, 3H, H_{11}), 1.58 (m, 4H, $H_{18,19}$), 1.41 (bs, 2H, H_{20}). **^{13}C NMR** (151 MHz, $CDCl_3$, **Annexure A - Spectrum 26**): δ 161.77 (C_7); 161.23 (C_2); 155.13 (C_9); 152.48 (C_4), 125.42 (C_5), 113.52 (C_3), 112.56 (C_6), 111.85 (C_{10}), 101.48 (C_8), 66.44 (C_{12}), 57.52 (C_{13}), 55.00 ($C_{16,17}$), 25.76 ($C_{18,19}$), 24.00 (C_{20}), 18.60 (C_{11}). **MS**: EIMS 315; EI-HRMS *m*/*z*: calculated for **$C_{17}H_{21}NO_3$**, 287.353, found 288.1593 (**Anneture B - Spectrum 41**). Yield: 810 mg, 2.82 mmol, 82.70 %.

3.5.14. 4-Methyl-7-[2-(morpholin-4-yl)ethoxy]-2*H*-chromen-2-one (BPR 14).

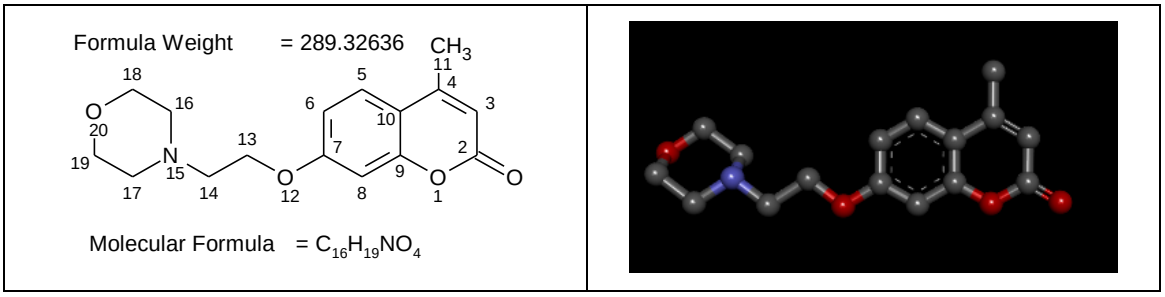

In a 50 mL flask, 4.09 mmol, 761 mg, 1.2 mol eqv. 4-(2-chloroethyl) morpholine hydrochloride; 3.41 mmol, 600 mg, 1.2 eqv. 4-methylated-7-hydroxycoumarin and 6.81 mmol, 941 mg, 2 mol eqv. K_2CO_3 was mixed in 30 mL anhydrous acetonitrile. The reaction was refluxed for 5 hours at 80 °C (the solution turns from white to light yellow), cooled down, filtered and evaporated to dryness. Following extraction with 100 mL brine and 2 x 30 mL Ethyl Acetate, the combined organic fractions was dried and filtered. The filtrate was concentrated and recrystallised at -2 °C until dark yellow, bulky crystals appeared.

R*f*: 0.381. Mp: 110.4 - 112.4 °C. **^{1}H NMR** (600 MHz, $CDCl_3$, **Annexure A - Spectrum 27**): δ 7.45 (d, *J* = 8.8 Hz, 1H, H_5), 6.82 (dd, *J* = 17.4, 8.7 Hz, 1H, H_6), 6.76 (d, *J* = 7.5 Hz, 1H, H_8), 6.09 (d, *J* = 0.9 Hz, 1H, H_3), 4.13 (t, *J* = 5.6 Hz, 2H, H_{13}), 3.78 – 3.60 (m, 4H, $H_{18,19}$), 2.80 (t, *J* = 5.6 Hz, 2H, H_{14}), 2.56 (m, 4H, $H_{16,17}$), 2.34 (dd, *J* = 16.2, 0.9 Hz, 3H, H_{11}). **^{13}C NMR** (151 MHz, $CDCl_3$, **Annexure A - Spectrum 28**): δ 161.60 (C_7), 161.20 (C_2), 155.12 (C_9), 152.49 (C_4), 125.49 (C_5), 113.64 (C_{10}), 112.58 (C_6), 111.95 (C_3), 101.40 (C_8), 66.74 (C_{13}), 66.20 ($C_{18,19}$), 57.23 (C_{14}), 53.99 ($C_{16,17}$), 18.60 (C_{11}). **MS**: EIMS 315; EI-HRMS *m*/*z*: calculated for **$C_{16}H_{19}NO_4$**, 289.3264, found 290.1380 (**Annexure B - Spectrum 42**). Yield: 390 mg, 1.35 mmol, 39.59 %.

3.6. CONCLUSION.

The synthesis of 14 novel coumarin conjugates [(coumarin(s) - esters and ethers were successfully accomplished. The yields ranged from 18.83 % [(**3.5.4.** 4,4'-[Butane-1,4-diylbis(oxy)]bis(2*H*-chromen-2-one)] to 28.89 % [(**3.5.5**. 4,4'-[Propane-1,3-diylbis(oxy)]bis(2*H*-chromen-2-one).]. The lower yields were attributed to the formation of by-products, lack of activation energy during and/or degradation of the novel compounds during synthetic procedures as well as inadequate purification. Optimisation of the various synthetic methods developed can further be advanced.

The more economical modified microwave-assisted synthesis improved both time and yield, e.g. an improved feasibility of 28.89 % [(**3.5.5** -. 4,4'-[propane-1,3-diylbis(oxy)]bis(2*H*-chromen-2-one)]. This is also a positive factor concerning further possibly of industrialisation/marketing of the product(s).

Structural confirmation was obtained using the analytical instrumentation and methods described in section 3.5 (TLC, Mp, MS, ^{1}HNMR and ^{13}CNMR). The R*f* value calculated using different concentrations of DCM:Cyclohexane as mobile phase, as well as the change in the 7-hydroxycoumarin's unique fluorescence that can clearly be observed on the TLC. MS, ^{1}HNMR and ^{13}CNMR presented characteristic signals for the specific compounds' structural confirmation.

Biological Evaluation and Molecular Modelling.

Chapter 4

4.1. INTRODUCTION.

In this chapter, an overview of the enzymes utilised in this study has been included, i.e. the enzyme kinetics; enzymology of both MAO-B and AChE. The biostudies conducted on these enzymes using the newly synthesised compounds are presented in the chapter, describing the methodologies and the results. Addtionally molecular modeling as an integral part of medicinal chemistry studies has been included. The modeling studies included computational chemistry investigations on both enzymes and interaction docking studies with selected structures showing the most promising biological results in order gain insite into the inter – relationship between these rudiments of structure and activity.

4.2 MONOAMINE OXIDASE.

Monoamine oxidases (MAO) (EC 1.4.3.4) are a family of enzymes that catalyse the oxidation of monoamines (Tripton *et al*., 2004; Edmondson *et al*., 2004). They are located bound to the mitochondria's outer membrane in most cell types in the body and belong to the flavin-containing amine oxidoreductases family of proteins. In humans there can be distinguished between MAO-A and MAO-B (Grimsby *et al*., 1990; Shih *et al*., 2004) according to their structural differences (refer to **chapter 2 - section 2.2.7**, **figure 2.36** and **table 2.3**) and substrate selectivity (refer to **chapter 2 - section 2.2.7, figure 2.32**): MAO-A catalyses the deamination of serotonin (5-HT), norephinephrine and epinephrine (refer to **chapter 2 - section 2.2.7**; **figure 2.32**) and inhibition results in an anti-depressant and anti-anxiety effect while MAO-B catalyses the deamination of Dopamine, ß-phenylethylamine and benzylamine **(refer to chapter 2 - section 2.2.7**; **figure 2.32**) and inhibition results in anti-PD and anti-AD effects (Ooms *et al*., 2003).

Beneficial properties of MAO-B inhibition include:

i. Decreased ROS formation resulting from metabolism of the biogenic amines, primarily dopamine which generates H_2O_2 causing oxidative Stress. (Cohen *et al*., 1989);
ii. Elevated MAO-B levels are present in the CSF, brain tissue and in the platelets of AD patients (Oreland *et al*., 1986 Riederer *et al.*, 1982);

iii. MAO-B inhibtors (e.g. selegiline) prevent the consequent activation of the environmental pre-toxins (Langston, 1990); and

iv. Its ability of the protective effects against neuronal apoptosis in cell culture (Suuronen *et al*., 2000).

4.2.1. Monoamine oxidase B (MAO-B).

The active site of the MAO-B enzyme (**Figure 4.1**) comprises of two cavities **(Chapter 2 - section 2.2.7**) namely the entrance cavity and the substrate cavity (Hubálek *et al*., 2005). The flavin adenine dinucleotide (FAD) coenzyme, which is covalently bound by an 8α-thioether linkage to CYS397, is at the end of the substrate cavity (Keraney *et al*., 1961).

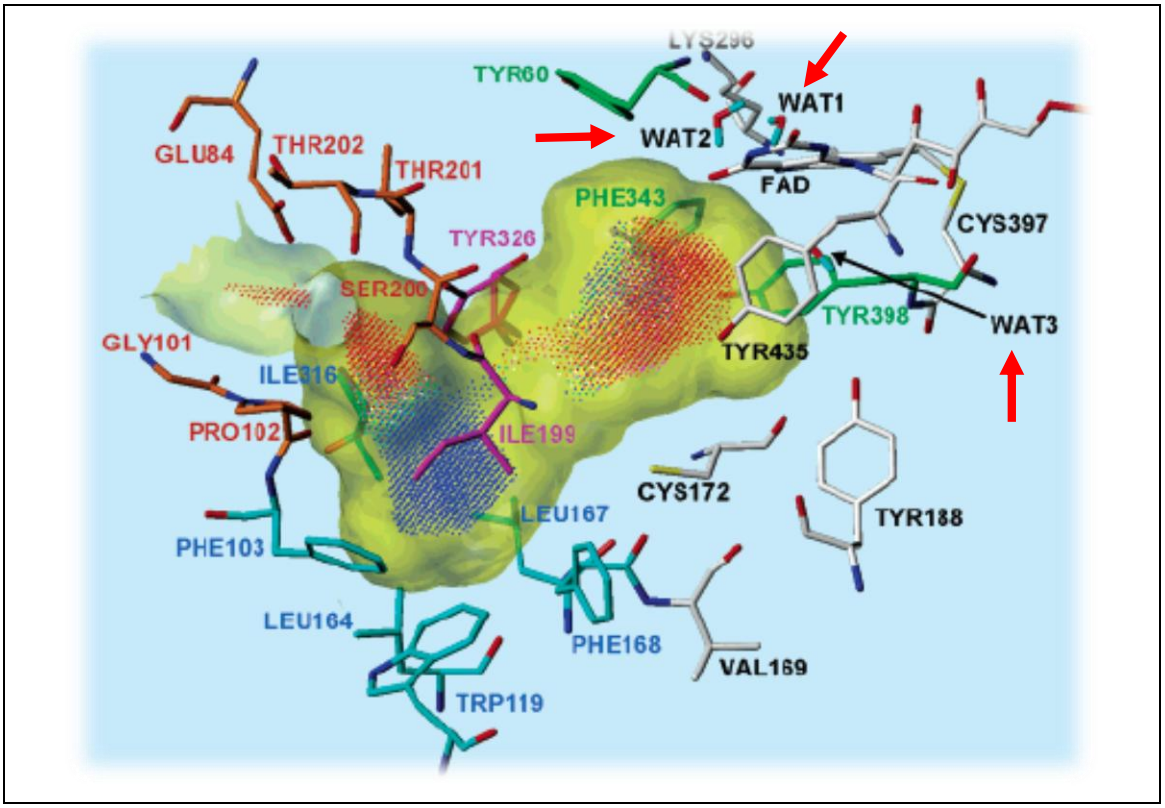

Figure 4:1: Binding site of MAO-B. The Connolly channel surface of the cavities is displayed in translucent yellow. The coloured dots describing the lipophilicity inside the pockets are colour-coded according to their MLP (Molecular lipophilicity potential) values. The amino acids potentially interacting with the ligands are color-coded following their localisation around the binding site. The FAD cofactor and the three selected water molecules (WAT 1, 2, 3; **red arrows**) are represented as an integral part of the MAO-B structure model (Novaroli *et al*., 2006).

The active site is hydrophobic in nature and favourable for amine binding near the FAD. TYR398 and TYR435 forms an 'aromatic cage' (**Figure 4.2**) and has catalytic function as is described in **section 4.2.1.2** (Edmonson *et al*., 2007). For MAO inhibition, the proposed/novel inhibitor should occupy at least the substrate cavity of the enzyme.

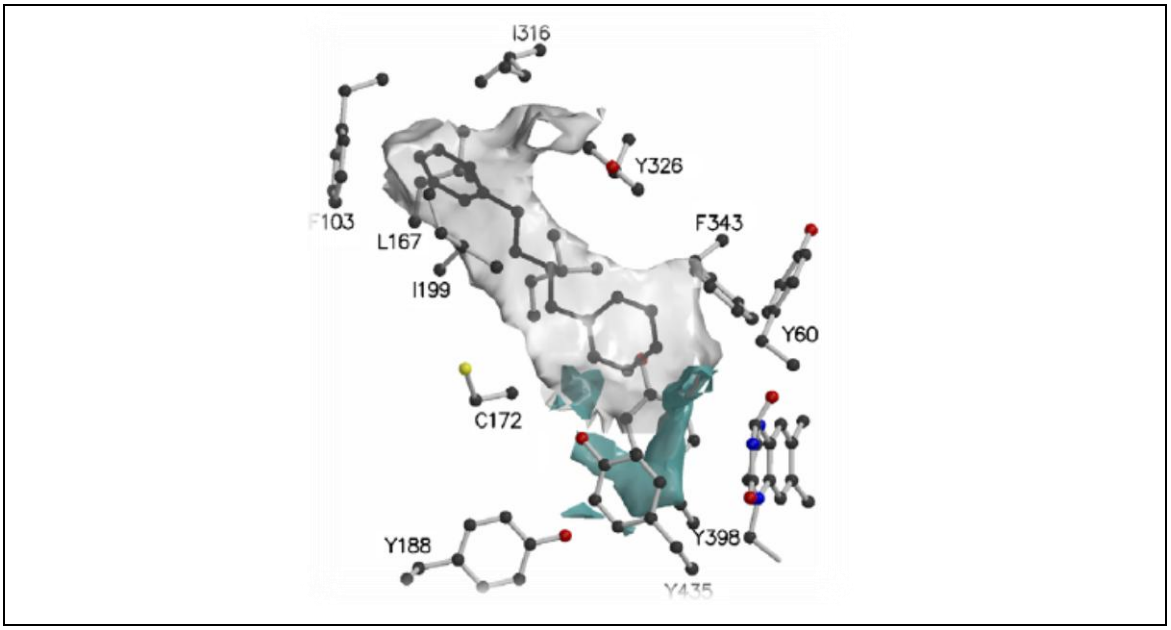

Figure 4:2: Molecular interaction fields, computed with an aromatic sp^2 carbon probe (gray) and a neutral NH_2 probe (cyan), of the coordinates represented by the fused entrance and substrate cavities in the human MAO-B complexed with 1,4-diphenyl-2-butene (Edmondson *et al*., 2007).

4.2.1.1. Mechanistic proposals for monoamine catalysed amine oxidation.

The function of the monoamine oxidase enzyme is to catalyse the α-carbon oxidation of amines to imines and iminium ions with simultaneous reduction of the covalently bound FAD cofactor. The enzyme is regenerated by re-oxidation of the reduced FAD with simultaneous reduction of molecular oxygen to liberate hydrogen peroxide (**Figure 4.3**). One mole of hydrogen peroxide is produced for each mole of substrate being oxidised.

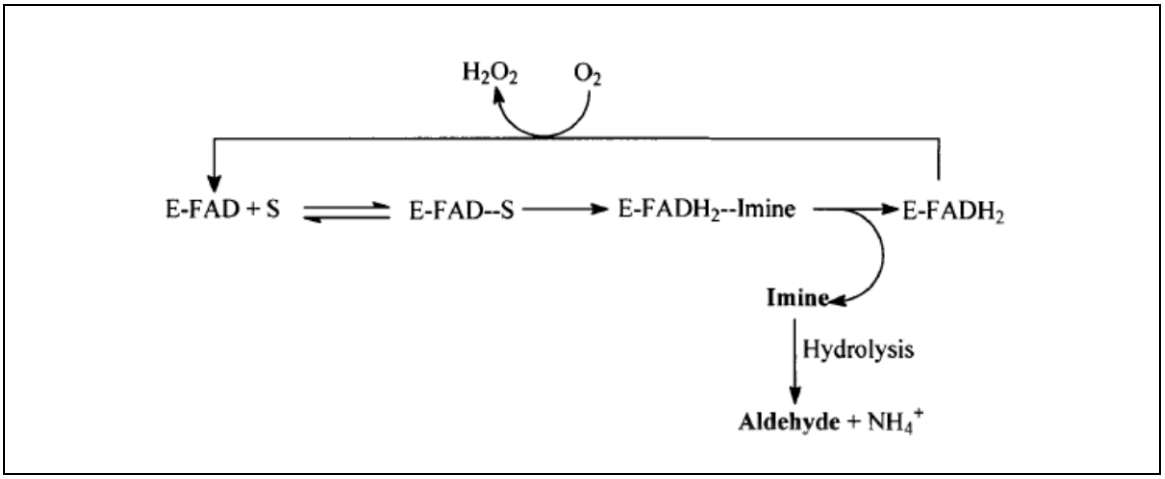

Figure 4:3: The kinetic mechanism of MAO-B. (E-FAD: monoamine oxidase, S: amine, E-$FADH_2$: reduced enzyme) (Edmondson *et al*., 2004).

The catalytic mechanism of MAO-B have been proposed to follow one of two pathways, namely the single electron transfer (SET) or the polar nucleophilic mechanism (Edmondson *et al*., 2007).

4.1.1.1.1. Single Electron Transfer (SET).

The first mechanism is through the single electron transfer (SET) pathway (Silverman, 1995). The mechanism is based on the foundation that one-electron oxidation of the substrate amine nitrogen results in labilisation of the α-CH bond to allow proton abstraction by a basic residue normally associated with proteins. This explains the oxidation observed (**Figure 4.4**) with cyclopropylamine substrate analogues (Lu *et al*., 2002).

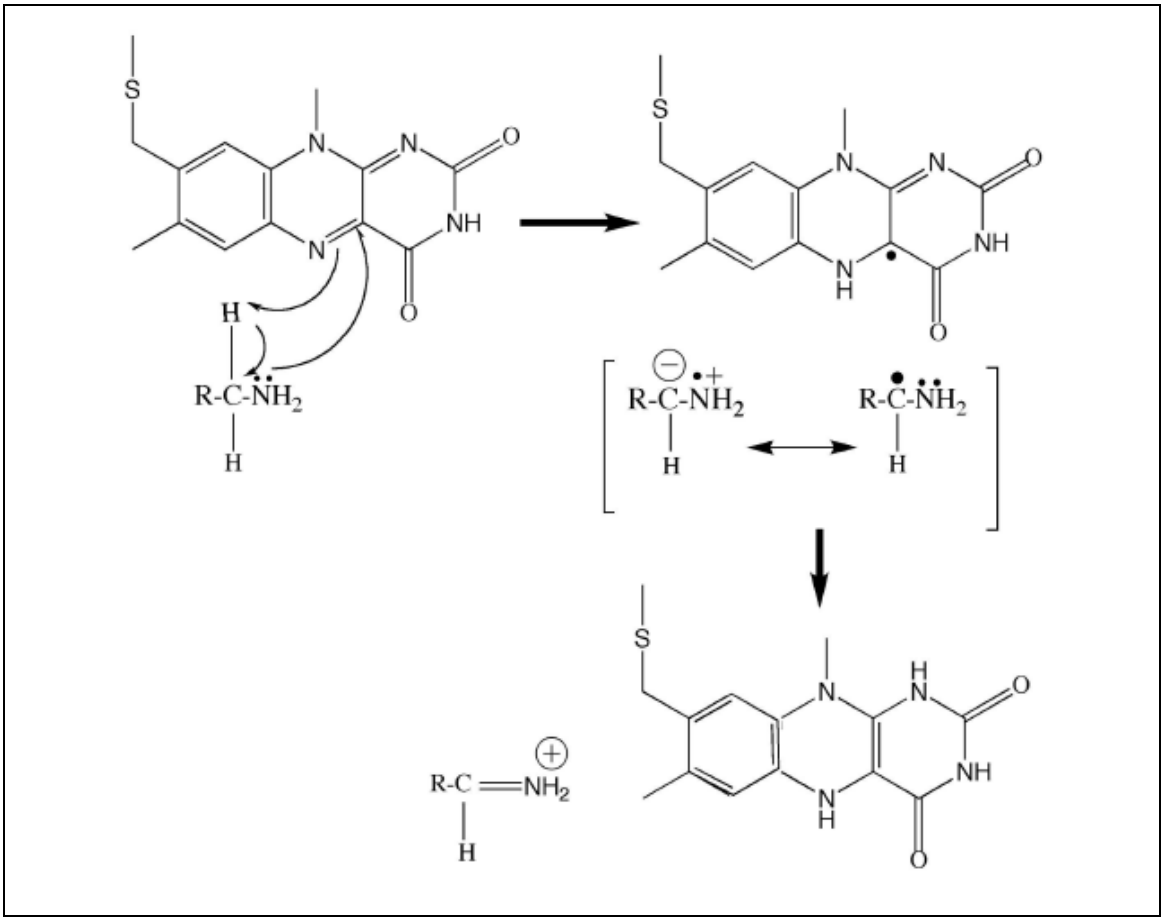

Figure 4:4: The proposed SET mechanism for MAO catalysis - oxidation of the substrate amine nitrogen results in labilisation of the α-CH bond (Lu *et al*., 2002).

According to this mechanism, one electron is transferred from the nitrogen lone pair to the oxidised FAD of MAO and an aminyl radical is generated. Following deprotonation of the α-carbon, a second electron is displaced to the flavin to liberate an iminium ion. Primary iminium ions are hydrolysed to the matching aldehyde **(Figure 4.5)**, hence the terminology oxidative deamination.

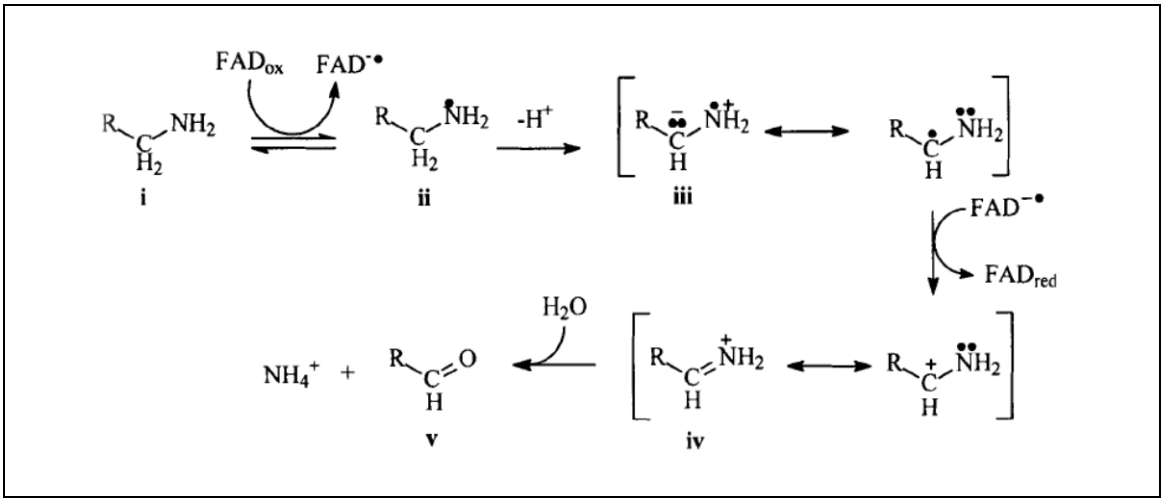

Figure 4:5: The proposed SET pathway - catalysed α-carbon oxidation of amines which produces (**i**) amine; (**ii**) aminyl radical; (**iii**) product after the loss of a proton; (**iv**) iminium ion; (**v**) corresponding aldehyde. (Lu *et al*., 2002).

4.1.1.1.2 Polar Nucleophilic Mechanism.

In the polar nucleophile or group transfer mechanism (**Figure 4.6**), MAO catalysis is postulated to occur *via* nucleophilic ‘‘attack’’ at the oxidised flavin 4α position by the amine. It has been suggested that an amino acid base in the active site facilitates the proton abstraction from the α-carbon of the amine-flavin adduct. The elimination of the reduced flavin results in the formation of the iminium product (Miller *et al*., 1999).

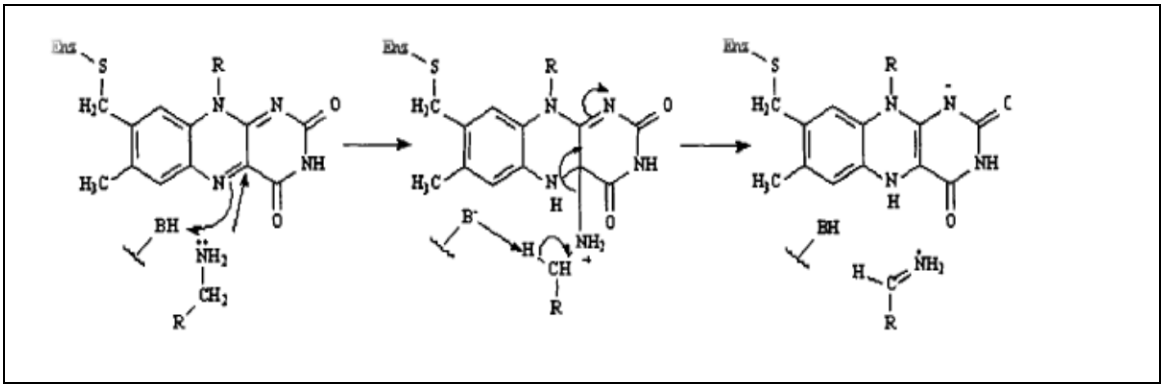

Figure 4:6: The proposed polar nucleophilic pathway for MAO catalysed α-carbon oxidation of amines to yield the corresponding iminium product (Miller *et al*., 1999).

Evidence for the polar nucleophilic mechanism has been based on binding analyses of Farnesol (Hubalék *et al*., 2005). Farnesol binds to MAO-B (**Figure 4.7**) with the OH group located at appropriate distance and angle with respect to the C4α position (3.4 Å and 23°) of the FAD while the α-CH_2 is situated at appropriate distance and angle direction (also 3.4 Å and 24°) of the FAD N5 site (Akyüz *et al*., 2007; Edmondson *et al*., 2007) Thus, Farnesol binds in a catalytically relevant conformation with turnover not being observed due to the lower nucleophilicity of the OH moiety relative to that of an amine group (Edmondson *et al*., 2007).

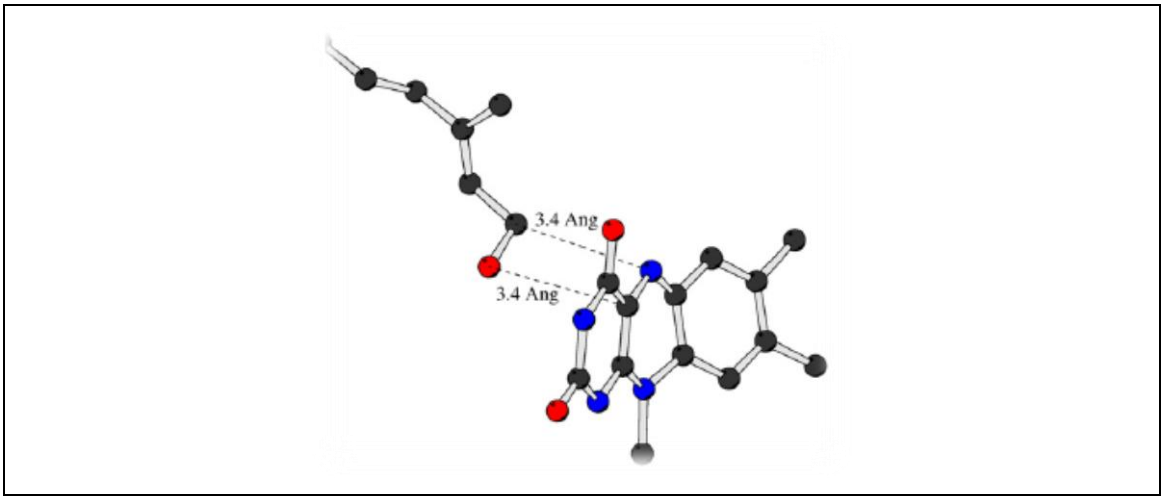

Figure 4:7: The CH_2-OH moiety of bound *trans-trans* Farnesol and the FAD of human MAO-B. The indicated distances are between: the oxygen (red) of Farnesol and the 4α-carbon (black) of the flavin ring, and the α-carbon (black) of Farnesol and the N5 position (blue) of the flavin ring (Edmondson *et al*., 2007).

4.2.1.2 Functional Role of The Aromatic Cage In MAO Catalysis.

Structural studies show that TYR398 and TYR435 in hMAO-B are located at appropriate distance and angle direction of the covalently bound flavin (Binda *et al*., 2002). To investigate the functional roles of these tyrosyl residues in the active site, a number of site directed mutants of TYR435 were expressed in hMAO-B and their structural properties compared (Li *et al*., 2006). These comparisons revealed a correlation exists between K_{cat}/K_m and the interaction energy of the dipole of the substrate amine moiety and the dipole of the substituent at TYR435. The 'aromatic cage' acts to polarise the substrate amine moiety to improve its efficiency (eg. **BPR10 in Figure 4.18, section 4.6.3.1**) as a nucleophile (**Figure 4.8**). It also directs the navigation of the substrate amine towards the reactive positions on the FAD (Akyüz *et al*., 2007).

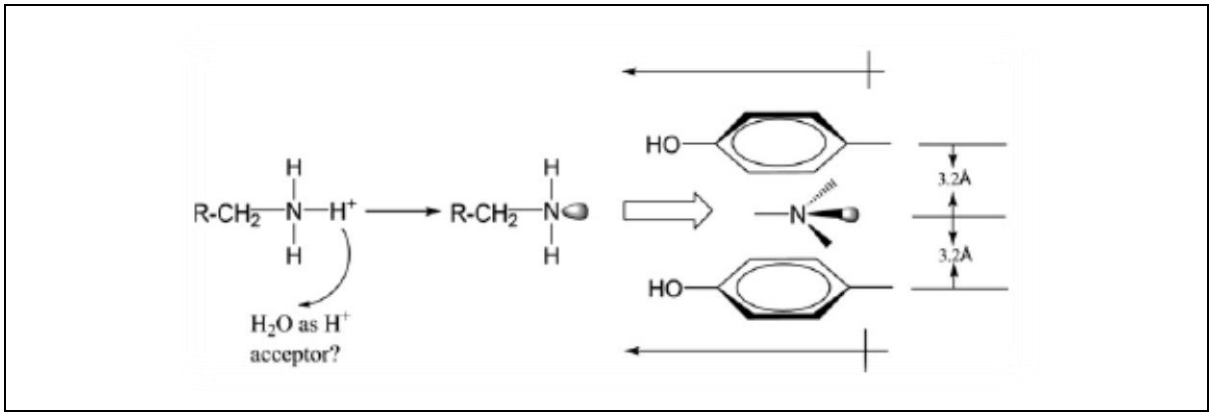

Figure 4:8: The effect of the dipole moments of TYR398 and TYR435 on the electron lone pair of the substrate amine moiety – which improves efficiency and navigates the substrate towards the FAD (Binda *et al*., 2002).

4.3 CHOLINESTERASE (ChE).

Cholinesterase is an esterase enzyme responsible to catalyse the hydrolysis of choline-based esters. Two types of cholinesterases can be distinguished namely, butyrylcholinesterase (BuChE) and acetylcholinesterase (AChE), the latter being the focus of this study. AChE in particular, plays a pivotal role in die pathology of AD (refer to **section 2.2.5**).

4.3.1. Acetylcholinesterase (AChE).

Acetylcholinesterase (AChE, E.C. 3.1.1.7) is the enzyme responsible for the termination of impulse transmission at cholinergic synapses through rapid hydrolysis of acetylcholine (ACh) into acetic acid and choline (**Figure 4.9**; Barnard 1974).

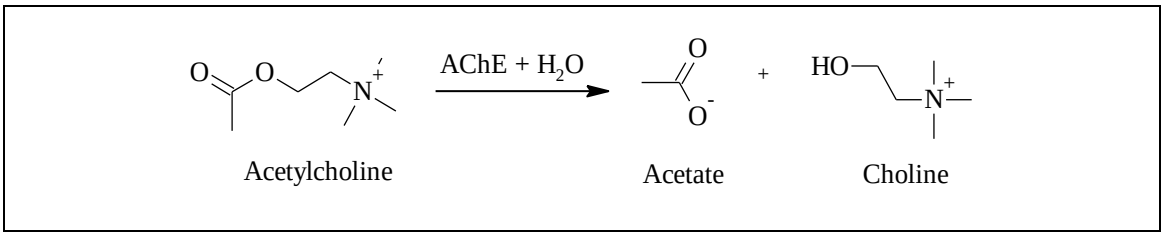

Figure 4.9: Enzymatic hydrolysis of ACh by AChE to yield acetate and choline.

In turn, Acetylcholinesterase inhibitors (AChEIs) reduces AChE induced metabolism of ACh in the synaptic cleft, resulting in the increased intra synaptic residence time of ACh, and facilitates interaction between ACh and the postsynaptic cholinergic receptor, thus contributing to their clinical benefits. AChEIs have also been reported to be beneficial not only on the cognitive performance in AD, but also in diffuse Lewy body disease (DLBD) as well as for the behavioural symptoms in dementia associated with PD (Aarsland *et al*., 2002, 2003; Werber *et al*., 2001; Giladi *et al*., 2003; Pakrasi *et al*., 2003; Leroi *et al*., 2004; Emre *et al*., 2004.). Fundamental studies further suggest that AChEIs might reduce APP (amyloid precursor protein) processing and provide some degree of neuroprotection (Mori *et al*., 2006).

4.3.2. Enzymology and catalytic mechanism.

AChEIs can be categorised into two classes namely organophosphorus [organophosphonate (nerve agents) and organophosphate (insecticides) compounds (OPs)], and carbamates (**Table 4.1**). The formers are generally insecticides, exhibiting higher toxicity (Marrs *et al*., 2000), with longer duration of action and generally cause CNS toxicity (Tareg *et al.* 2001).

Table 4.1: Classes of AChE inhibitors. "R" = various moieties attached to the basic structure. "P=S" of organophosphorus compounds can be substituted for "P=O.". "RL" oforganophosphates may attach via an "O" to "P." (Ecobichon, 1996).

Molecular structure of Organophosphorus compounds.		Carbamates.
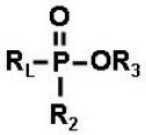 Organophosphonate (nerve agents)	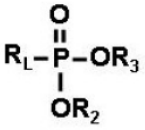 Organophospshate (insecticides)"	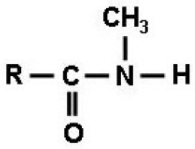

OPs such as nerve agents interact with the serine hydroxyl residue in the esteratic site (**Figure 4.10**) to block this hydrolysis.

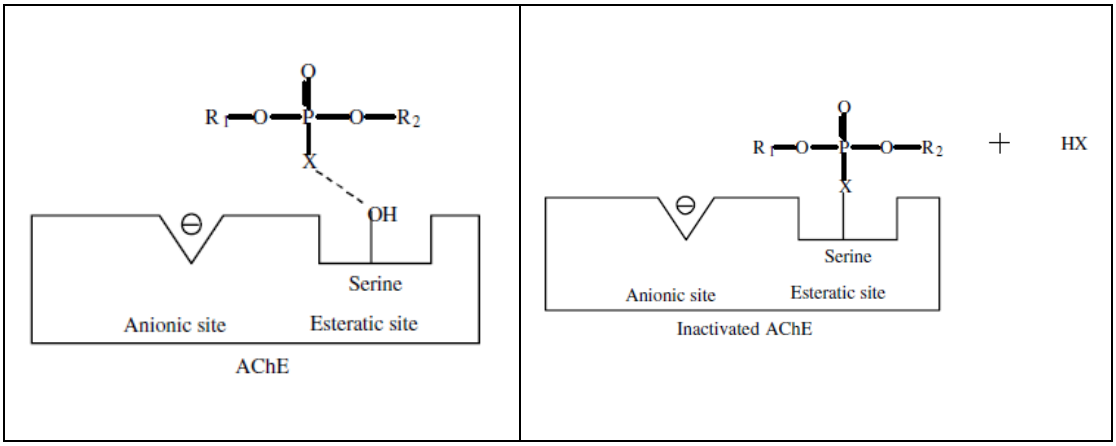

Figure 4.10: Mechanism of action of nerve agents. A nucleophillic attack by the free hydroxyl from the esteratic site's serine residue on the OP, subsequently blocks the site from action on ACh. If one of the R moieties disassociates, the enzyme has ''aged'' and inactivation is permanent (Wiener *et al*., 2004).

Knowledge of AChE's 3D structure is pivotal in recognising its unique catalytic mechanism, clarifying substrate – enzyme interactions and functional drug design. The crystal structure of *Torpedo californica* acetylcholinesterase (*Tc*AChE) was solved in 1991 (Sussman *et al*., 1991). A ribbon diagram of the catalytic subunit of *Tc*AChE (**Figure 4.11; left panel**) is illustrated and it was revealed to belong to the α/β hydrolase family (Ollis *et al*., 1992; Cygler *et al*., 1993).

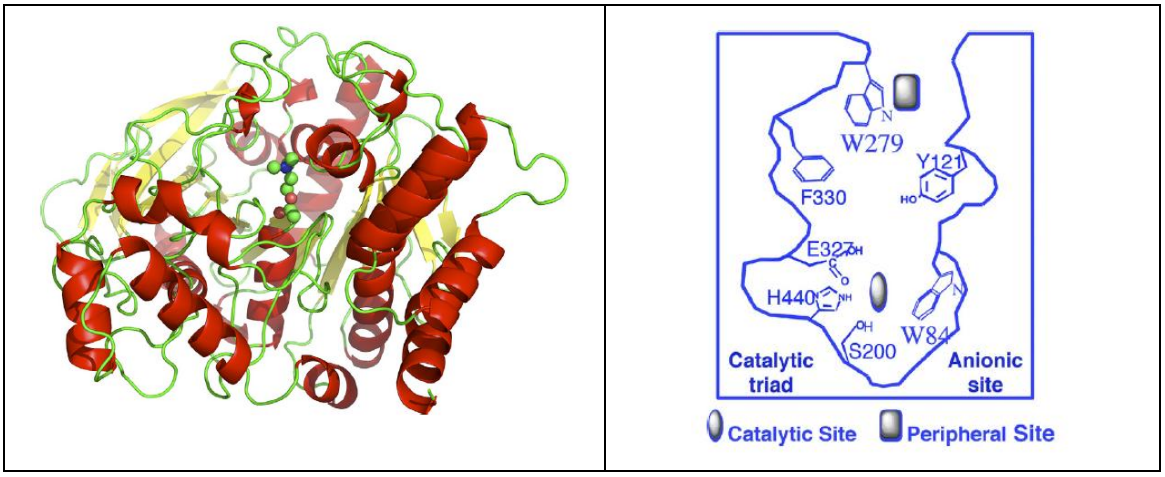

Figure 4.11: Ribbon diagram of *Tc*AChE with ACh docked in the active site **(left panel)**. Schematic cross-section of the active site gorge of *Tc*AChE **(right panel)**, with the principal catalytic acylation site (CAS) and peripheral anionic site (PAS) residues involved in the catalytic triad. (Silman *et al*., 2008).

The active site of AChE consists of a catalytic anionic/acylation site (CAS) and a peripheral anionic site (PAS). For its rapid catalytic activity, the active site is situated near the bottom of the deep, narrow gorge. (**Figure. 4.11; right panel**). The active site is constructed by ~14 conserved aromatic residues, which make up ~70% of its surface, with W84 and F330 contributing to the CAS, and TY70, TY121 and W279 to the PAS. This exceptional localisation of the active site (Harel *et al*., 1996) allows ACh to be bordered almost 360° by the enzyme residues, allowing increased substrate/enzyme interactions thus creating a more effective transition state.

Dual-site AChE inhibitors (molecules that interact simultaneously with both the CAS and PAS) appear to be a very promising therapeutic strategy as they not only stimulate the cholinergic system, but also inhibit the production and/or the aggregation of Aβ promoted by AChE (Munoz-Muriedas *et al.,* 2004). AChE can bind to the Aβ non-amyloidogenic form (refer to **chapter 2 - section 2.2.2.1**), inducing a conformational transition to the amyloidogenic conformation (refer to **chapter 2** - **section 2.2.2.1**) with subsequent amyloid fibril aggregation (Inestrosa *et al.,* 1996).

The narrow gorge of *Tc*AChE (**Figure 4.12**) is lined with aromatic residues and is about 20 Å deep, which allows ACh to penetrate nearly to the center of the 70 kDa catalytic subunit (Sussman *et al*., 1991). The acylation site (CAS-site) is at the base of the gorge where residue S203 (hAChE numbering) is acylated and de-acylated during substrate turnover. Residues H447 and E334 not only assist but participate with S203 in a catalytic triad (E–H–S), while W86 binds to the trimethylammonium moiety of ACh as acyl transfer to S203 is initiated (Schalk *et al*., 1992; Barak *et al*., 1994).

Ligands can also bind selectively either to the CAS or the PAS sites. Disadvantages of substrates that merely bind to the PAS site is that it (Szegletes *et al*., 1998) sterically obstruct the entrance to the CAS, which in turn reduces the flow rate of other molecules and allosteric activation (Rosenberry *et al*., 2005).

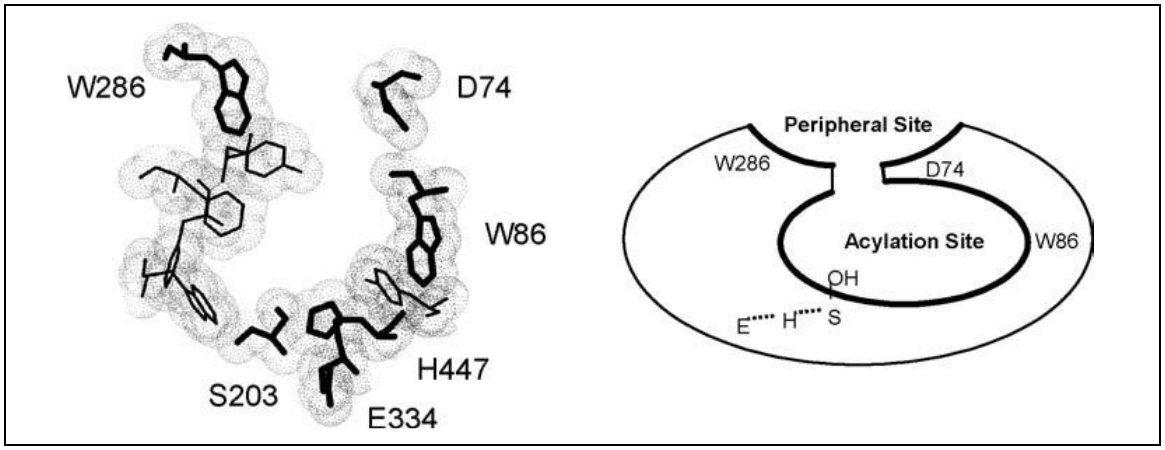

Figure 4.12: hAChE's active site. **Left panel**: residues from crystal structure that line the active site gorge of hAChE. **Right panel**: schematic representation of the two regions for ligand association within the AChE active site, the acylation and peripheral sites (Sussman *et al*., 1991).

4.4. ENZYME REACTIONS AND KINETICS : GENERAL PRINCIPLES.

Enzyme kinetics quantifies the rates of enzyme-catalysed reactions and the factors that influence it. This allows scientists to understand the individual steps how enzymes transform substrates into products. It also represents a critical part of drug discovery research to identify potential therapeutic agents.

The K_i value for competitive MAO-B inhibition by test inhibitors can be determined by the extent to which various concentrations of the test compounds reduce substrate oxidation to the corresponding product. The rates of enzyme-catalysed reactions are generally fast. Only traces of product accumulate, thus making the reverse reaction negligible. The reaction's initial velocity (V_i) is essentially that of the rate of the forward reaction. In enzyme assays a molar excess of substrate are used, making V_i proportional to the enzyme concentration. Measurements of the V_i allows researchers to quantity the enzyme present in a biologic sample.

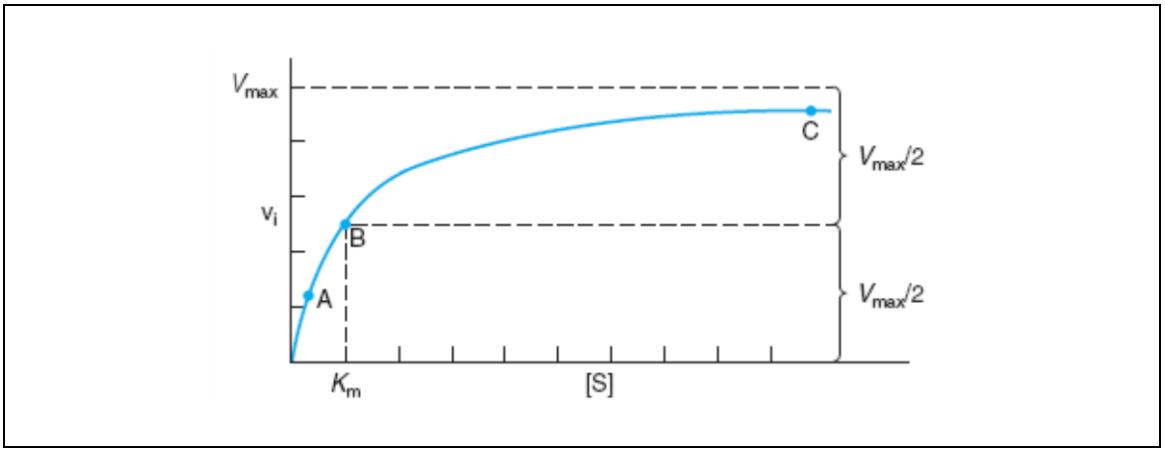

Graph 4.1: The substrate's concentration effect on the V_i of an enzyme-catalysed reaction (Murray *et al*., 2003).

As the concentration of the substrate ([S]) increases, V_i also esculates until a maximum value (V_{max}) is reached (**Graph 4.1**). The enzyme has reached a ''saturated'' point with the substrate and the curve of V_i *vs*. [S] (**Graph 4.1**) being hyperbolic. At this stage only substrate molecules that are combined with the enzyme (enzyme-substrate or ES) complex can be converted into product. Although the substrate is in excess, only the ES complex quantifies the enzyme present.

At points **A** or **B** (**Figure 4.13**), altering the [S] have a direct proportional effect on the ES complexes with an equivalent alteration in V_i. All the enzyme exist as an ES complex at higher [S] (**C** in **Figure 4.13)**.

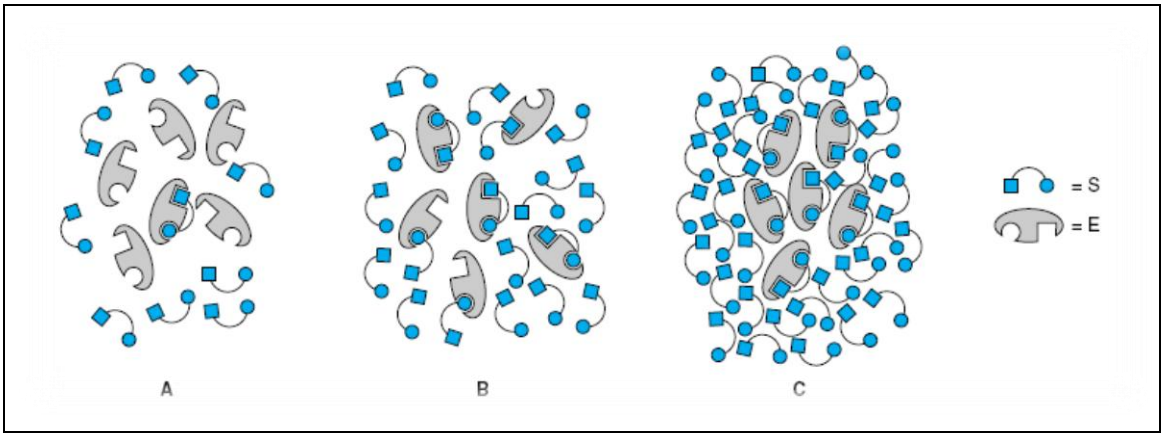

Figure 4.13: An enzyme at low (**A**), at high (**C**), and at [S] = K_m (**B**). (Murray *et al*., 2003).

When no free enzyme is available to form ES, further [S] escalation will not increase the reaction rate.

4.4.1 The Michaelis-Menten Equation

The Michaelis-Menten equation (**4.1**) represents the relationship between V_i and [S], as depicted in **Graph 4.1**.

Equation 4.1:

$$v_i = \frac{V_{\max}[S]}{K_m + [S]} \quad (\mathbf{4.1})$$

The Michaelis constant (K_m) is the [S] at which V_i is half the maximal velocity ($V_{max}/2$) achievable at a particular concentration of enzyme. V_i relies on [S] and K_m can be clarified under three conditions:

(1) When [S] < K_m (**A** in **Figure 4.13** and **Graph 4.1**), K_m. = K_m + [S]. Substition produces equation **4.2**. When [S] < K_m, the V_i are directly proportional to [S].

Equation 4.2:

$$v_{_1 i} \approx \frac{V_{\max}[S]}{K_m + [S]} \approx \left(\frac{V_{\max}}{K_m}\right)[S] \quad (\mathbf{4.2})$$

(2) If the [S] > K_m (**C** in **Figure 4.13** and **Graph 4.1**), [S] = K_m + [S]. Substitution yields equation **4.3**. The reaction velocity is maximal (V_{max}) and is not affected by additional increases in [S].

Equation 4.3:

$$v_i \approx \frac{V_{\max}[S]}{[S]} \approx V_{\max} \quad (\mathbf{4.3})$$

(3) When [S] = K_m (**B** in **Figure 4.13** and **Graph 4.1**), it is transformed to equation **4.4.** The V_i is now half-maximal ($V_{max}/2$).

Equation 4.4:

$$v_{_1 i} = \frac{V_{\max}[S]}{K_m + [S]} = \frac{V_{\max}[S]}{2[S]} = \frac{V_{\max}}{2} \quad (\mathbf{4.4})$$

4.4.2. Lineweaver-Burk plot.

The Lineweaver-Burk plot is used to calculate K_m and V_{max}. This linear form of the Michaelis-Menten equation avoids high [S] for saturated conditions and V_{max} and K_m can be calculated from V_i in non – saturating conditions.

Starting from **Equation 4.1**, **Equation 4.5** can be derived by inverse, factorisation and simplification.

Equation 4.5:

$$\frac{1}{v_i} = \left(\frac{K_m}{V_{\max}}\right)\frac{1}{[S]} + \frac{1}{V_{\max}} \quad (\mathbf{4.5})$$

Equation 4.5 forms a straight line (y = ax + b), where y = 1/ V_i and x = 1/[S]. A plot of $1/V_i$ *versus* 1/[S] results in a straight line with y intercept $1/V_{max}$ and slope K_m/V_{max} and is termed a double reciprocal / Lineweaver-Burk plot (**Graph 4.2**). K_m = the x intercept. (**Equation 4.6**).

$$0 = ax = b$$ therefore,

Equation 4.6:

$$x = \frac{-b}{a} = \frac{-1}{K_m} \quad (\mathbf{4.6})$$

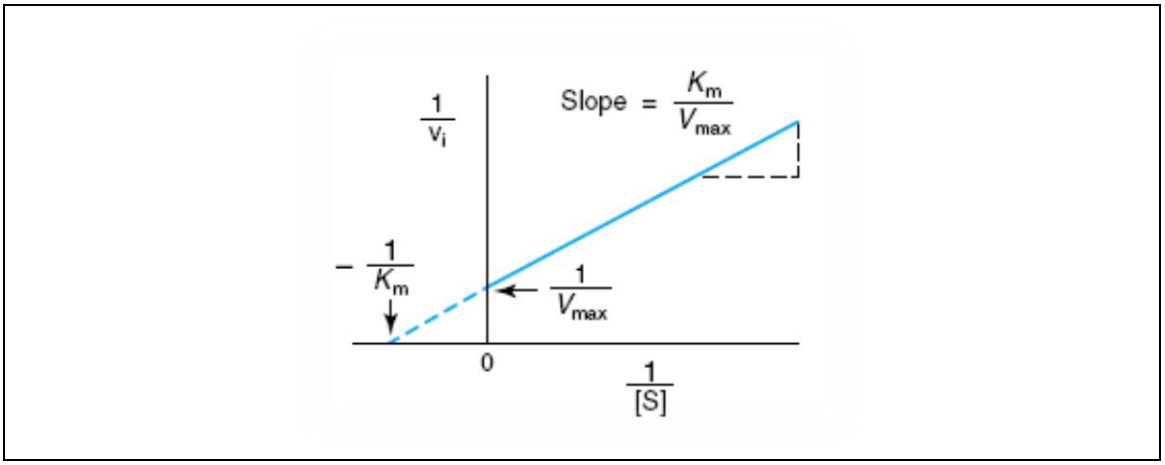

Graph 4.2: Double reciprocal / Lineweaver-Burk plot. (Murray *et al*., 2003).

4.4.3. Inhibitors

Inhibitors can be categorised according to their:

i. Site of action on the enzyme,
ii. potential to chemically modify the enzyme, or the
iii. kinetic parameters they affect.

Kinetically, three classes of inhibitors can be distinguished: Competitive, non-competitive and irreversible.

4.4.3.1. Competitive inhibitors.

By increasing the [S], this type of inhibitors' effect will be cancelled. It binds to the substrate-binding portion in the active site and prevents the substrate to interact with the enzyme. The development and dissociation of the enzyme-inhibitor (EI) complex is defined by:

Equation 4.7 where the free enzyme (*Enz*) and inhibitor (*I*):

$$Enz \underset{k2}{\overset{k1}{\leftrightarrow}} Enz + I \quad (\mathbf{4.7})$$

And the equilibrium constant (K_i) is:

Equation 4.8:

$$K_i = \frac{[Enz][I]}{[Enzl]} = \frac{k_1}{k_{-1}} \quad (\mathbf{4.8})$$

The quantity of free enzyme to form the ES decreases and consequently product formation as well. The Lineweaver-Burk plots differentiate between competitive and non - competitive inhibitors and reduce evaluation of inhibition constants (K_i). The V_i is calculated at several [S] both in the presence and in the absence of inhibitor (**Graph 4.3**).

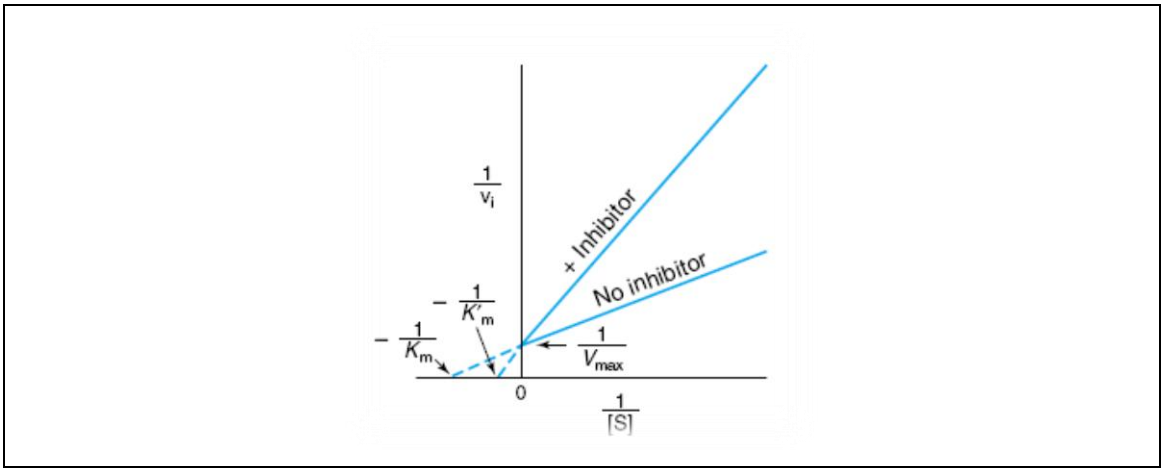

Graph 4.3: Lineweaver-Burk plot of competitive inhibition. No inhibition at high substrate concentration (Murray *et al*., 2003).

The y intercept = $1/V_{max}$, when 1/[S] reaches 0, V_i is independent of the presence of inhibitor. The x intercept varies with inhibitor concentration, $K_{m'}$ (the "apparent K_m") increases with increasing concentrations of inhibitor. V_{max} isn't affected by competitive inhibition, but raises K_m for the substrate. The x intercept is:

Equation 4.9:

$$x = \frac{-1}{K_m}\left(1 + \frac{[I]}{K_1}\right) \qquad (\mathbf{4.9})$$

The K_i can be determined from **Equation 4.9**. K_i values are used to compare different inhibitors of the same enzyme. A lower K_i value reflects a more potent inhibitor.

4.4.3.2. Elementary non-competitive inhibitors

In this case, substrate binding does not influence inhibitor binding and the development of EI (enzyme – inhibitor) and EIS (enzyme – inhibitor – substrate) complexes are achievable. The EI complex decreases the enzyme's ability to form the substrate product, and the V_{max}, is reduced. The E and EI retains the same affinity for substrate, and the EIS complex generates product at a minor rate (**Graph 4.4**).

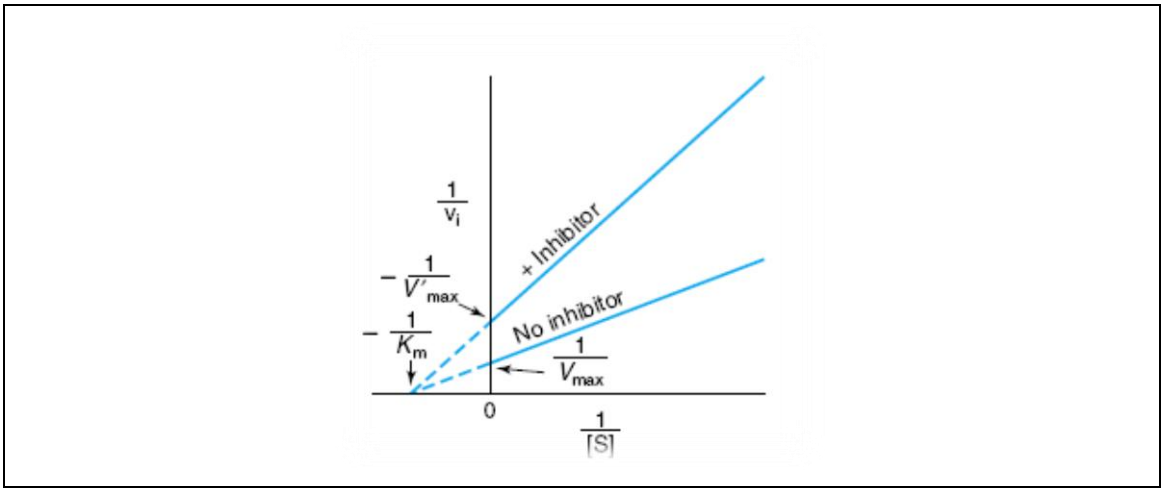

Graph 4.4: Lineweaver-Burk plot for simple non-competitive inhibition. More complex non-competitive inhibition occurs when binding of the inhibitor does affect the apparent affinity of the enzyme for substrate (Murray *et al*., 2003).

4.4.3.3. Irreversible inhibitors

This is where the inhibitor forms stable covalent bonds. This consequently inactivates the enzyme and *de novo* enzyme synthesis is normally required (Murray *et al*., 2003).

4.5. INHIBITION STUDIES.

The current study employed spectrophotometrical assays to determine the effect of the newly synthesised compounds on the MAO-B and AChE activity.

4.5.1. MAO-B Inhibition.

In general, the activity of MAO-B was measured by adding an appropriate substrate (which depends on parameters of the synthesised test compounds and consequently determines the method and instrumentation used for measurement e.g. UV, Fluorescent etc.) to the enzyme and then measuring the concentration of the product formed after a specified time. Recombinant human MAO-B was used in this study. A fluorometric assay was used to measure the enzyme activities with Kynuramine as substrate. Kynuramine were used as substrate and the assay is based on its MAO-B oxidisation to 4-hydroxyquinoline (**Figure 4.14**; Weissbach *et al*., 1960).

The concentrations of the 4-hydroxyquinoline produced were measured with a fluorescent spectrophotometer (excitation wavelength of 310 nm and an emission wavelength of 400 nm). The fluorescence intensity decreased as 4-hydroxyquinoline production is reduced by the MAO-B test inhibitors. The inhibition potencies were expressed as IC_{50} values.

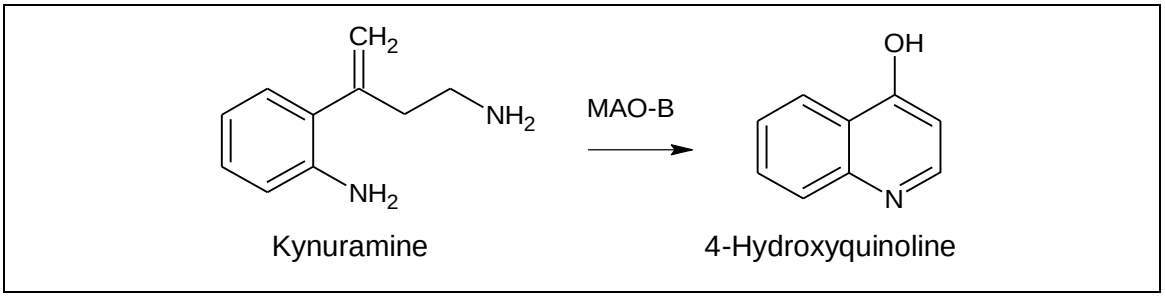

Figure 4.14: The MAO-B catalysed oxidation of Kynuramine (substrate) to yield 4-hydroxyquinoline (product).

4.5.1.1. Consumables and instrumentation.

The following were obtained from Sigma Aldrich: Kynuramine.2HBr, microsomes expressed in baculovirus infected BTI insects cells (Simon, S, 1997; Novaroli *et al*., 2005)) containing recombinant MAO-B (5 mg/mL), NaOH and DMSO. A Varian Cary Eclipse fluorescence spectrophotometer was utlised for fluorescence spectrophotometry.

4.5.1.2. Data Processing

GraphPad® Prism® V.5.03 software was utilised for data processing. The non-paramedic test application was used for significance comparability.

4.5.1.3. Method.

Recombinant hMAO-B (5 mg/mL) was pre-aliquoted and stored at -70 °C. The incubations were prepared in 500 µl potassium phosphate buffer (pH 7.4). Various concentrations of the test inhibitor (0 - 100 µM), in 4% DMSO as co-solvent was prepared. Kynuramine (30 µM) served as substrate and was added to each incubation. MAO-B (0.0075 mg/ml) was then added and the reactions were incubated for 20 min at 37 °C. The reaction was terminated by adding 400 µL NaOH (2 N) and distilled water (1000 µL) was added to each reaction. It was centrifugated (16000 g) for 10 minutes at room temperature to produce a supernatant.

Concentration measurements of 4-hydroxyquinoline of each incubation was carried out using a Varian Cary Eclipse fluorescence spectrophotometer (settings: medium PMT voltage with the excitation and emission slit widths set to 5 mm). The supernatant's fluorescence was measured at an excitation wavelength of 310 nm and an emission wavelength of 400 nm.

The initial rate of oxidation was plotted against the Logarithm of the inhibitor concentration ([I]) and the IC_{50} values were determined from the sigmoidal dose-response curves (**Graph 4.6**). Different inhibitor concentrations spanning at least 3 orders of magnitude were used for each sigmoidal curve (0; 0.1, 0.3; 1; 3; 10; 30; 100 µM). The inhibition data were fitted to the one site competition model (Legoabe *et al*., 2014) incorporated in the GraphPad® Prism® software package. The IC_{50} values were determined in triplicate and are expressed as mean ± standard deviation (SD). As a positive control, we used (*R*)-Deprenyl for its acknowledged MAO-B

selectivity of 0.020 µM (Matos *et al*., 2011) and parent compounds 7-hydroxycoumarin / umbelliferone because of its known MAO-B inhibitory activity of 28.583 µM (Kang *et al*., 2001).

4.5.1.4: Results: MOA-B inhibition activity

The results of the MAO-B inhibition activity of the newly synthesised compounds are presented in **Table 4.2** and **Graph 4.5**.

Table 4.2: Structures and MAO-B inhibition activity of synthesised compounds.

COMPOUND	IC_{50} (µM)	SD
(*R*)-Deprenyl 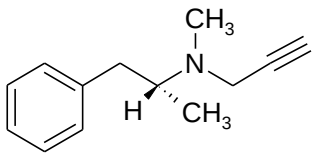	0.020	0.009
7C (7-Hydroxycoumarin) 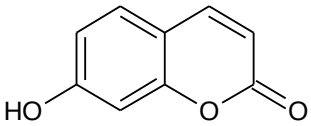	28.583	2.519
4MC (7-Hydroxy-4-methyl coumarin) 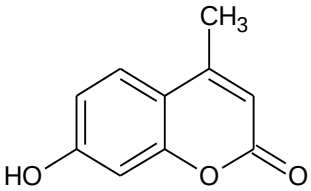	94.327	3.889
BPR 1 Oxo-2H-chromen-7-yl docos-24-enoate 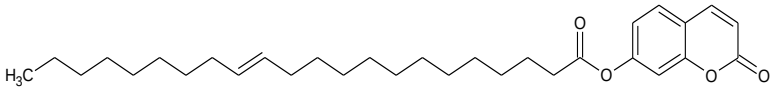	3.680	0.836
BPR 9 (4-[2-(Piperidin-1-yl)ethoxy]-2*H*-chromen-2-one). 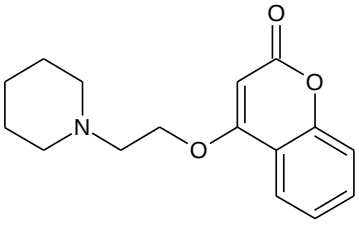	21.720	3.974

Table 4.2: Structures and MAO-B inhibition activity of synthesised compounds (continue).

BPR 10 (4-[2-(Morpholin-4-yl)ethoxy]-2*H*-chromen-2-one). 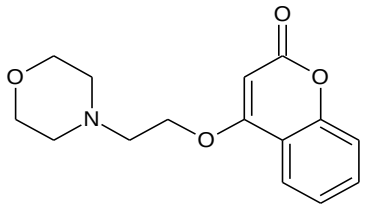	**0.372**	**0.026**
BPR 11 (7-[2-(Morpholin-4-yl)ethoxy]-2*H*-chromen-2-one). 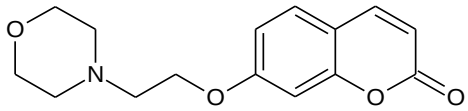	9.758	1.153
BPR 12 (7-[2-(Piperidin-1-yl)ethoxy]-2*H*-chromen-2-one). 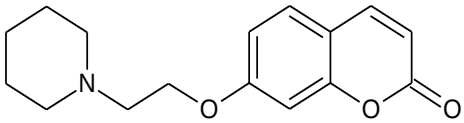	9.209	0.794
BPR 13 (4-Methyl-7-[2-(Piperidin-1-yl)ethoxy]-2*H*-chromen-2-one). 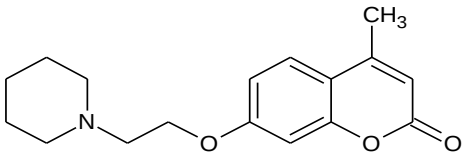	3.093	0.312
BPR 14 (4-Methyl-7-[2-(morpholin-4-yl)ethoxy]-2*H*-chromen-2-one). 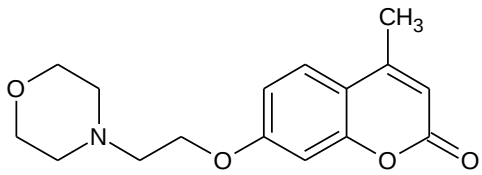	2.326	0.131

Note: Experiments were conducted in triplicate with the mean as IC_{50} value.

Compounds **BPR 2** – **8** and **4C** (4-Hydroxycoumarin) were devoid of MAO-B inhibitory activity and are not illustrated in the graph above. MAO-B inhibition activity (**Table 4.2; Graph 4.5)** was enhanced by nearly one log scale by conjugation of 7-Hydroxycoumarin (**7C**; IC_{50} = 28.583 µM) to erucic acid to form the coumarin ester, **BPR 1** (IC_{50} = 3.680 µM; **Table 4.2; Figure 4.5**), and with the sp2 carbon ‘‘spacer’’ to yield coumarin ethers of morpholine (**BPR 11**; IC_{50} = 9.758 µM) and piperidine (**BPR 12**; IC_{50} = 9.209 µM). The 4-methylated-7-Hydroxycoumarin (**4MC**; IC_{50} = 94.327 µM) conjugates also revealed a significant increase in activity with the sp^2 carbon ‘‘linker’’ and coumarin ether conjugates of piperidine (**BPR 13**; IC_{50} = 3.093 µM) and morpholine (**BPR 14**; IC_{50} = 2.326 µM). Although 4-hydroxycoumarin

exhibited the lowest inhibition activity, its ether conjugate with piperidine (**BPR 9**; IC_{50} = 21.720) showed activity and produced the most potent compound, this conjugate with morpholine (**BPR 10**; IC_{50} = 0.372 µM).

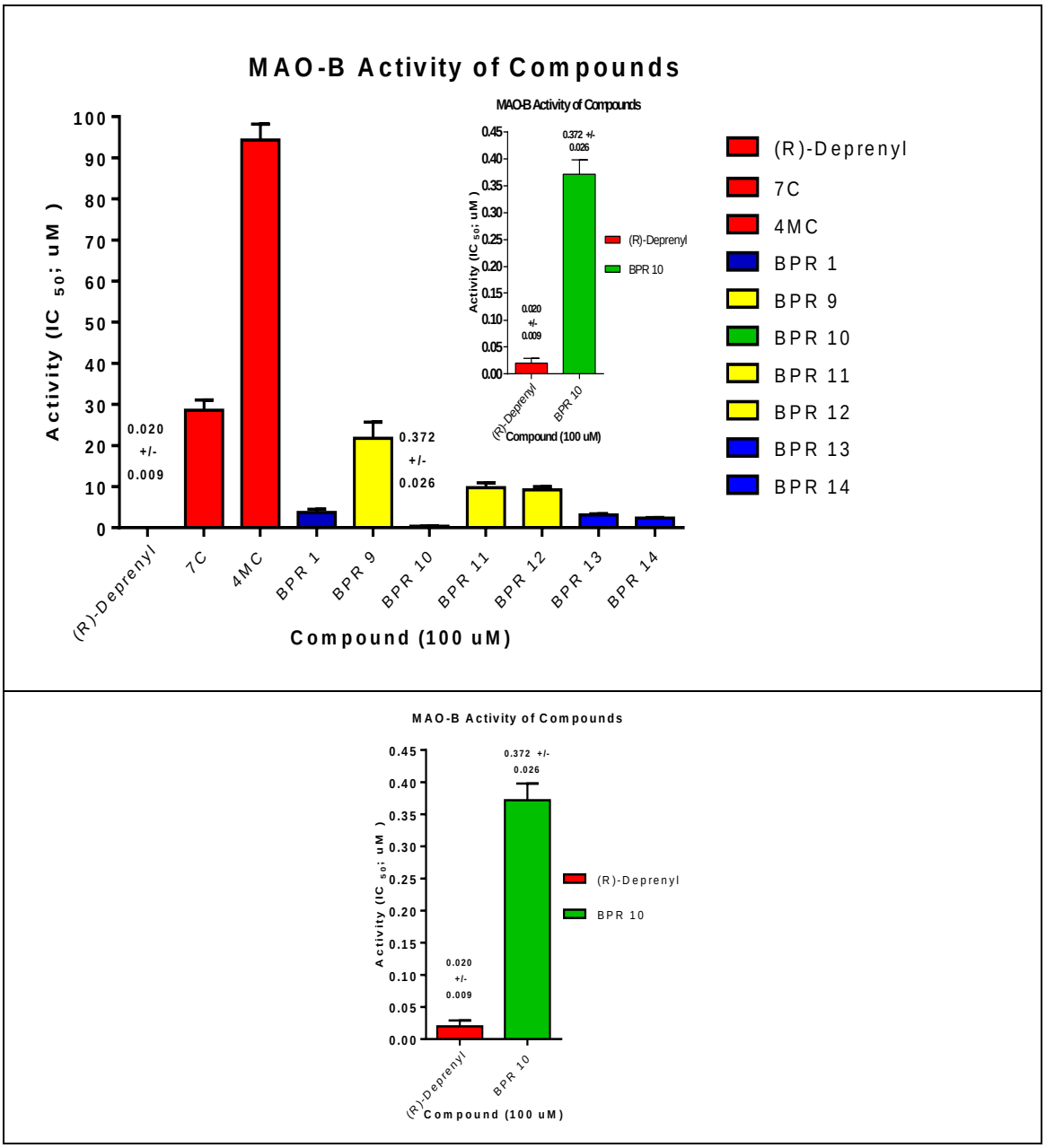

Graph 4.5: The MAO-B inhibition activity of synthesised inhibitors.

The 4-hydroxycoumarin - morpholine conjugate (**BPR10**; IC_{50} = 0.372 µM; **Graph 4.5**; green bar) revealed the most potent inhibitor, followed by **BPR14** (IC_{50} = 2.326 µM; **Graph 4.5**; blue bar); **BPR13** (IC_{50} = 3.093 µM; **Graph 4.5**; blue bar) and **BPR1** (IC_{50} = 3.680 µM; **Graph 4.5**; blue bar). **BPR9** (IC_{50} = 21.720 µM; **Graph 4.5**; yellow bar); **BPR11** (IC_{50} = 9.758 µM; Graph 4.5; yellow bar) and **BPR12** (IC_{50} = 9.209 µM; **Graph 4.5**; yellow bar) demonstrated moderate MAO-B activity as well as an increase in activity of their parent compounds.

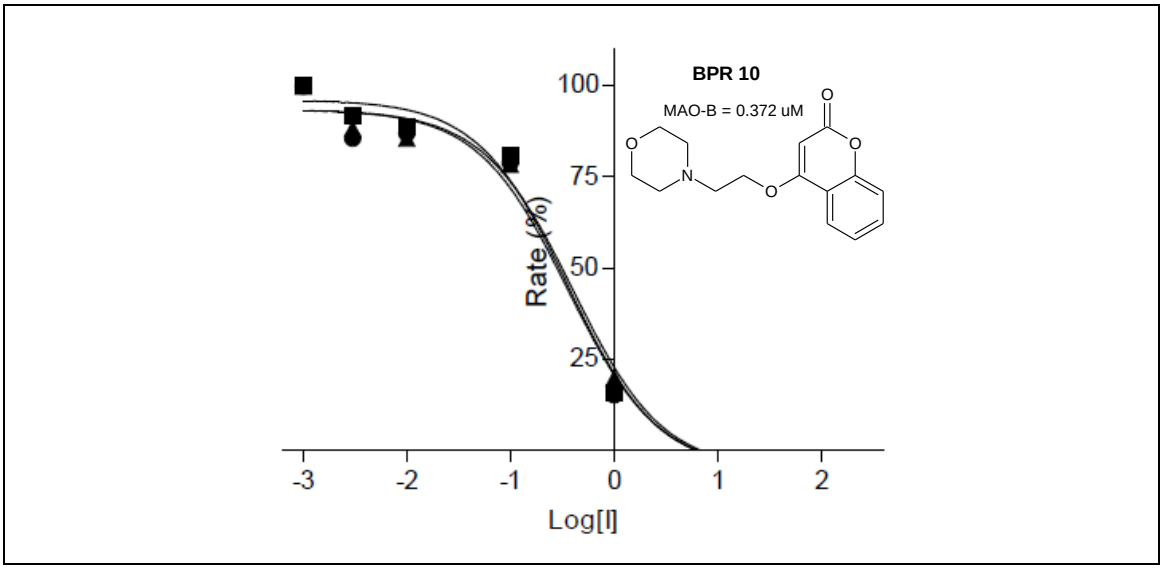

Graph 4.6: The sigmoidal curve of the most potent MAO-B inhibitor **BPR 10**.

Previous work on these compounds on MAO-B proved that coumarin conjugates without an alkyne/propargyl amine moiety (**Figure 4.15; B**) exhibit a competitive mode of inhibition. When 1/V vs. 1/[S] was plotted, the lines converged at the y-axis(**Figure 4.15; A**). The slope was obtained (**Figure 4.15; C**) and revealed a Ki of 0.688 µM and IC_{50} of 1.639 µM (Repsold, 2008). It is thus proposed that the newly synthesised compounds would exhibit the same mode of action (competitive inhibition).

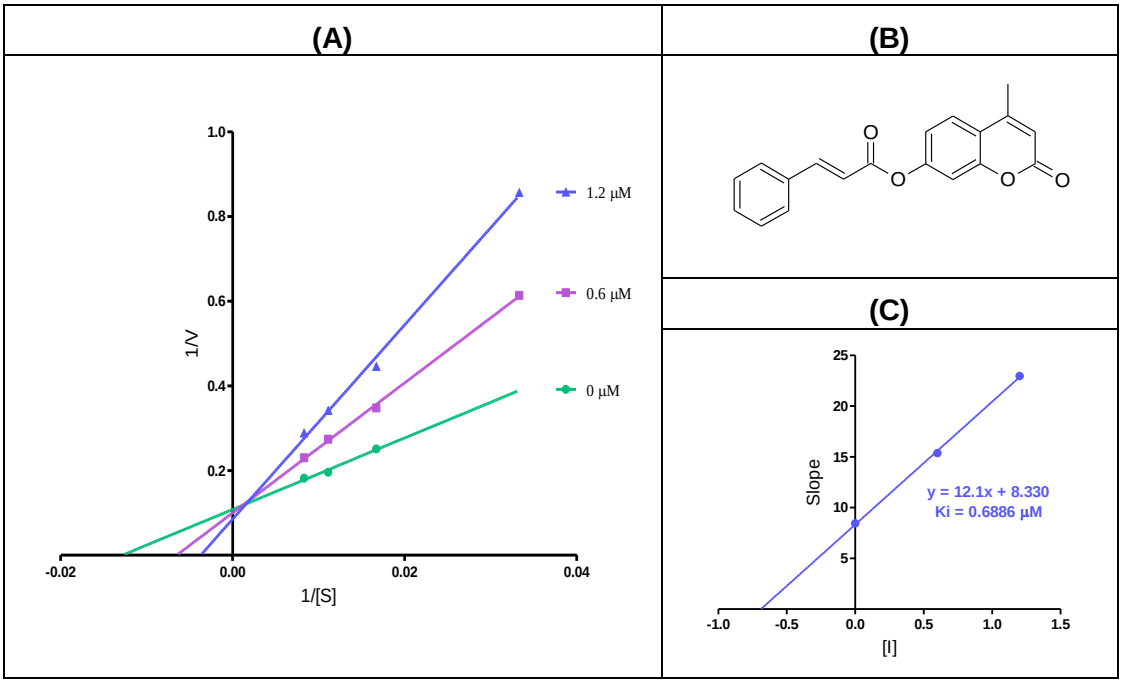

Figure 4.15: Lineweaver-Burk plot for simple competitive inhibition (Repsold, 2008).

4.5.2. Acetylcholinesterase Inhibition.

Employing an adapted version of the volumetric method using DTNB (Ellman *et al*., 1960), the test compound's inhibitory activity against EE AChE (Acetylcholinesterase from *Electrophorus electricus* / electric eel) was spectrophotometrically evaluated. It's based on the rationale of EE AChE hydrolysis of DTNB which is measured at 405 nm.

4.5.2.1. Consumables and instrumentation:

The following were purchased from Sigma Aldrich: DTNB [5,5'dithiobis(2-nitrobenzoic acid, 396.3g/mol)]; Acetylthiocholine iodide (289.18 g/mol); Acetylcholinesterase from *Electrophorus electricus* / EE AChE (electric eel, 500 UN); BSA (Albumin from Bovine serum); Trizma hydrochloride Reagent grade (157.60 g/mol); DMSO and NaOH. The Corning 96-well flat transparent plates were acquired from BioRad and a Rayto 6100 microplate reader (filter for 405 nm) was utilised.

4.5.2.2. Method:

Stock solutions of test compounds (1 µM and 100 µM) were prepared by dissolving it in DMSO and it was refrigerated until use. Trizma-Hydrochloride buffer was prepared (pH adjusted to 8 with diluted NaOH) and refrigerated until use. EE AChE (500 UN) was dissolved in 22.727 mL of Triz-buffer (38.43 nm) and pre-aliquoted (500 µL) and frozen. Thus, the final concentration of the aliquots contains 22 UN/mL in 34.43 mM Tris.

Acetylthiocholine iodide (15 mM - 5 mL, 21.69 mg), DTNB (1.5 mM – 10 mL, 5.94 g) and EE AChE (0.22 units/mL in 50 mM Tris-HCl and BSA 0.1%) were prepared directly preceding the assay and protected from light. Continuous thawing and refreezing of the above is not advisable.

148 µl DTNB and 50 µL of EE AChE solution was added to each of the required wells on the 96-well plate. DMSO (2 µL) was added to the control followed by the addition of 2 µL of the test compound stock solutions (**Table 4.3**) in consecutive wells to give test concentrations of 100 µM and 1 µM. The plate was incubated at 25 ˚C for 5 minutes. Acetylthiocholine iodide (30 µL) solution was added to respective wells by means of a multipipet. Absorbance was measured at 405 nm every 60 seconds for 20 minutes using the Rayto 6100 microplate reader. The activity (absorbance) were calculated and expressed in %.

To obtain a volume of 2 000 µL of 0.22 units/mL, 50 mM Tris, 0.1 % BSA (sufficient for 40 x 200 µL wells): 1 aliquot of EE AChE was thawed and 20 µL of the enzyme was used and 1980 µL Tris (50.12 nM – 5 mL, 39.50 mg) and 0.002 g BSA were added.

To compensate for the DMSO effect on activity, the concentration of DMSO where kept at (1 %) throughout the assays. This was achieved by the amount of DMSO added to a final volume of 200 µL in the wells, which was maintained at 2 µL (1 %).

Table 4.3: Preparation (Dilution) of novel compounds for EE AChE assay.

Stock solution concentration	**Volume added to well**	**Made up to**	**Final concentration in well for incubation (before addition of ATCI)**	**Final DMSO concentration**
10 mM	2 µL	200 µL	100 µM	1 %
1 mM	2 µL	200 µL	10 µM	1 %
0.1 mM	2 µL	200 µL	1 µM	1 %
0.01 mM	2 µL	200 µL	0.1 µM	1 %

$$\%\ \text{AchE inhibition} = \frac{\text{Control absorbance} - \text{Test compound absorbance}}{\text{Control Absorbance}}\ \text{X}\ 100$$

All data analysis and calculations were done using Prism 4.03® (GraphPhad, La Jolla, CA). Data analysis was carried out using the Student Newman Keuls multiple range tests and the level of significance was accepted at $p < 0.05$. Tacrine [100 uM] was used as positive control. The data in the table below was obtained using the the equation above.

4.5.2.3. Results: AChE inhibition activity

The results of the AChE inhibitory activity and structures of the newly synthesised compounds are presented in **Table 4.4**, **Graph 4.6** (100 µM) and **Graph 4.7** (1µM).

All of the synthesised compounds revealed weaker AChE potency than the positive control tacrine at both 100 µM and 1 µM.

Table 4.4: Structures and EE AChE inhibition activity (100 µM and 1µM) of the synthesised inhibitors.

COMPOUND	%EE AChE Inhibition (100 uM)	%EE AChE Inhibition [1 uM]
Tacrine 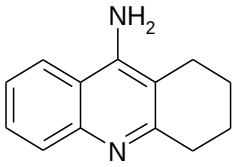	75.81± 1.845***	61.52± 5.369***
7C (7-Hydroxycoumarin). 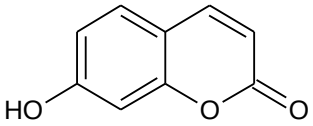	Insoluble	9.585± 2.135
4MC (7-Hydroxy-4-methyl coumarin) 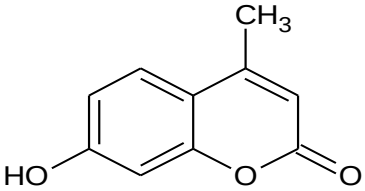	11.04± 6.362	8.415± 6.231
4C (4-Hydroxycoumarin). 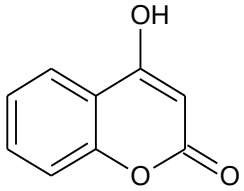	11.64± 6.054	12.910± 4.157
BPR1 (Oxo-2H-chromen-7-yl docos-24-enoate). 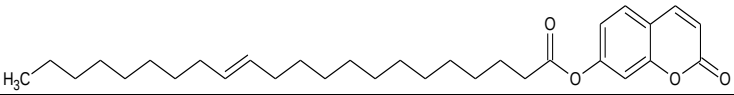	Insoluble	13.530± 5.265
BPR2 (2-Oxo-2H-chromen-4-yl docos-24-enoate). 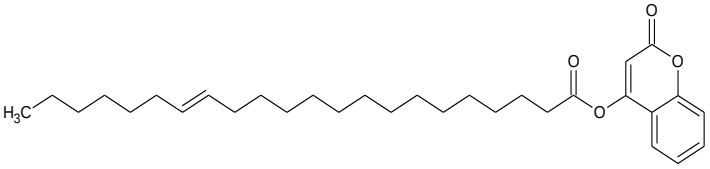	**Insoluble**	**22.460**± 6.959*
BPR3 (4-Methyl-2-oxo-2H-chromen-7-yl docos-25-enoate). 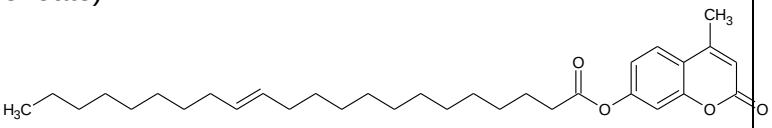	Insoluble	16.450± 8.583

BPR4 (4,4'-[Butane-1,4-diylbis(oxy)]bis(2*H*-chromen-2-one) 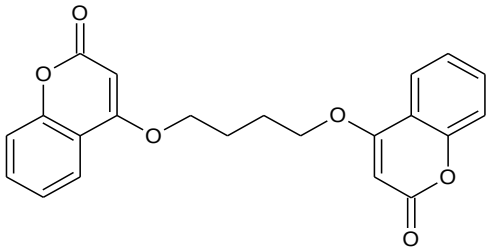	Insoluble	13.870± 4.875
BPR5 (4,4'-[Propane-1,3-diylbis(oxy)]bis(2*H*-chromen-2-one) 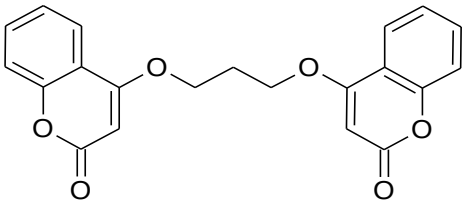	Insoluble	4.760± 7.258
BPR6 (7,7'-[Propane-1,3-diylbis(oxy)]bis(2*H*-chromen-2-one). 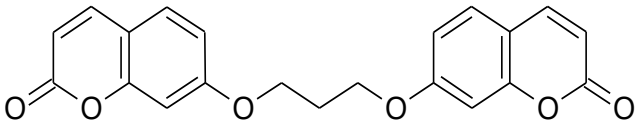	Insoluble	14.960± 4.512
BPR7 (7,7'-[Propane-1,3-diylbis(oxy)]bis(4-methyl-2*H*-chromen-2-one) 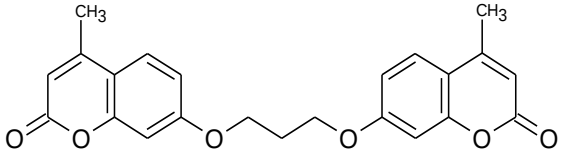	Insoluble	8.910± 3.265
BPR8 (Oxo-2*H*-chromen-7-yl thiophene-2-carboxylate). 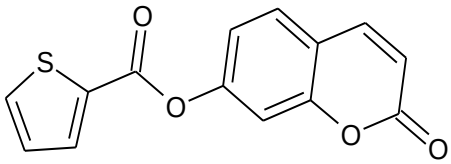	Insoluble	12.090± 3.257
BPR9 (4-[2-(Piperidin-1-yl)ethoxy]-2*H*-chromen-2-one). 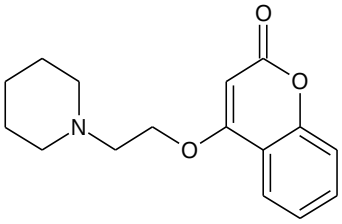	27.77± 8.243*	9.780± 4.268

BPR10 (4-[2-(Morpholin-4-yl)ethoxy]-2*H*-chromen-2-one). 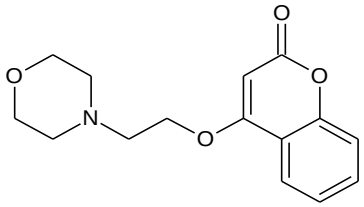	Insoluble	14.610± 4.568
BPR11 (7-[2-(Morpholin-4-yl)ethoxy]-2*H*-chromen-2-one). 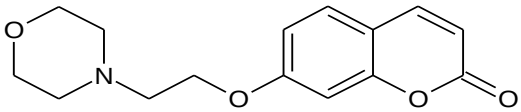	12.48± 8.075	6.750± 7.239
BPR12 (7-[2-(Piperidin-1-yl)ethoxy]-2*H*-chromen-2-one). 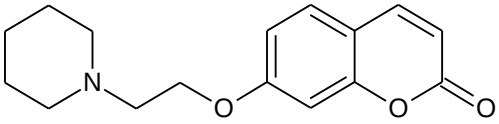	**52.90± 2.621*****	**30.900± 7.259****
BPR13 (4-Methyl-7-[2-(Piperidin-1-yl)ethoxy]-2*H*-chromen-2-one). 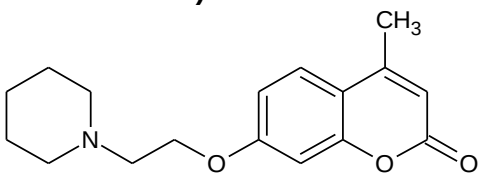	**57.43± 2.743*****	**21.560± 5.589***
BPR14 (4-Methyl-7-[2-(morpholin-4-yl)ethoxy]-2*H*-chromen-2-one). 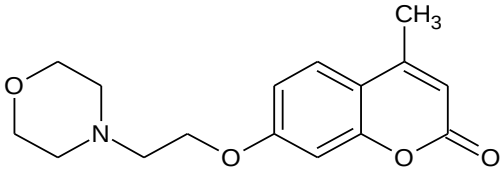	Insoluble	16.170± 11.250

Signifficance: p<0.05, **p<0.001, ***p<0.0001. All experiments were conducted in triplicate.

Coumarin – Erucic acid conjugates. **BPR1**, **BPR3** (**Graph 4.7**; blue bars) and **BPR2** (**Graph 4.7**; green bar) showed activity at 1 µM of 13.53 %, 16.46 % and 22.460 % respectively.

Coumarin Dimers. **BPR4**, **BPR6** (**Graph 4.7**; blue bars) and **BPR7** (**Graph 4.7**; yellow bar) also displayed activity in the same range (13.870 %; 14.960 % and 8.910 % at 1 µM respectively). **BPR5** (**Graph 4.7**; black bar) had weak EE AChE inhibition activity (even weaker than its corresponding starting material) of 4.760 % at 1 µM.

Coumarin – piperidine conjugates. **BPR12** (**Graph 4.7**; green bar) and **BPR13** (**Graph 4.7**; green bar) showed relatively potent activity of 30.90 % and 21.56 % at 1 µM. **BPR9** (**Graph 4.7**; yellow bar) revealed the weakest activity of this series with 9.780 % at 1 µM.

Coumarin – morpholine conjugates. **BPR11** (**Graph 4.7**; black bar) inhibited EE AChE 6.75 0 % at 1 µM. **BPR14** (**Graph 4.7**; blue bar) and **BPR10** (**Graph 4.7**; blue bar) exhibited activity in the same range of 14.61 % and 16.17 % at 1 µM.

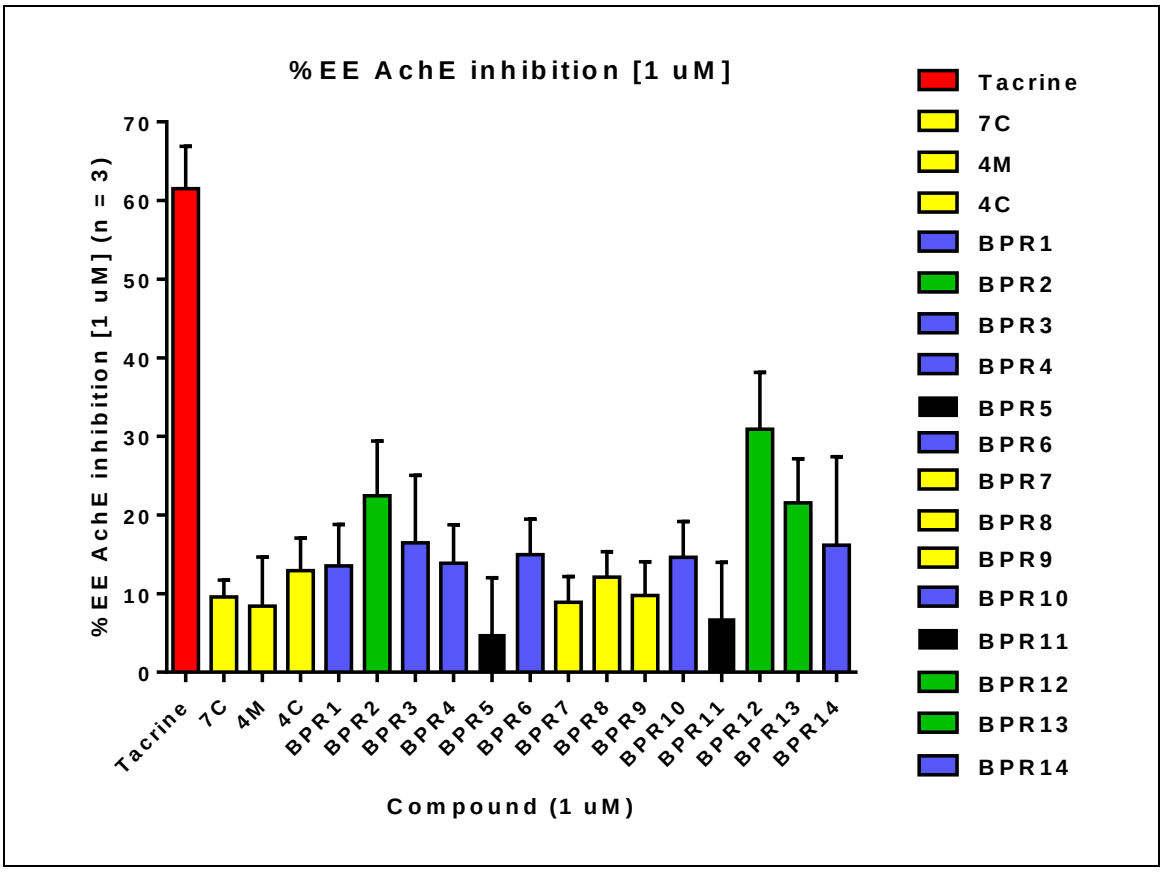

Graph 4.7: EE AChE inhibition activity (1 µM) in presence of synthesised inhibitors. Tacrine (red bar) represents the positive control. Green bars represent the most potent compounds, followed by compounds with moderate activity (blue bars) of the series. Yellow bars indicate moderate to weak activity while black bars very weak inhibition.

Positive control and parent compounds: Tacrine (positive control) revealed EE AChE inhibition of 75.81 % at 100 µM (**Graph 4.8**; red bar), **4MC** and **4C** (**Graph 4.8**; yellow bars) inhibitory activity of 11.04 % and 11.64 at 100 µM respectively.

Coumarin – piperidine conjugates. **BPR12** (**Graph 4.8**; green bar) had relatively potent activity of 52.90 % at 100 µM and **BPR13** (**Graph 4.8**; green bar) activity of 57.43 % at 100 µM. **BPR9** revealed the weakest activity of the piperidene series with 27.77 % at 100 µM (**Graph 4.8**; blue bar).

Coumarin – morpholine conjugates. **BPR11** revealed activity of 12.48 % at 100 µM (**Graph 4.8**; yellow bar). The parent compound **7C**, and compounds **BPR1** – **BPR8**, **BPR10** and **BPR14** were devoid of EE AChE activity at 100 µM.

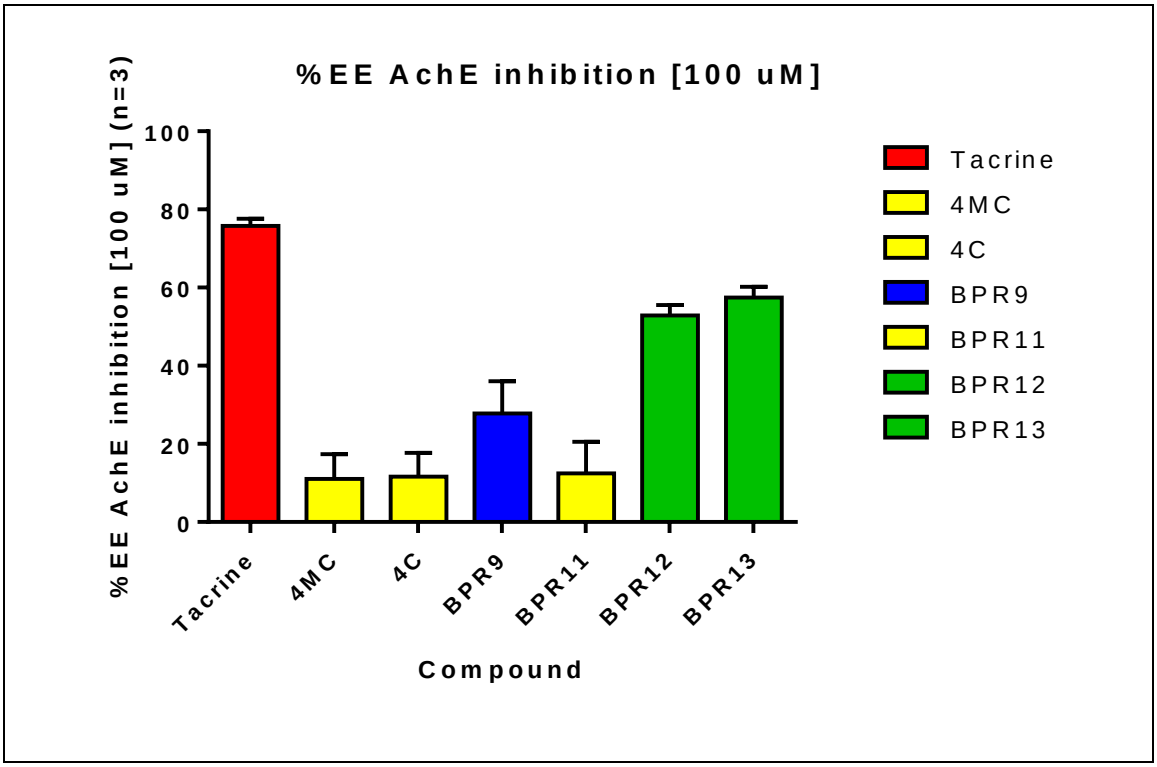

Graph 4.8: EE AChE inhibition (100 µM) activity of synthesised inhibitors. Tacrine (red bar) represents the positive control. Green bars represent potent activity, blue bars moderate activity and yellow bars weak activity.

In general, **BPR13** (57.43 % at 100 µM and 21.56 % at 1µM), **BPR12** (52.90 % at µM and 30.90 % at 1µM) and **BPR2** (22.46 % at 1 µM) were most promising coumarin hybrids.

4.6. MOLECULAR MODELLING.

Molecular Modelling / *In Silico* high-thoughput screening is the field of study that implements molecular graphics and computational chemistry techniques to build, simulate and analyse potential drug candidates within their specific pharmacological target protein(s) and performs numerous quantum mechanical calculations (Vlok *et al*., 2005).

4.6.1. Background.

Molecular Modelling enables the scientist to pre-select a large quantity of possible drug candidates (referred to as ligands) for a targeted protein(s). This method not only accelerates the drug design process, but avoids costly synthesis and *in vitro* and *in sito* biological evaluations (Krammer *et al*., 2005).

The Docking aspect includes docking and scoring. During docking, the ligands (key) are fitted within certain sites [usually the active site(s)] of the appropriate protein model (lock), and can metaphorically be described as the ‘‘key’’ and ‘‘lock’’ process (Yakunin *et al*., 2003). It views the ability of the 3D structure of the protein to accommodate / bind the ligands. Scoring

evaluates and quantifies the interactions between the different ways / poses in which the ligand binds within the protein. Numerous interactions (dispersion interactions, hydrogen bonding, ion-dipole, dipole-dipole, ion induced dipole interactions, charge transfer and covalent bonding) may occur between these two entities and determines therorectical binding affinities or interactions. The software employed prioritises and correlates (score) these binding interactions (Krammer *et al*., 2005).

4.6.2. Method

Material Studios Discovery Studios V3.1.1 software package (2012) with the CDOCKER application was used. The method can be summarised in three parts namely: preparing the protein, preparing the ligands, docking and scoring.

4.6.2.1. Preparing the Protein

From the Protein Data Bank (www.rcsb/pdb.org), the appropriate protein crystal structures: 4EY7 (Crystal structure of recombinant human Acetylcholinesterase in complex with Donepezil) and 2V61 (Structure of human MAO-B in complex with the selective inhibitor 7-(3-chlorobzloxy)-4-(methyl amino) methyl coumarin was downloaded. The downloaded file was opened in the Discovery Studios® and the protein report was used to confirm and check for any irregularities (crystallographic data, missing regions, alternate conformations, ligand co-crystallised, invalid residues, gaps in chains etc.).

The Prepare Protein function was used to correct the irregularities mentioned above (when applicable). The co-crystallised ligand was removed and the protein was then typed with CHARMm forcefield (Partial Charge: Momany-Rone) which assigned partial charges to the structure and it was saved. Subsequently, the ionisation and protonation state was optimised using ‘‘Protonate only the Protein and ‘‘Calculate Protein Ionisation and Residue pK’’ with settings: pH Range; From pH = 0; To pH = 14. The protein was minimised (to correct for any potential steric overlap due to the structure’s van der Waals interactions). Minimisation settings: Max Steps 5000, Implicit Solvent Model: Distance-Dependent Dielectric for 4EY7 and Generalised Born with Implicit Membrane for 2V61 was used since MAO-B is membrane bound. After completion of these modeling setup preparations the structure saved.

The active site (yellow sphere) of hMAO-B near the FAD (green ball-and-stick) co-crystallised with the selective inhibitor 7-(3-chlorobzloxy) 4-(methyl amino) methyl coumarin (gray ball-and-stick) was selected for MAO-B docking (**Figure 4.16**) as described in **section 4.6.1.1**

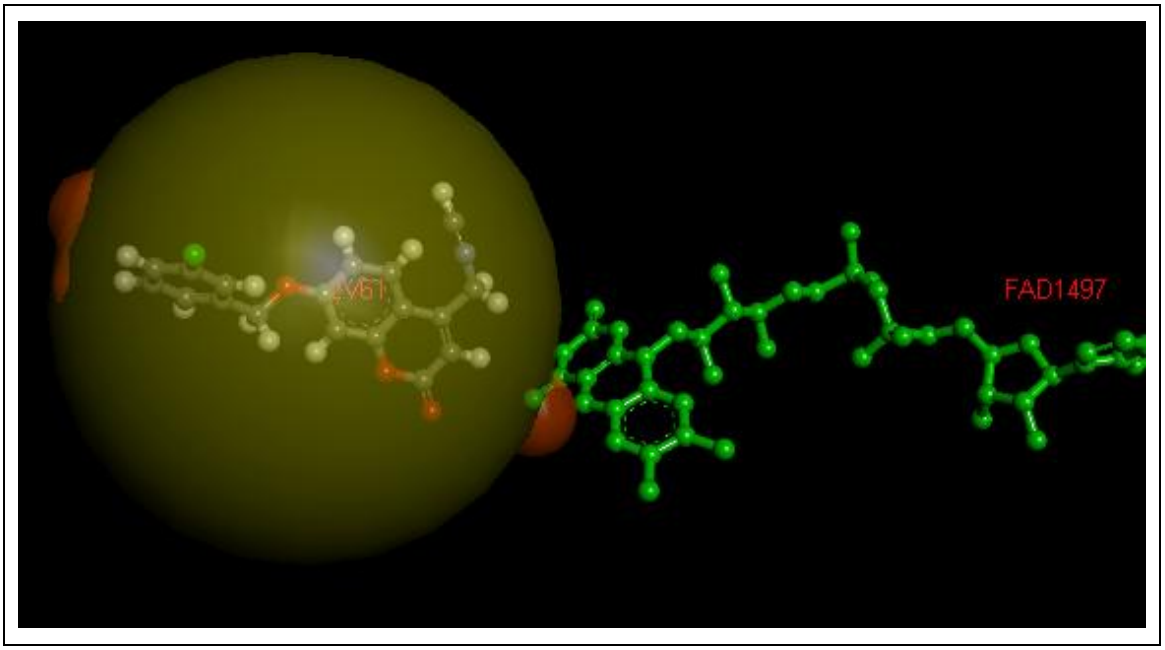

Figure 4.16: Structure of hMAO-B in complex with the selective inhibitor 7-(3-chlorobzloxy) 4-(methyl amino) methyl coumarin in the active site (**yellow sphere**) next to the FAD (**green ball-and stick**) – pdb file:2V61.

4.6.2.2. Prepare Ligands.

In a new window, the sketching function was used to sketch the ligands. Hydrogens were added, and the geometry ‘‘cleaned’’ (placing the structures in the correct and optimal conformation regarding their atomical angles). The ‘‘Prepare Ligands’’ utility was used with settings to true change ionisation, generate tautomers and correct for valencies according to the accurate settings and the file saved.

4.6.2.3. Docking.

The prepared protein was opened and typed with CHARMm forcefield. The prepared ligand file was recalled. In the CDOCKER®, the prepared protein and prepared ligand were loaded, and docked with random conformation set to 200, heating target temperature to 900 K and use full potential to true. The best poses (selected according the highest CDocker energy) of the docked ligand within the active site of the protein and the prominent side chains was documented and interpreted (According to Accelrys Discovery Studios V3.1.1 protocols, 2012). The CDocker energy is a quantitive indication of the ligand pose best accepted by the protein and includes numerous mathametical models.

4.6.3. Results:

The most potent novel compounds were selected for docking studies into the respective enzyme. **BPR10** into hMAO-B (2V61); **BPR2** and **BPR13** into hAChE (4EY7) with key interaction, active site and conserved residues are outlined in the following section.

4.6.3.1. Monoamine oxidase B (MAO-B)

The pyrone ring of the coumarin – morpholine conjugate (**BPR10**) revealed numerous interactions with pivotal residues in the substrate cavity. Hydrogen binding (distance: 2.015307 Å; angle:109.461123°) with CYS172 (dotted white line), PI interaction (distance: 6.514040 Å; angle: 22.164892°) with TYR398 (orange line) and Pi-Sigma interaction (distance: 2.911005 Å; angle: 27.035908°) with LEU171 (orange line) (**Figure 4.17**).

MAO-B IC_{50} = 0.372 µM	CDocker Energy = 18.9546

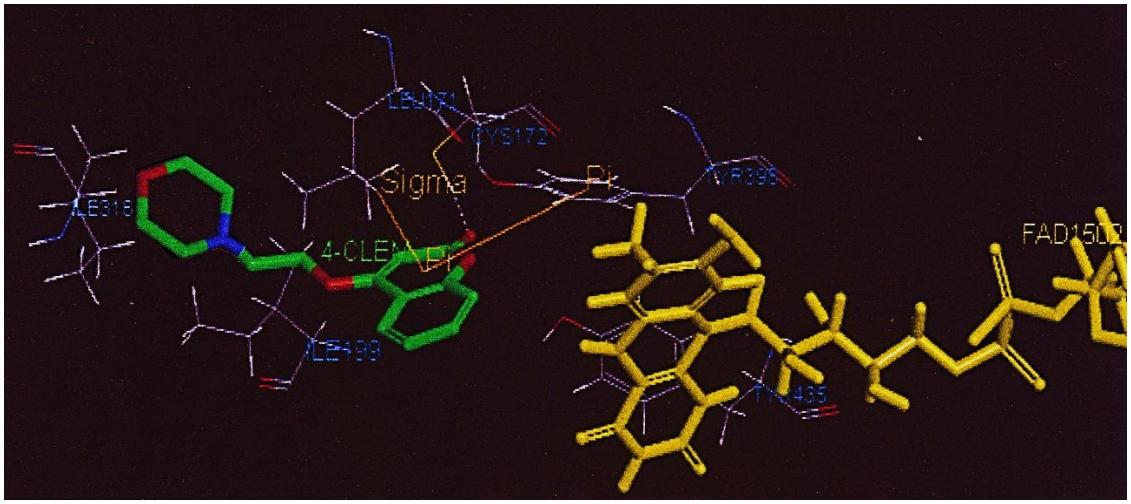

Figure 4.17: **BPR 10** (green ball-and-stick) docked in the hMAO-B protein (2V61). Pi-Pi interactions (orange), Pi-Sigma bindings (orange) and hydrogen binding (white dotted line) are observed in the substrate cavity.

Note the significance of TYR398 and TYR435 which directs a navigation path for the inhibitor towards the FAD (**Figure 4.18 and Figure 4.19**). This corresponds to the observation by Edmondson *et al*., 2007 (refer to **section 4.2.1.2**).

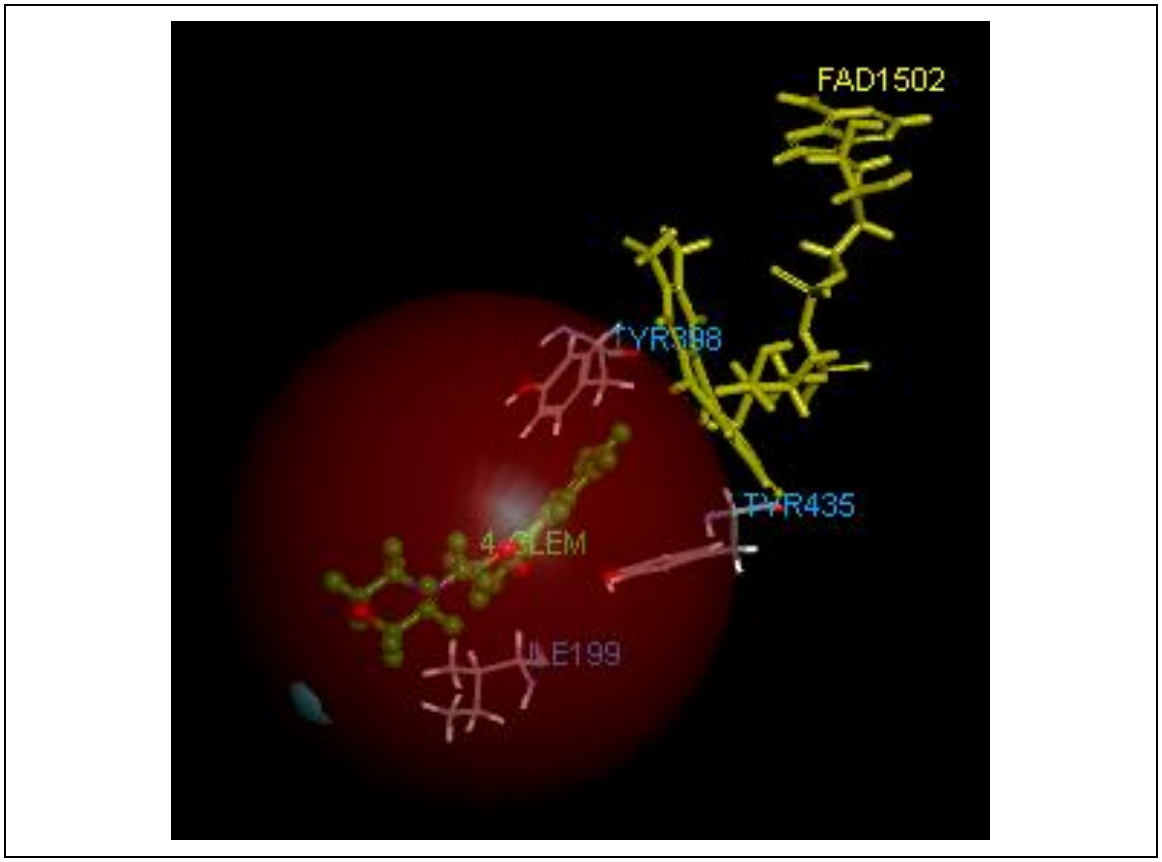

Figure 4.18: The active site (red sphere) of MAO-B near the FAD co-factor (yellow) with inhibitor **BPR10**/4-CLEM (green ball-and-stick). Residues TYR435, TYR398 and ILE199 (labelled in blue).

ILE199 is affected by the ether (although no bonding was observed), and served as a gateway for the compound to transverse and occupy both the substrate cavity and entrance cavity (**Figure 4.17 and Figure 4.18**, refer to **section 4.2.1.2**). Similar binding conformations was observed for all the coumarin conjugates.

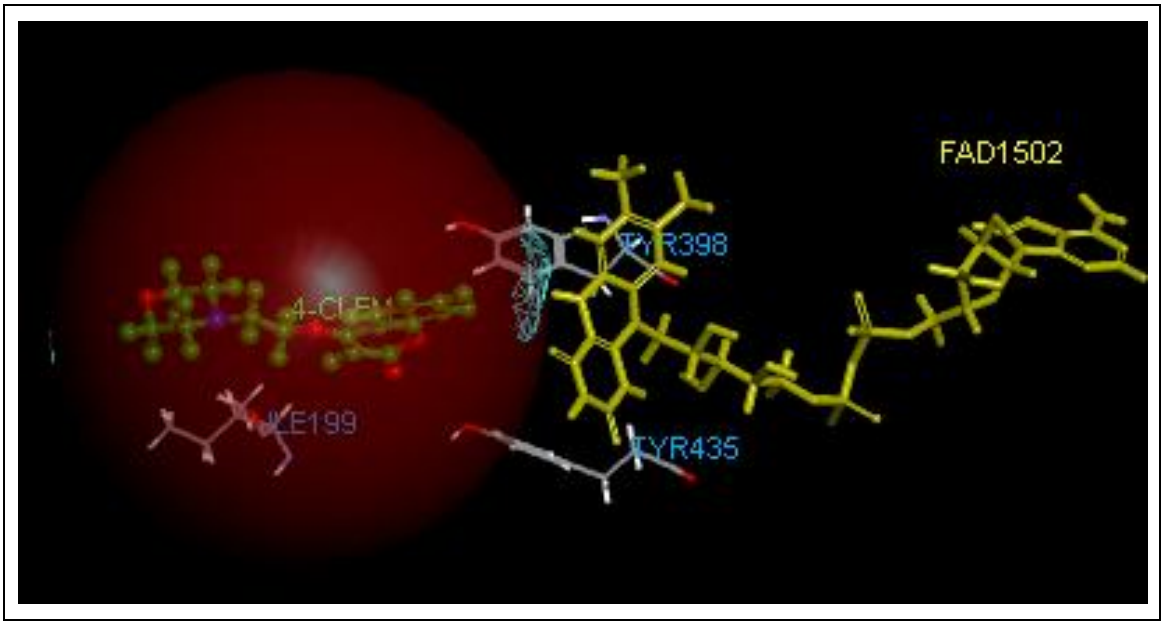

Figure 4.19: **BPR10** docked into hMAO-B.

This increased inhibitory activity can also be attributed to its hydrogen donor capacity (**Figure 4.20; A)** as well as its relative observed planarity (**Figure 4.20; B and C**).

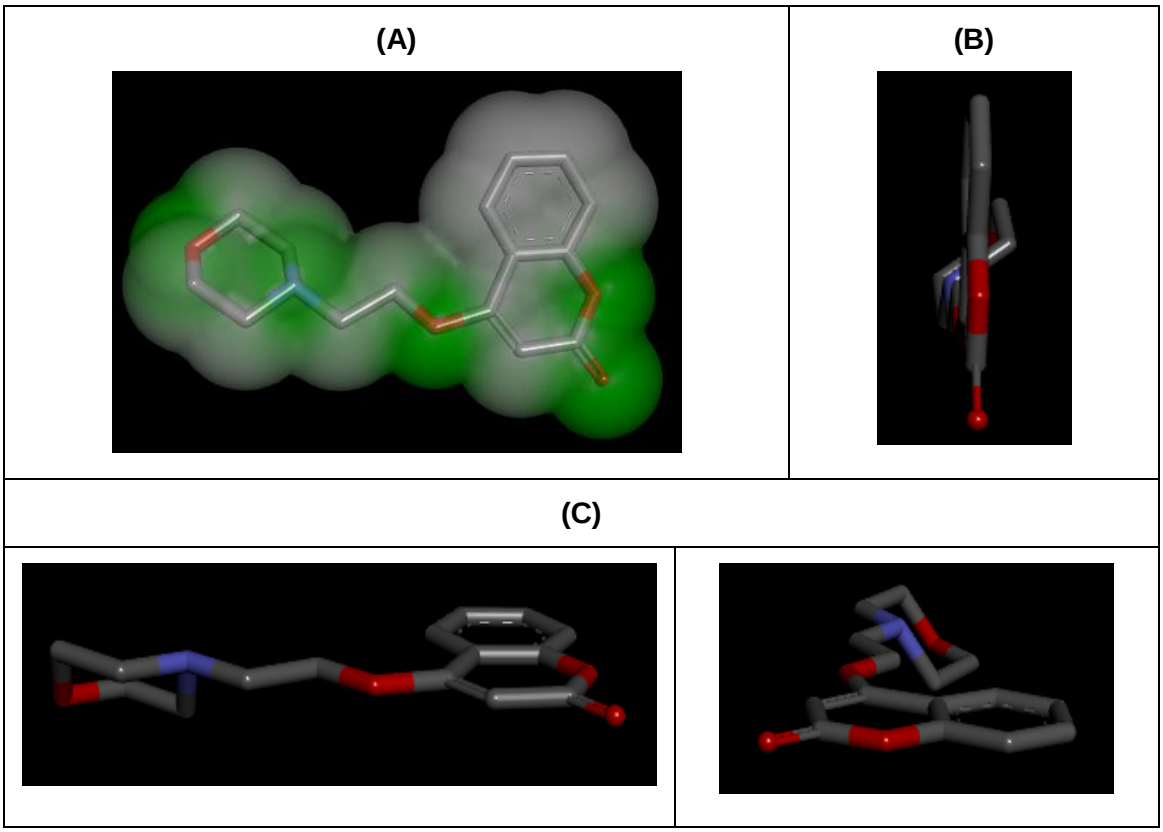

Figure 4.20: The hydrogen-donor capacity of **BPR10 (A)**. The conformations from different angles. **Note:** the relative observed planarity of the compound **(panes B and C)**.

4.6.3.2. Acetylcholinesterase (AChE)

BPR2 and **BPR13** were docked into hAChE to elucidate the binding mode of these novel inhibitors. The interactions with the protein's residues for each compound were described.

4.6.3.2.1. BPR2 hAChE Modelling

Since AChE' contains a long narrow gorge that leads towards the CAS (refer to **section 4.3.1.1**), the elongated fatty acid chain was preferred rather than a steric bulky conjugate. Thus, the coumarin entity of **BPR2** occupied the PAS while the erucic acid enitity was pushed in through the gorge into the CAS (**Figure 4.21 and Figure 4.22**). The rest of the elongated lipophillic entity was influenced by the neighbouring residues and fitted into the gorge to reach the CAS (although no further interactions was formed).

EE AChE Activity (1 µM): 22.460 %	CDocker Energy = 29.1198

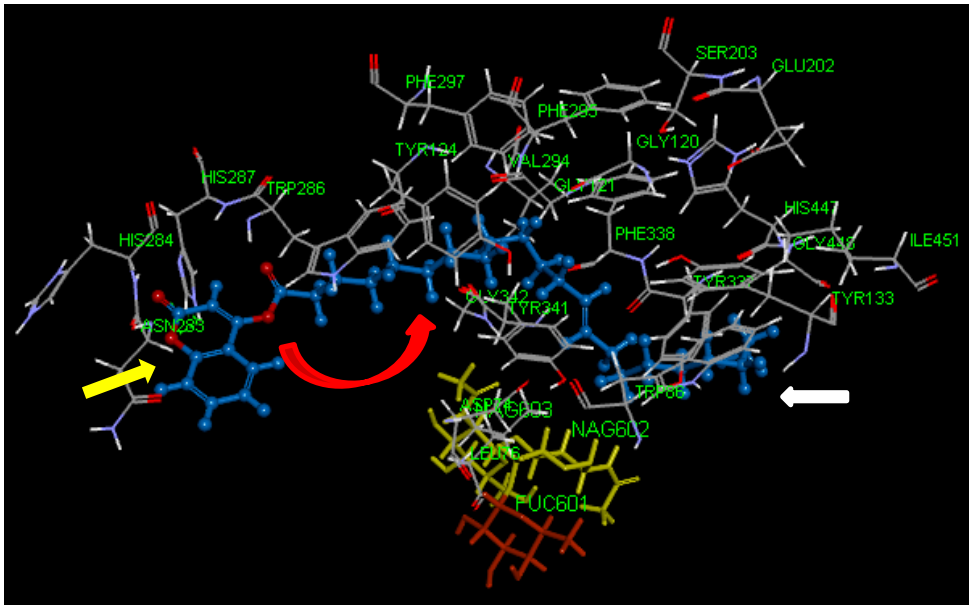

Figure 4.21: **BPR 2 (blue ball-and-stick)** docked in the hAChE protein with neighbouring atoms (**line models**). The coumarin entity (**yellow arrow**) inside the PAS with the elongated lipophillic entity (**red arrow and white arrow**) in the gorge and CAS.

Two hydrogen bonds between the pyrone ring of **BPR2** and HIS287 **were observed (Figure 4.24; yellow arrow; dotted orange and green line)** with influencencial neighbouring and the lipophillic entity strentching towards the CAS (Figure 24; blue sphere) through the gorge.

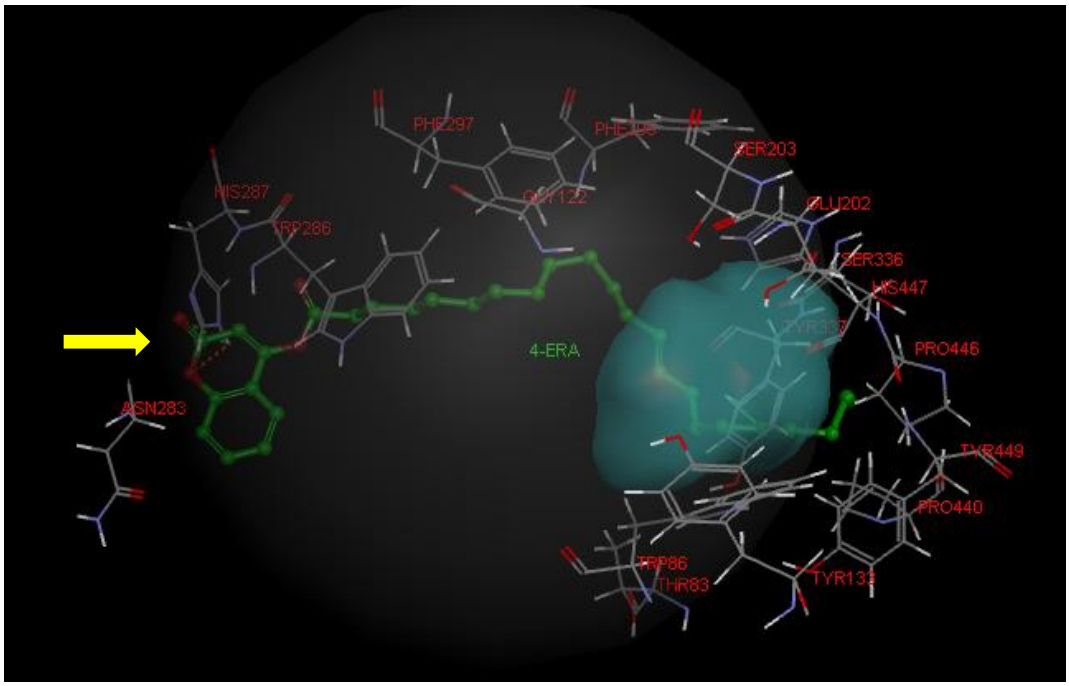

Figure 4.22: **BPR 2 (green ball-and-stick)** located in the PAS site of the actives site illustrated in transparent cyan, including the CAS site in transparent blue. Two hydrogen bonds between the pyrone ring of **BPR2** and HIS287 **(yellow arrow; dotted orange and green lines)** with influencencial neighbouring atoms **(line models)** are illustrated.

The pyrone ring of the 4-Hydroxycoumarin - erucic acid ester conjugate (**BPR2**) was in the ideal conformation to firstly interact with the HIS287 (**Figure 4.23)** *via* **two** hydrogen bonds (Distance:1.986887 Å; angle 86.104311° and distance :2.053422 Å; angle:45.252811°).

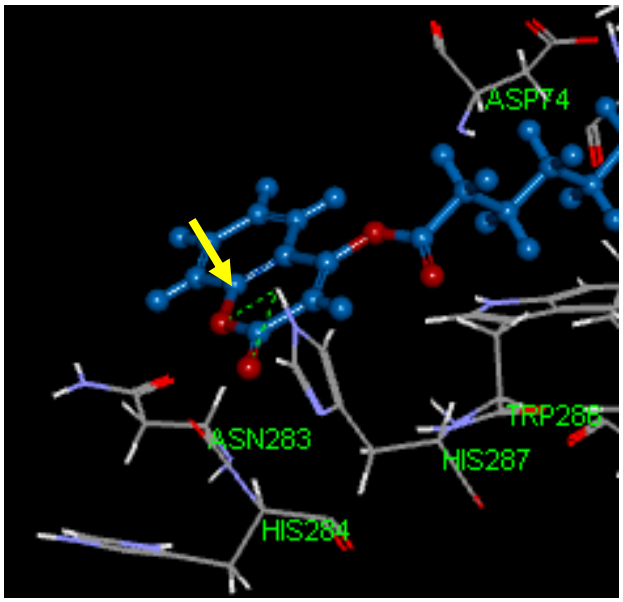

Figure 4.23: Enlargement of the two hydrogen bonds **(green dotted lines; yellow arrow)** between the pyrone ring of **BPR2 (blue ball-and-stick)** and HIS287.

4.6.3.2.2. BPR13 hAChE Modelling

BPR13 (**Figure 4.24**; blue ball-and-stick) were docked into hAChE. Hydrogen bonds (**Figure 4.24**; dotted green line) and Pi-interactions (**Figure 4.24**; orange lines) can be observed between the inhibitor and enzyme residues (**Figure 4.24)**.

EE AChE Activity (100 µM) = 57.43 %	EE AChE Activity (1 µM) = 21.560 %	CDocker Energy = 13.4973

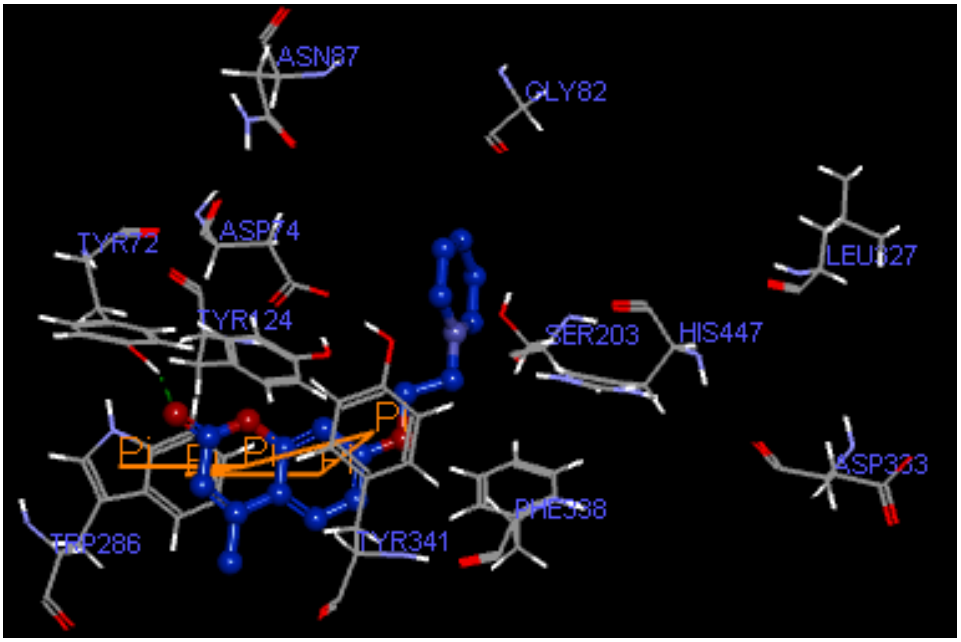

Figure 4.24: **BPR13** (**blue ball-and-stick**) docked into the active site of hAChE including interactions between residues.

5 Pi-Pi interactions (noncovalent interactions between aromatic rings) occurs (violet, pink, yellow, orange green lines) between **BPR13** and TYR283 and TRP341 and a H-bond (green dotted line) with TYR72 residues within the PAS **(Figure 4.25)**.

Pi-Pi interaction between TRP341 **(Figure 4.25)**: Orange Line between the phenol ring and TRP341 (Distance of 3.802244 Å and angle 19.229446 °); Violet Line between the pyrone ring and TRP341 (Distance of 4.869986 Å' and angle of 7.121048 °).

Pi-Pi interaction between TYR286 **(Figure 4.25)**: Yellow line between phenol ring en TYR286 (Distance of 5.215086 Å and angle of 9.396214 °); Green Line **(Figure 4.25)** between the pyrone ring and TYR286 (Distance of 4.868339 Å and angle of 22.783676 °) and Pink line **(Figure 4.25)** between the pyrone ring and TYR286 (Distance of 4.040728 Å and angle of 7.120387 °).

Hydrogen Bonding: Green dotted line between OH (white labelled) of the pyrone ring and TYR72 (Distance of 2.193334 Å and angle of 119.997215 °) depicted in **Figure 4.25.**

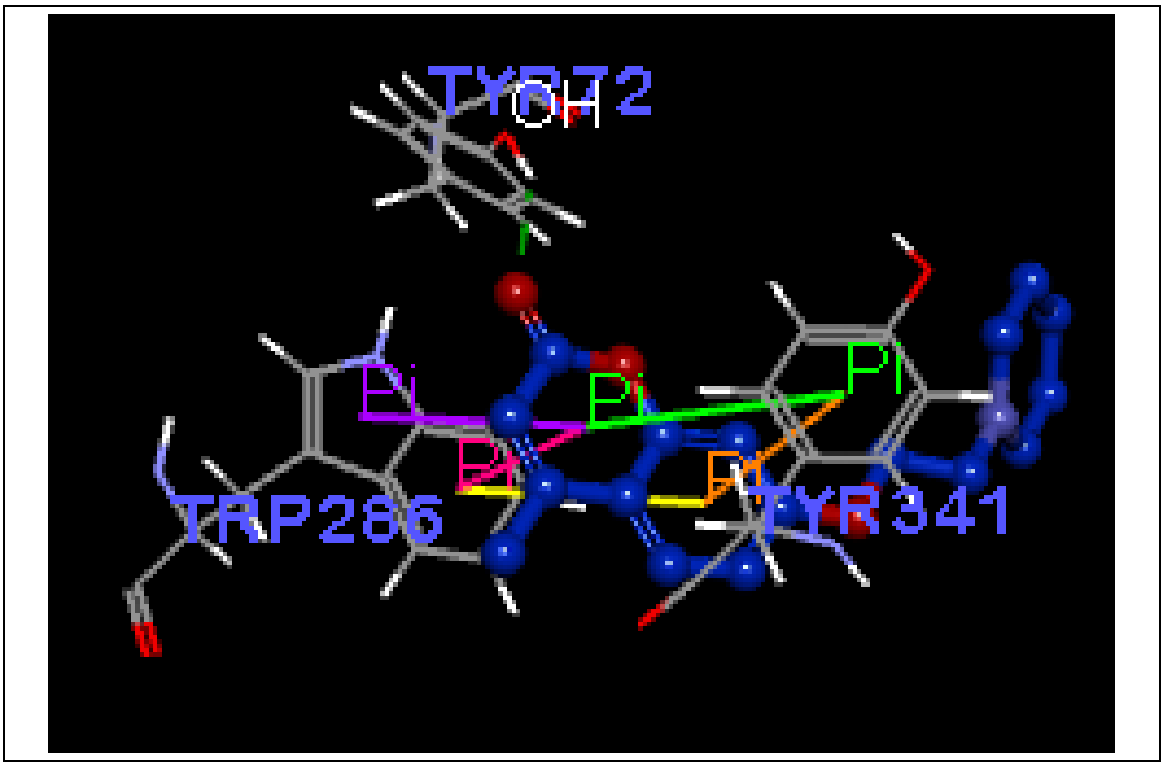

Figure 4.25: A detailed view of the 5 Pi-Pi interactions (**violet, pink, yellow, orange and green lines)** as well as the H-bond (**dotted green line**) between the compound and hAChE protein residues.

The docking of **BPR2** and **BPR13** illustrated similarity, with the coumarin moiety located in the PAS and the pyridine (**BPR13; Figure 4.24**) and the elongated fatty chain (**BPR2; Figures 4.21 and 4.22**) moiety in the gorge reaching towards the CAS of the enzyme.

4.7. SUMMARY.

4.7.1. Inhibition Studies.

The activities of the newly synthesised inhibitors were successfully evaluated against hMAO-B and EE AChE. The coumarin-morpholino ether conjugate, **BPR 10** (4-[2-(Morpholin-4-yl)ethoxy]-2*H*-chromen-2-one) was found be the most promising inhibitor of hMAO-B with an IC_{50} of 0.372 µM (**Table 4.2**; **Graph 4.5** and **Graph 4.6**). The coumarin-piperidine conjugates, **BPR 13** (4-Methyl-7-[2-(Piperidin-1-yl)ethoxy]-2H-chromen-2-one), was the most promising inhibitor of EE AChE at 100 µM (**Table 4.4**; **Graph 4.8**) with activity of 57.43 %. (21.560 % at 1µM). **BPR12** (7-[2-(Piperidin-1-yl)ethoxy]-2*H*-chromen-2-one) was the most potent at 1µM (**Table 4.4**; **Graph 4.7**) with inhibitory activity of 30.900 % (52.90 % at 100 µM).

4.7.2. Molecular Modelling.

BPR 10 was illustrated to transverse both the entrance cavity and substrate cavity of MAO-B with the lactam of the coumarin's pyrone ring forming hydrogen bonding with LEU171, PI interaction with TYR398 and Pi-Sigma interaction with LEU171 in the substrate cavity while the morpholine moiety is situated in the entrance cavity (**Figure 4.17**). Regarding AChE, the pyrone entity of **BPR13** formed 3 Pi-Pi bond interactions with TRP286, 2 Pi-Pi bond interactions with TYR341 and a H-bond with TYR72 in the PAS (**Figure 4.25**), while the piperidine moiety is situated in the gorge reaching towords the CAS (**Figure 4.24**).
The discussion and conclusion of the results are presented in **Chapter 5**.

Chapter 5 Discussion and Conclusion

5.1. INTRODUCTION.

Alzheimer's Disease (AD) is a multifaceted neurodegenerative disease characterised by a decline in cognitive abilities and non-cognitive abilities like anxiety, depression, apathy and psychosis (Assal *et al*., 2002). It's estimated that by the mid 21st century an individual in the United States will develop AD every 33 seconds (Alzheimer's Association, facts and figures, 2013), with a lifespan of 8 – 10 years (Small *et al*., 1997), placing a burden on the health sector.

Late-onset AD (LOAD) and early-onset familial AD (EOFAD) are distinguished, with aging and gene mutations respectively the cause (Serretti *et al.,* 2007). It affects multiple neurotransmitter systems with atrophy of the cholinergic system in the hippocampus the most dominant (Perry, 1986; Fibiger, 1991), while the dopamine and serotoninergic systems attributes to the non-cognitive symptoms (Assal *et al*., 2002; Erkinjuntti, 2002).

The hallmarks of AD (**Chapter 1 - Figures 1.1 and 1.2;)** include the presence of amyloid plaques (consisting of the Aβ protein), neurofibrillary tangles (composed of hyperphosphorylated tau) and neuro-inflammation caused by oxidative stress and numerous other factors (Saido T.C. 2003; Salloway *et al.,* 2008). Current treatment regimens (**Chapter 1 – section 1.1.4, Figure 1.3**) involve AChE inhibitors (donepezil, rivastigmine, galanthamine) and the NMDA antagonist, memantine, which is only available in the US and Europa (Mobius, 2008; Winblad *et al*., 2003; Rogawski *et al*., 2003; Reisberg *et al*., 2003).

5.2. PROBLEM STATEMENT AND HYPOTHESIS.

Current available drugs only provide symptomatic relieve, and because of the prevalence of parallel pathways (Frans *et al*., 2005; Mencher *et al.,* 2005) do not address the multifactorial underlying AD neurodegeneration pathology (Kasa *et al*., 1997; Gualtieri *et al*., 1996).

Thus, a new generation of drugs is required to treat the effects of the multifactorial underlying deficiency and a multi-target-directed (MTDLs) ligand approach could provide this (**Chapter 1 – section 1.2, Figure 1.4**). It can fundamentally be summarised as one compound that interacts with multiple targets (enzymes/receptors) to deliver a cumulative desired effect and addressing the multiple biological systems involved, where AChE and MAO-B are applicable in this study.

5.3. AIMS AND OBJECTIVES.

To achieve this, the coumarin chemical scaffold served as a nucleus/pharmacophore to synthesise novel compounds for MTDL activity. Molecular modelling studies were used to identify promising moieties to obtain the best biological activity. Rational and beneficial neuroprotective moieties (**Chapter 1** - **Table 1.1; section 1.3**) were conjugated in position 4 and 7 of the coumarin (*via* ether and esterification) to yield potential novel coumarin conjugates (**Table 5.1**).

Table 5.1: Novel synthesised coumarin conjugates.

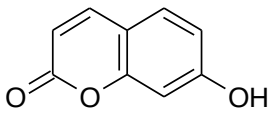 **7C**	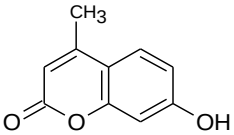 **4MC**	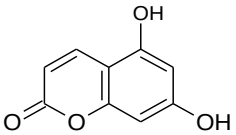 **4C**
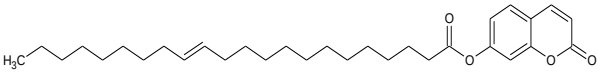 **BPR 1**	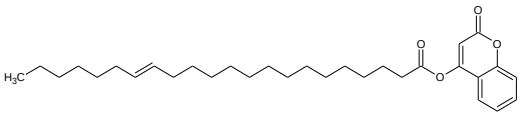 **BPR 2**	
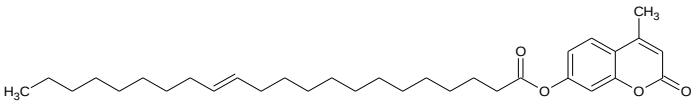 **BPR 3**	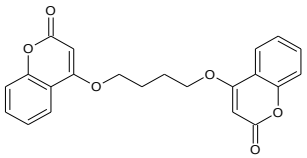 **BPR 4**	
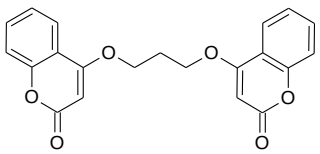 **BPR 5**	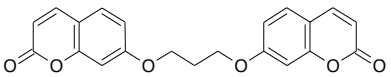 **BPR 6**	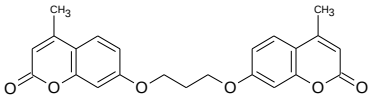 **BPR 7**
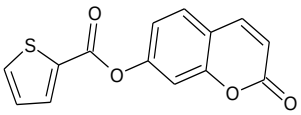 **BPR 8**	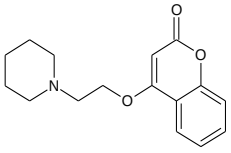 **BPR 9**	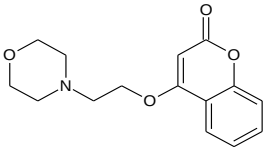 **BPR 10**
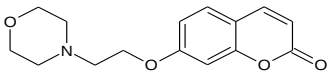 **BPR 11**	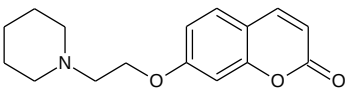 **BPR 12**	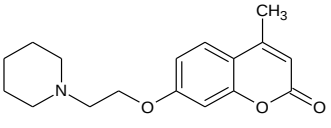 **BPR 13**
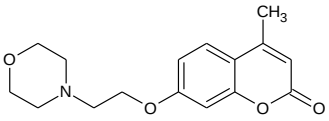 **BPR 14**		

This first series of compounds consist of different coumarins conjugated to erucic acid, which has numerous AD advantages (**Chapter 1 – section 1.3.5**), and esters **BPR1, BPR2 and BPR3** were synthesised **(Chapter 3 – section 3.4; scheme 3.4)**. Dimers has also been proven to be advantageous (**Chapter 1 – section 1.3.1**) and 4-hydroxycoumarin (**4C**) ester dimers were synthesised with 4 and 3 carbon spacers (**BPR4** and **BPR5**) respectively **(Chapter 3 – section 3.4; scheme 3.1)**. The 7-hydroxycoumarin (**7C**) dimer containing a 3 carbon spacer (**BPR6**) and a 7-Hydroxy-4-methyl coumarin (**4MC**) dimer (**BPR7**), were also synthesised **(Chapter 3 – section 3.4; scheme 3.1)**. The thiophene moiety, shown to exhibit a variety of neuroprotective properties **(Chapter 1 – section 1.3.4)** was conjugated to **7C** to yield the **BPR8** ester **(Chapter 3 – section 3.4; scheme 3.3)**. Piperidine, found in various compounds with anti-AD characteristics, was conjugated *via* a 2 carbon spacer to **7C**, **4MC** and **4C** to yield the respective coumarin – piperidine esters (**BPR12, BPR13, BPR9) (Chapter 3 – section 3.4; scheme 3.2)**. Similarly, the morpholine moiety (**Chapter 1 – section 1.3.3**) was conjugated to **7C**; **4MC** and **4C** to produce the coumarin – morpholine esters (**BPR11**, **BPR14**, **BPR10**) respectively **(Chapter 3 – section 3.4; scheme 3.3)**.

5.3.1. Outcomes:

- **i.** The desired compounds were successfully synthesised (**Chapter 3**) and their structures confirmed (^{1}H and ^{13}C NMR, MS Spectra and TLC was utilised).
- **ii.** AChE and MAO-B activities were determined (**Chapter 4**), and since MTDL design is the essence of this study, only the synthesised inhibtors that interact with both these target proteins were further discussed.
- **iii.** Molecular modeling determined the binding mode and key protein amino acid residue(s) interactions of the most potent inhibitor of each enzyme **(MAO-B – Figures 2.3 – 5.4 and AChE – Figure 5.10).** Physical-chemical and qualitative properties were identified which plays a pivotal role in activity.

5.4. CHEMISTRY.

For the purpose of the discussion of these compounds, a 7 substituted conjugate (**BPR12**) and a 7, 4 di-substituted conjugate (**BPR13**) were compared. The characteristic ^{1}H (**Table 5.2**; green) and ^{13}C NMR (**Table 5.2**; blue) signals of **BPR12** (**Spectra 5.1** and **5.2**) and **BPR13** (**Spectra 5.3** and **5.4**) show little variation in the chemical shift values and are depicted in **Table 5.2.** This can be utilised to accelerate the structure confirmation process for all compounds in this series.

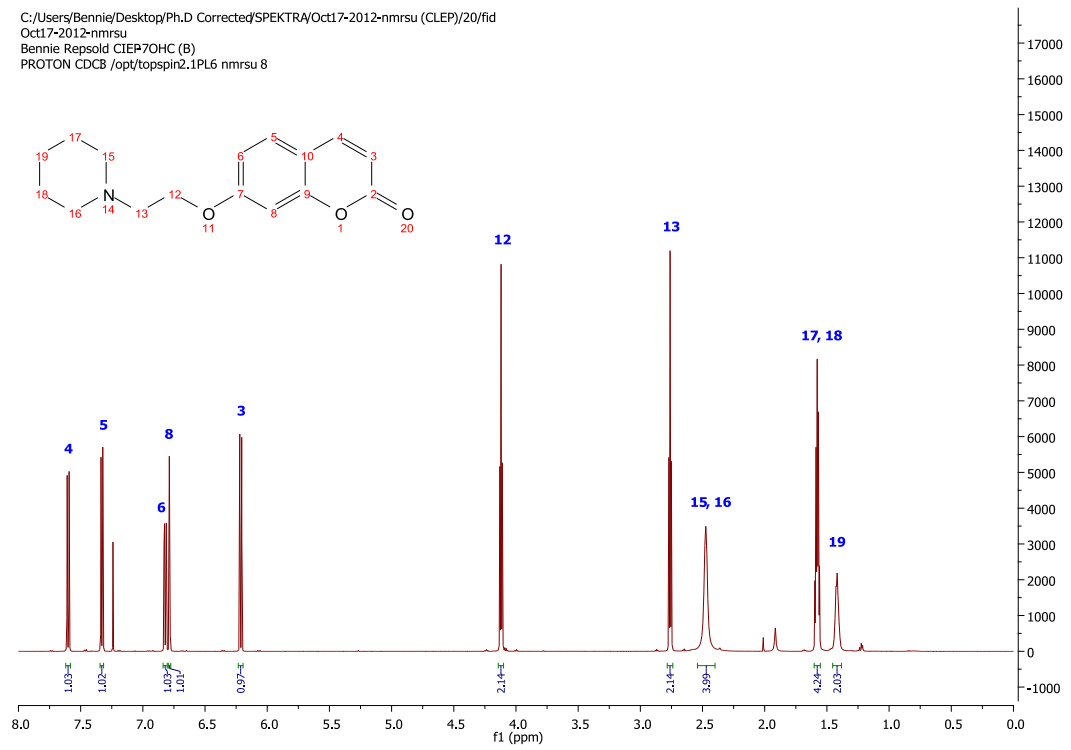

^{1}H NMR (600 MHz, $CDCl_3$,): δ 7.60 (d, J = 9.5 Hz, 1H, H_4); 7.33 (d, J = 8.6 Hz, 1H, H_5); 6.82 (dd, J = 8.6, 2.4 Hz, 1H, H_6); 6.79 (d, J = 2.4 Hz, 1H, H_8); 6.21 (d, J = 9.5 Hz, 1H, H_3); 4.12 (t, J = 6.0 Hz, 2H, H_{12}); 2.76 (t, J = 6.0 Hz, 2H, H_{13}); 2.47 (bs, 4H, $H_{15,16}$); 1.60 – 1.55 (m, 4H, $H_{17,18}$); 1.42 (bs, 2H, H_{19}).

Spectrum 5.1: Characteristic 1H NMR signals of **BPR12.**

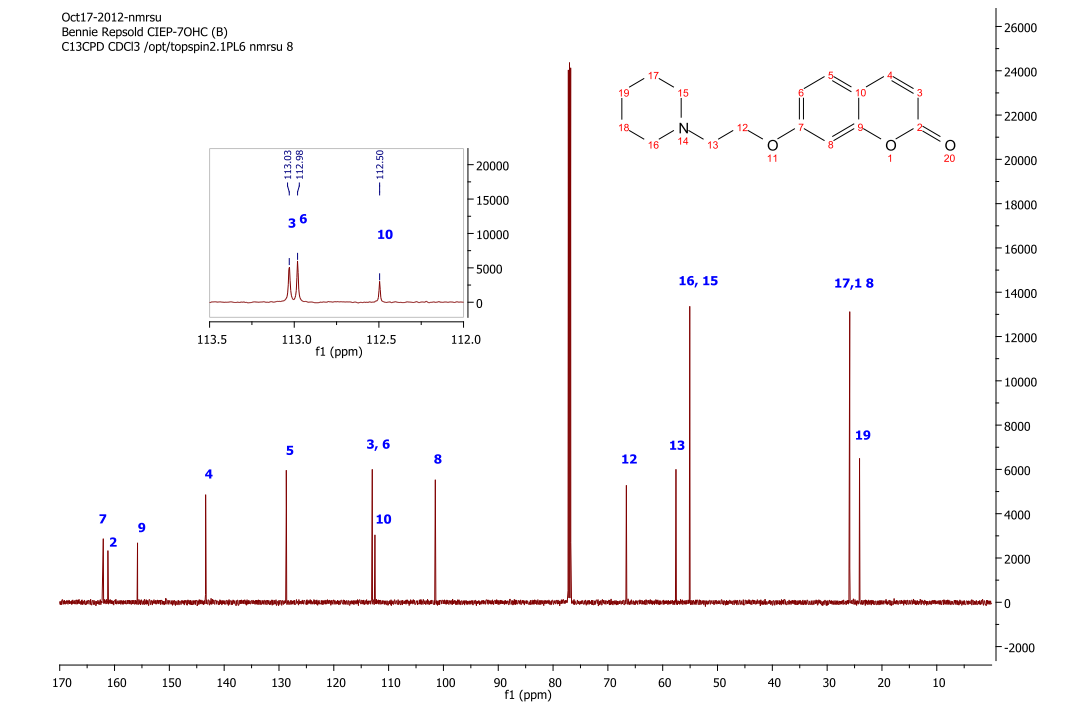

^{13}C NMR (151 MHz, $CDCl_3$,): δ 162.05 (C_7); 161.21 (C_2); 155.81 (C_9); 143.38 (C_4); 128.67 (C_5); 113.03 (C_3); 112.98 (C_6); 112.50 (C_{10}); 101.48 (C_8); 66.63 (C_{12}); 57.58 (C_{13}); 55.06 ($C_{15,\ 16}$); 25.88 ($C_{17,\ 18}$); 24.09 (C_{19}).

Spectrum 5.2: Characteristic ^{1}C NMR signals of **(BPR 12).**

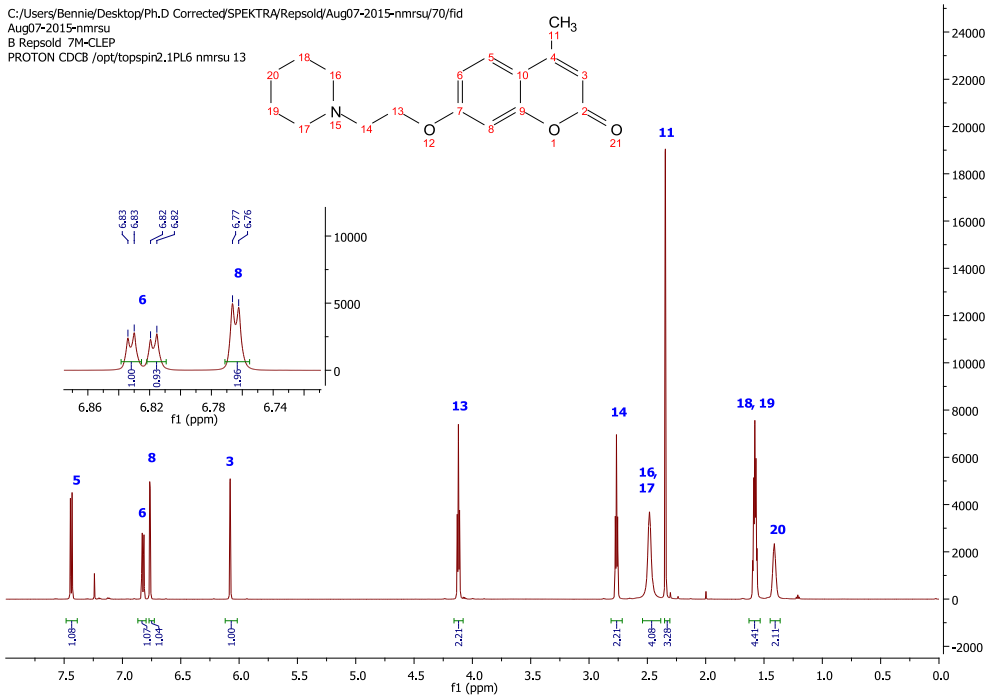

^{1}H NMR (600 MHz, $CDCl_3$,): δ 7.44 (d, J = 8.8 Hz, 1H, H_5), 6.82 (dd, J = 8.8, 2.4 Hz, 1H, H_6), 6.76 (d, J = 2.4 Hz, 1H, H_8), 6.08 (d, J = 0.9 Hz, 1H, H_3), 4.12 (t, J = 5.9 Hz, 2H, H_{13}), 2.76 (t, J = 5.9 Hz, 2H, H_{14}), 2.48 (bs, 4H, $H_{16,17}$), 2.35 (d, J = 1.0 Hz, 3H, H_{11}), 1.58 (m, 4H, $H_{18,19}$), 1.41 (bs, 2H, H_{20}).

Spectrum 5.3: Characteristic ^{1}H NMR signals of (**BPR13**).

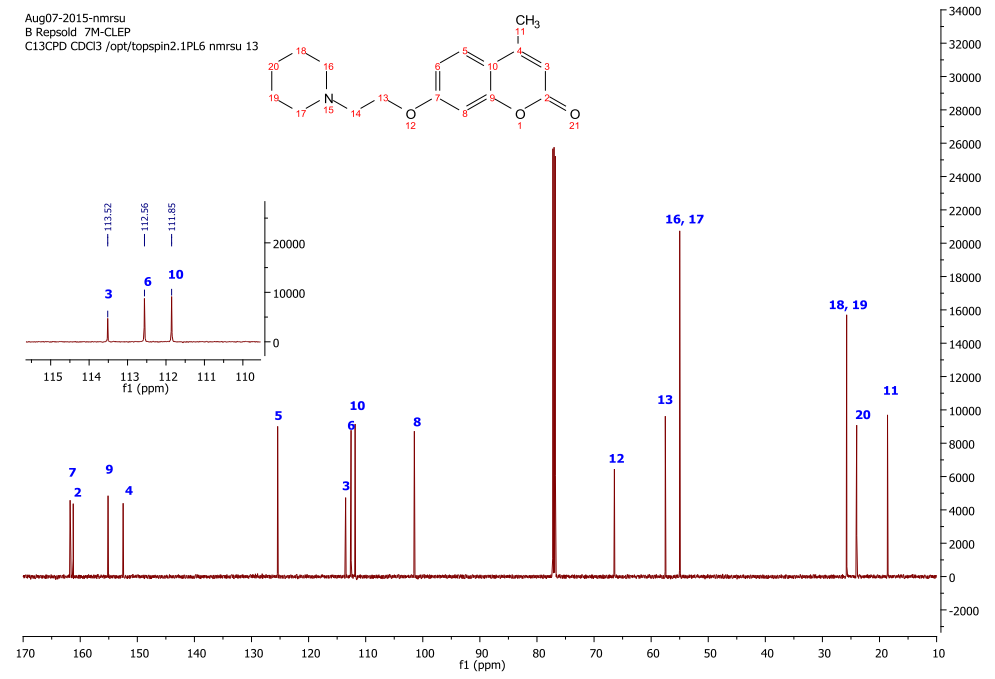

^{13}C NMR (151 MHz, $CDCl_3$,): δ 161.77 (C_7); 161.23 (C_2); 155.13 (C_9); 152.48 (C_4), 125.42 (C_5), 113.52 (C_3), 112.56 (C_6), 111.85 (C_{10}), 101.48 (C_8), 66.44 (C_{12}), 57.52 (C_{13}), 55.00 ($C_{16,17}$), 25.76 ($C_{18,19}$), 24.00 (C_{20}), 18.60 (C_{11}).

Spectrum 5.4: Characteristic ^{13}C NMR signals of **(BPR 13).**

H2, H4 if substituted and **H7, H9** and **H10,** which are saturated, will not reflect any ^{1}H NMR signals (ppm). The **H3** doublet (6.08 - 6.21) and the **H4** (unsubstituted) doublet (≈ 7.60) are clearly distinguished. The **H5** doublet (7.33 – 7.44), **H6** doublet of doublets (6.76 - 6.79) and the **H8** doublets (≈ 6.82) are also characteristic for these compounds.

The ^{13}C NMR signals (**Table 5.2**; **Figure 5.1**) of the coumarin nucleus (ppm) – from high field to low field: **C7 substituted** (161.77 - 162.05); **C2** (161.21 - 161.23); **C9** (155.81 - 155.13); **C4 unsubstituted** (≈ 143.38) but **C4 substituted** (≈ 152.48); **C5** (125.42 - 128.67); **C3** (113.03 - 113.52); **C6** (112.56 - 112.98); **C10** (111.85 - 112.50) and **C8** (≈ 101.48).

Table 5.2: Outlined characteristic ^{1}H and ^{13}C NMR signals of compounds **BPR12 (Spectra 5.1 and 5.2)** and **BPR13 (Spectra 5.3 and 5.4).**

BPR 12		**BPR13**	
^{1}H NMR signals (δ; ppm)	**^{13}C NMR signals (δ; ppm)**	**^{1}H NMR signals (δ; ppm)**	**^{13}C NMR signals (δ; ppm)**
7.60 (d, 1H, H_4)	162.05 (C_7)	7.44 (d, 1H, H_5)	161.77 (C_7)
7.33 (d, 1H, H_5)	161.21 (C_2)	6.82 (dd, 1H, H_6)	161.23 (C_2)
6.82 (dd, 1H, H_6)	155.81 (C_9)	6.76 (d, 1H, H_8)	155.13 (C_9)
6.79 (d, 1H, H_8)	143.38 (C_4)	6.08 (d, 1H, H_3)	152.48 (C_4)
6.21 (d, 1H, H_3)	128.67 (C_5)	4.12 (t, 2H, H_{13})	125.42 (C_5)
4.12 (t, 2H, H_{12})	113.03 (C_3)	2.76 (t, 2H, H_{14})	113.52 (C_3)
2.76 (t, 2H, H_{13})	112.98 (C_6)	2.48 (bs, 4H, $H_{16,17}$)	112.56 (C_6)
2.47 (bs, 4H, $H_{15,16}$)	112.50 (C_{10})	2.35 (d, 3H, H_{11})	111.85 (C_{10})
1.60 – 1.55 (m, 4H, $H_{17,18}$)	101.48 (C_8)	1.58 (m, 4H, $H_{18,19}$)	101.48 (C_8)
1.42 (bs, 2H, H_{19}).	66.63 (C_{12})	1.41 (bs, 2H, H_{20})	66.44 (C_{12})
	57.58 (C_{13})		57.52 (C_{13})
	55.06 ($C_{15, 16}$)		55.00 ($C_{16,17}$)
	25.88 ($C_{17, 18}$)		25.76 ($C_{18, 19}$)
	24.09 (C_{19})		24.00 (C_{20})
			18.60 (C_{11})

5.5. BIOLOGICAL EVALUATION.

The synthesised compounds were evaluated against recombinant hMAO-B (100 µM) and EE AChE (1 µM and 100 µM). Compound **BPR12** was the most effective AChE inhibitor at 100 µM and **BPR13** at 1 µM. Compound **BPR10** was the most potent MAO-B inhibitor. MAO-B values (IC_{50} µM) and AChE inhibition (expressed in percentage), were obtained. Due to the fact that both these enzymes do contribute to AD pathology, only compounds that interacts with both was further explored and discussed.

5.5.1. MAO-B Inhibition

All the novel synthesised compounds had lower MAO-B inhibitory activity than the reference compound **(*R*)-Deprenyl** as represented in **table 5.3.** The indication of **(*R*)-Deprenyl** is Parkinson's Disease, but its mechanism of action is highly selective, irreversible MAO-B inhibition. This pharmacological action makes it a suitable reference drug as a MTDL for AD as the MAO-B element plays a critical role in the pathology of AD.

MAO-B activity of the basic coumarinns were enhanced by nearly one log unit by conjugation of 7-hydroxycoumarin (**7C**; IC_{50} = 28.583 µM) to erucic acid to form the coumarin ester, **BPR 1** (IC_{50} = 3.680 µM). Introducing the 2 carbon ''spacer'' (an ethyl chain between the two moieties) yielded coumarin ethers of morpholine (**BPR 11**; IC_{50} = 9.758 µM) and piperidine (**BPR 12**; IC_{50} = 9.209 µM). This added distance between the coumarin and the entities endows the compounds the abiltiy to interact with more amino acid residues like ILE198 and ILE199, which consequently allows the compound to transverse the entrance cavity to access the substrate cavity of the active site of MAO-B e.g. which is also known as the "gating switch". The 4-methylated-7-hydroxycoumarin (**4MC**; IC_{50} = 94.327 µM) conjugate also revealed a significant increase in activity with the 2 carbon ''linker''. Both the piperidine coumarin ether (**BPR 13**; IC_{50} = 3.093 µM) and morpholine coumarin ether (**BPR 14**; IC_{50} = 2.326 µM) exhibited higher activity. Although 4-hydroxycoumarin (**4C**) was devoid of activity, its ether conjugate with piperidine (**BPR 9**; IC_{50} = 21.720) showed activity and it produced the most potent compound, the conjugate with morpholine (**BPR 10**; IC_{50} = 0.372 µM). With respect to the morpholine series: **BPR10** (0.372 µM) revealed a higher activity than **BPR14** (2.326 µM) of 6.253 fold (p = 0.246). **BPR10** is only substituted on the 4 position, making the coumarin pharmacophore more polar and placing it in an angular position suitably close to the FAD of hMAO-B. **BPR14**, on the other hand, is substituted on the 7 position and contains a methyl moiety on the 4 position. The methyl substitution resulted in a less polar coumarin nucleus but "fills the space" in the substrate cavity of the hMAOB's active site less optimally. It does however allow for possible intermolecular interaction between the compound and the protein's residues, resulting in a relatively low IC_{50}.

In the piperdine series; **BPR13** (3.093 µM) revealed a slightly higher activity than **BPR12** (9.209 µM) of 2.977 fold (p = 0.0338). **BPR12** is only conjugated on the 7 position a sp^2 piperidine moiety, which makes the coumarin nucleus more polar. **BPR13** is conjugated both with a sp^2 piperidine moiety on the 7 position and with a methyl group on the 4 position, resulting in a less polar coumarin nucleus. The 4 methyl substitution allows for additional intermolecular bonds between the compound and the substrate cavity's residues. This possibly contributes to higher activity.

Table 5.3: MAO-B inhibition values of the synthesised inhibitors including the relevant graphical representation. Red bars indicates the reference drug and parent compounds, green bar the most potent compound, blue and yellow bars activity in the same range.

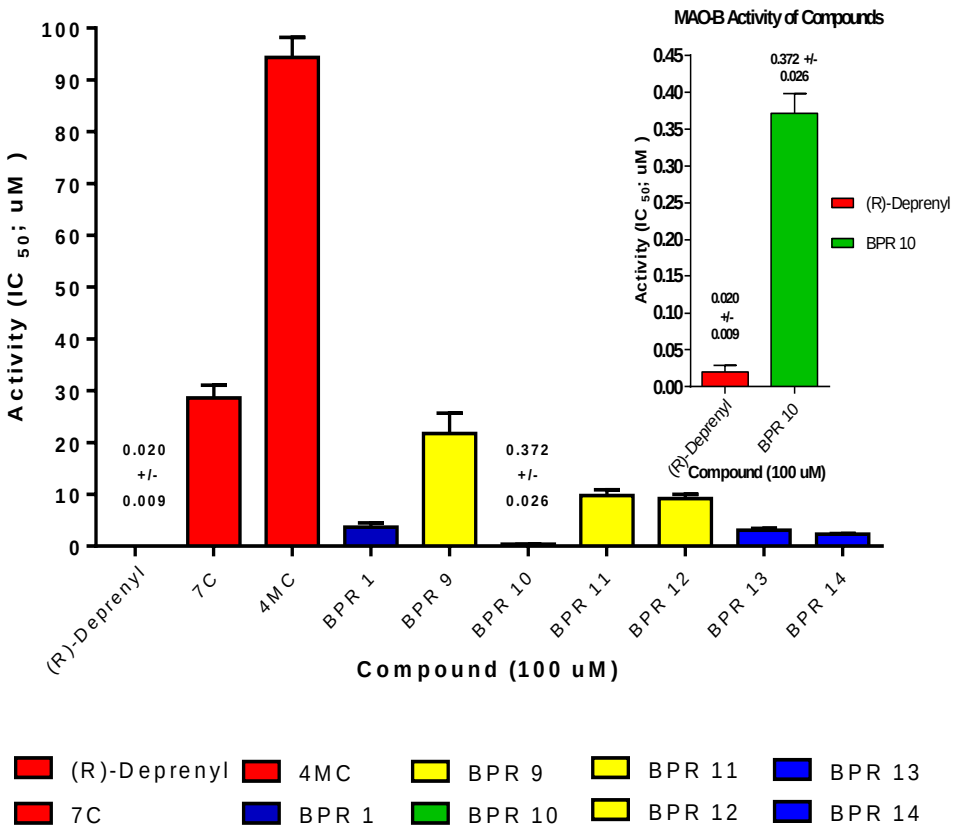

COMPOUND	IC_{50} (µM)	SD	COMPOUND	IC_{50} (µM)	SD
(R)-Deprenyl (control)	0.020	0.009	**BPR10**	**0.372**	**0.026**
7C	28.583	2.519	BPR11	9.758	1.153
4MC	94.327	3.889	BPR12	9.209	0.794
BPR1	3.680	0.836	BPR13	3.093	0.312
BPR9	21.720	3.974	BPR14	2.326	0.131
4C (a parent compound) and **BPR2 - BPR8** revealed no activity					

p<0.05, **p<0.001, ***p<0.0001. All experiments were conducted in triplicate.

The activity profile of the synthesised compounds can be divided into 3 groups: green bar (most potent), blue bars (relatively potent) and yellow bars (less potent). The most potent compound **BPR10** is indicated as the green bar relative to (*R*)-Deprenyl (**Table 5.3 - insert**). The blue bars presents compounds with relative activity (**Table 5.3 – BPR1, BPR13 - 14**) ranging from 2.326 µM to 3.680 µM. Compounds that are less potent are presented in yellow bars and ranged from 9.209 µM to 21.720 µM (**Table 5.3 – BPR9, BPR11 - 12**).

In order to assess the role of the lipophilicity of the test compounds - the Log P was calculated. **BPR10** (Log P = 0.67+/- 0.75) revealed a 6.253 fold increase in contrast with **BPR14** (Log P = 1.72+/- 0.45). MAO-B inhibition favours conjugation on the 4 position and less lipophilicity. **BPR13** (Log P = 3.38+/- 0.41) revealed a 2.977 fold increase to **BPR12** (Log P = 1.13+/- 0.46) – which indicates that the substrate cavity refers more polar inhibitor structures. Additionally, polarisability (an instrument to measure the polarity of a compound) was calculated for comparable compounds **BPR10** and **BPR12**. **BPR10** (Polarisability: 29.03 ± 0.5 $10^{-24}cm^3$; Log P = 0.67+/- 0.75) exhibited an increase of 24.755 fold approximate to **BPR12** (Polarisability: 28.82 ± 0.5 $10^{-24}cm^3$; 1.13+/- 0.46) a more polar conjugate (morpholine instead of piperidine) is preferred. The 4 substitution with morpholine (**BPR10**), piperidine (**BPR9**) or a small methyl entity (**BPR13, BPR14**) may play a role with conformational preference of these structures.

5.5.2. AChE Inhibition.

The synthesised compounds were evaluated against EE AChE at concentrations of 100 µM (**section 5.4.2.2.1**) and 1 µM (**section 5.4.2.2.2**). All of the synthesised compounds in **Figure 5.2** exhibited lower AChE potency than the reference compound Tacrine (75.81 % at 100 µM and 61.52 % at 1 µM). All compounds dissolved at 1 µM but only compounds **4MC, 4C, BPR9, BPR11 – BPR13** couldn't be evaluated 100 µM due to solubility problems with the rest of the compounds. Coumarin and the 7-hydroxycoumarin both have low water solubility (0.22 % and 0.031 %, respectively) resulting in low *in vivo* bioavailability (**Chapter 3 – section 3.2**).

5.5.2.1. AChE Inhibition at 100 µM.

The tested compounds revealed AChE inhibition of the enzyme that ranged from 11.040 % (**4MC**) to 57.430 % (**BPR13**) at 100 µM concentrations. **BPR13** proved to be the most potent inhibitor of the series followed by **BPR12** with inhibition of 57.430 % and 52.900 % respectively (**Table5.4; green bars**). The increased activity of **BPR13** (LogP = 3.38) is probably due to the 2 carbon spacer between the coumarin and piperidine, difference in binding conformation as well as a more lipophilic coumarin nucleus due to the methyl substitution on the 4 position, **BPR12** (LogP = 1.13) lack the latter characteristic. **BPR9** (**Table 5.4; blue bar**) expressed activity of 27.770 % while **BPR11** (12.480 %) and the parent compounds **4C** (11.640 %) and **4MC** (11.040 %) displayed activity in the same range (**Table 5.4; yellow bars**). The moderate activity of **BPR9** (LogP = 2.32) may prove that a spacer between the pharmacophore (coumarin) and a less polar conjugate (piperidine) improved activity in contrast with **BPR10** (LogP = 0.67) with a more polar conjugate (morpholine) which expressed no activity. AChE inhibition thus seem to favour a two carbon chain linkage as well as lipophilicity. Conformational flexibility of these structures may also allow for the potential binding abilities

in the active site. **7C, BPR1 – BPR8, BPR 10** and **BPR14** were devoid of EE AChE activity at 100 µM. **BPR13** (57.43 %) revealed a 1.320 fold (p = 0.0012) lesser potency than the reference compound Tacrine (75.81 %) but a 2.069 fold (p = 0.0169) and a 4.602 fold (p = 0.0059) higher activity **BPR11** (12.480 %). **BPR13** also exhibited a 5.221 fold (p = 0.0021) increase regarding its parent compound **4MC** (11.000 %).

Table 5.4: EE AChE inhibition activity of the synthesised inhibitors at 100 µM and 1 µM. Solid bars represent 100 µM activity and patterned bars 1 µM activity.

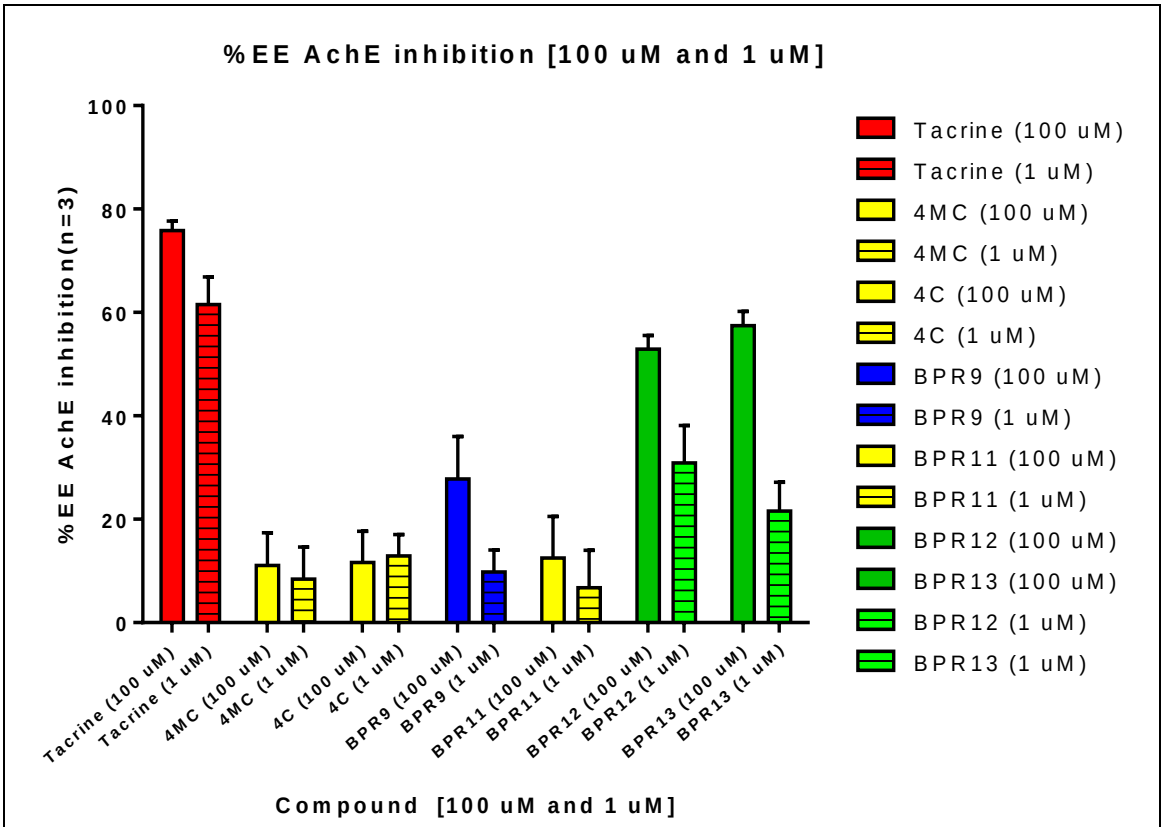

COMPOUND	% EE AChE activity, [100 µM]	% EE AChE activity, [1 µM]
Tacrine	75.81 ± 1.845***	61.52 ±5.369***
4MC	11.04 ± 6.362	8.415 ± 6.231
4C	11.64 ± 6.054	12.910 ± 4.157
BPR9	27.77 ± 8.243*	9.780 ± 4.268
BPR11	12.48 ± 8.075	6.750 ± 7.239
BPR12	52.90 ± 2.621***	**30.90 ± 7.259****
BPR13	**57.43 ± 2.743*****	21.560 ± 5.589*

Note: Significance =p<0.05, **p<0.001, ***p<0.0001. All experiments were conducted in triplicate.

The 1.320 fold increase of **BPR13** (Log P = 3.38+/- 0.41) *vs*. **BPR9** (Log P = 2.32+/- 0.75) is due to the conjugation of the coumarin on the 7 and the methylated 4 position.
The increase in lipophilicity and enhancement in AChE inhibitory activity of 7 substituted conjugates is ratified by various authors (Piazzi *et al*., 2007: **Chapter 2 – section 2.2.5.1; figure 2.21** and Fallarero *et al*., 2012: **Chapter 2 – section 2.2.5.1; .Figure 2.26**). The 4.602 fold increase of **BPR13** (Log P = 3.38+/- 0.41) compared to **BPR11** (Log P = 1.13+/- 0.46) proved the 4-methylated-coumarin to be more effective.

5.5.2.2. AChE Inhibition at 1 μM.

The most potent EE AChE inhibitors *of this series* at the lower concentration were **BPR12** (30.90 %), **BPR2** (22.460 %) and **BPR13** (21.560 %) at 1 μM (**Table 5.6; green bars**). Inhibition in the same range were exhibited by **BPR3, BPR14, BPR6, BPR10, BPR4** and **BPR1** at 16.450 %, 16.170 %, 14.960 %, 14.610 %, 13.870 % and 13.530 % (**Table 5.6; blue bars**). Compounds that revealed slightly less activity in the same range were **BPR8**, **BPR9** and **BPR7** (12.090 %, 9.780 % and 8.910 %) respectively (**Table 5.5; yellow bars**). Compounds with activity weaker than its respective parent compounds were **BPR 5** (4.760 %) and **BPR 11** (6.750 %), (**Table 5.5; black bars**). The parent compounds **4C, 7C** and **4MC** revealed EE AChE inhibition of 12.910 %, 9.585 % and 8.415 % individually at 1 μM (**Table 5.5; red bars**).

BPR12 (30.900 %) revealed a decrease of 1.991 fold (p = 0.0054) compare to the reference compound, Tacrine (61.520), but **BPR12** revealed an increase when compared to: **BPR9** (9.780 %) of 3.160 fold (p = 0.0193); **BPR11** (6.750 %) of 4.578 fold (p = 0.0151); **BPR10** (14.610 %) of 2.115 fold (p = 0.0389); **BPR6** (14.960 %) of 2.066 fold (p = 0.0413); **BPR7** (8.910 %) of 3.468 fold (p = 0.0206); **BPR4** (13.870 %) of 2.228 fold (p = 0.0343); **BPR5** (4.760 %) of **6.492** fold (p = 0.0116) and **BPR1** (13.530 %) of 2.284 fold (p = 0.0327). Parent compound **7C** (9.585 %) is 3.224 fold (p = 0.0285) less active than its conjugate **BPR12** (30.900 %)**.**

The enhanced activity of **BPR2** (22.460 %) is probably due to the methyl substitution on the 4 position of the coumarin which prevent steric hindrance and beneficially allows for elevated lipophilicity. This enables the pyrone entity to interact with more pivotal residues in the PAS and the elongated lipophilic erucic acid conjugate in the gorge and CAS.

Table 5.5: EE AChE inhibition values of synthesised inhibitors at 1 µM including the appropriate graph. Red bars indicates the reference drug and parent compounds, green bars the most potent compounds, blue and yellow bars activity in the same range and black bars compounds with weaker activity in relation to their respective parent compounds.

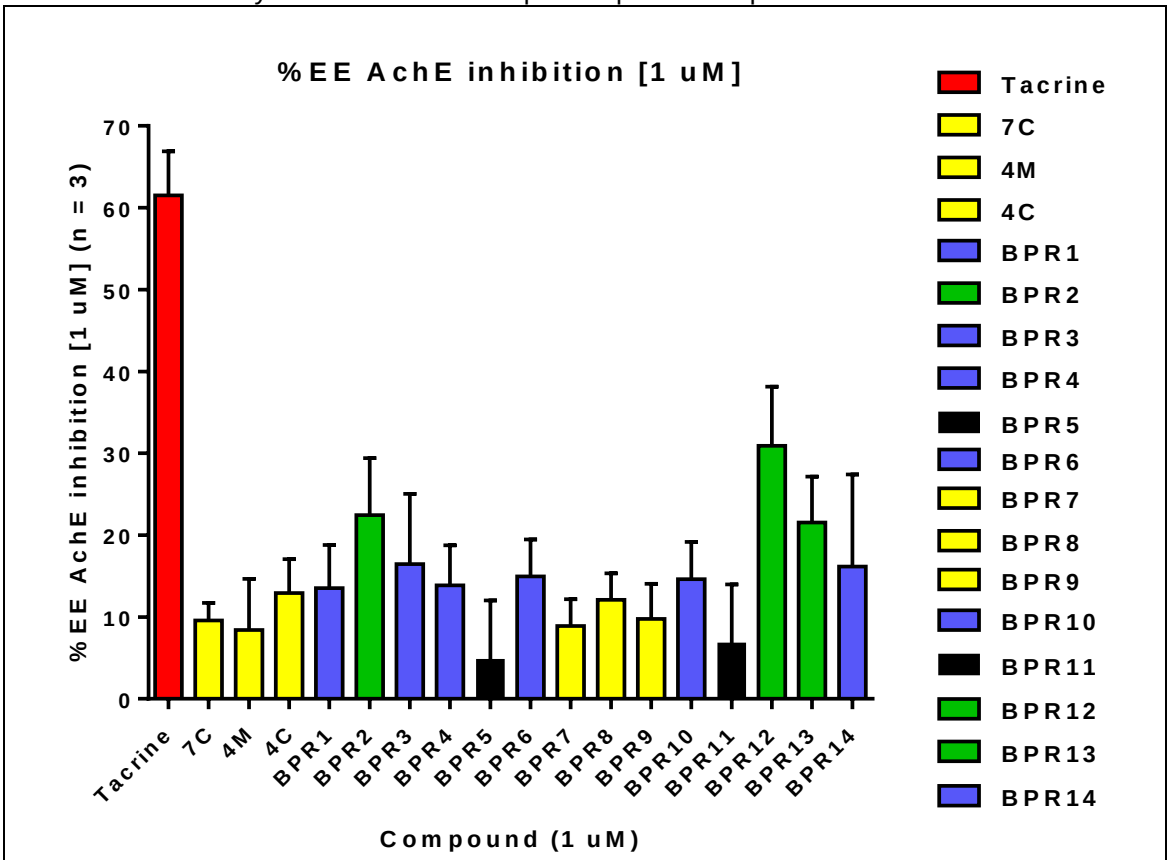

Compound	% EE AChE activity(n=3), [1 µM]	Compound	% EE AChE activity(n=3), [1 µM]	Compound	% EE AChE activity(n=3), [1 µM]
Tacrine	61.52 ± 5.369***	BPR3	16.450± 8.583	BPR9	9.780 ± 4.268
7C	9.585 ± 2.135	BPR4	13.870 ± 4.875	BPR10	14.610 ± 4.568
4MC	8.415 ± 6.231	BPR5	4.760 ± 7.258	BPR11	6.750 ± 7.239
4C	12.910 ± 4.157	BPR6	14.960 ± 4.512	**BPR12**	**30.90 ± 7.259****
BPR1	13.530 ± 5.265	BPR7	8.910 ± 3.265	BPR13	21.560 ± 5.589*
BPR2	22.460± 6.959*	BPR8	12.090 ± 3.257	BPR14	16.170 ± 11.25

p<0.05, **p<0.001, ***p<0.0001. All experiments were conducted in triplicate.

BPR12 (30.900 % at 1 µM and 52.900 % at 100 µM) exhibited activity in the same range of **BPR13** (21.560 at 1 µM and 57.430 % at 100 µM). Interesting to note that **BPR12** exhibited the most promising activity at 100 µM, whereas **BPR13** at 1 µM. This non-linear concentration effect on activity (**BPR13** being more potent at 100 µM and **BPR12** more potent at 1 µM) may be due to the difference in the degree of solubility of these compounds or experimental variation.

5.6. MOLECULAR MODELLING.

Molecular Modelling implements molecular graphics and computational chemistry techniques to build, simulate and analyse potential drug candidates (ligands) within their specific pharmacological target protein(s) and performs numerous quantum mechanical calculations (Vlok *et al*., 2005). This involves docking and scoring (**Chapter 4 – section 4.6.2**). Docking is concerned with the "fitting" of the ligand into a specific area (site) of the protein's amino acid residues (usually the active site) whereas scoring consists of analysing and interpreting the ligand-protein interactions (Yakunin *et al*., 2003; Krammer *et al*., 2005).

5.6.1. Intermolecular interaction parameters.

The docking results are dependent on a set of parameters between the ligand and the protein's amino acid residue(s) e.g. type of bond (mostly van der Waals), bond lengths and bond angles which in turn determines the strength of the interaction(s). This consequently influences the potency or type of activity of the compound. A hydrogen bond with a distance closer than ≈ 2 Å and Pi-interactions closer than ≈ 5 Å are considered strong. The angle between the two entities (ligand atom and protein residue) determines the type of Pi-bond for example Pi-Pi, Pi-Sigma, Pi-Cation etc. (Huyskens, P. 1991).

There a possibility or a great probability for the applicable interaction according to the following parameters:

I. **Hydrogen bonds:** The maximum distance is 2.5 Å the minimum acceptor angle is 90.0°. The C–H•••O angle is usually linear (180°), and the closer the angle is to 180°, the stronger is the hydrogen bond and the shorter is the H•••O distance (Arunan *et al*., 2010).

II. **Pi-Pi stacking**

The angle between the ring planes is less than 30° and the distance between the ring centroids is less than 4.4 Å for face-to-face interaction (**Figure 5.1 (A)**). For edge-to-face interaction the angle between the ring planes is between 60° and 120° and the distance between the ring centroids is less than 5.5 Å (**Figure 5.1 (B)** (http://www.schrodinger.com/kb/1556).

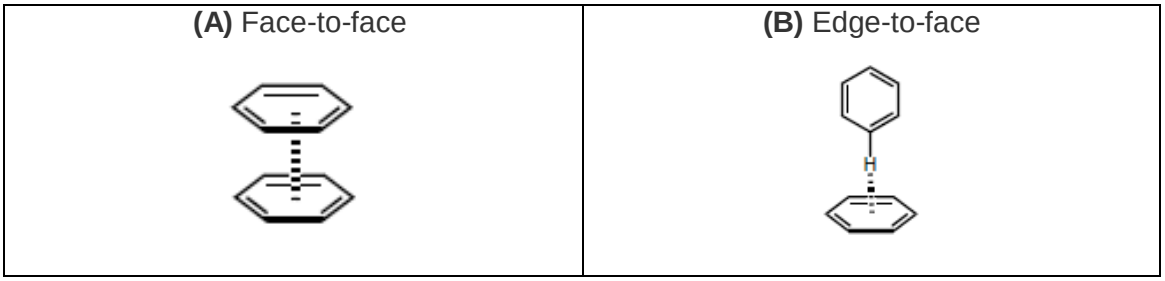

Figure 5.1: The different Pi-Pi interactions. **(A)** Face-to-face on the left panel. **(B)** Edge-to-face on the tight panel (Burley, Science, 1985, 229, 23).

III. **Pi-cation interaction:** The maximum distance between the cation center (**Figure 5.2**) and the ring center is 6.6 Å and the angle between the ring plane and the line between the cation center and the ring center does not deviate from the perpendicular by more than 30° (http://www.schrodinger.com/kb/1556).

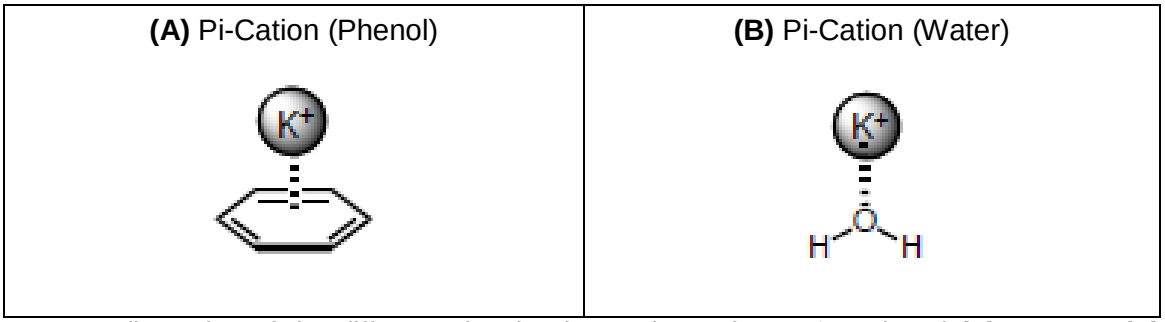

Figure 5.2: Illustration of the different Pi-cation interactions where K^+ = phenol **(A)** or water **(B)** (Kebarle, J. Phys. Chem., **1981,** 85, 1814).

5.6.2. hMAO-B Modelling.

BPR 10 (green ball-and-stick model) was illustrated to transverse both the entrance cavity and substrate cavity. The lactam entity of the coumarin moiety formed hydrogen bonding (white dotted line) with CYS172 and is located in the substrate cavity near the FAD co-factor (stick-model in yellow) in the vicinity of pivotal protein residues. The pyrone ring of the coumarin formed strong Pi-Pi and Pi-Sigma (solid orange line) interactions with TYR398 and LUE171 (review **section 5.4.2.3**) respectively. The morpholine moiety is situated in the entrance cavity, with the 2 carbon ‘‘spacer’’ in the vicinity of ILE199 and ILE198, so that the coumarin entity can access the entrance cavity (**Figure 5.3**). The compound seems to be guided toward the “aromatic cage” *via* TYR398 and TYR435 which improved its effectiveness (**Chapter 4 - section 4.6.3.1; Figure 4.18**).

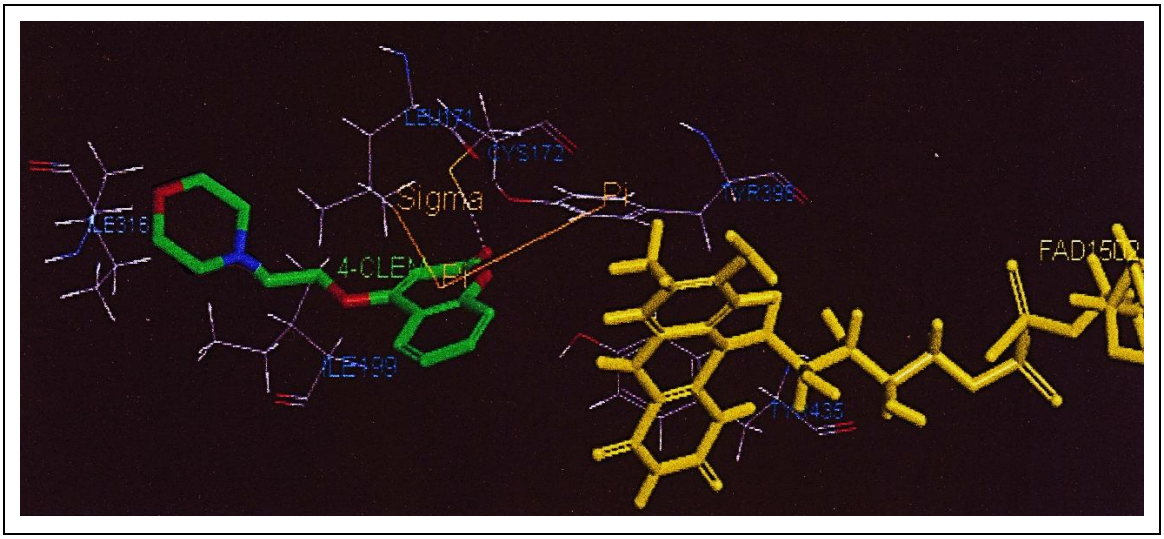

Figure 5.3: **BPR 10/4CLEM** (green ball-and-stick) docked in the hMAO-B protein (2V61). Pi-Pi interactions (orange), Pi-Sigma bonds (orange) and hydrogen bonds (white dotted line) are observed in the substrate cavity.

Pi-Pi, Pi-Sigma as well as an H-bonds are presented **(Table 5.6)** including distances and angles. These latter parameters (**section 5.4.2.1**) indicates relative bonding strengtht between the compound and the neighbouring residues in the substrate active site of hMAO-B.

Table 5.6: Different types of intermolecular bonds between **BPR10** and hMAO-B including the relevant distances and angles.

Coumarin	Residue	Type	Distance (Å)	Angle (°)
Pyrone ring	TYR398	Pi-Pi	6.514	22.164
Pyrone ring	LUE171	Pi-Sigma	2.911	27.035
Pyrone ring (O11)	CYS172	H-bond	2.015	109.461

This increased activity of **BPR10** may be attributed to its hydrogen acceptor capacity (**Figure 5.4; A)** as well as its relative planarity (**Figure 5.3; B and C**) (**Figure 5.4**) and the compounds' position in relation to the FAD co-factor (**Figure 5.4**) and other neighbouring residues in the vicinity (**Figures 5.5 – 5.7**).

The substrate cavity of hMAO-B is shaped like a flat, elongated disc with the longer axis perpendicular to the FAD (Edmondson *et al*., 2004; **Chapter 2 – section 2.2.7**). The longer, narrower active site of MAO B (~700 $Å^3$) compared to the shorter but wider (~ 550 $Å^3$) active site of hMAO-A (deColibus *et al*., 2005), favours planar inhibitors (**Chapter 2 - section 2.2.7; figure 2.36**). The substrate cavity is also more sterically constrained than the entrance cavity (Novaroli *et al*., 2006) – resulting in the occupation of non - bulky compounds.

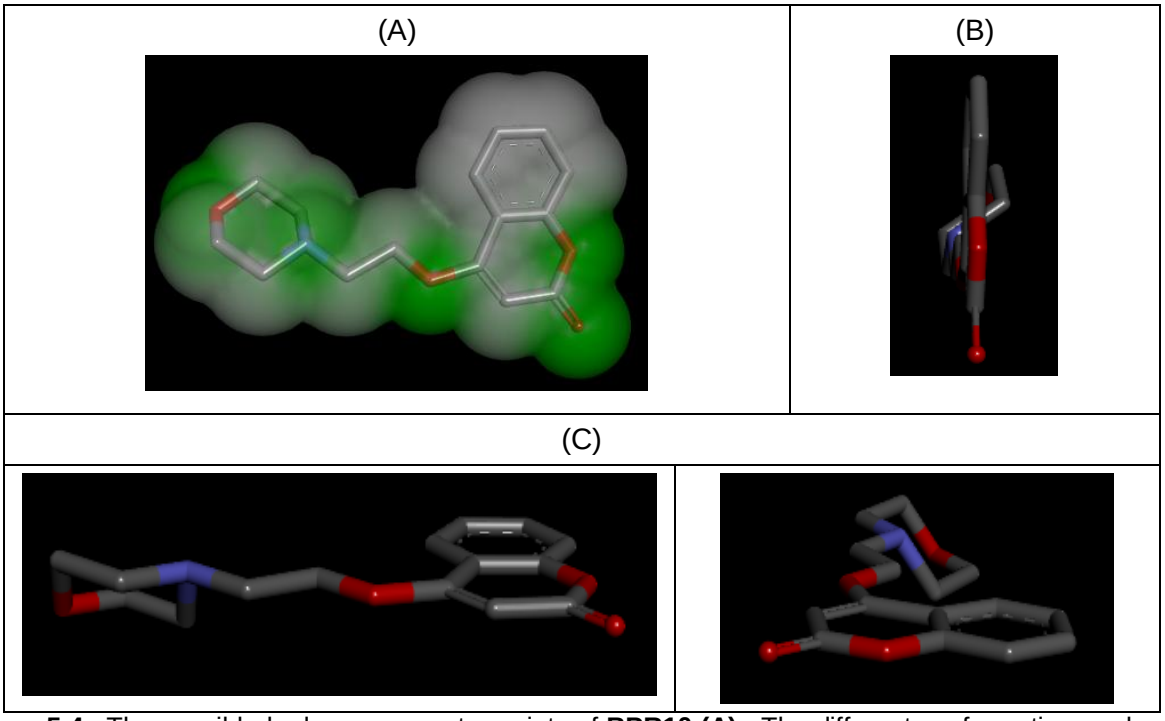

Figure 5.4: The possible hydrogen-acceptor points of **BPR10 (A)**. The different conformation angles of **BPR10**. **NOTE:** the relative observed planarity of the compound **(plans B and C)**.

A notable observation is the position of compounds **BPR10** and **BPR11** relation to the FAD co-factor that involves different key residues. **BPR10** is located perpendicular to the FAD which means that the 4-substituted coumarin will have interactions with different pivotal residues near the FAD. The O4 and O11 atoms of the pyrone ring of **BPR10** is in a favourable position for interaction with the N5 and O2 groups of the FAD moiety. The pyrone ring of **BPR10** interacts through Pi-bonds with CYS172 (**Figure 5.5; dotted violet line and arrow**), LEU171 (**Figure 5.5; dotted yellow line and arrow**) and with ILE198 (**Figure 5.5; dotted blue line and arrow**). The phenyl forms a Pi-bond with LEU171 (**Figure 5.5; dotted gray line and arrow**). A relative strong H-bond (distance: 2.015307 Å; angle:109.461 °) is also present (**Figure 5.5; dotted green line**). The difference in the orientation of the coumarin moiety favours a **Pi bond between the pyrone and ILE198 (Figure 5.5).** Refer to **chapter 4 – section 4.6.3.1** for an in detailed discussion.

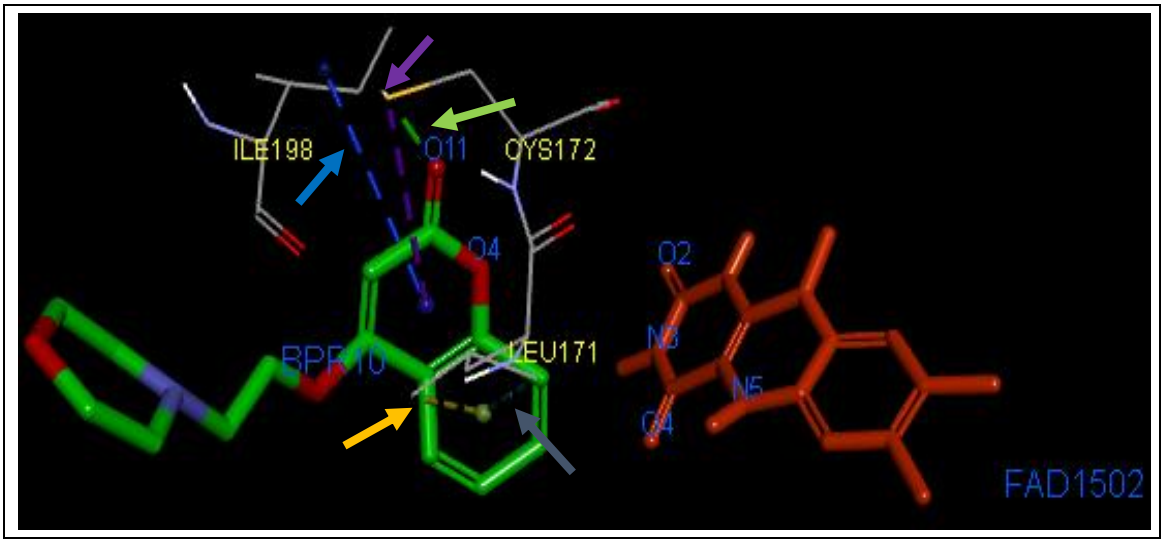

Figure 5.5: **BPR 10** (green line model) docked in hMAO-B with relation to FAD (orange line model), including the Pi-interactions (dotted blue, violet, yellow, gray lines and arrows) and H-bonds (green dotted line and arrow).

A relative strong H-bond as well as different Pi-bonds are presented in **table 5.7**. The strength of the H-bond as well as the Pi-Sigma bonds' distances while the angle of the Pi-Alkyl bonds are the contributing factors (**Table 5.7; section 5.6.1**).

Table 5.7: Different type of intermolecular bonds between compound **BPR10** and hMAO-B including relevant distances and angles.

Coumarin	Residue	Colour	Type	Distance (Å)	Angle (°)
Pyrone Ring	ILE198	Blue	Pi-Alkyl	5.444	53.651
Pyrone Ring	CYS172	Violet	Pi-Alkyl	4.741	51.896
H-Bond (O11)	CYS171	Geen	H-Bond	2.021	109.461
Phenol ring	CYS171	Gray	Pi-Sigma	3.654	53.861
Phenol ring	CYS172	Yellow	Pi-Sigma	2.210	53.461

BPR11 is located more horizontal relative to the FAD, which in turns involves different residues near the FAD vicinity. The O4 and O15 atoms of the pyrone ring of **BPR11** is in a less favourable position for interaction with the O4 and N5 groups of the FAD and more angular towards FAD.

Two Pi-bonds occurs between the pyrone group of **BPR11** and LEU171 (**Figure 5.6; green and light yellow line and arrows**), while another Pi-bond is present between the phenol and CYS172 (**Figure 5.6; blue line and arrow**) and a unique Pi-bond between the TYR326 (**Figure 5.6; violet line and arrow**). The difference in orientation of the coumarin in relation to the FAD resulted in **Pi interaction between the phenol ring and TYR326.**

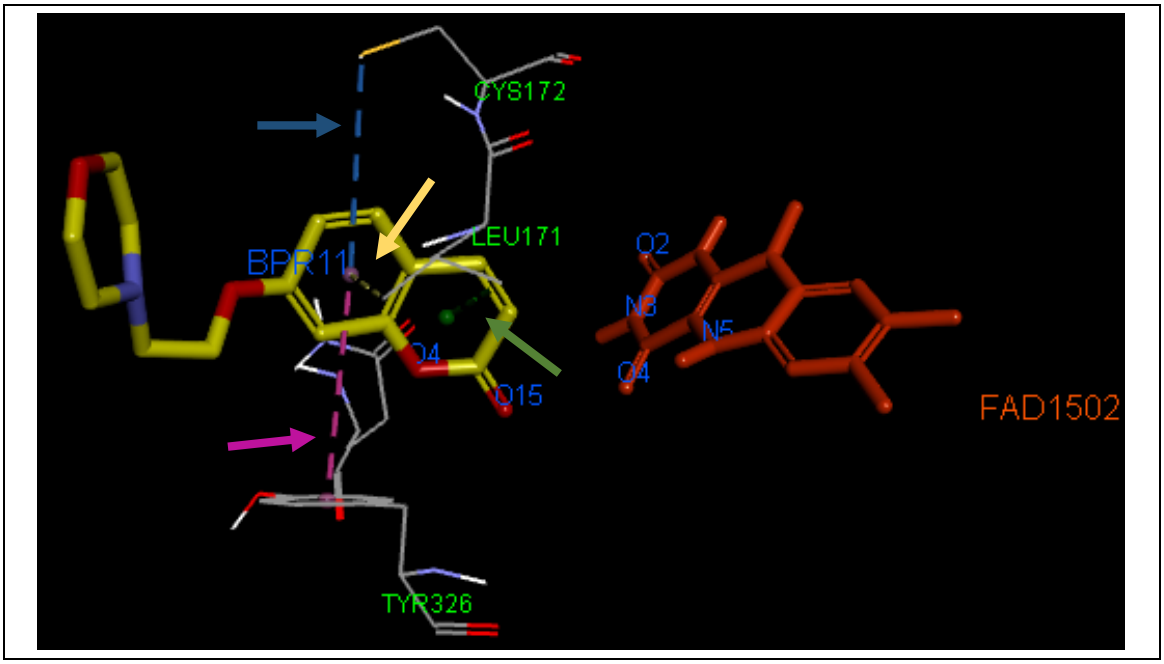

Figure 5.6: **BPR 11** (yellow line model) docked in hMAO-B with relation to FAD (orange line model), Pi-interactions (dotted blue, violet, green and light yellow lines and arrows) are illustrated.

Table 5.8: Intermolecular Pi-bonds between **BPR11** and hMAO-B.

Coumarin	Residue	Colour	Type	Distance (Å)	Angle (°)
Phenol	CYS172	Blue	Pi-Sulphur	4.932	84.486
Phenol	TYR326	Violet	Pi-Pi T-shaped	5.188	79.245
Pyrone	LEU171	Green	Pi-Sigma	3.248	26.175
Phenol	LEU171	Yellow	Pi-Sigma	2.134	3.940

It appears that the distances of the Pi-Sigma bonds rather than the angles are the determining factors for these intermolecular bonds. Both the distance and angles of the Pi-sulphur contributes to its intermolecular bond strength (**Table 5.8**; **section 5.6.1**).

Substitution on the 7 position resulted in the different orientation of **BPR11** (**Figure 5.7**; yellow line model) relative to the FAD which in turn led to the **Pi interaction of the phenol with TYR326 (Figure 5.7; dotted violet line).** **BPR10** had substitution on the 7 position which resulted in a different orientation of the pyrone ring relative to the FAD which in turn formed Pi-inertactions between pyrone and **ILE198** (**Figure 5.7**).

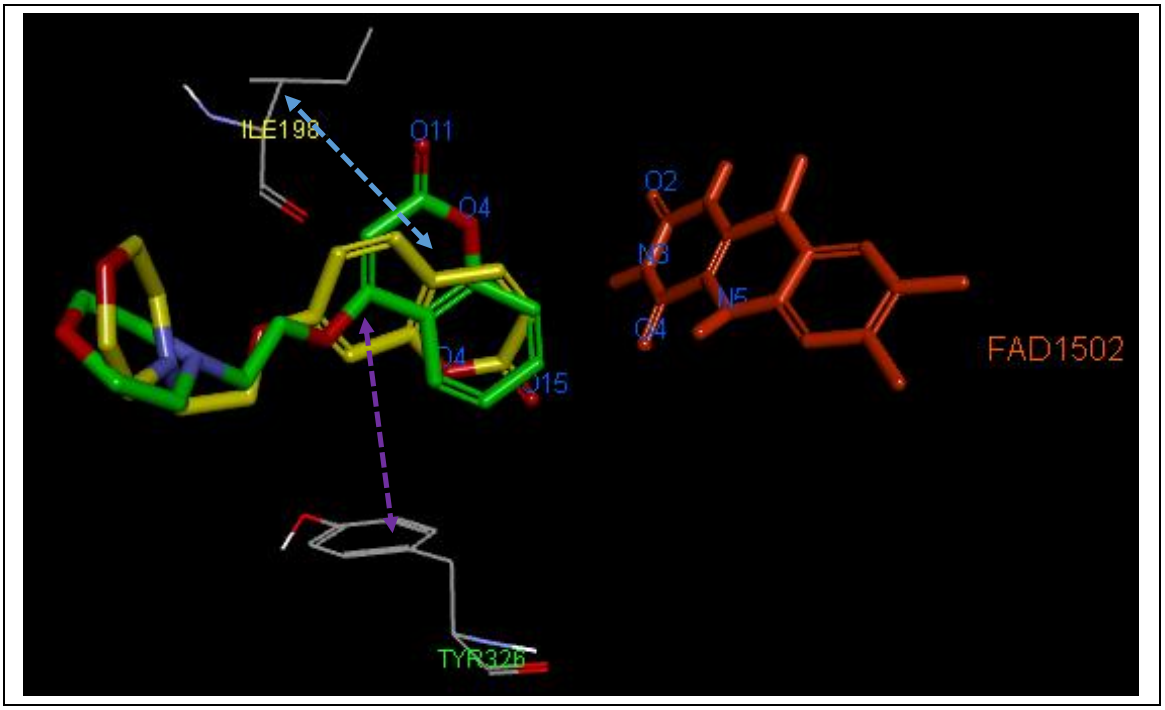

Figure 5.7: An overlay of **BPR10** and **BPR11** with relation with FAD of hMAO-B and the interactions (dotted light blue and violet lines) with the respective unique residues TYR326 (for **BPR11**) and ILE198 (for **BPR10**).

An overlay of these two compounds' conformations clearly illustrates that the pyrone ring of **BPR10** is in the vicinity of the N3 and O2 atoms of the FAD which resulted in a Pi-bond between the pyrone ring and ILE198. **BPR11** is in the region of the O4 and N5 atoms of the FAD, which in turns results in a Pi-bond between the phenol ring and TYR326. This difference in conformations thus resulted in interactions with different residues.

Both **BPR10** and **BPR11** seems to be guided by the "aromatic cage" formed by TYR398 and TYR435 (Akyüz *et al*., 2007; Binda *et al*., 2002) towards the FAD and so improve their binding effectivity (**Figure 5.8**; **Figure 4.18; section 4.6.3.1**).

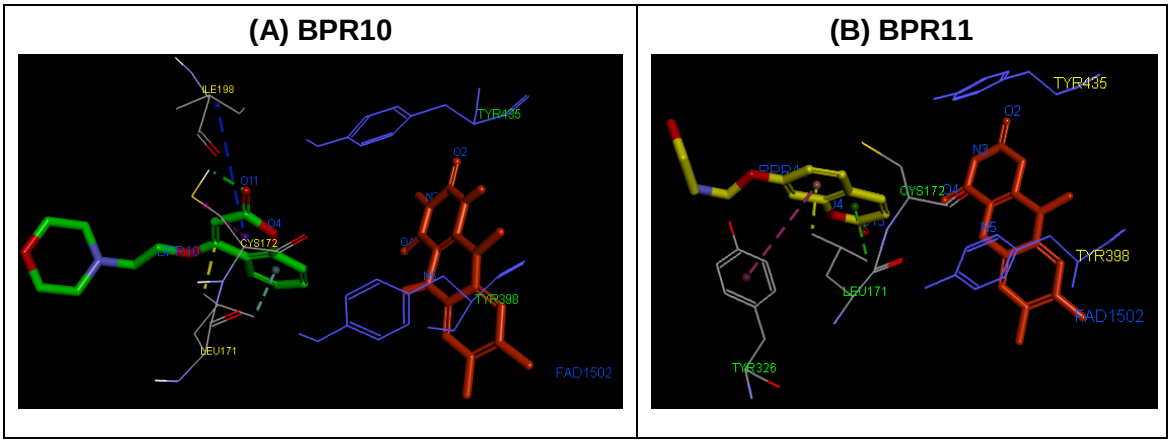

Figure 5.8: The aromatic cage in the substrate cavity of hMAO-B docked with **BPR10 (Left Panel)** and **BPR11 (Right Panel)**.

BPR9 (IC_{50} = 21.720 µM) revealed weaker activity compared to **BPR12** (IC_{50} = 9.209 µM) and **BPR13** (IC_{50} = 3.093 µM) but substitution in general led to an increase in activity with regards to their parent compounds: **BPR13** (IC_{50} = 3.039 µM) *vs*. **4MC** (IC_{50} = 94.327 µM); **BPR 12** (IC_{50} = 3.093 µM) *vs*. **7C** (IC_{50} = 28.583 µM) and **BPR9** (IC_{50} = 21.720 µM) *vs*. **4C** with no activity.

BPR13 (57.43 % at 100 µM) revealed a 2.069 fold (p = 0.0169) increase over **BPR9** (27.770 % at 100 µM). This is probably due to substitution of a small lipophilic entity on the 4 position of the coumarin without causing any steric hindrance instead of a larger H-donating entity with the piperidine moiety.

5.6.3. AChE Modelling.

BPR2 and **BPR13** were docked into the hAChE (4EY7) protein (**Chapter 4 – section 4.3.2.6**). **BPR 2** (ball-and-stick in blue) interacted with both the PAS and CAS of AChE. The coumarin moiety is located within the PAS with two hydrogen bonds between the pyrone entity of the coumarin and HIS284 (**Figure 5.9; yellow arrow** and **Figure 5.10**). The extended flexible erucic chain is located near the co-factors (stick models in yellow and orange) and because of influence of the numerous neighbouring residues (illustrated as line models) penetrates into the deep, narrow gorge of the CAS (**Figure 5.9**).

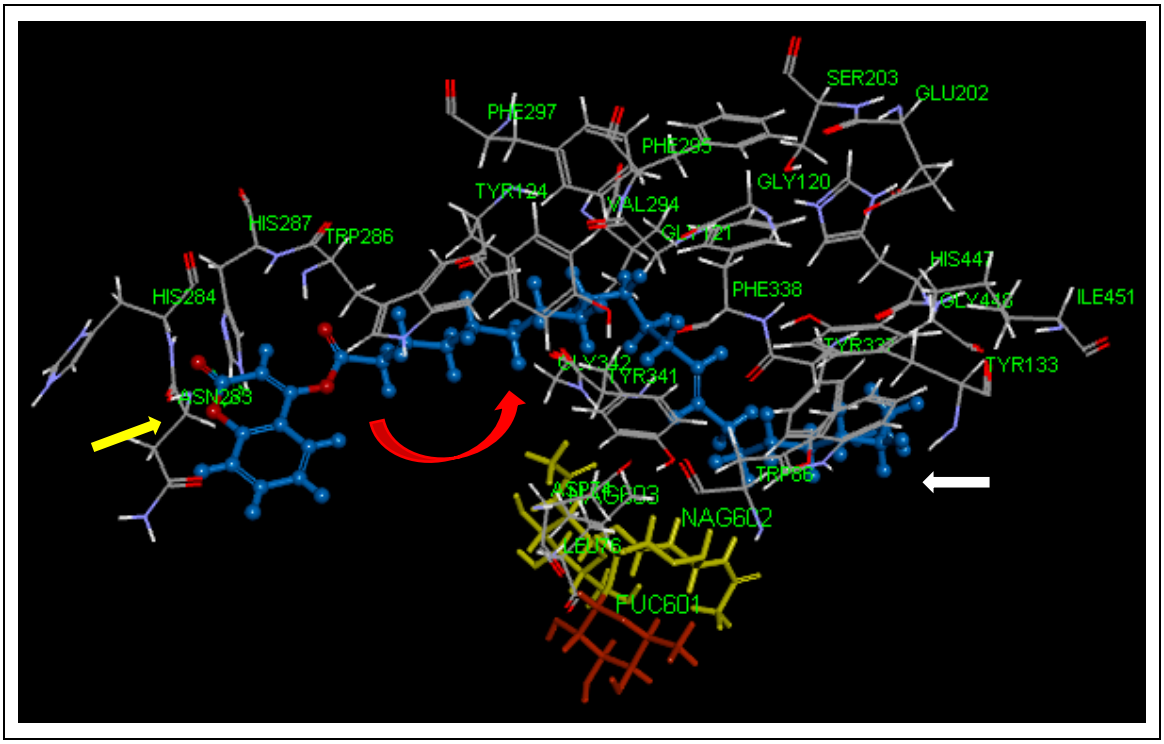

Figure 5.9: BPR 2 (blue ball-and-stick) docked in the hAChE protein with neighbouring atoms (**line models**). The coumarin entity (**yellow arrow**) inside the PAS with the elongated lipophillic entity in the gorge (**red arrow)** and CAS **(white arrow**).

The pyrone ring of the 4-hydroxycoumarin - erucic acid ester conjugate (**BPR2**) is in the ideal conformation to interact with the HIS287 (**Figure 5.10)** *via* **two** hydrogen bonds (Distance: 1.986887 Å; angle 86.104311 ° and distance: 2.053422 Å; angle;45.252811 °).

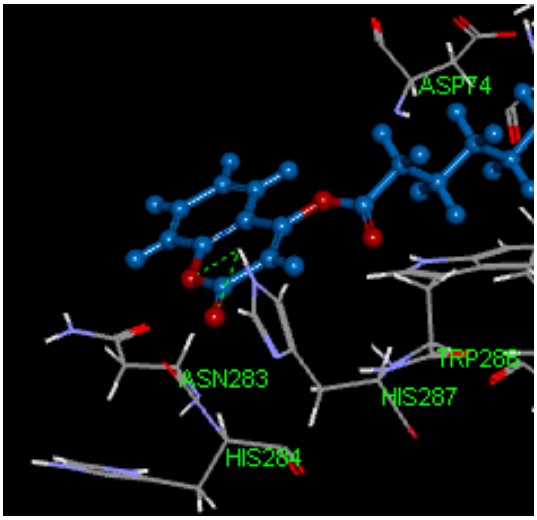

Figure 5.10: Enlargement of the two hydrogen bonds **(green dotted lines)** between the pyrone ring of **BPR 2 (blue ball-and-stick)** and HIS287.

As can be seen from **Table 5.9**, the distances are the main contributing factors of the intermolecular H-bonds, although the angles are not planar (**section 5.6.1**).

Table 5.9: Intermolecular H-bonds between compound **BPR2** and residue HIS287 of EE AChE.

Coumarin	Residue	Type	Distance (Å)	Angle (°)
Pyrone (O1)	HIS287	H-bonds	1.986	86.104
Pyrone (O11)	HIS287	H-bonds	2.053	45.252

The O11 atom and the O11 atom of the pyrone moiety of the coumarin formed relative (see **section 5.4.3.3**) hydrogen-bonds with HIS289 residue of AChE.

The 7-hydroxycoumarin and 4-methylated-7-hydroxycoumarin – erucic acid (**BPR1** and **BPR3**) conjugates were devoid of AChE inhibitory activity simply because the pyrone ester is situated in an unfavourable position for interaction with the residues in the PAS. This explains the fact that **BPR1** and **BPR3** (where the esters and pyrone ring are located in the opposite position) didn't reveal activity (**Figure 5.11**). It also explains why **BPR1** and **BPR2** docking were not successful.

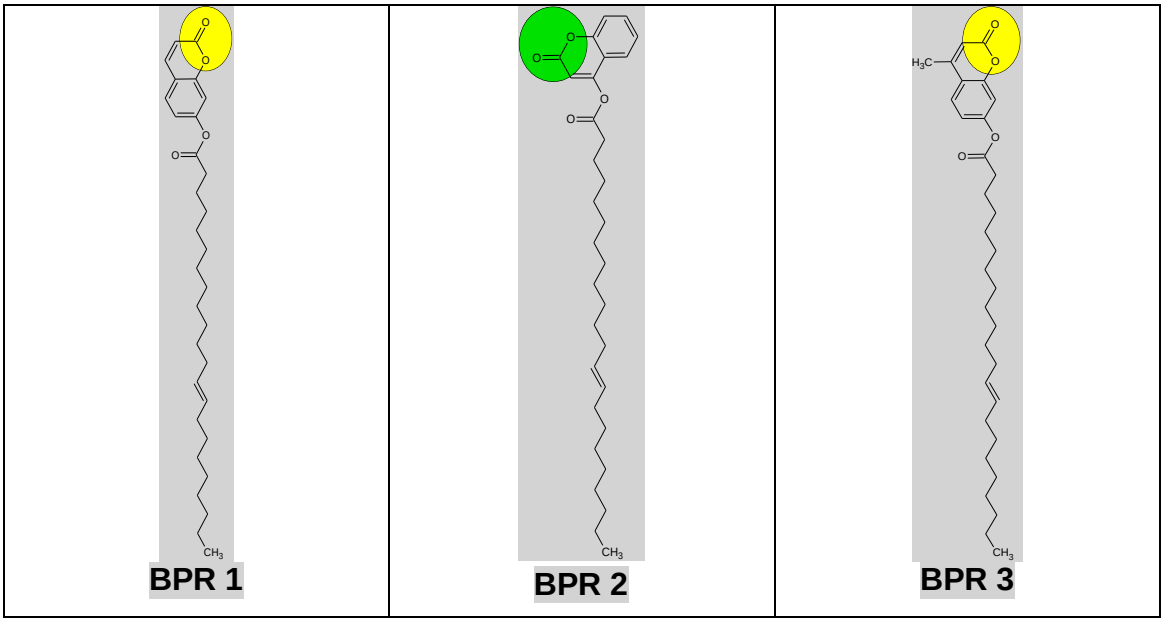

Figure 5.11: Different orientations of **BPR1**, **BPR2** and **BPR3**. The pyrone ring of **BPR2** (green circle) is in an ideal orientation to form **two** hydrogen-bonds with HIS284, while **BPR1** and **BPR3** (yellow circles) lacks this characteristic.

BPR13 (**Figure 5.12**; blue ball-and-stick) were docked into hAChE. A H-bond (**Figure 5.12; A**; dotted green line) and several Pi-interactions (**Figure 5.12; A - orange lines**) can be observed between the inhibitor and enzyme residues.

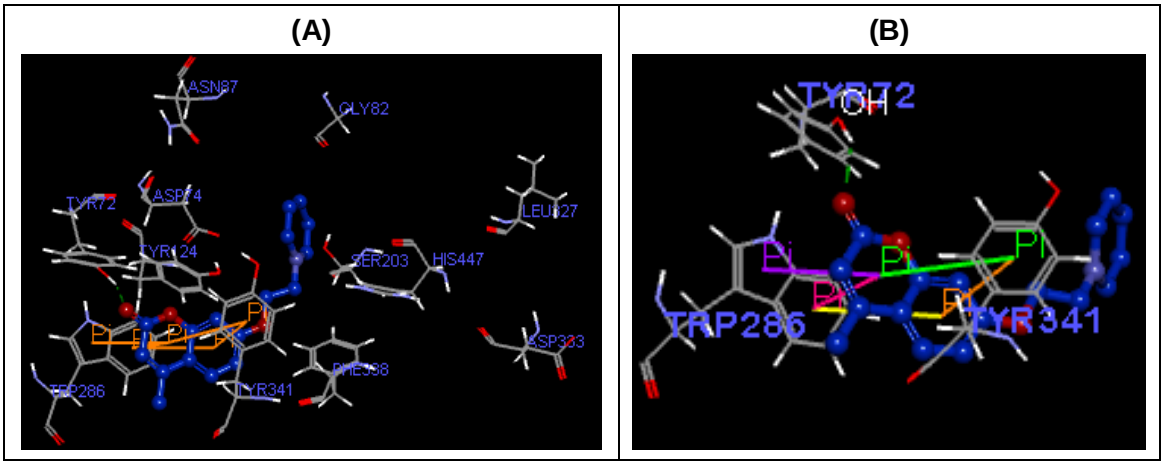

Figure 5.12: **BPR13** (**blue ball-and-stick**) docked into the active site of hAChE including interactions between residues **(A)**. An expanded view of the 5 Pi-Pi interactions (**violet, pink, yellow, orange and green lines)** as well as the H-bond (**dotted green line**) between the compound and hAChE protein residues **(B)**.

The 5 Pi-interactions occurs (violet, pink, yellow, orange green lines) between **BPR13** and TYR283 and TRP341 and H-bonds (green dotted line) with TYR72 within the PAS **(Figure 5.12; B and Table 5.10)**.

Pi – Interactions are as follows: Orange line is between the phenol ring and TRP341, violet line between the pyrone ring and TRP341, yellow line between phenol ring en TYR286, green

line between the pyrone ring and TYR286 and pink line between the pyrone ring and TYR286 **(Figure 5.12; B and Table 5.7).** The hydrogen bond (Distance of 2.193334 Å and angle of 119.997215 °) between the OH (white labelled) of TYR72 and the pyrone ring is depicted as a green dotted line in **Figure 5.12, B.** For a detailed description (distances and angles of Pi-interactions), review **chapter 4 – section 4.6.3.2.**

Table 5.10: Outline of the intermolecular interactions between **BPR13** and hAChE with respective distances and angles.

Coumarin	Residue	Colour	Type	Distance (Å)	Angle (°)
Phenol ring	TRP341	Orange	Pi-Pi	3.802	19.229
Pyrone ring	TRP341	Violet	Pi-Pi	4.869	7.121
Phenol ring	TYR286	Yellow	Pi-Pi	5.215	9.396
Pyrone ring	TYR286	Green	Pi-Pi	4.868	22.783
Pyrone ring	TYR286	Pink	Pi-Pi	4.040	7.120
Pyrone ring (O11)	TYR72	Green	H-bond	2.193	119.997

Due to the Pi-bonds' and H-bonds' distances, rather than the angles, these intermolecular bonds are relative strong (**Table 5.10; section 5.6.1**).

The hypothesis that if an inhibitor interacts with both the PAS and CAS sites, $A\beta_{40}$ formation decreases (Piazzi *et al*., 2003), thus endows **BPR2** with possible additional beneficial effect e.g. compound **AP 2238** (**Chapter 2; Figure 2.20 - section 2.2.5**).

5.7. Mutual AChE and MAO-B inhibitors.

In order to address diseases with multifactorial, underlying pathology e.g. AD (Kasa *et al*., 1997), a multi-target-directed ligand (MTDL) approach was employed. This is where one compound interacts with multiple targets (enzymes/receptors) – in which AChE and MAO-B were selected for this study.

MAO-B Inhibition: BPR10; BPR14; BPR13; BPR1; BPR12; BPR11; BPR9; 7C and 4MC.

AChE Inhibition at 100 µM: BPR13; BPR12; BPR9; BPR11; 4C and 4MC.

AChE Inhibition at 1 µM: BPR12; BPR13; BPR2; BPR14; BPR3; BPR6; BPR10; BPR4; BPR1; 4C; BPR8; 7C; BPR9; 4MC; BPR11 and BPR5.

The results of the current study indicate that of the 17 compounds, 9 compounds (highlighted in green) revealed dual-mechanism activity or could be MTDLs for both AChE and MAO-B: 7C;BPR1; BPR14; BPR13; BPR12; BPR11; BPR10; BPR9; 4MC.

This is however only a qualitative indication to identify dual enzyme inhibition because of the unknown MAO-B and AChE distribution in the affected CNS areas. For the purpose of this study compounds interacting with both MAO-B and AChE, was regarded potential MTDL.

5.8. RECOMMENDATIONS.

As shown in this study, the coumarin scaffold serves as a promising pharmacophore and inhibitors synthesised by conjugation to elongated proton acceptor moieties has the potential to increase both MAO-B and AchE inhibitory activity (**Table 5.3 - 5.6**). Numerous promising neuroprotective entities can additionally be conjugated to the synthesised coumarin – morpholine/piperidine scaffolds. Intensive molecular modelling can be conducted to elucidate the intermolecular interactions of these compounds. In additional, *in vivo* studies of relevant potential targets (see section below and **Figure 5.13**) can be performed. AD pathology consists of multiple targets (e.g. BACE1, APOE, ACE, NOS) (**Chapter 2**), beyond the two targets this study focussed on, and these could be investigated in future studies. **Figure 5.13** outlines the potential MTDLs and references to the specific coumarin conjugates.

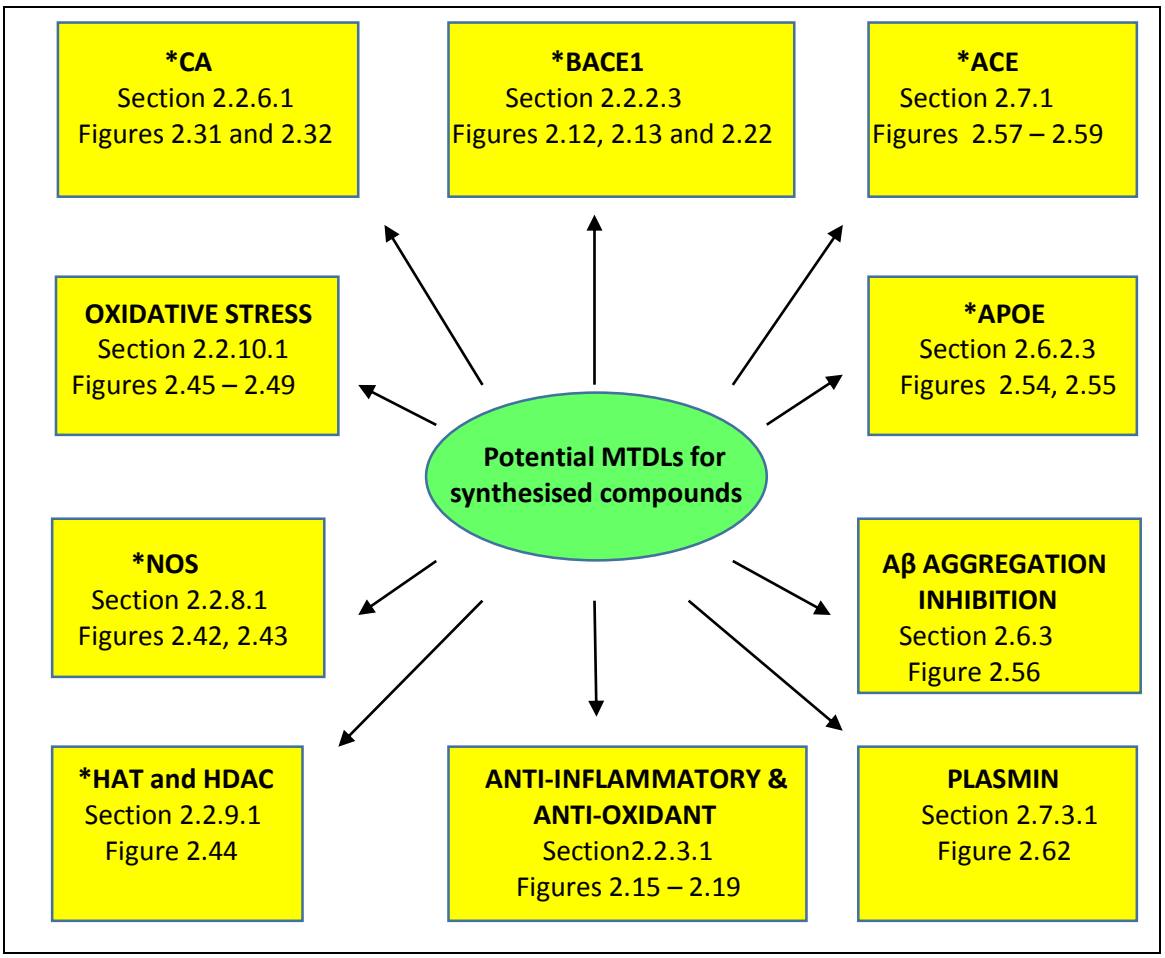

Figure 5.13: Possible targets for further coumarins as MTDLs for AD.*__CA__ (Carbonic Anhydrase); **BACE1** (β-sectretase enzyme); **ACE** (Angiotensin converting enzyme); **APOE** (Apolipoprotein E); **NOS** (Nitric oxide synthase); **HAT** (Histone acetyltransferase; **HDAC** (Histone deacetyltransferase).

5.9. CONCLUSION.

The activity of the synthesised coumarin-type inhibitors was successfully evaluated against hMAO-B and EE AChE (**Chapter 4 – section 4.5**). The coumarin - morpholine ether, **BPR 10** (4-[2-(Morpholin-4-yl)ethoxy]-2H-chromen-2-one) proved to be the most promising inhibitor of hMAO-B with an IC_{50} of 0.372 µM, though at least one log unit less potent than the irreversible reference MAO-B inhibitor (*R*)-Deprenyl (**Table 5.3, section 5.2.1**). This could be ascribed to its position of conjugation, relative planarity as well as multiple hydrogen accepting points (**Table 5.3; Figure 5.4**). In docking studies, **BPR 10** was illustrated to transverse both the entrance cavity and substrate cavity of MAO-B with the coumarin moiety forming a hydrogen bond with LEU171, Pi-Pi interaction with TYR398 and Pi-Sigma interaction with LEU171 in the substrate cavity while the morpholine moiety is situated in the entrance cavity (**Figure 5.3**). Its relative position in the substrate cavity towards FAD also have an influential effect. **BPR10** (4 substituted) formed an interaction with ILE198 (**Figures 5.5 - 5.7**) compared to **BPR11** (7 substituted) which interacted with TYR326 (**Figures 5.6 - 5.8**).

The coumarin-piperidine conjugate, **BPR13** (4-Methyl-7-[2-(Piperidin-1-yl)ethoxy]-2H-chromen-2-one), was the most potent inhibitor of EE AChE with inhibitory activity of 57.430 % at 100 µM and 21.560 % at 1µM (**Table 5.4 and 5.5**) while **BPR12** [(7-[2-(Piperidin-1-yl)ethoxy]-2H-chromen-2-one)] was the most potent EE AChE inhibitor at 1 µM with activity of 30.900 % (**Table 5.5**). Both are however still significantly lower than the reference AChE inhibitor, Tacrine. Docking the compounds into the hAChE, **BPR 2** was found to occupy both the PAS and CAS of AChE. The coumarin moiety is located within the PAS with the pyrone ring of the coumarin forming two hydrogen bonds with HIS284. The extended flexible erucic chain is influenced by the neighbouring residues that allows it to penetrate into the deep, narrow gorge of the CAS of AChE (**Figure 5.9 and 5.10**). **BPR13** formed 3 Pi-bonds with TRP286, 2 Pi-bonds with TYR341 (**Table 5.10**) and a H-bond with TYR72 in the PAS (**Figure 5.13**). The coumarin occupying the PAS site correlates with previous studies of AChE e.g. compound AP 228 **(Chapter 2 - section 2.2.5; Figure 2.20**; Piazzi *et al*., 2004**)**.

The coumarin thus served as an adequate pharmacophoric scaffold and conjugated **BPR13** (57.43 %) exhibited significant AChE inhibition at at 100 µM (**Table 5.4, section 5.4.2.2.1**) and **BPR12** (30.900 %) at 1 µM (**Table 5.5, section 5.4.2.2.2**), though still significantly lower than the reference AChE inhibitor, Tacrine. Compounds exhibited potential for both MAO-B and AChE inhibition in AD and wualifies as MTDLs are **BPR 9** – **BPR 14**. Different lipophilic neuroprotective moieties can further be conjugated on the notional positions of the coumarin to increase or modify activity.

ANNEXURE A:
NMR (^{1}H and ^{13}C) Spectra

Spectrum 1: ^{1}H NMR of 2-Oxo-2*H*-chromen-7-yl docos-24-enoate **(BPR1).**

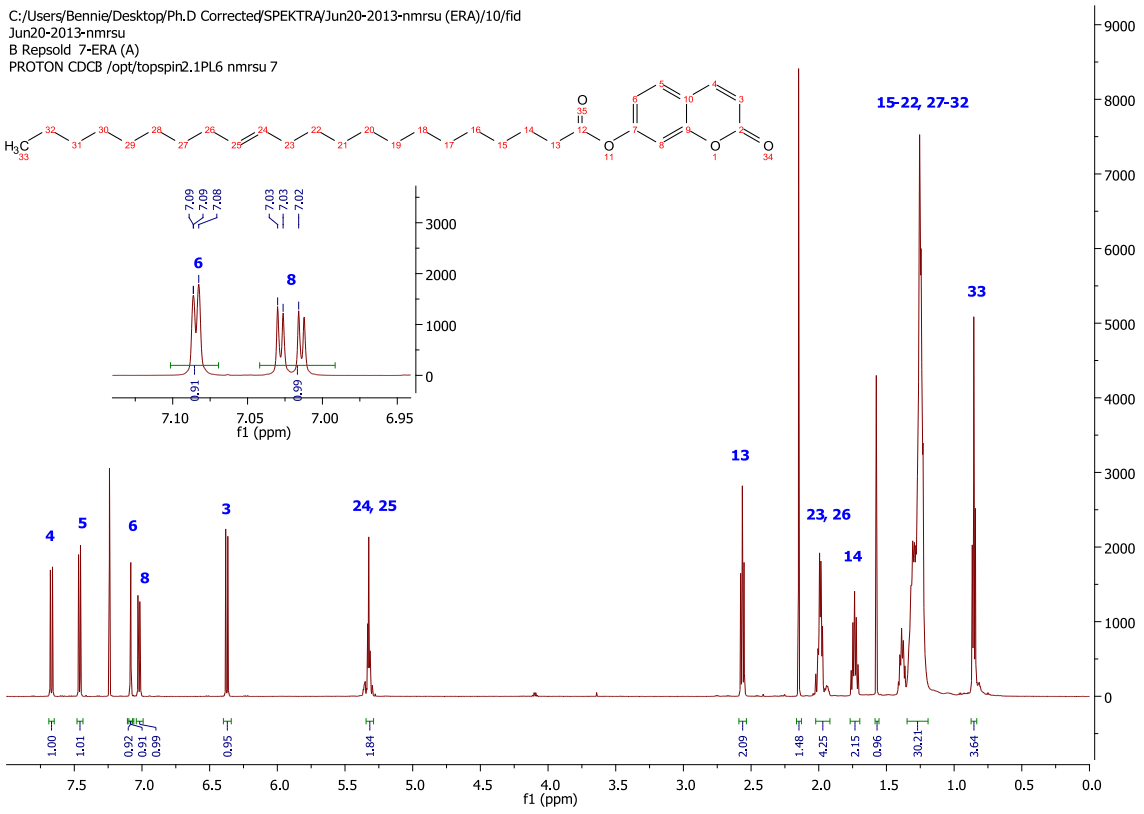

^{1}H NMR (600 MHz, $CDCl_3$, **Spectrum 1**): δ 7.67 (d, *J* = 9.5 Hz, 1H, H_4); 7.46 (d, *J* = 8.4 Hz, 1H, H_5); 7.08 (d, *J* = 2.1 Hz, 1H, H_6); 7.04 – 6.99 (m, 1H, H_8); 6.37 (d, *J* = 9.5 Hz, 1H, H_3); 5.32 (t, *J* = 4.7 Hz, 2H, $H_{24,\ 25}$); 2.56 (t, *J* = 7.5 Hz, 2H, H_{13}); 1.99 (m, 4H, $H_{23,\ 26}$); 1.77 – 1.70 (m, 4H, H_{14}); 1.35 – 1.19 (m, 28H, $H_{15\ -\ 22,\ 27\ -\ 32}$); 0.85 (t, *J* = 7.0 Hz, 3H, H_{33}).

Spectrum 2: ^{13}C NMR of 2-Oxo-2*H*-chromen-7-yl docos-24-enoate **(BPR1).**

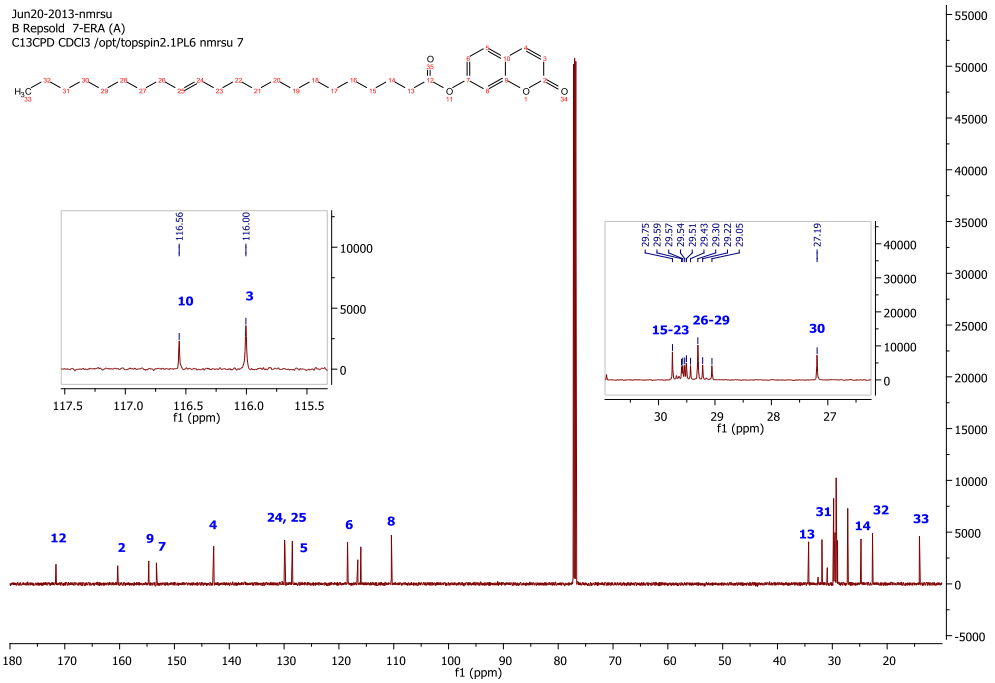

^{13}C NMR (151 MHz, $CDCl_3$. **Spectrum 2**): δ 171.61 (C_{12}); 160.35 (C_2); 154.68 (C_9); 153.29 (C_7); 142.84 (C_4); 129.91 (C_{24}); 129.85 (C_{25}); 118.43 (C_5); 116.56 (C_6); 116.00 (C_{10}); 110.43 (C_3); 34.32 (C_8); 31.89 (C_{13}); 30.92 (C_{31}); 29.75 - 29.05($C_{15-23,\ 26-29}$); 27.19(C_{30}); 24.77(C_{14}); 22.67(C_{32}); 14.18 (C_{33}).

Spectrum 3: ^{1}H NMR of 2-Oxo-2*H*-chromen-4-yl docos-24-enoate **(BPR 2).**

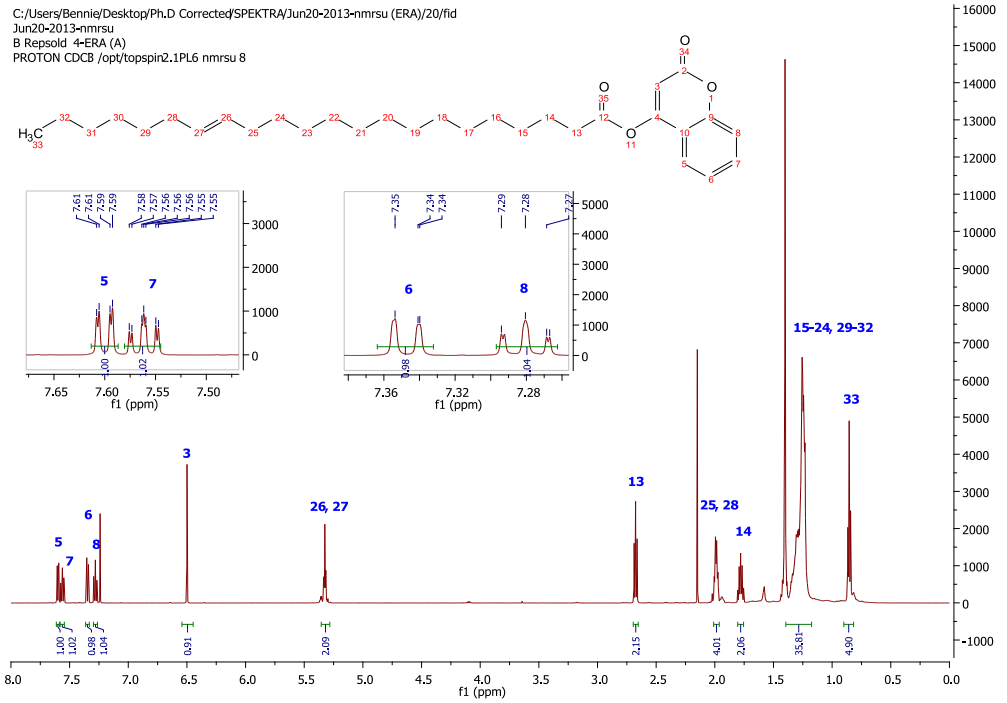

^{1}H NMR (600 MHz, $CDCl_3$, **Spectrum 3**): δ 7.60 (dd, J = 7.9, 1.5 Hz, 1H, H_5); 7.56 (m, 1H, H_7); 7.34 (dd, J = 1, 0.6 Hz, 1H, H_6); 7.30 – 7.26 (m, 1H, H_8); 6.50 (s, 1H, H_3), 5.33 (m, 2H, $H_{26,27}$); 2.68 (t, J = 7.5 Hz, 2H, H_{13}); 1.77 (m, 4H, $H_{25,28}$); 1.39 – 1.17 (m, 28H, $H_{15-24,29-32}$); 0.85 (t, J = 7.0 Hz, 3H, H_{33}).

Spectrum 4: ^{13}C NMR of 2-Oxo-2*H*-chromen-4-yl docos-24-enoate **(BPR2).**

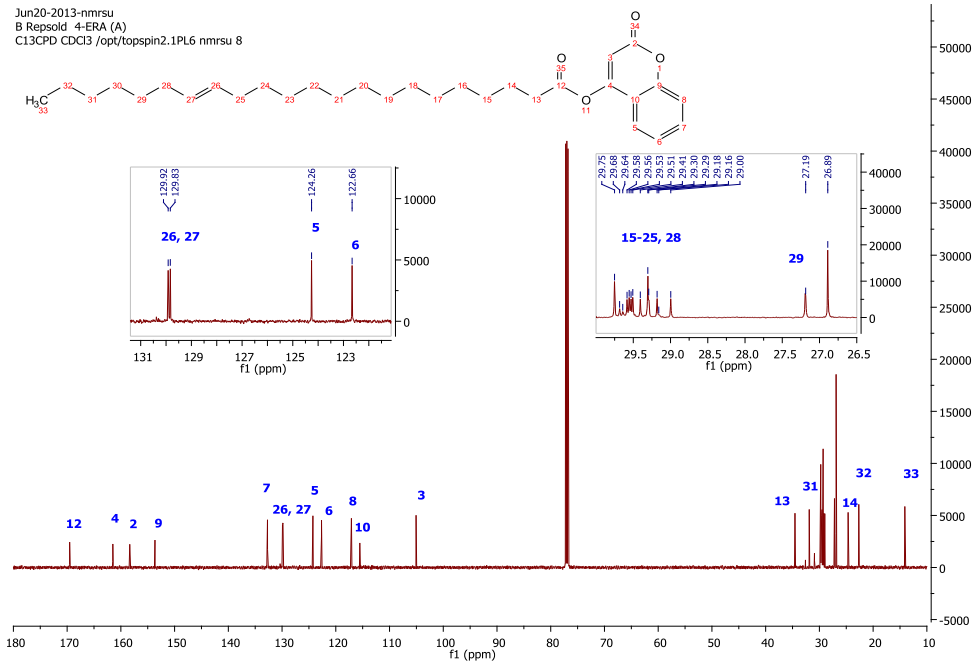

^{13}C NMR (151 MHz, $CDCl_3$, **Spectrum 4**): δ 169.53 (C_{12}); 161.50 (C_4); 158.34 (C_2); 153.65 (C_9); 132.71 (C_7); 129.92 (C_{26}); 129.83 (C_{27}); 124.26 (C_5); 122.66 (C_6); 117.09 (C_8); 115.53 (C_{10}); 105.06 (C_3); 34.55 (C_{13}); 30.92 (C_{31}); 29.75 - 29.16 ($C_{15\text{ - }25}$); 29.00 (C_{28}); 27.19 (C_{29}); 26.89 (C_{30}); 24.65 (C_{14}); 22.67 (C_{32}); 14.10 (C_{33}).

Spectrum 5: ^{1}H NMR of 4-Methyl-2-oxo-2*H*-chromen-7-yl docos-25-enoate **(BPR3).**

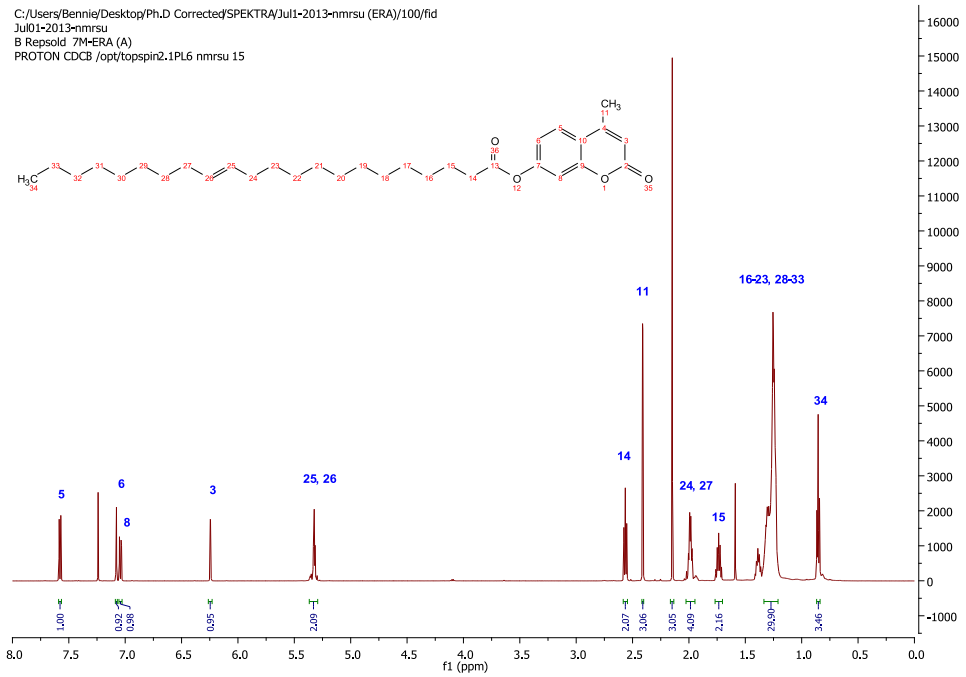

^{1}H NMR (600 MHz, $CDCl_3$, Spectrum 5): δ 7.58 (d, *J* = 8.6 Hz, 1H, H_5); 7.08 (d, *J* = 2.2 Hz, 1H, H_6); 7.04 (dd, *J* = 8.6, 2.3 Hz, 1H, H_8); 6.24 (s, 1H, H_3); 5.37 – 5.29 (m, 2H, $H_{25,26}$); 2.56 (t, *J* = 7.5 Hz, 2H, H_{14}); 2.41 (s, 3H, H_{11}); 2.03 – 1.95 (m, 4H, $H_{24,27}$); 1.77 – 1.70 (m, 2H, H_{15}); 1.33 - 1.21 (m, 28H, $H_{16\text{ – }13,28\text{ - }33}$); 0.85 (t, *J* = 7.0 Hz, 3H, H_{34}).

Spectrum 6: ^{13}C NMR of 4-Methyl-2-oxo-2*H*-chromen-7-yl docos-25-enoate **(BPR3).**

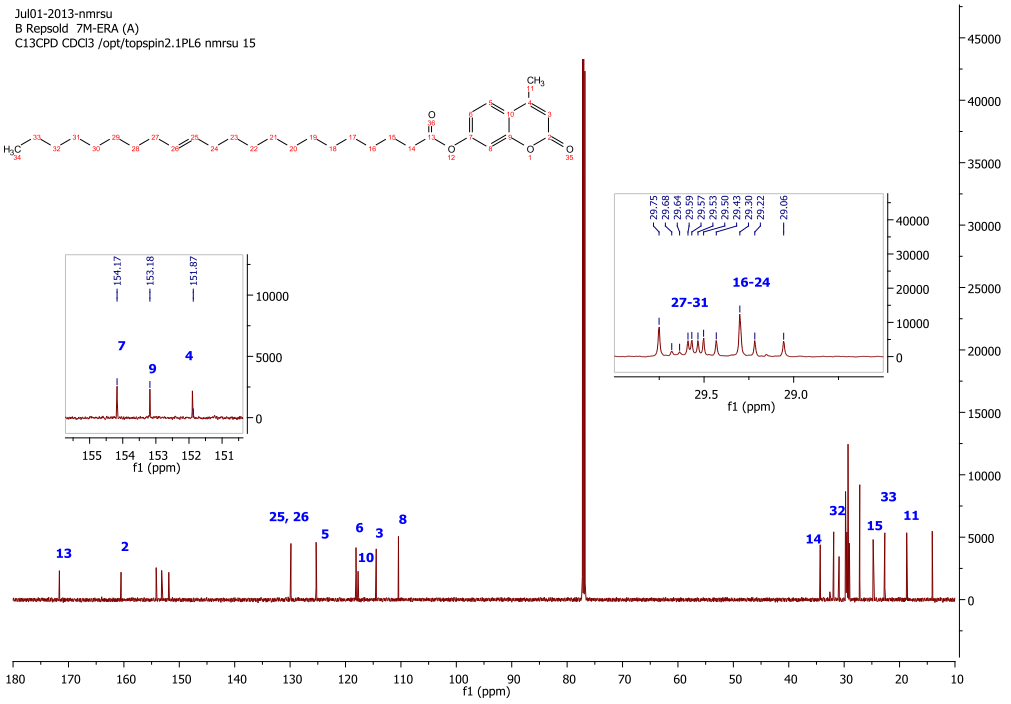

^{13}C NMR (151 MHz, $CDCl_3$, **Spectrum 6**): δ 171.64 (C_{13}); 160.51 (C_2); 154.17 (C_7); 153.18 (C_9); 151.87 (C_4); 129.90 (C_{25}); 125.30 (C_{26}); 118.11 (C_5); 117.73 (C_6); 114.45 (C_{10}); 110.44 (C_3); 34.32 (C_8); 31.89 (C_{14}); 30.92 (C_{32}); 29.75 - 27.19 ($C_{27\text{ - }31,\ 16\text{ - }24}$); 24.77 ($C_{15}$); 22.67 ($C_{33}$); 18.71 ($C_{11}$); 14.10 ($C_{34}$).

Spectrum 7: ^{1}H NMR of 4,4'-[Butane-1,4-diylbis(oxy)]bis(2*H*-chromen-2-one) **(BPR4).**

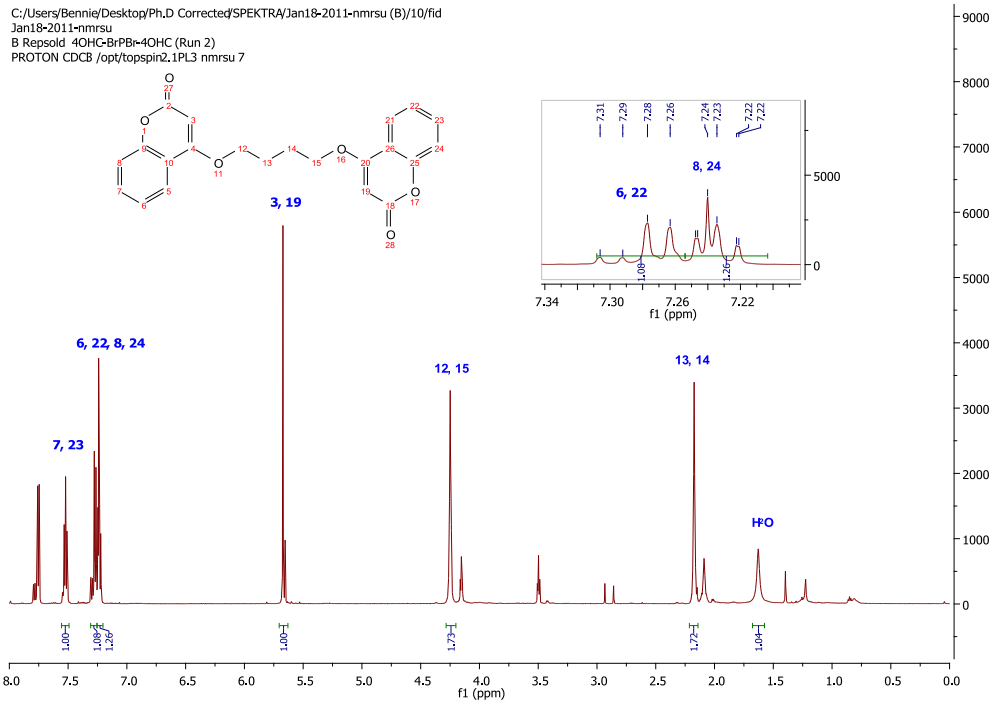

^{1}H NMR (600 MHz, $CDCl_3$, Spectrum 7): δ 7.77 (dd, *J* = 7.9, 1.4 Hz, 2H, $H_{5,21}$); 7.56 – 7.49 (m, 2H, $H_{7,23}$); 7.28 - 7.20 (m, 4H, $H_{6,\ 22,\ 8,\ 24}$); 5.66 (s, 2H, $H_{3,19}$); 4.29 (bs, 2H, $H_{12,15}$); 2.23 (bs, 2H, $H_{13,14}$); 1.63 (s, 2H, H_2O; $CDCL_3$).

Spectrum 8: ^{13}C NMR of 4,4'-[Butane-1,4-diylbis(oxy)]bis(2*H*-chromen-2-one) **(BPR4).**

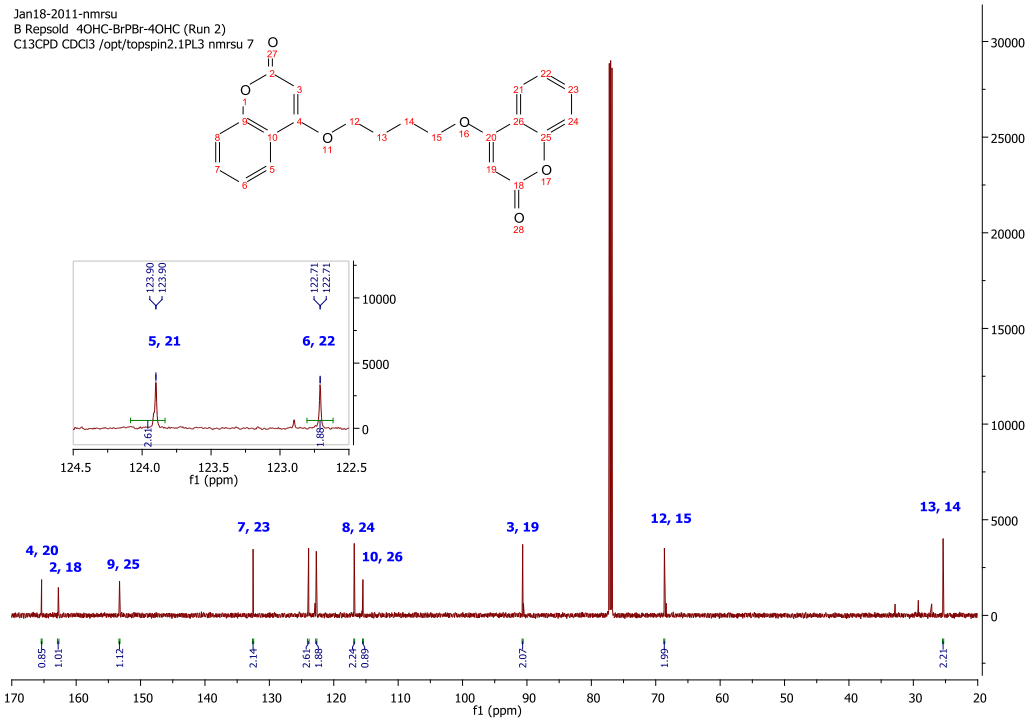

^{13}C NMR (151 MHz, $CDCl_3$,): δ 165.37 ($C_{4,20}$); 162.77 ($C_{2,18}$); 153.26 ($C_{9,25}$); 132.53 ($C_{7,23}$); 123.90 ($C_{5,21}$); 122.71 ($C_{6,22}$); 116.82 ($C_{8,24}$); 115.47 ($C_{10,26}$); 90.66 ($C_{3,19}$); 68.66 ($C_{12,15}$); 25.38 ($C_{13,14}$).

Spectrum 9: ^{1}H NMR of 4,4'-[Propane-1,3-diylbis(oxy)]bis(2*H*-chromen-2-one) **(BPR5).**

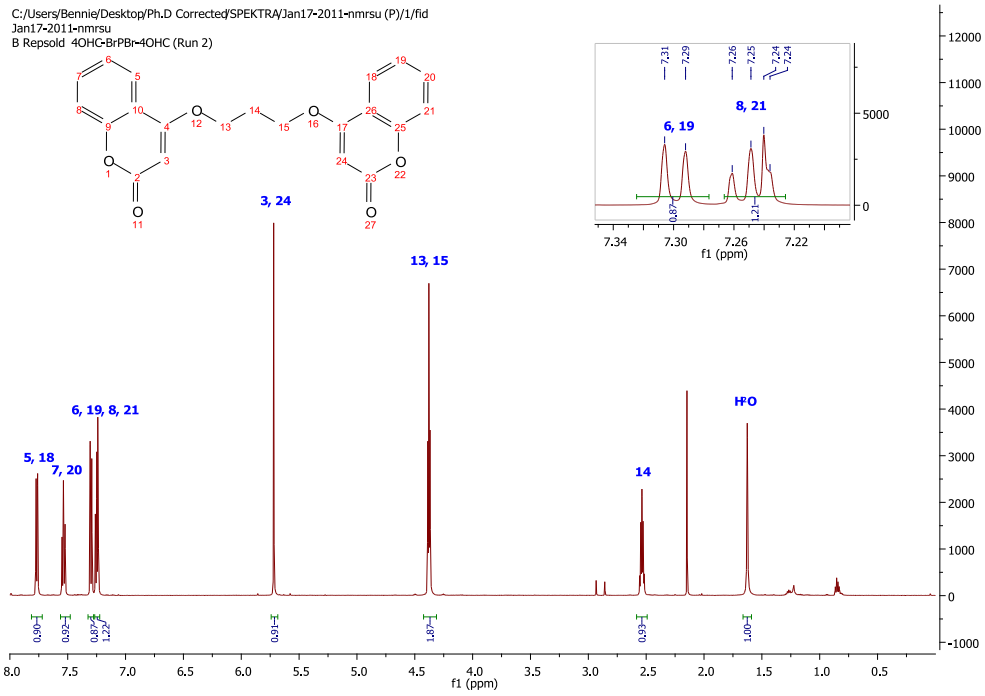

^{1}H NMR (600 MHz, $CDCl_3$, Spectrum 9): δ 7.77 (dd, *J* = 7.9, 1.3 Hz, 2H, $H_{5,18}$); 7.56 – 7.48 (m, 2H, $H_{7,20}$); 7.30 (m, 2H, $H_{6,19}$), 7.25 (dd, *J* = 10.1, 5.0 Hz, 2H, $H_{8,21}$); 5.72 (s, 2H, $H_{3,24}$); 4.38 (t, *J* = 5.9 Hz, 2H, $H_{13,15}$); 2.54 (m, 1H, H_{14}); 1.63 (s, 2H, H_2O; $CDCL_3$).

Spectrum 10: ^{13}C NMR of 4,4'-[Propane-1,3-diylbis(oxy)]bis(2*H*-chromen-2-one) **(BPR5).**

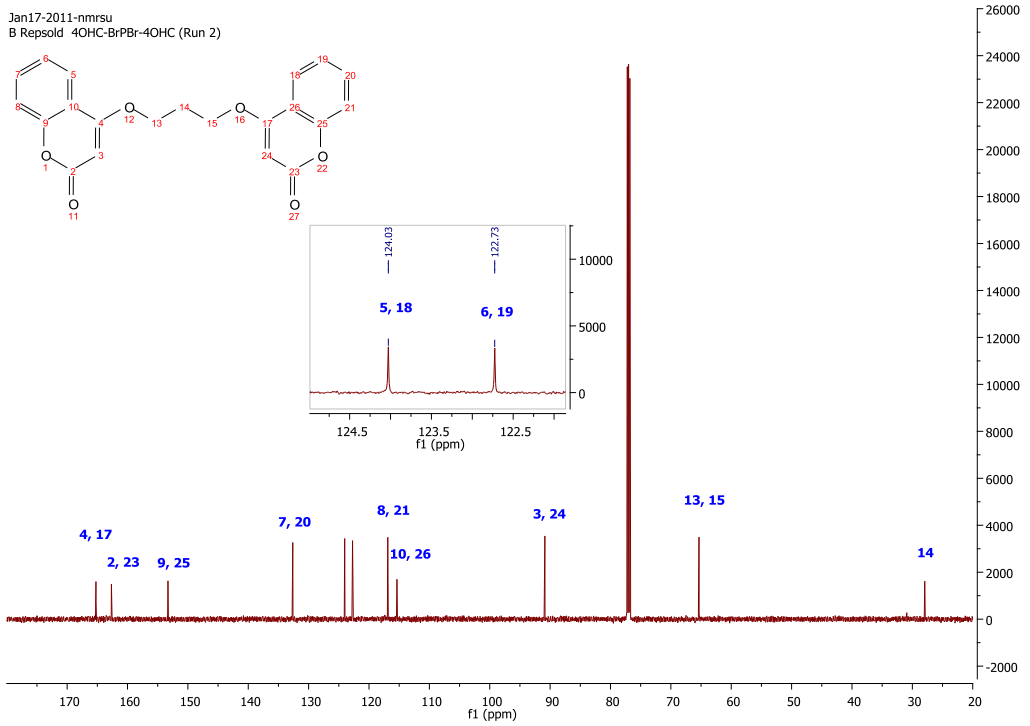

^{13}C NMR (151 MHz, $CDCl_3$, **Spectrum 10**): δ 165.22 ($C_{4,17}$); 162.66 ($C_{2,23}$); 153.29 ($C_{9,25}$); 132.62 ($C_{7,20}$); 124.03 ($C_{5,18}$); 122.73 ($C_{6,19}$); 116.89 ($C_{8,21}$); 115.37 ($C_{10,26}$); 90.87 ($C_{3,24}$); 65.34 ($C_{13,15}$); 27.95 (C_{14}).

Spectrum 11: ^{1}H NMR of 7,7'-[Propane-1,3-diylbis(oxy)]bis(2H-chromen-2-one) (**BPR 6**).

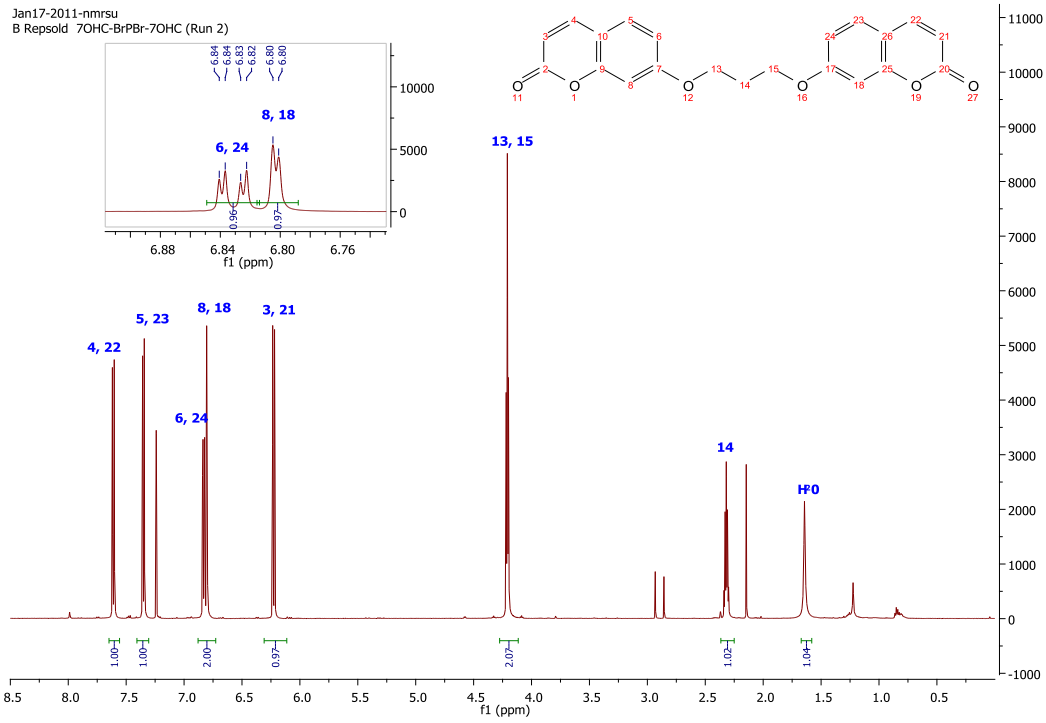

^{1}H NMR (600 MHz, $CDCl_3$, **Spectrum 11**): δ 7.61 (d, *J* = 9.5 Hz, 2H,$H_{4,22}$); 7.35 (d, *J* = 8.6 Hz, 2H,$H_{5,23}$); 6.88 (dd, J = 8.6, 2.4 Hz, 2H, $H_{6,24}$); 6.73 (s, 2$H_{8,18}$); 6.23 (d, *J* = 9.5 Hz, 2H,$H_{3,21}$); 4.21 (t, *J* = 6.0 Hz, 4H, $H_{13,15}$); 2.32 (m, 2H, H_{14}); 1.64 (s, 2H, H_2O; $CDCL_3$).

Spectrum 12: ^{13}C NMR of 7,7'-[Propane-1,3-diylbis(oxy)]bis(2*H*-chromen-2-one) **(BPR6).**

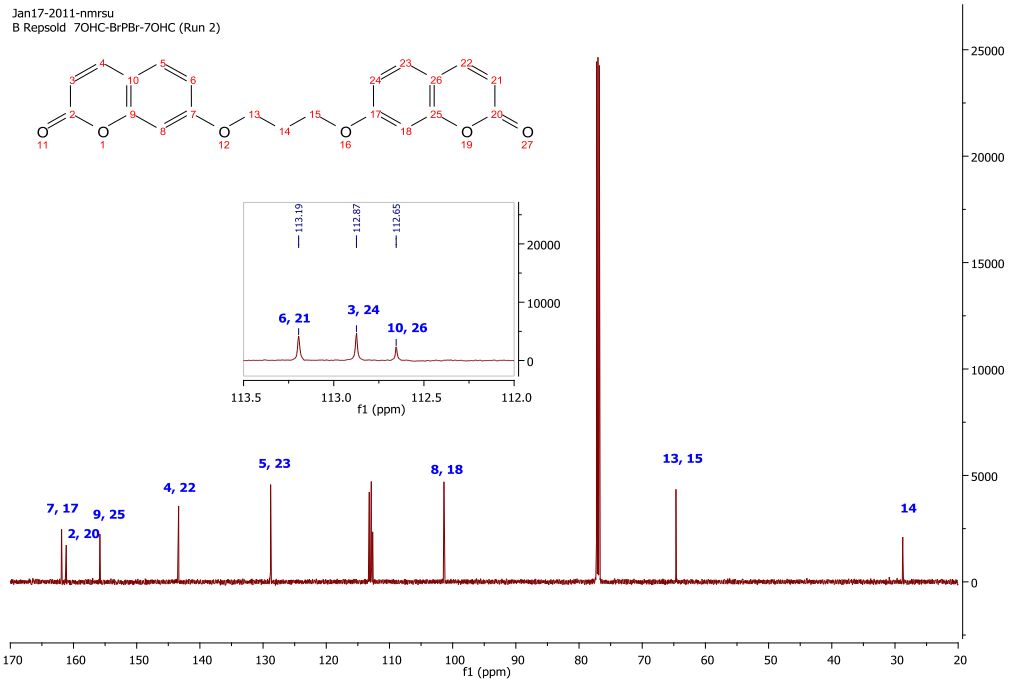

^{13}C NMR (151 MHz, $CDCl_3$, **Spectrum 12**): δ 161.89 ($C_{7,17}$); 161.15 ($C_{2,20}$); 155.82 ($C_{9,25}$); 143.36 ($C_{4,22}$), 128.80 ($C_{5,23}$), 113.19 ($C_{6,21}$); 112.87 ($C_{3,24}$), 112.36 ($C_{10.26}$), 101.37 ($C_{8,18}$), 64.66 ($C_{13,\ 15}$), 28.77 (C_{14}).

Spectrum 13: ^{1}H NMR of 7,7'-[Propane-1,3-diylbis(oxy)]bis(4-methyl-2*H*-chromen-2-one). **(BPR7).**

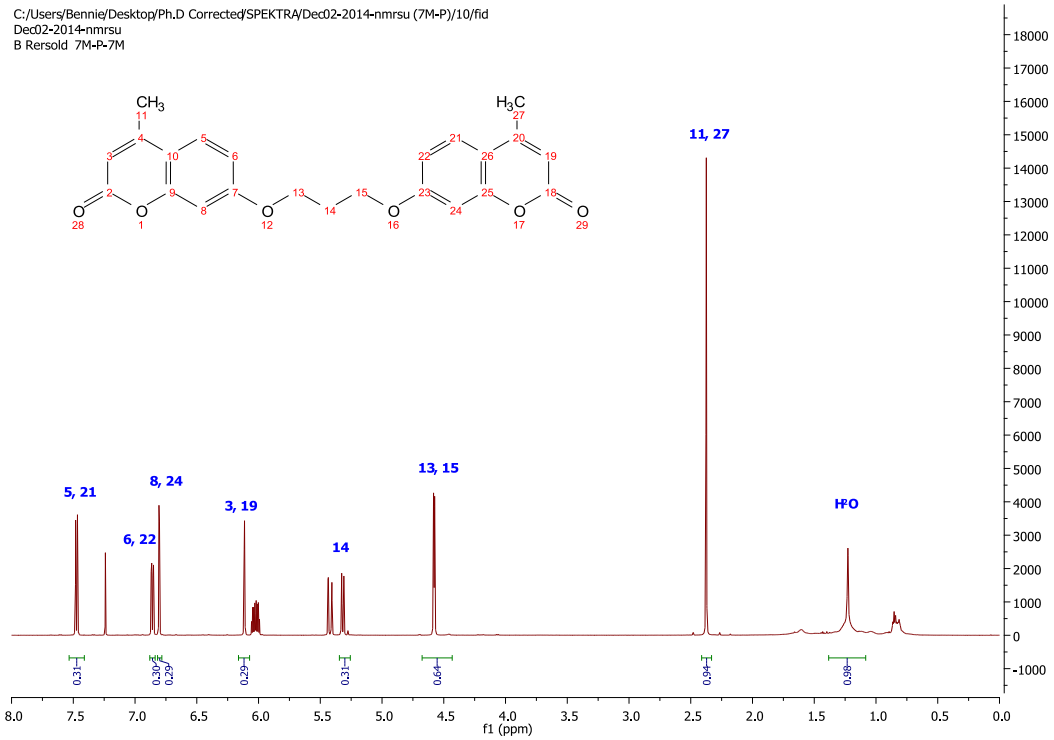

^{1}H NMR (600 MHz, $CDCl_3$, **Spectrum 13**): δ 7.47 (d, *J* = 7.0 Hz, 2H, $H_{5,\ 21}$); 6.86 (dd, J = 8.8. 2.5 Hz, 2H, $H_{6,\ 22}$); 6.80 (d, *J* = 2.5 Hz, 2H,$H_{8,24}$) 6.11 (s, 2H,$H_{3,\ 19}$); 4.58 (m, 4H, $H_{13,15}$); 5.42 (dd, *J* = 17.3, 1.4 Hz, 2H, H_{14}); 2.37 (s, 6H, $H_{11,27}$); 1.26 (s, 2H, H_2O; $CDCL_3$).

Spectrum 14: ^{13}C NMR of 7,7'-[Propane-1,3-diylbis(oxy)]bis(4-methyl-2*H*-chromen-2-one). **(BPR7).**

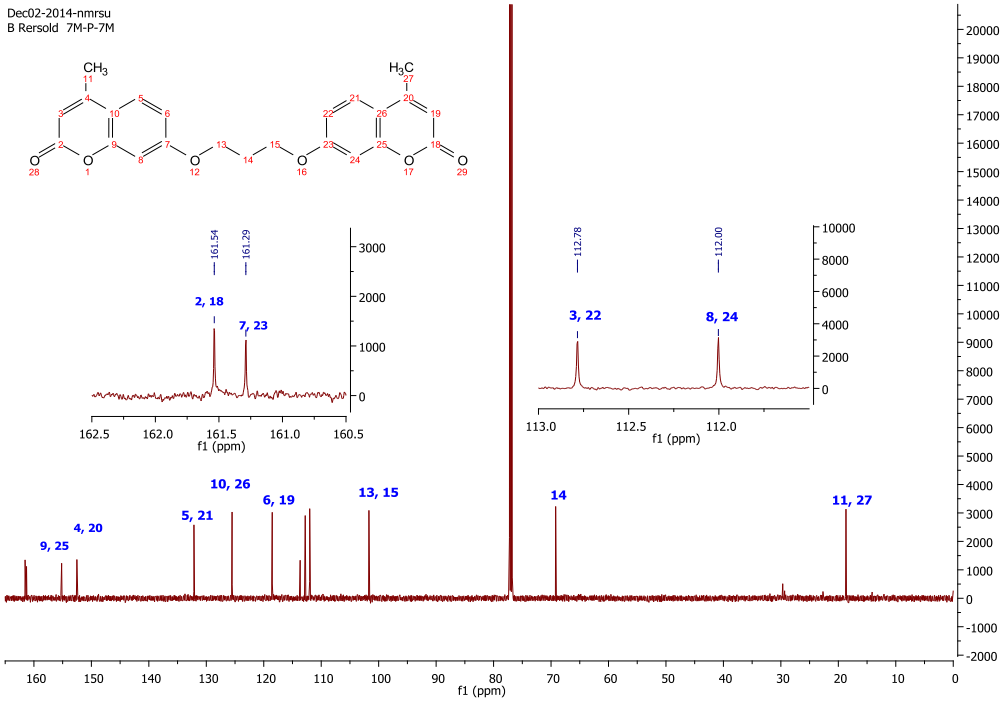

^{13}C NMR (151 MHz, $CDCl_3$, **Spectrum 14**): δ 161.54 (C2, 18); 161.29 (C7, 23); 155.18 (C9, 25); 152.52 (C4, 20); 132.15 (C5, 21); 125.51 (C10, 26); 118.52 (C6, 22); 112.78 (C3, 19); 112.00 (C8, 24); 101.70 (C13, 15); 69.20 (C14); 18.67 (C11, 27).

Spectrum 15: ^{1}H NMR of 2-Oxo-2*H*-chromen-7-yl thiophene-2-carboxylate **(BPR8).**

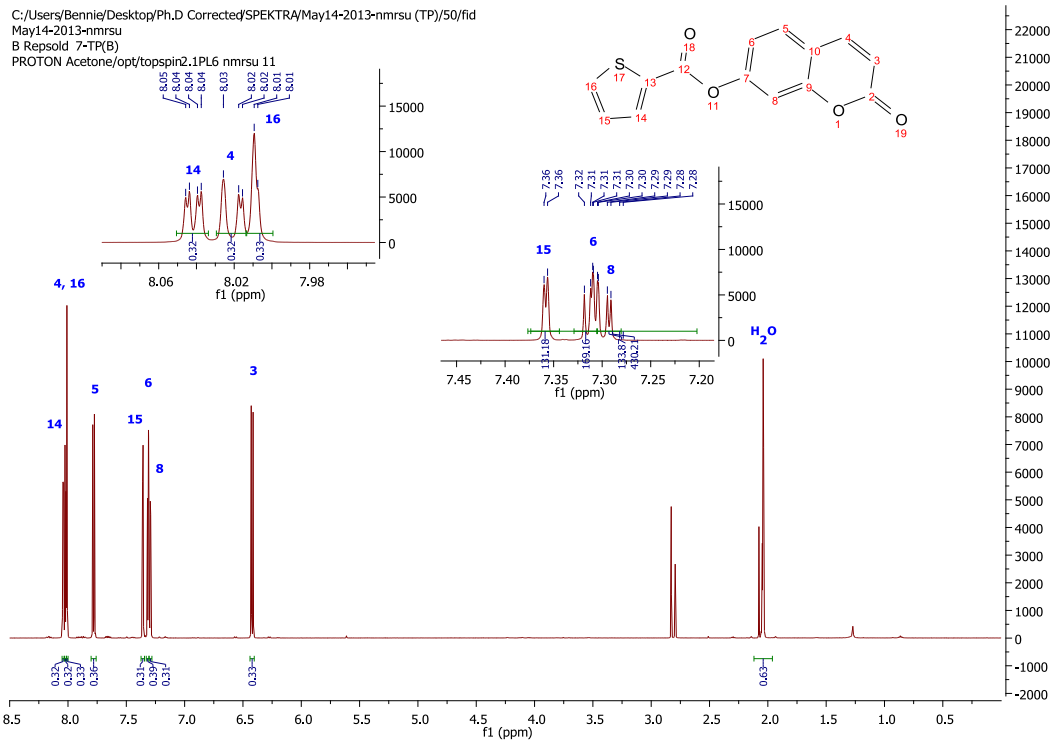

^{1}H NMR (600 MHz, Acetone; **Spectrum 15**): δ 8.04 (dd, *J* = 3.8, 1.2 Hz, 1H, H_{14}); 8.03 – 8.01 (m, 1H, H_4); 8.01 (d, *J* = 1.1 Hz, 1H, H_{16}); 7.78 (d, *J* = 6.6 Hz, 1H, H_5); 7.36 (m, 1H, H_{15}); 7.31 (dd, J = 3.4, 2.1 Hz, 1H, H_6); 7.30 (dd, *J* = 6.9, 1.4 Hz, 1H, H_8); 6.42 (dd, *J* = 9.6, 3.9 Hz, 1H, H_3); 2.12 – 1.96 (m, 2H, H_2O; Acetone).

Spectrum 16: ^{13}C NMR of 2-Oxo-2*H*-chromen-7-yl thiophene-2-carboxylate **(BPR8).**

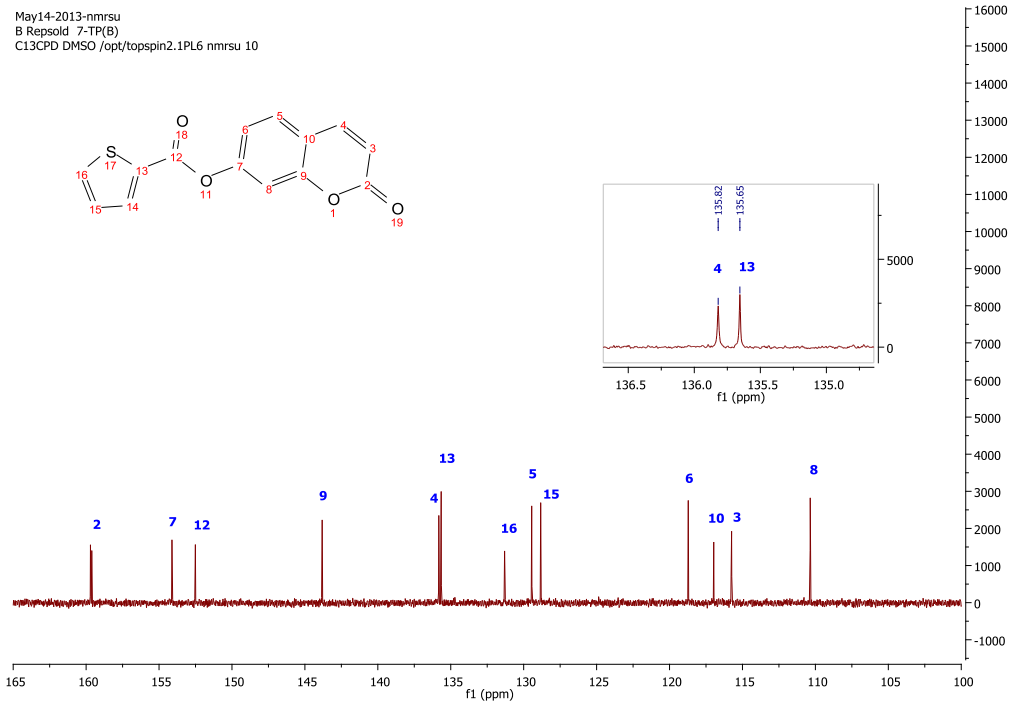

^{13}C NMR (151 MHz, DMSO, **Spectrum 16**): δ159.61 (C_2); 154.11 (C_7); 152.51 (C_{12}); 143.82 (C_9); 135.82 (C_4); 135.65 (C_{13}); 131.31 (C_{16}); 129.45 (C_5); 128.83 (C_{15}); 118.72 (C_6); 116.97 (C_{10}); 115.74 (C_3); 110.35 (C_8).

Spectrum 17: ^{1}H NMR of 4-[2-(Piperidin-1-yl)ethoxy]-2*H*-chromen-2-one **(BPR9).**

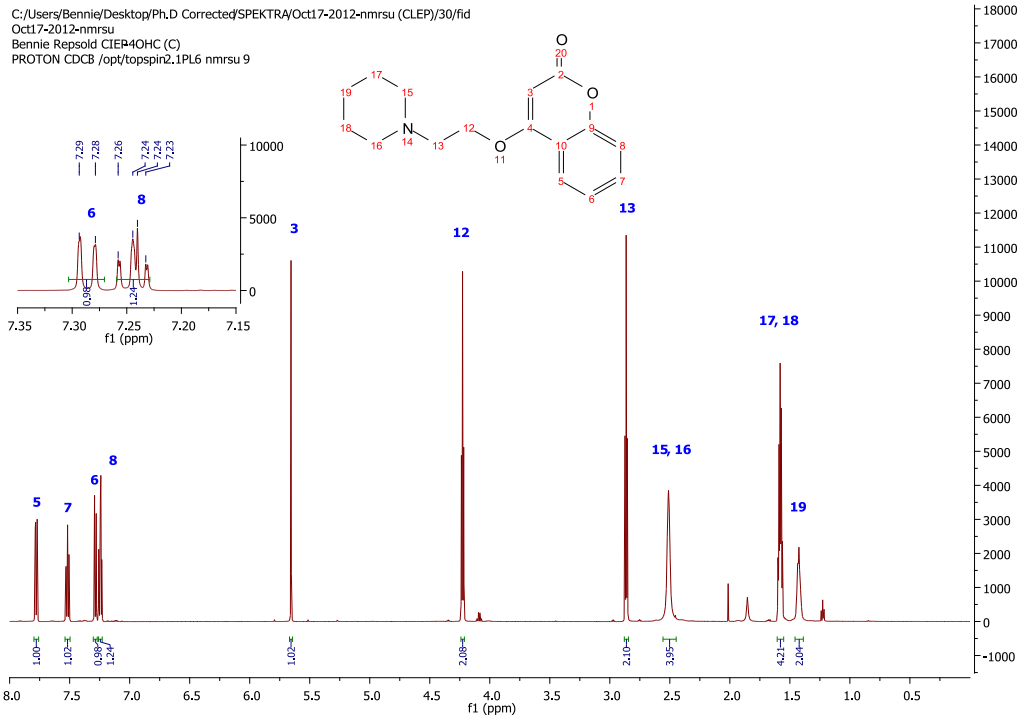

^{1}H NMR (600 MHz, $CDCl_3$, Spectrum 17): δ 7.78 (dd, *J* = 7.9, 1.5 Hz, 1H, H_5); 7.54 – 7.50 (m, 1H, H_7); 7.29 (dd, *J* = 8.3, 0.6 Hz, 1H, H_6); 7.24 (m, 1H, H_8); 5.66 (s, 1H, H_3); 4.23 (t, *J* = 5.8 Hz, 2H, H_{12}); 2.86 (t, *J* = 5.8 Hz, 2H, H_{13}); 2.51 (s, 4H, $H_{15,16}$); 1.61 – 1.55 (m, 4H, $H_{17,18}$); 1.46 – 1.39 (m, 2H, H_{19}).

Spectrum 18: ^{13}C NMR of 4-[2-(Piperidin-1-yl)ethoxy]-2*H*-chromen-2-one **(BPR9).**

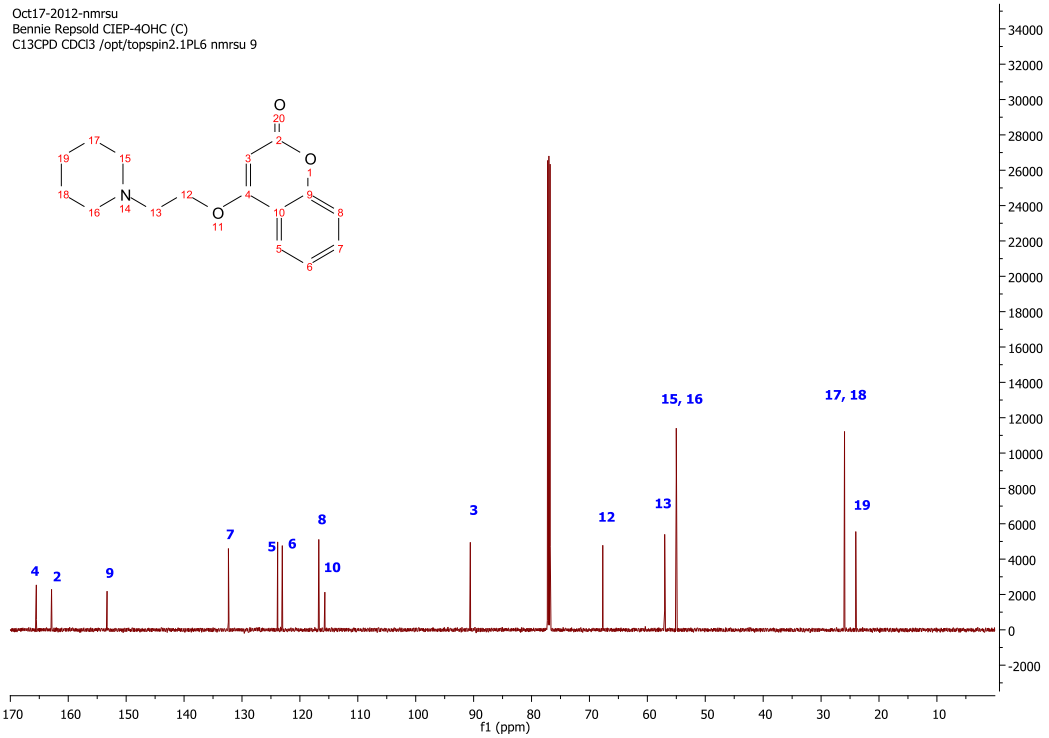

^{13}C NMR (151 MHz, $CDCl_3$, **Spectrum 18**): δ 165.51 (C_4); 162.88 (C_2); 153.30 (C_9); 132.34 (C_7); 123.84 (C_5); 123.04 (C_6); 116.74 (C_8); 115.69 (C_{10}); 90.57 (C_3); 67.70 (C_{12}); 57.01 (C_{13}); 55.01 ($C_{16,15}$); 25.95 ($C_{17,18}$); 24.01(C_{19}).

Spectrum 19: ^{1}H NMR of 4-[2-(Morpholin-4-yl)ethoxy]-2*H*-chromen-2-one **(BPR10).**

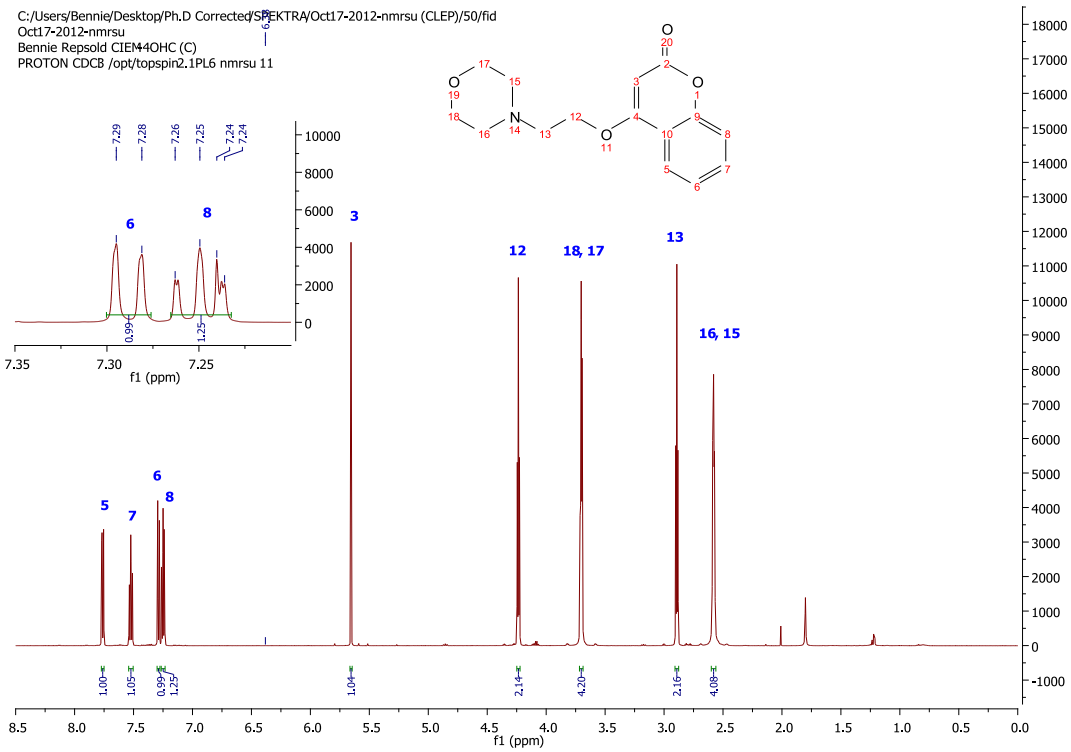

^{1}H NMR (600 MHz, $CDCl_3$. Spectrum 19): δ 7.76 (dd, *J* = 7.9, 1.5 Hz, 1H, H_5); 7.54 – 7.50 (m, 1H, H_7); 7.29 (d, *J* = 8.3 Hz, 1H, H_6); 7.27 – 7.23 (m, 1H, H_8); 5.66 (s, 1H, H_3); 4.24 (t, *J* = 5.5 Hz, 2H, H_{12}); 3.72 – 3.69 (m, 4H, $H_{17,18}$); 2.89 (t, *J* = 5.5 Hz, 2H, H_{13}); 2.60 – 2.56 (m, 4H, $H_{15,16}$).

Spectrum 20: ^{13}C NMR of 4-[2-(Morpholin-4-yl)ethoxy]-2*H*-chromen-2-one **(BPR10)**.

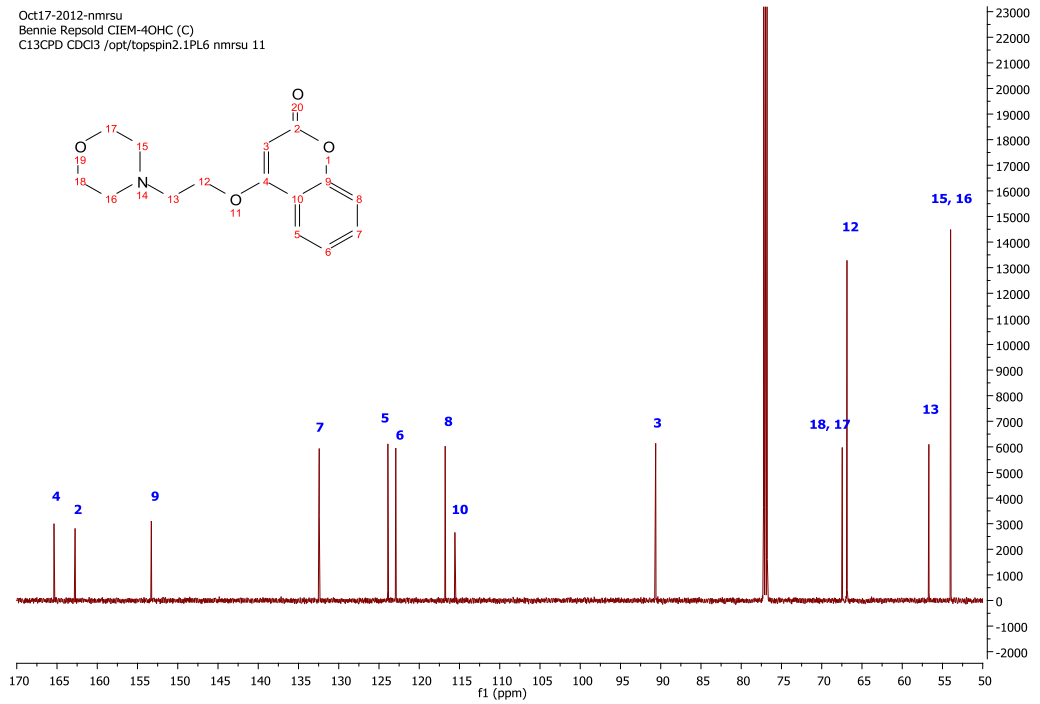

^{13}C NMR (151 MHz, $CDCl_3$, **Spectrum 20**): δ 165.38 (C_4); 162.75 (C_2); 153.28 (C_9); 132.48 (C_7); 123.86 (C_5); 122.92 (C_6); 116.78 (C_8); 115.57 (C_{10}); 90.63 (C_3); 67.45 ($C_{17,18}$); 66.86 (C_{12}); 56.69 (C_{13}); 53.99 ($C_{15,16}$).

Spectrum 21: ^{1}H NMR of 7-[2-(Morpholin-4-yl)ethoxy]-2*H*-chromen-2-one. **(BPR11).**

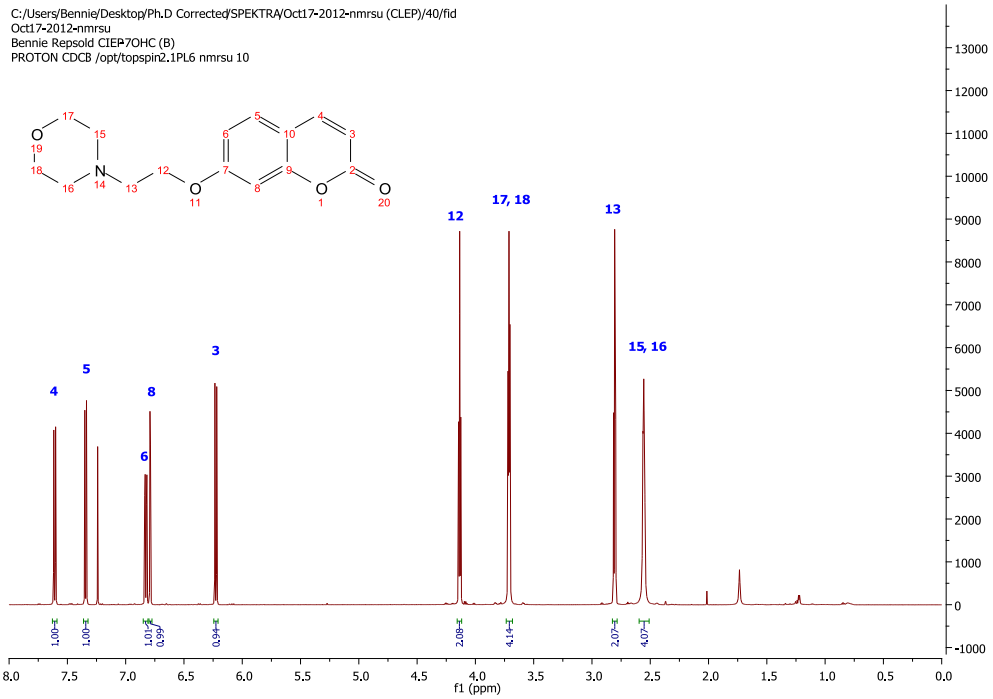

^{1}H NMR (600 MHz, $CDCl_3$, **Spectrum 21**): δ 7.61 (d, J = 9.5 Hz, 1H, H_4); 7.34 (d, J = 8.6 Hz, 1H, H_5); 6.83 (dd, J = 8.6, 2.4 Hz, 1H, H_6); 6.79 (d, J = 2.4 Hz, 1H, H_8); 6.23 (d, J = 9.5 Hz, 1H, H_3); 4.13 (t, J = 5.6 Hz, 2H, H_{12}); 3.74 – 3.68 (m, 4H, $H_{17,18}$); 2.81 (t, J = 5.6 Hz, 2H, H_{13}); 2.56 (s, 4H, $H_{15,16}$).

Spectrum 22: ^{13}C NMR of 7-[2-(Morpholin-4-yl)ethoxy]-2*H*-chromen-2-one.**(BPR11).**

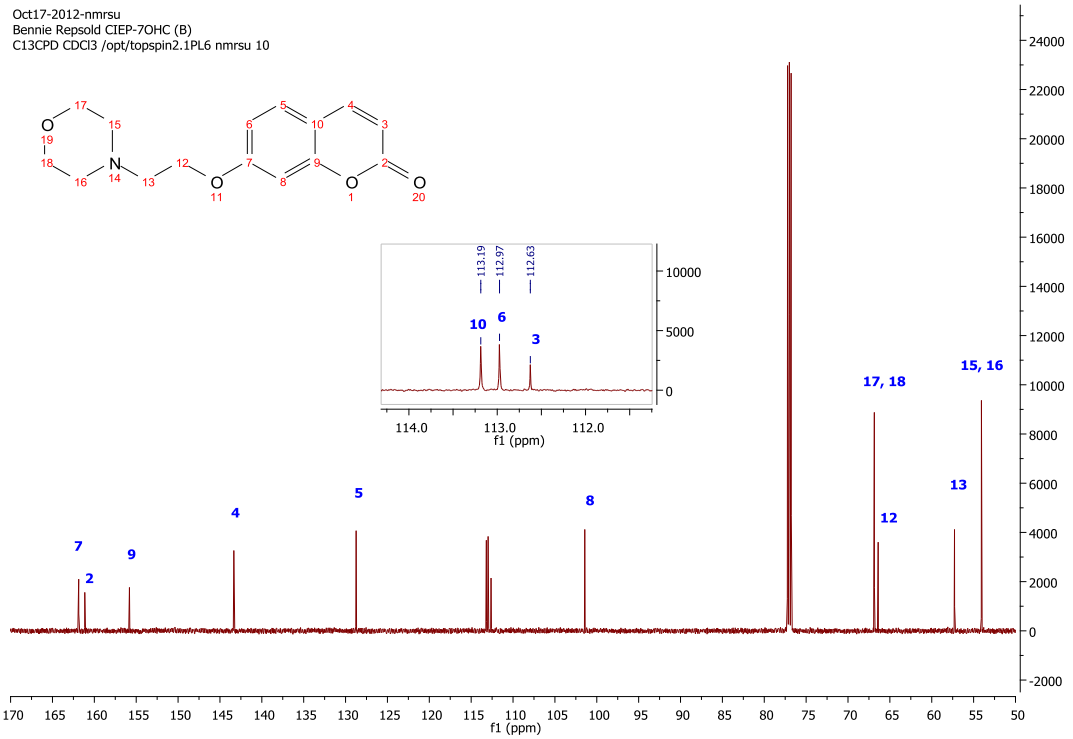

^{13}C NMR (151 MHz, $CDCl_3$, **Spectrum 22**): δ 161.87 (C_7); 161.14 (C_2); 155.81 (C_9); 143.34 (C_4); 128.74 (C_5); 113.19 (C_{10}); 112.97 (C_6); 112.63 (C_3); 101.43 (C_8); 66.85 ($C_{17,18}$); 66.40 (C_{12}); 57.28 (C_{13}); 54.07 ($C_{15,16}$).

Spectrum 23: ^{1}H NMR of 7-[2-(Piperidin-1-yl)ethoxy]-2*H*-chromen-2-one. **(BPR12).**

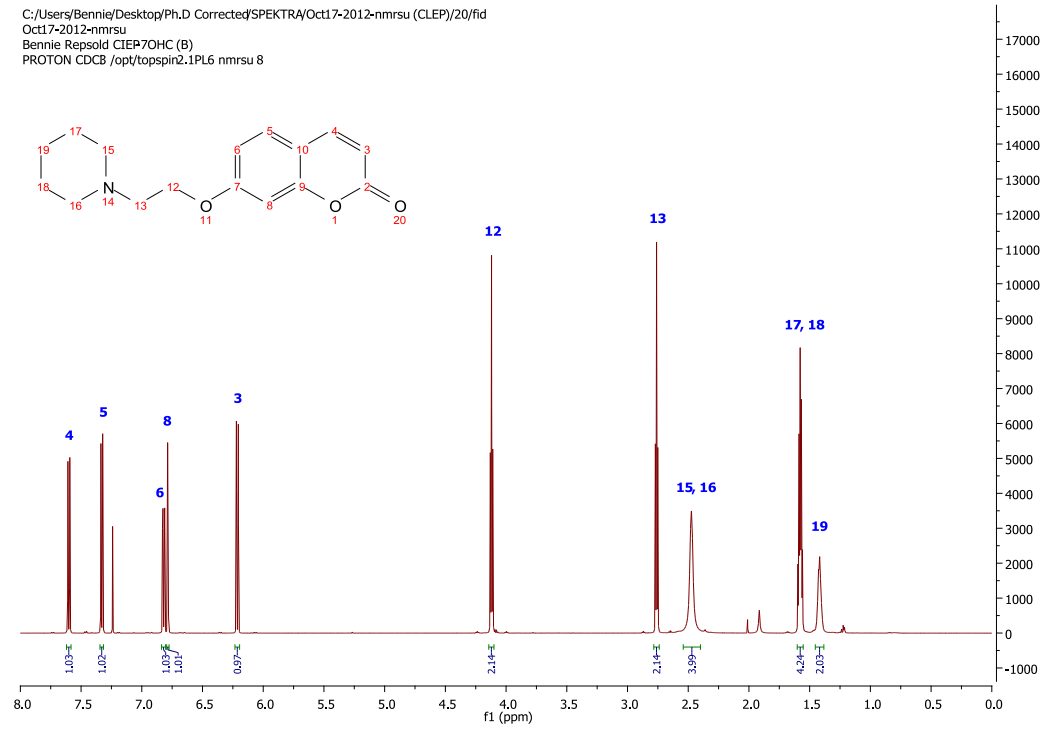

^{1}H NMR (600 MHz, $CDCl_3$, **Spectrum 23**): δ 7.60 (d, *J* = 9.5 Hz, 1H, H_4); 7.33 (d, *J* = 8.6 Hz, 1H, H_5); 6.82 (dd, *J* = 8.6, 2.4 Hz, 1H, H_6); 6.79 (d, *J* = 2.4 Hz, 1H, H_8); 6.21 (d, *J* = 9.5 Hz, 1H, H_3); 4.12 (t, *J* = 6.0 Hz, 2H, H_{12}); 2.76 (t, *J* = 6.0 Hz, 2H, H_{13}); 2.47 (bs, 4H, $H_{15,16}$); 1.60 – 1.55 (m, 4H, $H_{17,18}$); 1.42 (bs, 2H, H_{19}).

Spectrum 24: ^{13}C NMR of 7-[2-(Piperidin-1-yl)ethoxy]-2*H*-chromen-2-one. **(BPR12).**

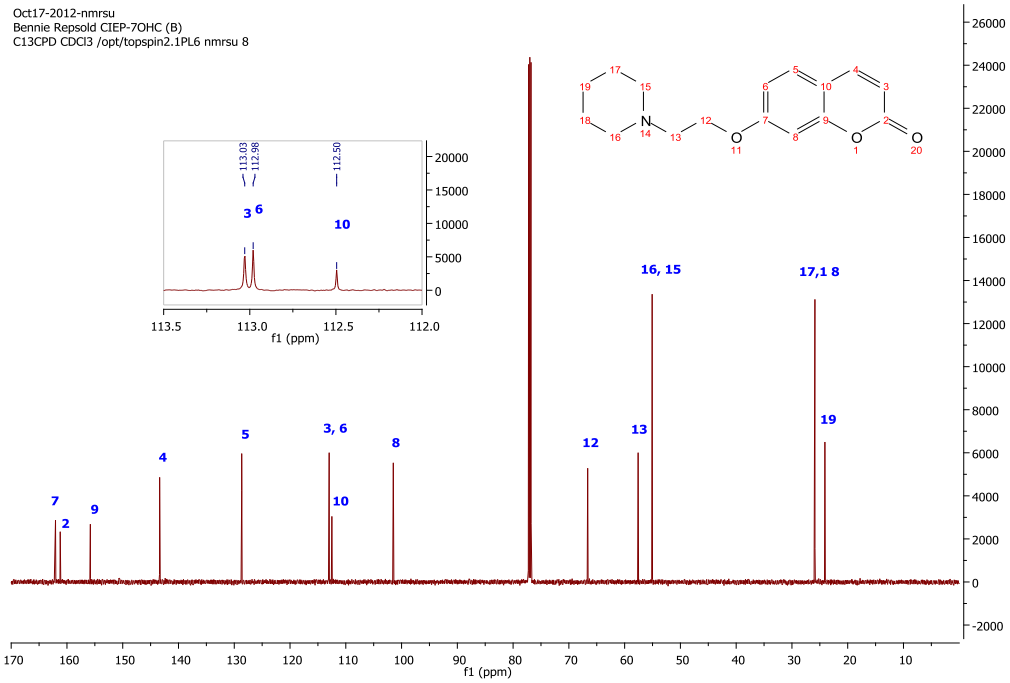

^{13}C NMR (151 MHz, $CDCl_3$, **Spectrum 24**): δ 162.05 (C_7); 161.21 (C_2); 155.81 (C_9); 143.38 (C_4); 128.67 (C_5); 113.03 (C_3); 112.98 (C_6); 112.50 (C_{10}); 101.48 (C_8); 66.63 (C_{12}); 57.58 (C_{13}); 55.06 ($C_{15, 16}$); 25.88 ($C_{17, 18}$); 24.09 (C_{19}).

Spectrum 25: ^{1}H NMR of 4-Methyl-7-[2-(piperidin-1-yl)ethoxy]-2*H*-chromen-2-one. **(BPR13).**

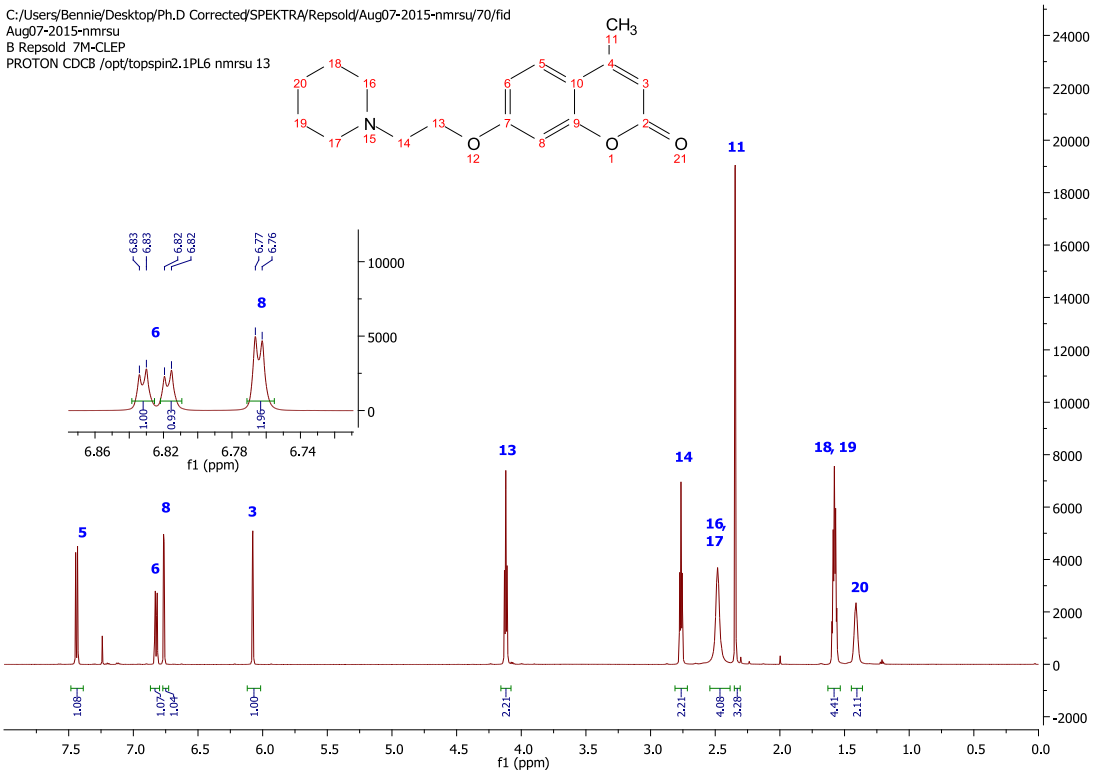

^{1}H NMR (600 MHz, $CDCl_3$, **Spectrum 25**): δ 7.44 (d, *J* = 8.8 Hz, 1H, H_5), 6.82 (dd, *J* = 8.8, 2.4 Hz, 1H, H_6), 6.76 (d, *J* = 2.4 Hz, 1H, H_8), 6.08 (d, *J* = 0.9 Hz, 1H, H_3), 4.12 (t, *J* = 5.9 Hz, 2H, H_{13}), 2.76 (t, *J* = 5.9 Hz, 2H, H_{14}), 2.48 (bs, 4H, $H_{16,17}$), 2.35 (d, *J* = 1.0 Hz, 3H, H_{11}), 1.58 (m, 4H, $H_{18,19}$), 1.41 (bs, 2H, H_{20}).

Spectrum 26: ^{13}C NMR of 4-Methyl-7-[2-(piperidin-1-yl)ethoxy]-2*H*-chromen-2-one. **(BPR13).**

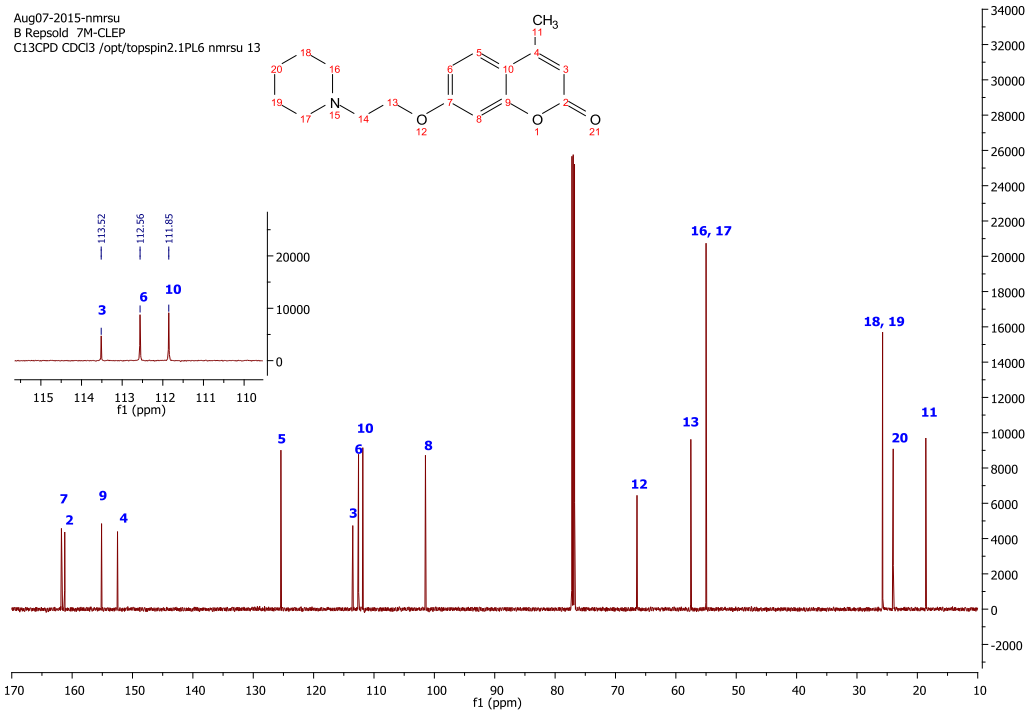

^{13}C NMR (151 MHz, $CDCl_3$, **Spectrum 26**): δ 161.77 (C_7); 161.23 (C_2); 155.13 (C_9); 152.48 (C_4), 125.42 (C_5), 113.52 (C_3), 112.56 (C_6), 111.85 (C_{10}), 101.48 (C_8), 66.44 (C_{12}), 57.52 (C_{13}), 55.00 ($C_{16,17}$), 25.76 ($C_{18,19}$), 24.00 (C_{20}), 18.60 (C_{11}).

Spectrum 27: ^{1}H NMR of 4-Methyl-7-[2-(morpholin-4-yl)ethoxy]-2*H*-chromen-2-one. **(BPR14).**

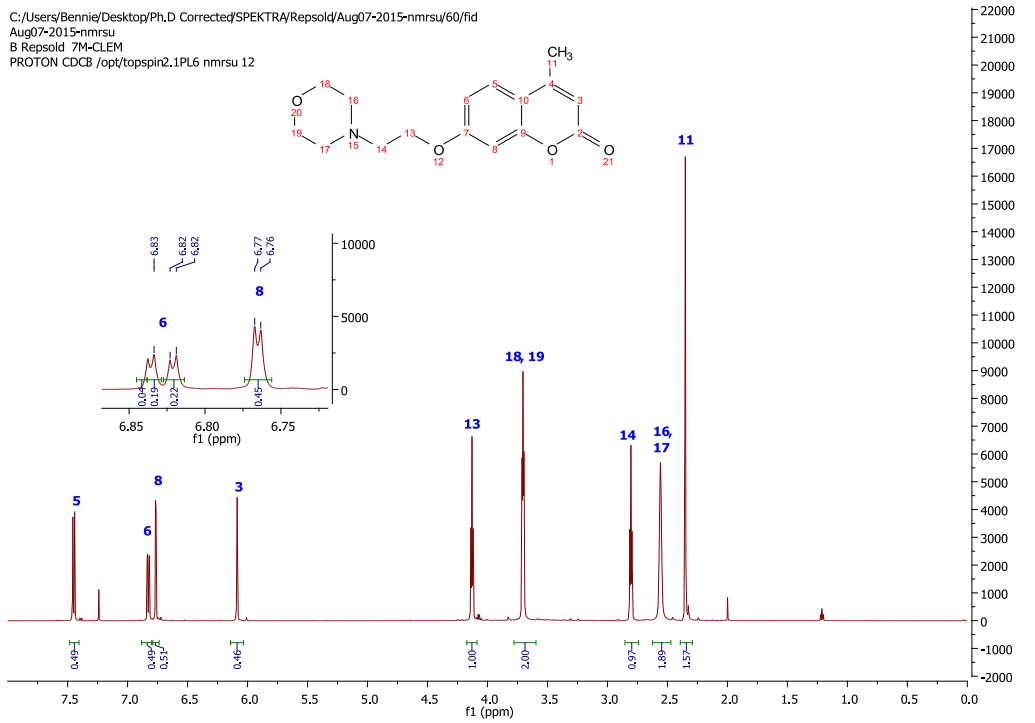

^{1}H NMR (600 MHz, $CDCl_3$, **Spectrum 27**): δ 7.45 (d, *J* = 8.8 Hz, 1H, H_5), 6.82 (dd, *J* = 17.4, 8.7 Hz, 1H, H_6), 6.76 (d, *J* = 7.5 Hz, 1H, H_8), 6.09 (d, *J* = 0.9 Hz, 1H, H_3), 4.13 (t, *J* = 5.6 Hz, 2H, H_{13}), 3.78 – 3.60 (m, 4H, $H_{18,19}$), 2.80 (t, *J* = 5.6 Hz, 2H, H_{14}), 2.56 (m, 4H, $H_{16,17}$), 2.34 (dd, *J* = 16.2, 0.9 Hz, 3H, H_{11}).

Spectrum 28: ^{13}C NMR of 4-Methyl-7-[2-(morpholin-4-yl)ethoxy]-2*H*-chromen-2-one. **(BPR14).**

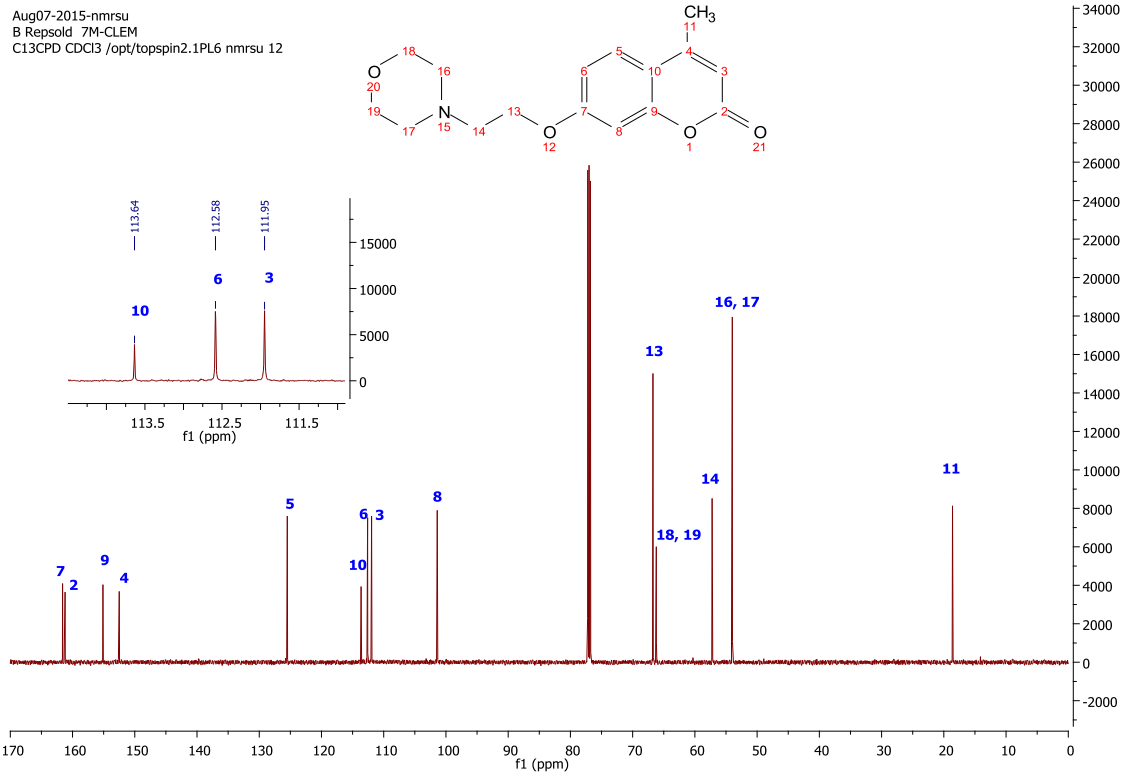

^{13}C NMR (151 MHz, $CDCl_3$, **Spectrum 28**): δ 161.60 (C_7), 161.20 (C_2), 155.12 (C_9), 152.49 (C_4), 125.49 (C_5), 113.64 (C_{10}), 112.58 (C_6), 111.95 (C_3), 101.40 (C_8), 66.74 (C_{13}), 66.20 ($C_{18,19}$), 57.23 (C_{14}), 53.99 ($C_{16,17}$), 18.60 (C_{11}).

ANNEXURE B: Mass Spectra

Spectrum 29: 2-Oxo-2*H*-chromen-7-yl docos-24-enoate **(BPR1).**

Mass Spectrum SmartFormula Report

Analysis Info

Analysis Name	D:\Data\21062013\LADMS000001.d	Acquisition Date	6/21/2013 8:02:03 AM
Method	tune_low12062013.m	Operator	JHL Jordaan
Sample Name	7-ERA_A	Instrument / Ser#	micrOTOF-Q II 10390
Comment			

Acquisition Parameter

Source Type	APCI	Ion Polarity	Positive	Set Nebulizer	1.6 Bar
Focus	Not active	Set Capillary	4500 V	Set Dry Heater	200 °C
Scan Begin	50 m/z	Set End Plate Offset	-500 V	Set Dry Gas	8.0 l/min
Scan End	1500 m/z	Set Collision Cell RF	100.0 Vpp	Set Divert Valve	Waste

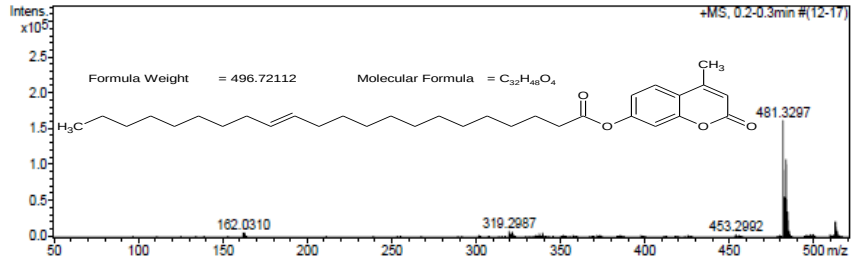

Meas. m/z	#	Formula	Score	m/z	err [mDa]	err [ppm]	mSigma	rdb	N-Rule	e⁻ Conf
481.3297	1	C 31 H 45 O 4	100.00	481.3312	1.6	3.3	318.0	9.5	ok	even
	2	C 27 H 41 N 6 O 2	61.52	481.3286	-1.1	-2.3	324.0	10.5	ok	even
483.3446	1	C 27 H 43 N 6 O 2	100.00	483.3442	-0.4	-0.8	10.1	9.5	ok	even
	2	C 31 H 47 O 4	30.24	483.3469	2.3	4.7	10.1	8.5	ok	even
	3	C 26 H 47 N 2 O 6	38.05	483.3429	-1.7	-3.6	19.3	4.5	ok	even
512.3351	1	C 30 H 40 N 8	53.12	512.3370	1.9	3.8	32.5	15.0	ok	odd
	2	C 31 H 46 N O 5	50.44	512.3371	2.0	3.8	34.3	9.5	ok	even
	3	C 29 H 44 N 4 O 4	100.00	512.3357	0.6	1.2	40.1	10.0	ok	odd
	4	C 28 H 48 O 8	71.12	512.3344	-0.7	-1.4	49.8	5.0	ok	odd

MS: EIMS 315; EI-HRMS *m/z*: calculated for $\mathbf{C_{31}H_{46}O_4}$, 482.6945, found 481.3297 (**Spectrum 29**).

Spectrum 30: 2-Oxo-2*H*-chromen-4-yl docos-24-enoic carboxylate **(BPR2).**

Mass Spectrum SmartFormula Report

Analysis Info

Analysis Name	D:\Data\21062013\LADMS000003.d	Acquisition Date	6/21/2013 9:57:16 AM
Method	tune_low12062013.m	Operator	JHL Jordaan
Sample Name	4-ERA_A	Instrument / Ser#	micrOTOF-Q II 10390
Comment			

Acquisition Parameter

Source Type	APCI	Ion Polarity	Positive	Set Nebulizer	1.6 Bar
Focus	Not active	Set Capillary	4500 V	Set Dry Heater	200 °C
Scan Begin	50 m/z	Set End Plate Offset	-500 V	Set Dry Gas	8.0 l/min
Scan End	1500 m/z	Set Collision Cell RF	100.0 Vpp	Set Divert Valve	Waste

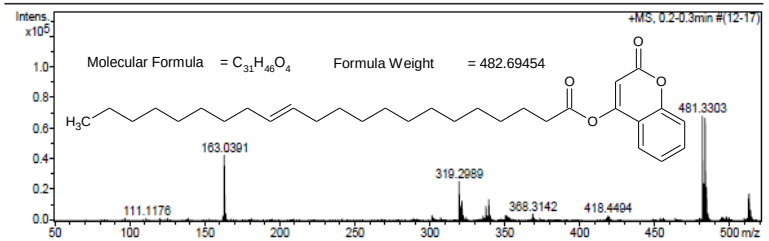

Meas. m/z	#	Formula	Score	m/z	err [mDa]	err [ppm]	mSigma	rdb	N-Rule	e⁻ Conf
163.0391	1	C 9 H 7 O 3	100.00	163.0390	-0.2	-1.0	0.3	6.5	ok	even
	2	C 7 H 5 N 3 O 2	41.40	163.0376	-1.5	-9.2	7.2	7.0	ok	odd
319.2989	1	C 22 H 39 O	100.00	319.2995	0.7	2.0	285.5	3.5	ok	even
	2	C 20 H 37 N 3	61.76	319.2982	-0.7	-2.2	288.7	4.0	ok	odd
481.3303	1	C 31 H 45 O 4	100.00	481.3312	1.0	2.0	483.3	9.5	ok	even
	2	C 29 H 43 N 3 O 3	78.51	481.3299	-0.4	-0.8	486.2	10.0	ok	odd
	3	C 27 H 41 N 6 O 2	20.06	481.3286	-1.7	-3.6	489.3	10.5	ok	even
483.3456	1	C 27 H 43 N 6 O 2	97.90	483.3442	-1.4	-2.9	7.3	9.5	ok	even
	2	C 31 H 47 O 4	100.00	483.3469	1.3	2.6	9.5	8.5	ok	even
512.3362	1	C 30 H 40 N 8	91.90	512.3370	0.9	1.7	25.4	15.0	ok	odd
	2	C 31 H 46 N O 5	88.18	512.3371	0.9	1.7	27.0	9.5	ok	even
	3	C 29 H 44 N 4 O 4	100.00	512.3357	-0.5	-0.9	32.8	10.0	ok	odd
	4	C 27 H 42 N 7 O 3	39.02	512.3344	-1.8	-3.5	38.6	10.5	ok	even
	5	C 28 H 48 O 8	35.09	512.3344	-1.8	-3.5	42.6	5.0	ok	odd

MS: EIMS 315; EI-HRMS *m/z*: calculated for $\mathbf{C_{31}H_{46}O_4}$, 482.6945, found 481.303 (**Spectrum 30**).

Spectrum 31: 4-Methyl-2-oxo-2*H*-chromen-7-yl docos-25-enoic carboxylate **(BPR3).**

Mass Spectrum SmartFormula Report

Analysis Info

Analysis Name	D:\Data\11122014\LADM3000001.d	Acquisition Date	12/11/2014 11:42:18 AM
Method	tune_low_14082014_tune.m	Laboratory	Laboratory for Analytical Services
Sample Name	7M-ERA	Operator	JHL Jordaan
Comment		Instrument / Ser#	micrOTOF-Q II 10390

Acquisition Parameter

Source Type	APCI	Ion Polarity	Positive	Set Nebulizer	1.6 Bar
Focus	Not active	Set Capillary	4500 V	Set Dry Heater	200 °C
Scan Begin	50 m/z	Set End Plate Offset	-500 V	Set Dry Gas	8.0 l/min
Scan End	3000 m/z	Set Collision Cell RF	150.0 Vpp	Set Divert Valve	Waste

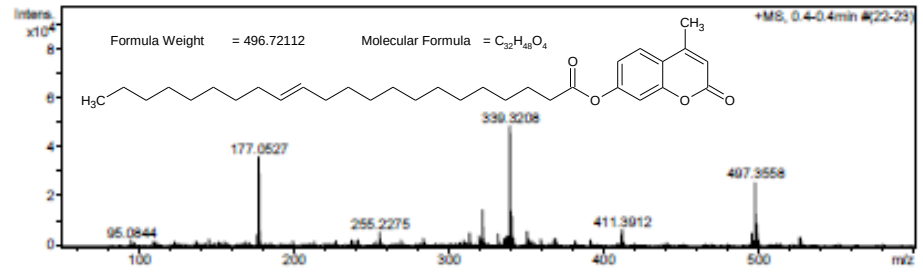

Meas. m/z	#	Formula	Score	m/z	err [mDa]	err [ppm]	mSigma	rdb	N-Rule	e⁻ Conf
496.3396	1	C 32 H 47 O 4	0.26	496.3469	7.3	14.7	651.8	9.5	ok	even
	2	C 31 H 45 N O 4	8.11	496.3343	-5.3	-10.6	652.0	10.0	ok	odd
	3	C 30 H 45 N 3 O 3	2.18	496.3455	6.0	12.0	652.9	10.0	ok	odd
	4	C 29 H 43 N 4 O 3	0.68	496.3330	-6.6	-13.4	653.1	10.5	ok	even
	5	C 28 H 43 N 6 O 2	11.71	496.3442	4.6	9.3	654.1	10.5	ok	even
	6	C 35 H 45 N O	0.00	496.3496	10.0	20.2	654.2	14.0	ok	odd
	7	C 27 H 41 N 7 O 2	0.04	496.3316	-8.0	-16.1	654.3	11.0	ok	odd
	8	C 34 H 43 N 2 O	100.00	496.3370	-2.6	-5.2	654.4	14.5	ok	even
	9	C 33 H 43 N 4	0.01	496.3482	8.6	17.4	654.5	14.5	ok	even
	10	C 32 H 41 N 5	23.28	496.3356	-3.9	-7.9	654.7	15.0	ok	odd
	11	C 26 H 41 N 9 O	0.00	496.3429	3.3	6.6	731.6	11.0	ok	odd
496.3427	1	C 35 H 44 O 2	0.00	496.3336	-9.1	-18.3	573.9	14.0	ok	odd
	2	C 34 H 44 N 2 O	91.41	496.3448	2.1	4.3	575.5	14.0	ok	odd
	3	C 32 H 42 N 5	100.00	496.3435	0.8	1.6	578.9	14.5	ok	even
	4	C 31 H 46 N O 4	22.52	496.3421	-0.5	-1.1	585.9	9.5	ok	even
	5	C 29 H 44 N 4 O 3	4.08	496.3408	-1.9	-3.8	589.7	10.0	ok	odd
	6	C 28 H 44 N 6 O 2	0.00	496.3520	9.4	18.9	591.1	10.0	ok	odd
	7	C 27 H 42 N 7 O 2	0.51	496.3395	-3.2	-6.5	593.5	10.5	ok	even
	8	C 26 H 42 N 9 O	0.00	496.3507	8.0	16.2	685.6	10.5	ok	even
	9	C 25 H 40 N 10 O	0.00	496.3381	-4.6	-9.2	688.4	11.0	ok	odd
	10	C 24 H 40 N 12	0.00	496.3493	6.7	13.4	689.7	11.0	ok	odd
	11	C 23 H 38 N 13	0.00	496.3368	-5.9	-11.9	692.5	11.5	ok	even
	12	C 23 H 44 N 8 O 4	0.00	496.3480	5.3	10.8	698.0	6.0	ok	odd
	13	C 22 H 42 N 9 O 4	0.00	496.3354	-7.2	-14.6	700.8	6.5	ok	even
	14	C 21 H 42 N 11 O 3	0.00	496.3467	4.0	8.0	702.5	6.5	ok	even
	15	C 20 H 40 N 12 O 3	0.00	496.3341	-8.6	-17.3	705.3	7.0	ok	odd
	16	C 19 H 40 N 14 O 2	0.00	496.3453	2.7	5.3	707.0	7.0	ok	odd
	17	C 18 H 38 N 15 O 2	0.00	496.3327	-9.9	-20.0	709.8	7.5	ok	even
	18	C 17 H 38 N 17 O	0.00	496.3440	1.3	2.6	711.8	7.5	ok	even
	19	C 15 H 36 N 20	0.00	496.3426	-0.0	-0.1	716.1	8.0	ok	odd
	20	C 14 H 40 N 16 O 4	0.00	496.3413	-1.4	-2.8	724.6	3.0	ok	odd

Mass Spectrum SmartFormula Report

Meas. m/z	#	Formula	Score	m/z	err [mDa]	err [ppm]	mSigma	rdb	N-Rule	e⁻ Conf
497.3558	1	C 32 H 49 O 4	0.23	497.3625	6.8	13.6	10.7	8.5	ok	even
	2	C 31 H 47 N O 4	1.24	497.3500	-5.8	-11.6	11.5	9.0	ok	odd
	3	C 30 H 47 N 3 O 3	2.06	497.3612	5.4	10.9	13.4	9.0	ok	odd
	4	C 29 H 45 N 4 O 3	0.11	497.3486	-7.1	-14.3	15.6	9.5	ok	even
	5	C 32 H 43 N 5	7.88	497.3513	-4.5	-9.0	16.7	14.0	ok	odd
	6	C 28 H 45 N 6 O 2	11.70	497.3599	4.1	8.2	17.8	9.5	ok	even
	7	C 33 H 45 N 4	0.01	497.3639	8.1	16.3	18.7	13.5	ok	even
	8	C 34 H 45 N 2 O	33.15	497.3526	-3.1	-6.3	19.9	13.5	ok	even
	9	C 27 H 43 N 7 O 2	0.01	497.3473	-8.5	-17.0	20.7	10.0	ok	odd
	10	C 35 H 47 N O	0.00	497.3652	9.5	19.0	22.6	13.0	ok	odd
	11	C 26 H 43 N 9 O	40.06	497.3585	2.8	5.5	26.7	10.0	ok	odd
	12	C 25 H 41 N 10 O	0.00	497.3459	-9.8	-19.7	30.3	10.5	ok	even
	13	C 24 H 41 N 12	100.00	497.3572	1.4	2.8	32.2	10.5	ok	even

MS: EIMS 315; EI-HRMS *m/z*: calculated for $\mathbf{C_{32}H_{48}O_4}$, 496.721, found 497.3558 (**Spectrum 31**).

Spectrum 32: 4,4'-[Butane-1,4-diylbis(oxy)]bis(2*H*-chromen-2-one) **(BPR4).**

Mass Spectrum SmartFormula Report

Analysis Info

Analysis Name	D:\Data\Bennie Repsold\4OHC-BrBBr_4OHC_APCI000001.d	Acquisition Date	5/18/2012 3:44:04 PM
Method	tune low_APCI.m	Operator	Dr JHL Jordaan
Sample Name	OHC-BrBBr_4OHC_APCI	Instrument / Ser#	micrOTOF-Q II 10390
Comment			

Acquisition Parameter

Source Type	APCI	Ion Polarity	Positive	Set Nebulizer	1.6 Bar
Focus	Not active	Set Capillary	4000 V	Set Dry Heater	200 °C
Scan Begin	50 m/z	Set End Plate Offset	-500 V	Set Dry Gas	1.5 l/min
Scan End	3000 m/z	Set Collision Cell RF	140.0 Vpp	Set Divert Valve	Waste

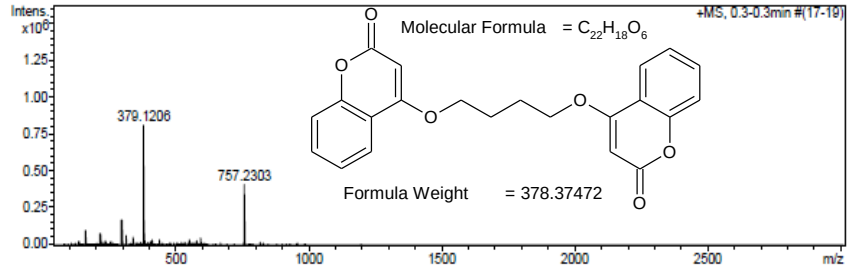

Meas. m/z	#	Formula	Score	m/z	err [mDa]	err [ppm]	mSigma	rdb	e⁻ Conf	N-Rule
379.1206	1	C 28 H 15 N 2	100.00	379.1235	2.9	7.7	197.3	22.5	even	ok
	2	C 25 H 17 N O 3	5.22	379.1208	0.2	0.6	248.6	18.0	odd	ok
	3	C 23 H 15 N 4 O 2	1.70	379.1195	-1.1	-2.9	255.1	18.5	even	ok
	4	C 21 H 13 N 7 O	0.31	379.1182	-2.4	-6.4	261.9	19.0	odd	ok
	5	C 19 H 11 N 10	0.04	379.1168	-3.8	-10.0	268.2	19.5	even	ok
	6	C 15 H 23 O 11	0.06	379.1240	3.4	9.1	268.8	4.5	even	ok
	7	C 22 H 19 O 6	0.14	379.1182	-2.4	-6.4	269.4	13.5	even	ok
	8	C 20 H 17 N 3 O 5	0.02	379.1168	-3.8	-10.0	275.9	14.0	odd	ok
	9	C 13 H 11 N 14 O	0.00	379.1240	3.4	9.0	297.9	15.5	even	ok
	10	C 11 H 9 N 17	0.00	379.1227	2.1	5.5	304.2	16.0	odd	ok

MS: EIMS 315; EI-HRMS *m/z*: calculated for $\mathbf{C_{22}H_{18}O_6}$, 378.3747, found 379.1206 (**Spectrum 32**).

Spectrum 33: 4,4'-[Propane-1,3-diylbis(oxy)]bis(2*H*-chromen-2-one) **(BPR5).**

Mass Spectrum SmartFormula Report

Analysis Info

Analysis Name	D:\Data\Bennie Repsold\4OHC-BrPBr-4OHC_Apci_run2000001.d	Acquisition Date	5/17/2012 3:34:02 PM
Method	tune low_APCI.m	Operator	Dr JHL Jordaan
Sample Name	4OHC-BrPBr-4OHC_Apci_run2	Instrument / Ser#	micrOTOF-Q II 10390
Comment			

Acquisition Parameter

Source Type	APCI	Ion Polarity	Positive	Set Nebulizer	1.6 Bar
Focus	Not active	Set Capillary	4000 V	Set Dry Heater	200 °C
Scan Begin	50 m/z	Set End Plate Offset	-500 V	Set Dry Gas	1.5 l/min
Scan End	3000 m/z	Set Collision Cell RF	140.0 Vpp	Set Divert Valve	Waste

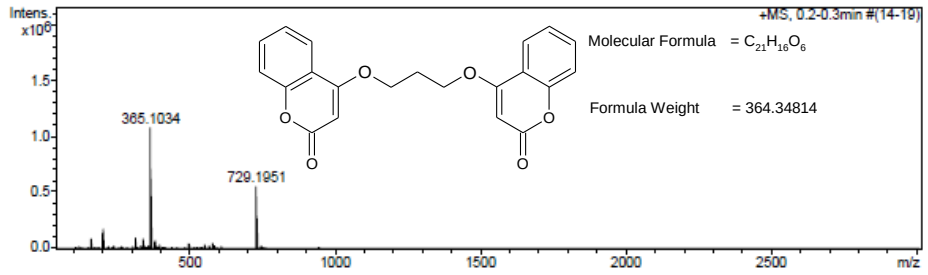

Meas. m/z	#	Formula	Score	m/z	err [mDa]	err [ppm]	mSigma	rdb	e⁻ Conf	N-Rule
365.1034	1	C 22 H 13 N 4 O 2	100.00	365.1039	0.5	1.3	190.4	18.5	even	ok
	2	C 18 H 9 N 10	11.09	365.1012	-2.2	-6.1	203.4	19.5	even	ok
	3	C 21 H 17 O 6	24.73	365.1025	-0.9	-2.4	204.7	13.5	even	ok
	4	C 17 H 13 N 6 O 4	0.90	365.0998	-3.6	-9.7	217.5	14.5	even	ok
	5	C 11 H 13 N 10 O 5	0.05	365.1070	3.7	10.0	246.7	10.5	even	ok
	6	C 7 H 9 N 16 O 3	0.11	365.1044	1.0	2.7	259.9	11.5	even	ok
	7	C 10 H 17 N 6 O 9	0.04	365.1057	2.3	6.4	260.8	5.5	even	ok
	8	C 9 H 21 N 2 O 13	0.03	365.1044	1.0	2.7	272.1	0.5	even	ok
	9	C 3 H 5 N 22 O	0.02	365.1017	-1.7	-4.7	273.0	12.5	even	ok
	10	C 6 H 13 N 12 O 7	0.03	365.1030	-0.4	-1.0	273.7	6.5	even	ok

MS: EIMS 315; EI-HRMS *m/z*: calculated for $\mathbf{C_{21}H_{16}O_6}$, 364.348, found 365.1034 (**Spectrum 33**).

Spectrum 34: 7,7'-[Propane-1,3-diylbis(oxy)]bis(2*H*-chromen-2-one) **(BPR6).**

Mass Spectrum SmartFormula Report

Analysis Info

Analysis Name	D:\Data\Bennie Repsold\7OHC_BrPBr_7OHC_run2000001.d	Acquisition Date	5/17/2012 2:39:45 PM
Method	tune low_APCI.m	Operator	Dr JHL Jordaan
Sample Name	7OHC_BrPBr_7OHC_run2	Instrument / Ser#	micrOTOF-Q II 10390
Comment			

Acquisition Parameter

Source Type	APCI	Ion Polarity	Positive	Set Nebulizer	1.6 Bar
Focus	Not active	Set Capillary	4000 V	Set Dry Heater	200 °C
Scan Begin	50 m/z	Set End Plate Offset	-500 V	Set Dry Gas	1.5 l/min
Scan End	3000 m/z	Set Collision Cell RF	140.0 Vpp	Set Divert Valve	Waste

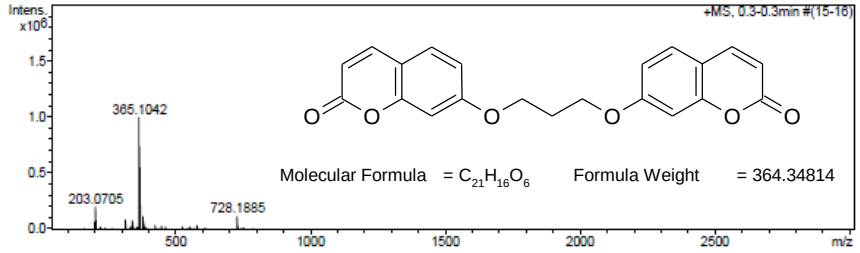

Meas. m/z	#	Formula	Score	m/z	err [mDa]	err [ppm]	mSigma	rdb	e⁻ Conf	N-Rule
365.1042	1	C 27 H 13 N 2	100.00	365.1079	3.6	10.0	225.4	22.5	even	ok
	2	C 22 H 13 N 4 O 2	1.68	365.1039	-0.4	-1.0	287.6	18.5	even	ok
	3	C 18 H 9 N 10	0.05	365.1012	-3.1	-8.4	300.6	19.5	even	ok
	4	C 21 H 17 O 6	0.14	365.1025	-1.7	-4.7	301.9	13.5	even	ok
	5	C 11 H 13 N 10 O 5	0.00	365.1070	2.8	7.7	343.9	10.5	even	ok
	6	C 7 H 9 N 16 O 3	0.00	365.1044	0.1	0.3	357.0	11.5	even	ok
	7	C 10 H 17 N 6 O 9	0.00	365.1057	1.5	4.0	358.0	5.5	even	ok
	8	C 9 H 21 N 2 O 13	0.00	365.1044	0.1	0.4	369.3	0.5	even	ok
	9	C 3 H 5 N 22 O	0.00	365.1017	-2.6	-7.0	370.2	12.5	even	ok
	10	C 6 H 13 N 12 O 7	0.00	365.1030	-1.2	-3.3	370.9	6.5	even	ok

MS: EIMS 315; EI-HRMS *m/z*: calculated for $\mathbf{C_{21}H_{16}O_6}$, 364.3481, found 365.1042 (**Spectrum 34**).

Spectrum 35: 7,7'-[Propane-1,3-diylbis(oxy)]bis(4-methyl-2*H*-chromen-2-one) **(BPR 7).**

Mass Spectrum SmartFormula Report

Analysis Info

Analysis Name	D:\Data\Bennie Repsold\4OH-IPCL-P(5.2)_APCI000001.d	Acquisition Date	6/29/2012 9:01:41 AM
Method	tune low_APCI.m	Operator	Dr JHL Jordaan
Sample Name	4OH-IPCL-P(5.2)_APCI	Instrument / Ser#	micrOTOF-Q II 10390
Comment	External calibration 28062012		

Acquisition Parameter

Source Type	APCI	Ion Polarity	Positive	Set Nebulizer	1.6 Bar
Focus	Not active	Set Capillary	4000 V	Set Dry Heater	200 °C
Scan Begin	50 m/z	Set End Plate Offset	-500 V	Set Dry Gas	1.5 l/min
Scan End	3000 m/z	Set Collision Cell RF	140.0 Vpp	Set Divert Valve	Waste

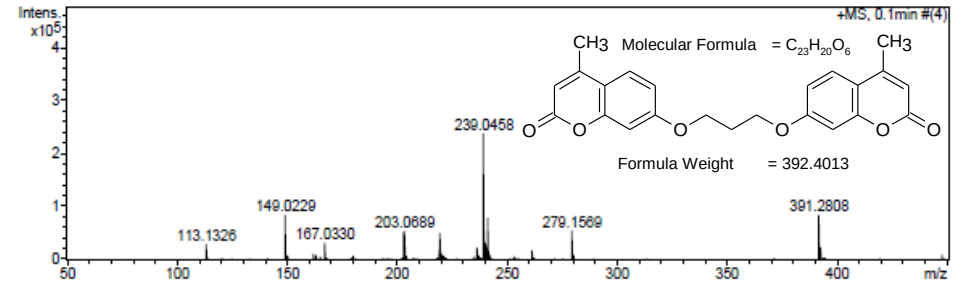

Meas. m/z	#	Formula	Score	m/z	err [mDa]	err [ppm]	mSigma	rdb	e⁻ Conf	N-Rule
239.0458	1	C 12 H 12 Cl O 3	100.00	239.0469	1.2	4.9	2.7	6.5	even	ok
	2	C 13 H 7 N 2 O 3	0.04	239.0451	-0.7	-2.8	182.2	11.5	even	ok

MS: EIMS 315; EI-HRMS *m/z*: calculated for $\mathbf{C_{23}H_{20}O_6}$, 392.4013, found 391.2808 (**Spectrum 35**).

Spectrum 36: 2-Oxo-2*H*-chromen-7-yl thiophene-2-carboxylate **(BPR8).**

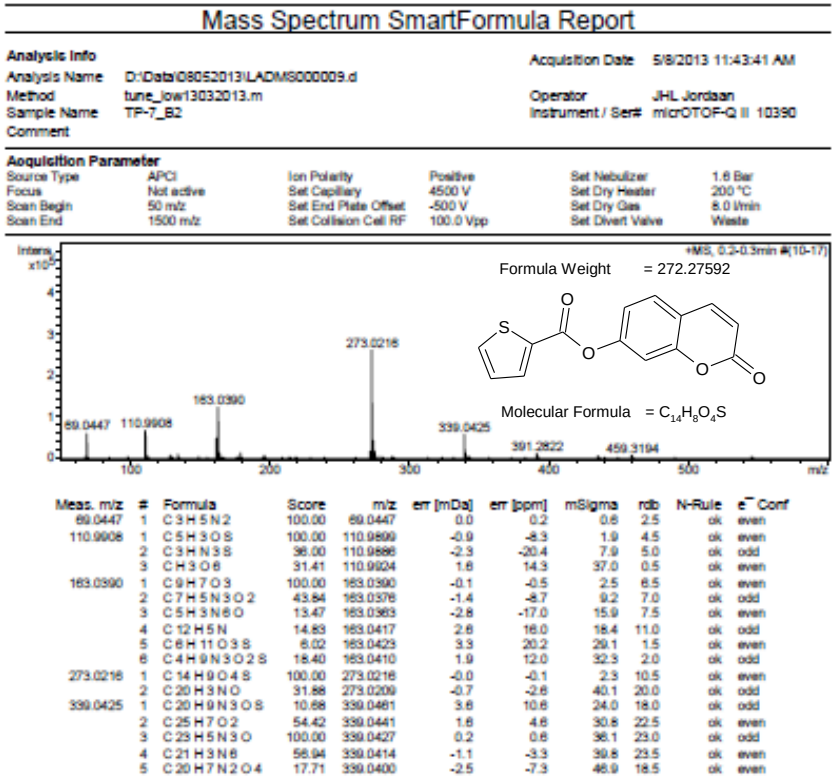

Mass Spectrum SmartFormula Report

Analysis Info

Analysis Name	D:\Data\08052013\LADMS000009.d	Acquisition Date	5/8/2013 11:43:41 AM
Method	tune_low13032013.m	Operator	JHL Jordaan
Sample Name	TP-7_B2	Instrument / Ser#	micrOTOF-Q II 10390
Comment			

Acquisition Parameter

Source Type	APCI	Ion Polarity	Positive	Set Nebulizer	1.6 Bar
Focus	Not active	Set Capillary	4500 V	Set Dry Heater	200 °C
Scan Begin	50 m/z	Set End Plate Offset	-500 V	Set Dry Gas	8.0 l/min
Scan End	1500 m/z	Set Collision Cell RF	100.0 Vpp	Set Divert Valve	Waste

Meas. m/z	#	Formula	Score	m/z	err [mDa]	err [ppm]	mSigma	rdb	N-Rule	e⁻ Conf
69.0447	1	C 3 H 5 N 2	100.00	69.0447	0.0	0.2	0.6	2.5	ok	even
110.9908	1	C 5 H 3 O S	100.00	110.9899	-0.9	-8.3	1.9	4.5	ok	even
	2	C 3 H N 3 S	36.00	110.9886	-2.3	-20.4	7.9	5.0	ok	odd
	3	C H 3 O 6	31.41	110.9924	1.6	14.3	37.0	0.5	ok	even
183.0390	1	C 9 H 7 O 3	100.00	183.0390	-0.1	-0.5	2.5	6.5	ok	even
	2	C 7 H 5 N 3 O 2	43.84	183.0376	-1.4	-8.7	9.2	7.0	ok	odd
	3	C 5 H 3 N 6 O	13.47	183.0363	-2.8	-17.0	15.9	7.5	ok	even
	4	C 12 H 5 N	14.83	183.0417	2.6	16.0	18.4	11.0	ok	odd
	5	C 6 H 11 O 3 S	6.02	183.0423	3.3	20.2	29.1	1.5	ok	even
	6	C 4 H 9 N 3 O 2 S	18.40	183.0410	1.9	12.0	32.3	2.0	ok	odd
273.0216	1	C 14 H 9 O 4 S	100.00	273.0216	-0.0	-0.1	2.3	10.5	ok	even
	2	C 20 H 3 N O	31.88	273.0209	-0.7	-2.6	40.1	20.0	ok	odd
339.0425	1	C 20 H 9 N 3 O S	10.68	339.0461	3.6	10.6	24.0	18.0	ok	odd
	2	C 25 H 7 O 2	54.42	339.0441	1.6	4.6	30.8	22.5	ok	even
	3	C 23 H 5 N 3 O	100.00	339.0427	0.2	0.6	36.1	23.0	ok	odd
	4	C 21 H 3 N 6	56.94	339.0414	-1.1	-3.3	39.8	23.5	ok	even
	5	C 20 H 7 N 2 O 4	17.71	339.0400	-2.5	-7.3	46.9	18.5	ok	even

MS: EIMS 315; EI-HRMS *m/z*: calculated for $\mathbf{C_{16}H_{18}SO_4}$, 272.2759, found 273.0218 (**Spectrum 36**).

Spectrum 37: 4-[2-(Piperidin-1-yl)ethoxy]-2*H*-chromen-2-one **(BPR9).**

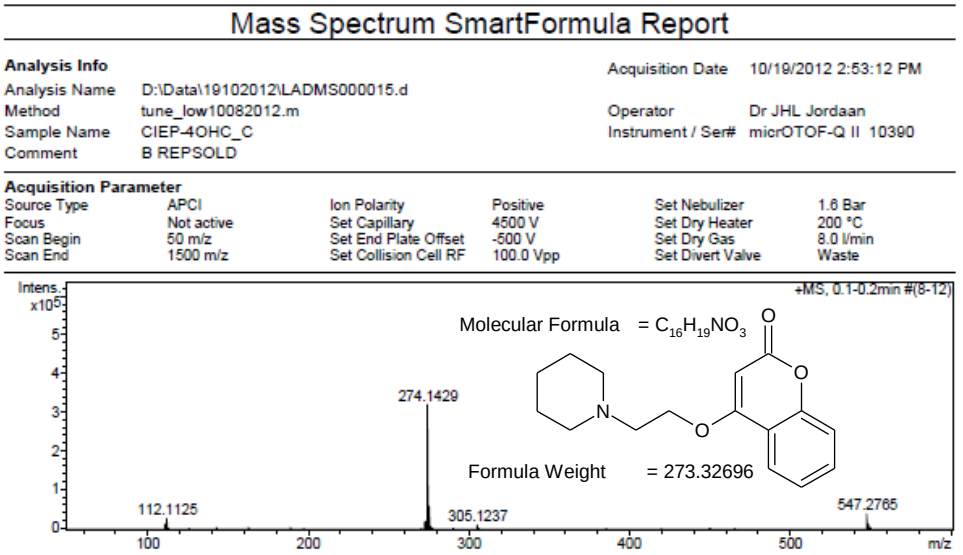

Mass Spectrum SmartFormula Report

Analysis Info

Analysis Name	D:\Data\19102012\LADMS000015.d	Acquisition Date	10/19/2012 2:53:12 PM
Method	tune_low10082012.m	Operator	Dr JHL Jordaan
Sample Name	CIEP-4OHC_C	Instrument / Ser#	micrOTOF-Q II 10390
Comment	B REPSOLD		

Acquisition Parameter

Source Type	APCI	Ion Polarity	Positive	Set Nebulizer	1.6 Bar
Focus	Not active	Set Capillary	4500 V	Set Dry Heater	200 °C
Scan Begin	50 m/z	Set End Plate Offset	-500 V	Set Dry Gas	8.0 l/min
Scan End	1500 m/z	Set Collision Cell RF	100.0 Vpp	Set Divert Valve	Waste

Meas. m/z	#	Formula	Score	m/z	err [mDa]	err [ppm]	mSigma	rdb	e⁻ Conf	N-Rule
112.1125	1	C 7 H 14 N	100.00	112.1121	-0.4	-3.5	0.7	1.5	even	ok
274.1429	1	C 16 H 20 N O 3	100.00	274.1438	0.9	3.3	6.4	7.5	even	ok
	2	C 12 H 16 N 7 O	43.59	274.1411	-1.8	-6.5	19.8	8.5	even	ok
	3	C 11 H 20 N 3 O 5	10.10	274.1397	-3.1	-11.4	33.3	3.5	even	ok
547.2765	1	C 32 H 39 N 2 O 6	9.09	547.2803	3.7	6.8	7.2	14.5	even	ok
	2	C 28 H 35 N 8 O 4	82.26	547.2776	1.0	1.9	10.5	15.5	even	ok
	3	C 29 H 31 N 12	30.75	547.2789	2.4	4.3	12.7	20.5	even	ok
	4	C 27 H 39 N 4 O 8	100.00	547.2762	-0.3	-0.6	19.3	10.5	even	ok
	5	C 24 H 31 N 14 O 2	41.28	547.2749	-1.7	-3.0	24.7	16.5	even	ok
	6	C 26 H 43 O 12	38.02	547.2749	-1.6	-3.0	28.5	5.5	even	ok
	7	C 39 H 35 N 2 O	17.18	547.2744	-2.2	-3.9	44.3	23.5	even	ok

MS: EIMS 315; EI-HRMS *m/z*: calculated for $\mathbf{C_{16}H_{19}NO_3}$, 273.3270, found 274.1429 (**Spectrum 37**).

Spectrum 38: 4-[2-(Morpholin-4-yl)ethoxy]-2*H*-chromen-2-one **(BPR 10)**.

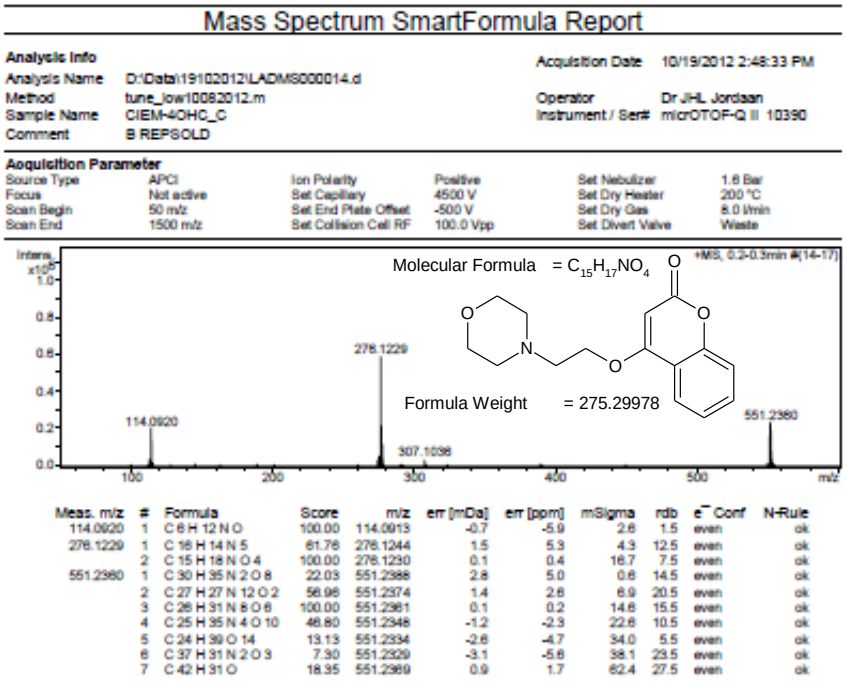

Mass Spectrum SmartFormula Report

Analysis Info

Analysis Name	D:\Data\19102012\LADMS000014.d	Acquisition Date	10/19/2012 2:48:33 PM
Method	tune_low10082012.m	Operator	Dr JHL Jordaan
Sample Name	CIEM-4OHC_C	Instrument / Ser#	micrOTOF-Q II 10390
Comment	B REPSOLD		

Acquisition Parameter

Source Type	APCI	Ion Polarity	Positive	Set Nebulizer	1.6 Bar
Focus	Not active	Set Capillary	4500 V	Set Dry Heater	200 °C
Scan Begin	50 m/z	Set End Plate Offset	-500 V	Set Dry Gas	8.0 l/min
Scan End	1500 m/z	Set Collision Cell RF	100.0 Vpp	Set Divert Valve	Waste

Meas. m/z	#	Formula	Score	m/z	err [mDa]	err [ppm]	mSigma	rdb	e⁻ Conf	N-Rule
114.0920	1	C 6 H 12 N O	100.00	114.0913	-0.7	-5.9	2.6	1.5	even	ok
278.1229	1	C 16 H 14 N 5	61.76	278.1244	1.5	5.3	4.3	12.5	even	ok
	2	C 15 H 18 N O 4	100.00	278.1230	0.1	0.4	16.7	7.5	even	ok
551.2360	1	C 30 H 35 N 2 O 8	22.03	551.2388	2.8	5.0	0.6	14.5	even	ok
	2	C 27 H 27 N 12 O 2	58.96	551.2374	1.4	2.6	6.9	20.5	even	ok
	3	C 28 H 31 N 8 O 6	100.00	551.2361	0.1	0.2	14.6	15.5	even	ok
	4	C 25 H 35 N 4 O 10	46.80	551.2348	-1.2	-2.3	22.6	10.5	even	ok
	5	C 24 H 39 O 14	13.13	551.2334	-2.6	-4.7	34.0	5.5	even	ok
	6	C 37 H 31 N 2 O 3	7.30	551.2329	-3.1	-5.6	38.1	23.5	even	ok
	7	C 42 H 31 O	18.35	551.2369	0.9	1.7	62.4	27.5	even	ok

MS: EIMS 315; EI-HRMS *m*/*z*: calculated for **$C_{15}H_{17}NO_4$**, 275.2998, found 278.1229 (**Spectrum 38**).

Spectrum 39: 7-[2-(Morpholin-4-yl)ethoxy]-2*H*-chromen-2-one **(BPR 11).**

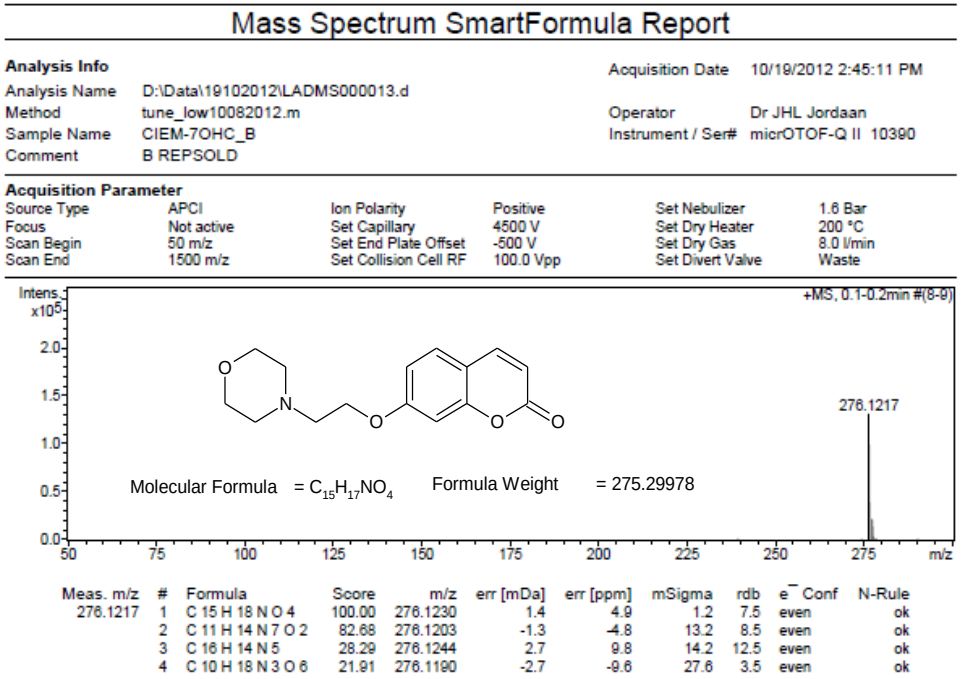

Mass Spectrum SmartFormula Report

Analysis Info

Analysis Name	D:\Data\19102012\LADMS000013.d	Acquisition Date	10/19/2012 2:45:11 PM
Method	tune_low10082012.m	Operator	Dr JHL Jordaan
Sample Name	CIEM-7OHC_B	Instrument / Ser#	micrOTOF-Q II 10390
Comment	B REPSOLD		

Acquisition Parameter

Source Type	APCI	Ion Polarity	Positive	Set Nebulizer	1.6 Bar
Focus	Not active	Set Capillary	4500 V	Set Dry Heater	200 °C
Scan Begin	50 m/z	Set End Plate Offset	-500 V	Set Dry Gas	8.0 l/min
Scan End	1500 m/z	Set Collision Cell RF	100.0 Vpp	Set Divert Valve	Waste

Meas. m/z	#	Formula	Score	m/z	err [mDa]	err [ppm]	mSigma	rdb	e⁻ Conf	N-Rule
276.1217	1	C 15 H 18 N O 4	100.00	276.1230	1.4	4.9	1.2	7.5	even	ok
	2	C 11 H 14 N 7 O 2	82.68	276.1203	-1.3	-4.8	13.2	8.5	even	ok
	3	C 16 H 14 N 5	28.29	276.1244	2.7	9.8	14.2	12.5	even	ok
	4	C 10 H 18 N 3 O 6	21.91	276.1190	-2.7	-9.6	27.6	3.5	even	ok

MS: EIMS 315; EI-HRMS *m*/*z*: calculated for **$C_{15}H_{17}NO_4$**, 275.2999, found 276.1217 (**Spectrum 39**).

Spectrum 40: 7-[2-(Piperidin-1-yl)ethoxy]-2*H*-chromen-2-one **(BPR12).**

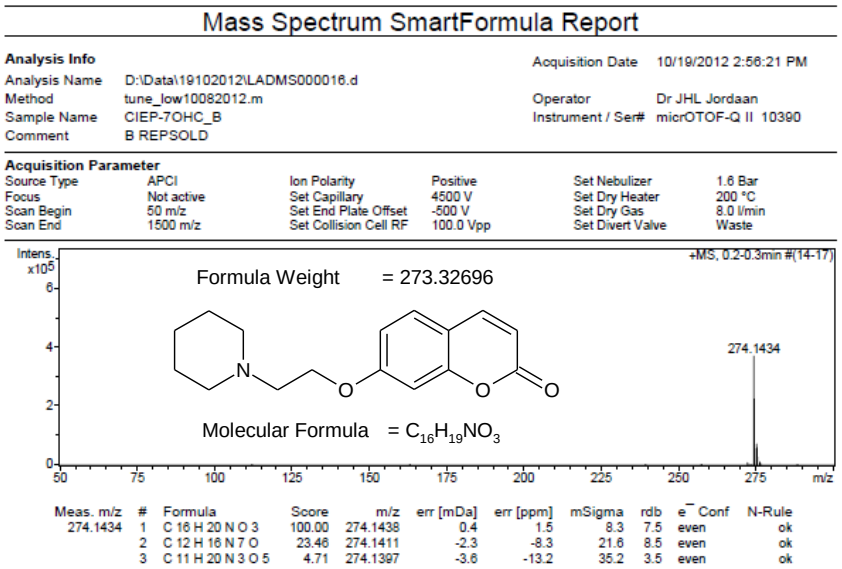

Mass Spectrum SmartFormula Report

Analysis Info

Analysis Name	D:\Data\19102012\LADMS000016.d	Acquisition Date	10/19/2012 2:56:21 PM
Method	tune_low10082012.m	Operator	Dr JHL Jordaan
Sample Name	CIEP-7OHC_B	Instrument / Ser#	micrOTOF-Q II 10390
Comment	B REPSOLD		

Acquisition Parameter

Source Type	APCI	Ion Polarity	Positive	Set Nebulizer	1.6 Bar
Focus	Not active	Set Capillary	4500 V	Set Dry Heater	200 °C
Scan Begin	50 m/z	Set End Plate Offset	-500 V	Set Dry Gas	8.0 l/min
Scan End	1500 m/z	Set Collision Cell RF	100.0 Vpp	Set Divert Valve	Waste

Meas. m/z	#	Formula	Score	m/z	err [mDa]	err [ppm]	mSigma	rdb	e⁻ Conf	N-Rule
274.1434	1	C 16 H 20 N O 3	100.00	274.1438	0.4	1.5	8.3	7.5	even	ok
	2	C 12 H 16 N 7 O	23.46	274.1411	-2.3	-8.3	21.6	8.5	even	ok
	3	C 11 H 20 N 3 O 5	4.71	274.1397	-3.6	-13.2	35.2	3.5	even	ok

MS: EIMS 315; EI-HRMS *m/z*: calculated for **$C_{16}H_{19}NO_3$**, 273.3267, found 274.1434 (**Spectrum 40**).

Spectrum 41: 4-Methyl-7-[2-(piperidin-1-yl)ethoxy]-2*H*-chromen-2-one **(BPR13).**

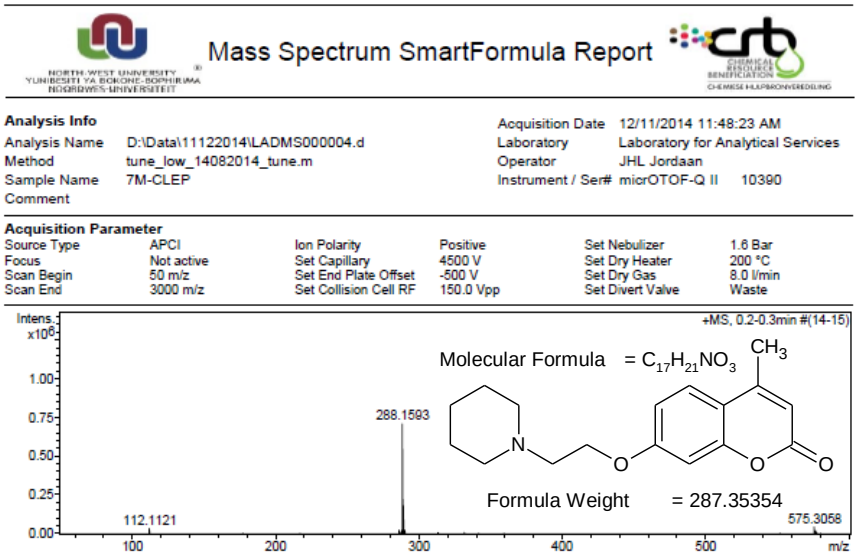

Mass Spectrum SmartFormula Report

Analysis Info

Analysis Name	D:\Data\11122014\LADMS000004.d	Acquisition Date	12/11/2014 11:48:23 AM
Method	tune_low_14082014_tune.m	Laboratory	Laboratory for Analytical Services
Sample Name	7M-CLEP	Operator	JHL Jordaan
Comment		Instrument / Ser#	micrOTOF-Q II 10390

Acquisition Parameter

Source Type	APCI	Ion Polarity	Positive	Set Nebulizer	1.6 Bar
Focus	Not active	Set Capillary	4500 V	Set Dry Heater	200 °C
Scan Begin	50 m/z	Set End Plate Offset	-500 V	Set Dry Gas	8.0 l/min
Scan End	3000 m/z	Set Collision Cell RF	150.0 Vpp	Set Divert Valve	Waste

Meas. m/z	#	Formula	Score	m/z	err [mDa]	err [ppm]	mSigma	rdb	N-Rule	e⁻ Conf
288.1593	1	C 20 H 20 N 2	33.25	288.1621	2.8	9.8	46.8	12.0	ok	odd
	2	C 17 H 22 N O 3	100.00	288.1594	0.1	0.5	67.5	7.5	ok	even
	3	C 15 H 20 N 4 O 2	45.64	288.1581	-1.2	-4.2	73.9	8.0	ok	odd
	4	C 13 H 18 N 7 O	13.06	288.1567	-2.5	-8.8	80.4	8.5	ok	even
	5	C 11 H 16 N 10	2.57	288.1554	-3.9	-13.5	86.6	9.0	ok	odd
	6	C 14 H 24 O 6	9.43	288.1567	-2.5	-8.8	88.3	3.0	ok	odd
	7	C 12 H 22 N 3 O 5	1.83	288.1554	-3.9	-13.5	94.5	3.5	ok	even

MS: EIMS 315; EI-HRMS *m/z*: calculated for **$C_{17}H_{21}NO_3$**, 287.353, found 288.1593 (**Spectrum 41**).

Spectrum 42: 4-Methyl-7-[2-(morpholin-4-yl)ethoxy]-2*H*-chromen-2-one **(BPR14).**

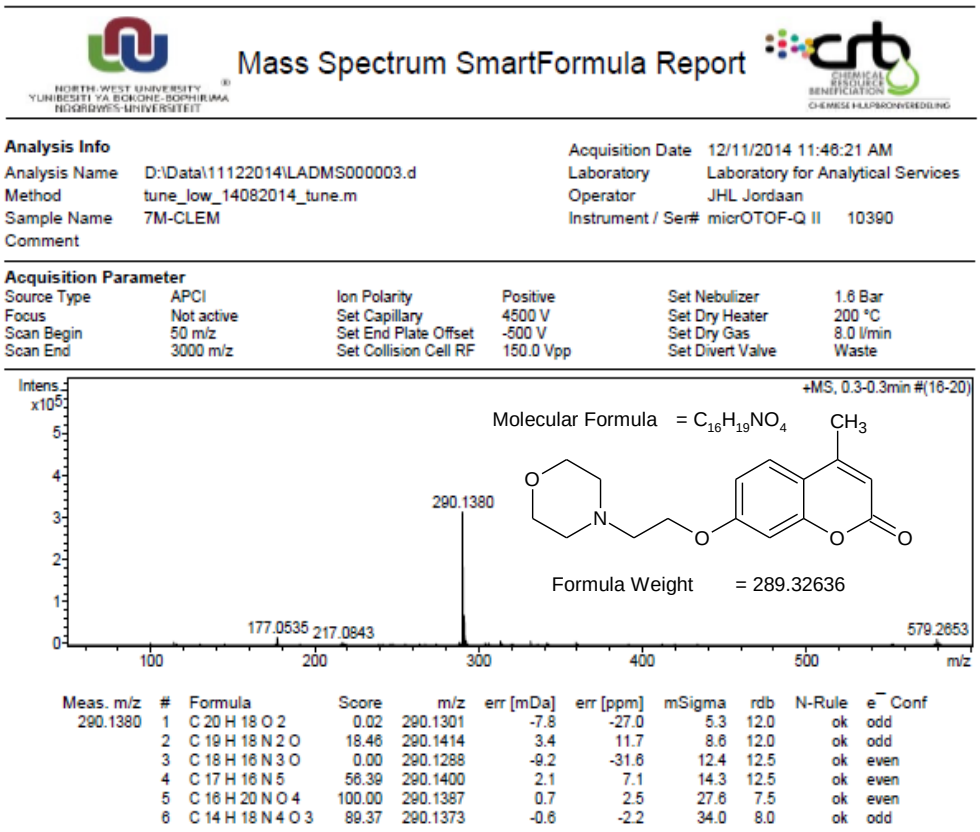

Mass Spectrum SmartFormula Report

Analysis Info

Analysis Name	D:\Data\11122014\LADMS000003.d	Acquisition Date	12/11/2014 11:46:21 AM
Method	tune_low_14082014_tune.m	Laboratory	Laboratory for Analytical Services
Sample Name	7M-CLEM	Operator	JHL Jordaan
Comment		Instrument / Ser#	micrOTOF-Q II 10390

Acquisition Parameter

Source Type	APCI	Ion Polarity	Positive	Set Nebulizer	1.6 Bar
Focus	Not active	Set Capillary	4500 V	Set Dry Heater	200 °C
Scan Begin	50 m/z	Set End Plate Offset	-500 V	Set Dry Gas	8.0 l/min
Scan End	3000 m/z	Set Collision Cell RF	150.0 Vpp	Set Divert Valve	Waste

Meas. m/z	#	Formula	Score	m/z	err [mDa]	err [ppm]	mSigma	rdb	N-Rule	e⁻ Conf
290.1380	1	C 20 H 18 O 2	0.02	290.1301	-7.8	-27.0	5.3	12.0	ok	odd
	2	C 19 H 18 N 2 O	18.46	290.1414	3.4	11.7	8.6	12.0	ok	odd
	3	C 18 H 16 N 3 O	0.00	290.1288	-9.2	-31.6	12.4	12.5	ok	even
	4	C 17 H 16 N 5	56.39	290.1400	2.1	7.1	14.3	12.5	ok	even
	5	C 16 H 20 N O 4	100.00	290.1387	0.7	2.5	27.6	7.5	ok	even
	6	C 14 H 18 N 4 O 3	89.37	290.1373	-0.6	-2.2	34.0	8.0	ok	odd

MS: EIMS 315; EI-HRMS *m/z*: calculated for **$C_{16}H_{19}NO_4$**, 289.3264, found 290.1380 (**Spectrum 42**).

ANNEXURE C: MAO-B Results

7C IC_{50}: 28.583 ± 2.519 µM

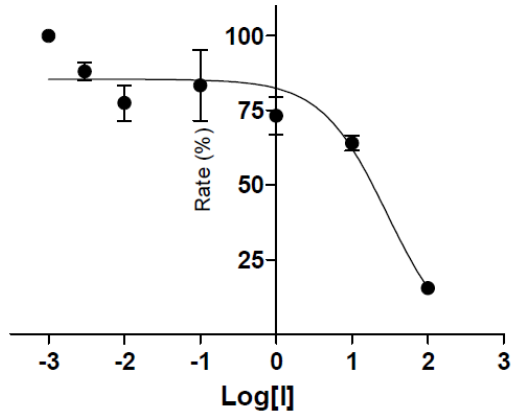

4MC IC_{50}: 94.327 ± 3.889 µM

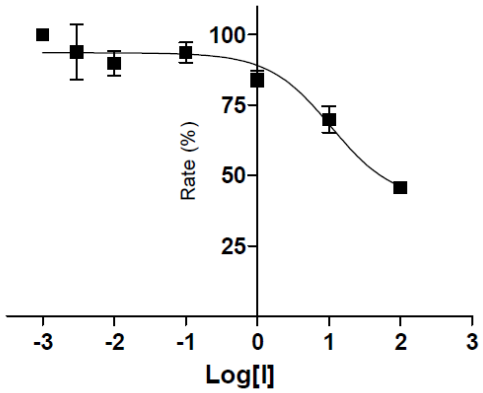

BPR 1 IC_{50}: 3.680 ± 0.836 µM

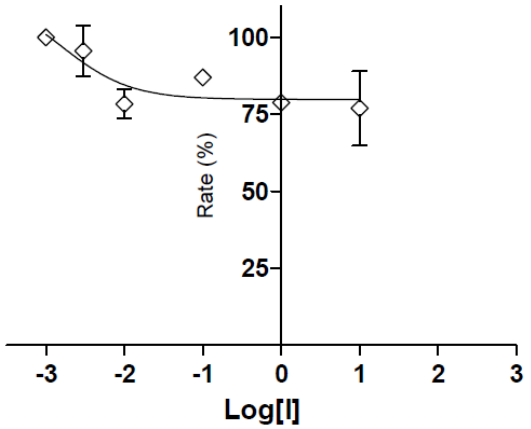

BPR 9 IC_{50}: 21.720 ± 3.974 µM

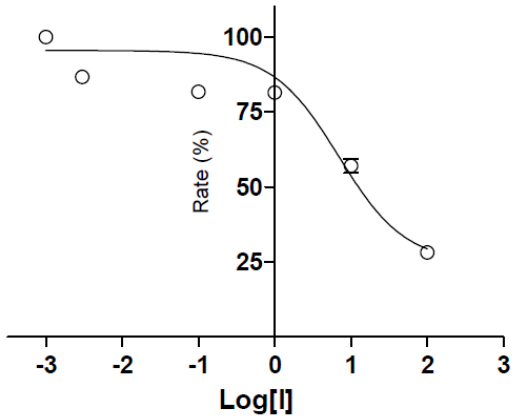

BPR 10 IC_{50}: 0.372 ± 0.026 µM

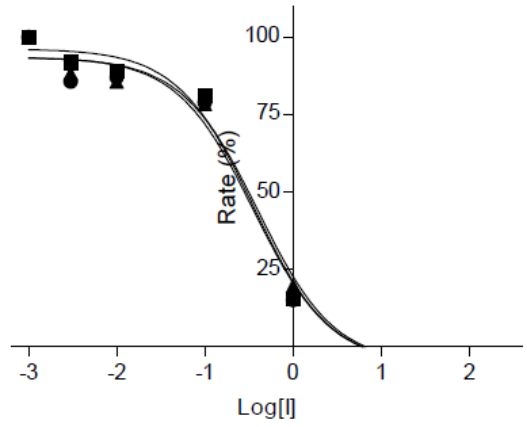

BPR 11 IC_{50}: 9.758 ± 1.153 µM

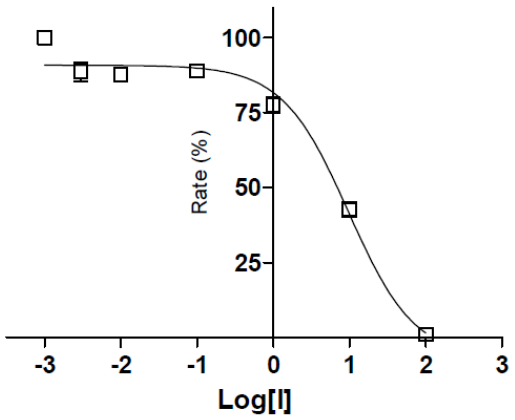

BPR 12 IC_{50}: 9.209 ± 0.794 µM

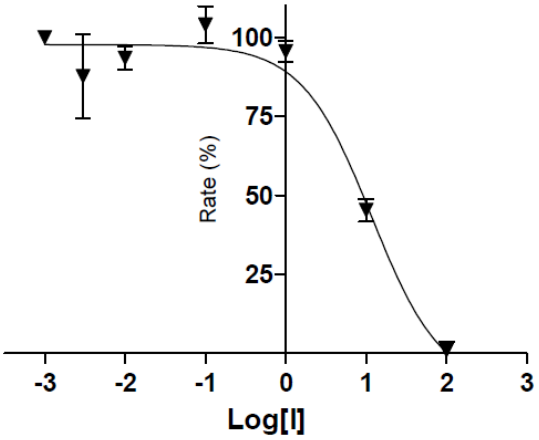

BPR 13 IC_{50}: 3.093 ± 0.312 µM

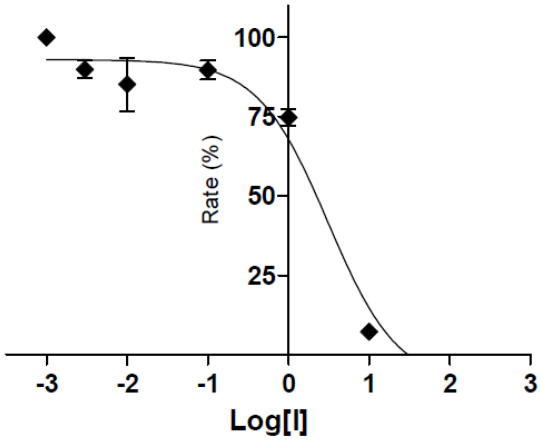

BPR 14 IC_{50}: 2.326 ± 0.131 µM

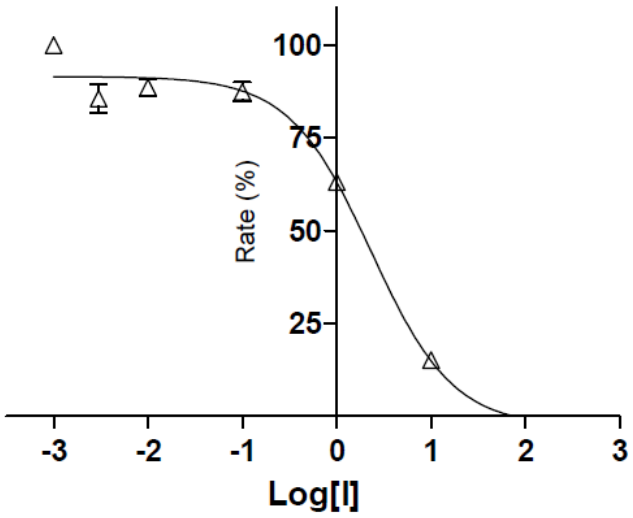

References

Aalten, P., Verhey, F.R., Boziki, M., Brugnolo, A., Bullock, R., Byrne, E.J., Camus, V., Caputo, M., Collins, D., De Deyn, P.P., Elina, K., Frisoni, G., Holmes, C., Hurt, C., Marriott, A., Mecocci, P., Nobili, F., Ousset, P.J., Reynish, E., Salmon, E., Tsolaki, M., Vellas, B. & Robert, P.H. 2008, "Consistency of neuropsychiatric syndromes across dementias: results from the European Alzheimer Disease Consortium. Part II", *Dementia and geriatric cognitive disorders,* vol. 25, no. 1, pp. 1-8.

Abad-Rodriguez, J., Ledesma, M.D., Craessaerts, K., Perga, S., Medina, M., Delacourte, A., Dingwall, C., De Strooper, B. & Dotti, C.G. 2004, "Neuronal membrane cholesterol loss enhances amyloid peptide generation", *The Journal of cell biology,* vol. 167, no. 5, pp. 953-960.

Abel, T. & Kandel, E. 1998, "Positive and negative regulatory mechanisms that mediate long-term memory storage", *Brain research.Brain research reviews,* vol. 26, no. 2-3, pp. 360-378.

Abraham, K., Wohrlin, F., Lindtner, O., Heinemeyer, G. & Lampen, A. 2010, "Toxicology and risk assessment of coumarin: focus on human data", *Molecular nutrition & food research,* vol. 54, no. 2, pp. 228-239.

Ahmed, S., Arnold, R., Thompson, S.A., Graham, K.S. & Hodges, J.R. 2008, "Naming of objects, faces and buildings in mild cognitive impairment", *Cortex; a journal devoted to the study of the nervous system and behavior,* vol. 44, no. 6, pp. 746-752.

Akama, K.T., Albanese, C., Pestell, R.G. & Van Eldik, L.J. 1998, "Amyloid beta-peptide stimulates nitric oxide production in astrocytes through an NFkappaB-dependent mechanism", *Proceedings of the National Academy of Sciences of the United States of America,* vol. 95, no. 10, pp. 5795-5800.

Akyuz, M.A., Erdem, S.S. & Edmondson, D.E. 2007, "The aromatic cage in the active site of monoamine oxidase B: effect on the structural and electronic properties of bound benzylamine and p-nitrobenzylamine", *Journal of neural transmission (Vienna, Austria : 1996),* vol. 114, no. 6, pp. 693-698.

Alarcon, J.M., Malleret, G., Touzani, K., Vronskaya, S., Ishii, S., Kandel, E.R. & Barco, A. 2004, "Chromatin acetylation, memory, and LTP are impaired in CBP+/- mice: a model for the cognitive deficit in Rubinstein-Taybi syndrome and its amelioration", *Neuron,* vol. 42, no. 6, pp. 947-959.

Ali, J.A., Jackson, A.P., Howells, A.J. & Maxwell, A. 1993, "The 43-kilodalton N-terminal fragment of the DNA gyrase B protein hydrolyzes ATP and binds coumarin drugs", *Biochemistry,* vol. 32, no. 10, pp. 2717-2724.

Allan, R.K., Mok, D., Ward, B.K. & Ratajczak, T. 2006, "Modulation of chaperone function and cochaperone interaction by novobiocin in the C-terminal domain of Hsp90: evidence that coumarin antibiotics disrupt Hsp90 dimerization", *The Journal of biological chemistry,* vol. 281, no. 11, pp. 7161-7171.

Allinson, T.M., Parkin, E.T., Turner, A.J. & Hooper, N.M. 2003, "ADAMs family members as amyloid precursor protein alpha-secretases", *Journal of neuroscience research,* vol. 74, no. 3, pp. 342-352.

Alvarez, A., Alarcon, R., Opazo, C., Campos, E.O., Munoz, F.J., Calderon, F.H., Dajas, F., Gentry, M.K., Doctor, B.P., De Mello, F.G. & Inestrosa, N.C. 1998, "Stable complexes involving acetylcholinesterase and amyloid-beta peptide change the biochemical properties of the enzyme and increase the neurotoxicity of Alzheimer's fibrils", *The Journal of neuroscience : the official journal of the Society for Neuroscience,* vol. 18, no. 9, pp. 3213-3223.

Alvarez, A., Opazo, C., Alarcon, R., Garrido, J. & Inestrosa, N.C. 1997, "Acetylcholinesterase promotes the aggregation of amyloid-beta-peptide fragments by forming a complex with the growing fibrils", *Journal of Molecular Biology,* vol. 272, no. 3, pp. 348-361.

Alvarez, A., Toro, R., Caceres, A. & Maccioni, R.B. 1999, "Inhibition of tau phosphorylating protein kinase cdk5 prevents beta-amyloid-induced neuronal death", *FEBS letters,* vol. 459, no. 3, pp. 421-426.

Amin, K.M., Awadalla, F.M., Eissa, A.A., Abou-Seri, S.M. & Hassan, G.S. 2011, "Design, synthesis and vasorelaxant evaluation of novel coumarin-pyrimidine hybrids", *Bioorganic & medicinal chemistry,* vol. 19, no. 20, pp. 6087-6097.

Anderson, J.J., Holtz, G., Baskin, P.P., Turner, M., Rowe, B., Wang, B., Kounnas, M.Z., Lamb, B.T., Barten, D., Felsenstein, K., McDonald, I., Srinivasan, K., Munoz, B. & Wagner, S.L. 2005, "Reductions in beta-amyloid concentrations in vivo by the gamma-secretase inhibitors BMS-289948 and BMS-299897", *Biochemical pharmacology,* vol. 69, no. 4, pp. 689-698.

Ando, K., Iijima, K.I., Elliott, J.I., Kirino, Y. & Suzuki, T. 2001, "Phosphorylation-dependent regulation of the interaction of amyloid precursor protein with Fe65 affects the production of beta-amyloid", *The Journal of biological chemistry,* vol. 276, no. 43, pp. 40353-40361.

Atwood, C.S., Moir, R.D., Huang, X., Scarpa, R.C., Bacarra, N.M., Romano, D.M., Hartshorn, M.A., Tanzi, R.E. & Bush, A.I. 1998, "Dramatic aggregation of Alzheimer abeta by Cu(II) is induced by conditions representing physiological acidosis", *The Journal of biological chemistry,* vol. 273, no. 21, pp. 12817-12826.

Atwood, C.S., Scarpa, R.C., Huang, X., Moir, R.D., Jones, W.D., Fairlie, D.P., Tanzi, R.E. & Bush, A.I. 2000, "Characterization of copper interactions with alzheimer amyloid beta peptides: identification of an attomolar-affinity copper binding site on amyloid beta1-42", *Journal of neurochemistry,* vol. 75, no. 3, pp. 1219-1233.

Au, N. & Rettie, A.E. 2008, "Pharmacogenomics of 4-hydroxycoumarin anticoagulants", *Drug metabolism reviews,* vol. 40, no. 2, pp. 355-375.

Augustinack, J.C., Sanders, J.L., Tsai, L.H. & Hyman, B.T. 2002, "Colocalization and fluorescence resonance energy transfer between cdk5 and AT8 suggests a close association in pre-neurofibrillary tangles and neurofibrillary tangles", *Journal of neuropathology and experimental neurology,* vol. 61, no. 6, pp. 557-564.

Bach, A.W., Lan, N.C., Johnson, D.L., Abell, C.W., Bembenek, M.E., Kwan, S.W., Seeburg, P.H. & Shih, J.C. 1988, "cDNA cloning of human liver monoamine oxidase A and B: molecular basis of differences in enzymatic properties", *Proceedings of the National Academy of Sciences of the United States of America,* vol. 85, no. 13, pp. 4934-4938.

Baek, S.H., Ohgi, K.A., Rose, D.W., Koo, E.H., Glass, C.K. & Rosenfeld, M.G. 2002, "Exchange of N-CoR corepressor and Tip60 coactivator complexes links gene expression by NF-kappaB and beta-amyloid precursor protein", *Cell,* vol. 110, no. 1, pp. 55-67.

Barak, D., Kronman, C., Ordentlich, A., Ariel, N., Bromberg, A., Marcus, D., Lazar, A., Velan, B. & Shafferman, A. 1994, "Acetylcholinesterase peripheral anionic site degeneracy conferred by amino acid arrays sharing a common core", *The Journal of biological chemistry,* vol. 269, no. 9, pp. 6296-6305.

Barnham, K.J., Haeffner, F., Ciccotosto, G.D., Curtain, C.C., Tew, D., Mavros, C., Beyreuther, K., Carrington, D., Masters, C.L., Cherny, R.A., Cappai, R. & Bush, A.I. 2004, "Tyrosine gated electron transfer is key to the toxic mechanism of Alzheimer's disease beta-amyloid", *The FASEB journal : official publication of the Federation of American Societies for Experimental Biology,* vol. 18, no. 12, pp. 1427-1429.

Berger, S.L. 2007, "The complex language of chromatin regulation during transcription", *Nature,* vol. 447, no. 7143, pp. 407-412.

Bharate, S.B., Guo, L., Reeves, T.E., Cerasoli, D.M. & Thompson, C.M. 2009, "New series of monoquaternary pyridinium oximes: Synthesis and reactivation potency for paraoxon-inhibited electric eel and recombinant human acetylcholinesterase", *Bioorganic & medicinal chemistry letters,* vol. 19, no. 17, pp. 5101-5104.

Bibb, J.A., Snyder, G.L., Nishi, A., Yan, Z., Meijer, L., Fienberg, A.A., Tsai, L.H., Kwon, Y.T., Girault, J.A., Czernik, A.J., Huganir, R.L., Hemmings, H.C.,Jr, Nairn, A.C. & Greengard, P. 1999, "Phosphorylation of DARPP-32 by Cdk5 modulates dopamine signalling in neurons", *Nature,* vol. 402, no. 6762, pp. 669-671.

Biernat, J., Gustke, N., Drewes, G., Mandelkow, E.M. & Mandelkow, E. 1993, "Phosphorylation of Ser262 strongly reduces binding of tau to microtubules: distinction between PHF-like immunoreactivity and microtubule binding", *Neuron,* vol. 11, no. 1, pp. 153-163.

Binda, C., Hubalek, F., Li, M., Edmondson, D.E. & Mattevi, A. 2004, "Crystal structure of human monoamine oxidase B, a drug target enzyme monotopically inserted into the mitochondrial outer membrane", *FEBS letters,* vol. 564, no. 3, pp. 225-228.

Binda, C., Hubalek, F., Li, M., Herzig, Y., Sterling, J., Edmondson, D.E. & Mattevi, A. 2004, "Crystal structures of monoamine oxidase B in complex with four inhibitors of the N-propargylaminoindan class", *Journal of medicinal chemistry,* vol. 47, no. 7, pp. 1767-1774.

Binda, C., Li, M., Hubalek, F., Restelli, N., Edmondson, D.E. & Mattevi, A. 2003, "Insights into the mode of inhibition of human mitochondrial monoamine oxidase B from high-resolution crystal structures", *Proceedings of the National Academy of Sciences of the United States of America,* vol. 100, no. 17, pp. 9750-9755.

Binda, C., Mattevi, A. & Edmondson, D.E. 2002, "Structure-function relationships in flavoenzyme-dependent amine oxidations: a comparison of polyamine oxidase and monoamine oxidase", *The Journal of biological chemistry,* vol. 277, no. 27, pp. 23973-23976.

Binda, C., Newton-Vinson, P., Hubalek, F., Edmondson, D.E. & Mattevi, A. 2002, "Structure of human monoamine oxidase B, a drug target for the treatment of neurological disorders", *Nature structural biology,* vol. 9, no. 1, pp. 22-26.

Blennow, K. & Hampel, H. 2003, "CSF markers for incipient Alzheimer's disease", *Lancet neurology,* vol. 2, no. 10, pp. 605-613.

Bliss, T.V. & Collingridge, G.L. 1993, "A synaptic model of memory: long-term potentiation in the hippocampus", *Nature,* vol. 361, no. 6407, pp. 31-39.

Bourre, J.M. 2005, "Dietary omega-3 Fatty acids and psychiatry: mood, behaviour, stress, depression, dementia and aging", *The journal of nutrition, health & aging,* vol. 9, no. 1, pp. 31-38.

Bourtchuladze, R., Frenguelli, B., Blendy, J., Cioffi, D., Schutz, G. & Silva, A.J. 1994, "Deficient long-term memory in mice with a targeted mutation of the cAMP-responsive element-binding protein", *Cell,* vol. 79, no. 1, pp. 59-68.

Bramblett, G.T., Goedert, M., Jakes, R., Merrick, S.E., Trojanowski, J.Q. & Lee, V.M. 1993, "Abnormal tau phosphorylation at Ser396 in Alzheimer's disease recapitulates development and contributes to reduced microtubule binding", *Neuron,* vol. 10, no. 6, pp. 1089-1099.

Brouwers, N., Sleegers, K. & Van Broeckhoven, C. 2008, "Molecular genetics of Alzheimer's disease: an update", *Annals of Medicine,* vol. 40, no. 8, pp. 562-583.

Brown, A.M., Tummolo, D.M., Rhodes, K.J., Hofmann, J.R., Jacobsen, J.S. & Sonnenberg-Reines, J. 1997, "Selective aggregation of endogenous beta-amyloid peptide and soluble amyloid precursor protein in cerebrospinal fluid by zinc", *Journal of neurochemistry,* vol. 69, no. 3, pp. 1204-1212.

Bruneton, J. 1999, "Pharmacognosy, Phytochemistry, Medicinal Plants" in , Second Edition edn, Intercept Ltd, Hampshire UK, pp. 263-277.

Burton, E.J., Barber, R., Mukaetova-Ladinska, E.B., Robson, J., Perry, R.H., Jaros, E., Kalaria, R.N. & O'Brien, J.T. 2009, "Medial temporal lobe atrophy on MRI differentiates Alzheimer's disease from dementia with Lewy bodies and vascular cognitive impairment: a prospective study with pathological verification of diagnosis", *Brain : a journal of neurology,* vol. 132, no. Pt 1, pp. 195-203.

Bush, A.I., Pettingell, W.H.,Jr, Paradis, M.D. & Tanzi, R.E. 1994, "Modulation of A beta adhesiveness and secretase site cleavage by zinc", *The Journal of biological chemistry,* vol. 269, no. 16, pp. 12152-12158.

Bush, A.I., Pettingell, W.H., Multhaup, G., d Paradis, M., Vonsattel, J.P., Gusella, J.F., Beyreuther, K., Masters, C.L. & Tanzi, R.E. 1994, "Rapid induction of Alzheimer A beta amyloid formation by zinc", *Science (New York, N.Y.),* vol. 265, no. 5177, pp. 1464-1467.

Buxbaum, J.D., Thinakaran, G., Koliatsos, V., O'Callahan, J., Slunt, H.H., Price, D.L. & Sisodia, S.S. 1998, "Alzheimer amyloid protein precursor in the rat hippocampus: transport and processing through the perforant path", *The Journal of neuroscience : the official journal of the Society for Neuroscience,* vol. 18, no. 23, pp. 9629-9637.

Caccamo, A., Oddo, S., Sugarman, M.C., Akbari, Y. & LaFerla, F.M. 2005, "Age- and region-dependent alterations in Abeta-degrading enzymes: implications for Abeta-induced disorders", *Neurobiology of aging,* vol. 26, no. 5, pp. 645-654.

Cao, X. & Sudhof, T.C. 2001, "A transcriptionally [correction of transcriptively] active complex of APP with Fe65 and histone acetyltransferase Tip60", *Science (New York, N.Y.),* vol. 293, no. 5527, pp. 115-120.

Carpentier, M., Robitaille, Y., DesGroseillers, L., Boileau, G. & Marcinkiewicz, M. 2002, "Declining expression of neprilysin in Alzheimer disease vasculature: possible involvement in cerebral amyloid angiopathy", *Journal of neuropathology and experimental neurology,* vol. 61, no. 10, pp. 849-856.

Carta, F., Maresca, A., Scozzafava, A. & Supuran, C.T. 2012, "Novel coumarins and 2-thioxo-coumarins as inhibitors of the tumor-associated carbonic anhydrases IX and XII", *Bioorganic & medicinal chemistry,* vol. 20, no. 7, pp. 2266-2273.

Causing, C.G., Gloster, A., Aloyz, R., Bamji, S.X., Chang, E., Fawcett, J., Kuchel, G. & Miller, F.D. 1997, "Synaptic innervation density is regulated by neuron-derived BDNF", *Neuron,* vol. 18, no. 2, pp. 257-267.

Cecilia, R., Kunz, U. & Turek, T. 2007, "Possibilities of process intensification using microwaves applied to catalytic microreactors", *Chemical Engineering and Processing: Process Intensification; Selected Papers from the European Process Intensification Conference (EPIC), Copenhagen, Denmark, September 19-20, 2007,* vol. 46, no. 9, pp. 870-881.

Chartier-Harlin, M.C., Crawford, F., Houlden, H., Warren, A., Hughes, D., Fidani, L., Goate, A., Rossor, M., Roques, P. & Hardy, J. 1991, "Early-onset Alzheimer's disease caused by mutations at codon 717 of the beta-amyloid precursor protein gene", *Nature,* vol. 353, no. 6347, pp. 844-846.

Chen, J., Zhou, Y., Mueller-Steiner, S., Chen, L.F., Kwon, H., Yi, S., Mucke, L. & Gan, L. 2005, "SIRT1 protects against microglia-dependent amyloid-beta toxicity through inhibiting NF-kappaB signaling", *The Journal of biological chemistry,* vol. 280, no. 48, pp. 40364-40374.

Chen, Q.S., Wei, W.Z., Shimahara, T. & Xie, C.W. 2002, "Alzheimer amyloid beta-peptide inhibits the late phase of long-term potentiation through calcineurin-dependent mechanisms in the hippocampal dentate gyrus", *Neurobiology of learning and memory,* vol. 77, no. 3, pp. 354-371.

Chen, T., Liu, W., Chao, X., Qu, Y., Zhang, L., Luo, P., Xie, K., Huo, J. & Fei, Z. 2011, "Neuroprotective effect of osthole against oxygen and glucose deprivation in rat cortical neurons: involvement of mitogen-activated protein kinase pathway", *Neuroscience,* vol. 183, pp. 203-211.

Cherny, R.A., Atwood, C.S., Xilinas, M.E., Gray, D.N., Jones, W.D., McLean, C.A., Barnham, K.J., Volitakis, I., Fraser, F.W., Kim, Y., Huang, X., Goldstein, L.E., Moir, R.D., Lim, J.T., Beyreuther, K., Zheng, H., Tanzi, R.E., Masters, C.L. & Bush, A.I. 2001, "Treatment with a copper-zinc chelator markedly and rapidly inhibits beta-amyloid accumulation in Alzheimer's disease transgenic mice", *Neuron,* vol. 30, no. 3, pp. 665-676.

Cherny, R.A., Legg, J.T., McLean, C.A., Fairlie, D.P., Huang, X., Atwood, C.S., Beyreuther, K., Tanzi, R.E., Masters, C.L. & Bush, A.I. 1999, "Aqueous dissolution of Alzheimer's disease Abeta amyloid deposits by biometal depletion", *The Journal of biological chemistry,* vol. 274, no. 33, pp. 23223-23228.

Chung, H.M. & Struhl, G. 2001, "Nicastrin is required for Presenilin-mediated transmembrane cleavage in Drosophila", *Nature cell biology,* vol. 3, no. 12, pp. 1129-1132.

Cleveland, D.W., Hwo, S.Y. & Kirschner, M.W. 1977, "Purification of tau, a microtubule-associated protein that induces assembly of microtubules from purified tubulin", *Journal of Molecular Biology,* vol. 116, no. 2, pp. 207-225.

Close, J., Heidebrecht, R.,Jr, Hendrix, J., Li, C., Munoz, B., Surdi, L., Kattar, S., Tempest, P., Moses, P., Geng, X., Hughes, B., Smotrov, N., Moxham, C., Chapnick, J., Kariv, I., Nikov, G., Burke, J.E., Deshmukh, S., Jeliazkova-Mecheva, V., Leach, J.K., Diaz, D., Xu, L., Yang, Z., Kwei, G., Moy, L., Shah, S., Tanga, F., Kenefic, C., Savage, D., Shearman, M., Ball, R.G., McNevin, M.J., Markarewicz, A. & Miller, T. 2012, "Lead optimization of 4,4-biaryl piperidine amides as gamma-secretase inhibitors", *Bioorganic & medicinal chemistry letters,* vol. 22, no. 9, pp. 3203-3207.

Cohen, G. & Spina, M.B. 1989, "Deprenyl suppresses the oxidant stress associated with increased dopamine turnover", *Annals of Neurology,* vol. 26, no. 5, pp. 689-690.

Connell-Crowley, L., Le Gall, M., Vo, D.J. & Giniger, E. 2000, "The cyclin-dependent kinase Cdk5 controls multiple aspects of axon patterning in vivo", *Current biology : CB,* vol. 10, no. 10, pp. 599-602.

Cooke, D. 1999, *Studies on the Mode of Action of Coumarins (Coumarin, 6-hydroxycoumarin, 7-hydroxycoumarin and Esculetin) at a Cellular Level.*, Ph.D Thesis edn, Dublin City University, Dublin, Ireland, Dublin, Ireland,.

Corder, E.H., Saunders, A.M., Risch, N.J., Strittmatter, W.J., Schmechel, D.E., Gaskell, P.C.,Jr, Rimmler, J.B., Locke, P.A., Conneally, P.M. & Schmader, K.E. 1994, "Protective effect of apolipoprotein E type 2 allele for late onset Alzheimer disease", *Nature genetics,* vol. 7, no. 2, pp. 180-184.

Corder, E.H., Saunders, A.M., Strittmatter, W.J., Schmechel, D.E., Gaskell, P.C., Small, G.W., Roses, A.D., Haines, J.L. & Pericak-Vance, M.A. 1993, "Gene dose of apolipoprotein E type 4 allele and the risk of Alzheimer's disease in late onset families", *Science (New York, N.Y.),* vol. 261, no. 5123, pp. 921-923.

Cuajungco, M.P., Goldstein, L.E., Nunomura, A., Smith, M.A., Lim, J.T., Atwood, C.S., Huang, X., Farrag, Y.W., Perry, G. & Bush, A.I. 2000, "Evidence that the beta-amyloid plaques of Alzheimer's disease represent the redox-silencing and entombment of abeta by zinc", *The Journal of biological chemistry,* vol. 275, no. 26, pp. 19439-19442.

Dall'Acqua, S., Maggi, F., Minesso, P., Salvagno, M., Papa, F., Vittori, S. & Innocenti, G. 2010, "Identification of non-alkaloid acetylcholinesterase inhibitors from Ferulago campestris (Besser) Grecescu (Apiaceae)", *Fitoterapia,* vol. 81, no. 8, pp. 1208-1212.

Davis, T.J., Soto-Ortega, D.D., Kotarek, J.A., Gonzalez-Velasquez, F.J., Sivakumar, K., Wu, L., Wang, Q. & Moss, M.A. 2009, "Comparative study of inhibition at multiple stages of amyloid-beta self-assembly provides mechanistic insight", *Molecular pharmacology,* vol. 76, no. 2, pp. 405-413.

De Strooper, B. 2003, "Aph-1, Pen-2, and Nicastrin with Presenilin generate an active gamma-Secretase complex", *Neuron,* vol. 38, no. 1, pp. 9-12.

de, l.H., Diaz-Ortiz, A. & Moreno, A. 2005, "Microwaves in organic synthesis. Thermal and non-thermal microwave effects", *Chemical Society Reviews,* vol. 34, no. 2, pp. 164-178.

Deane, R., Du Yan, S., Submamaryan, R.K., LaRue, B., Jovanovic, S., Hogg, E., Welch, D., Manness, L., Lin, C., Yu, J., Zhu, H., Ghiso, J., Frangione, B., Stern, A., Schmidt, A.M., Armstrong, D.L., Arnold, B., Liliensiek, B., Nawroth, P., Hofman, F., Kindy, M., Stern, D. & Zlokovic, B. 2003, "RAGE mediates amyloid-beta peptide transport across the blood-brain barrier and accumulation in brain", *Nature medicine,* vol. 9, no. 7, pp. 907-913.

Dhavan, R., Greer, P.L., Morabito, M.A., Orlando, L.R. & Tsai, L.H. 2002, "The cyclin-dependent kinase 5 activators p35 and p39 interact with the alpha-subunit of Ca2+/calmodulin-dependent protein kinase II and alpha-actinin-1 in a calcium-dependent manner", *The Journal of neuroscience : the official journal of the Society for Neuroscience,* vol. 22, no. 18, pp. 7879-7891.

Dhavan, R. & Tsai, L.H. 2001, "A decade of CDK5", *Nature reviews.Molecular cell biology,* vol. 2, no. 10, pp. 749-759.

Diaz, A., Limon, D., Chavez, R., Zenteno, E. & Guevara, J. 2012, "Abeta25-35 injection into the temporal cortex induces chronic inflammation that contributes to neurodegeneration and spatial memory impairment in rats", *Journal of Alzheimer's disease : JAD,* vol. 30, no. 3, pp. 505-522.

Diaz, A., Mendieta, L., Zenteno, E., Guevara, J. & Limon, I.D. 2011, "The role of NOS in the impairment of spatial memory and damaged neurons in rats injected with amyloid beta 25-35 into the temporal cortex", *Pharmacology, biochemistry, and behavior,* vol. 98, no. 1, pp. 67-75.

Dietschy, J.M. & Turley, S.D. 2004, "Thematic review series: brain Lipids. Cholesterol metabolism in the central nervous system during early development and in the mature animal", *Journal of lipid research,* vol. 45, no. 8, pp. 1375-1397.

Dietschy, J.M. & Turley, S.D. 2001, "Cholesterol metabolism in the brain", *Current opinion in lipidology,* vol. 12, no. 2, pp. 105-112.

Dovey, H.F., John, V., Anderson, J.P., Chen, L.Z., de Saint Andrieu, P., Fang, L.Y., Freedman, S.B., Folmer, B., Goldbach, E., Holsztynska, E.J., Hu, K.L., Johnson-Wood, K.L., Kennedy, S.L., Kholodenko, D., Knops, J.E., Latimer, L.H., Lee, M., Liao, Z., Lieberburg, I.M., Motter, R.N., Mutter, L.C., Nietz, J., Quinn, K.P., Sacchi, K.L., Seubert, P.A., Shopp, G.M., Thorsett, E.D., Tung, J.S., Wu, J., Yang, S., Yin, C.T., Schenk, D.B., May, P.C., Altstiel, L.D., Bender, M.H., Boggs, L.N., Britton, T.C., Clemens, J.C., Czilli, D.L., Dieckman-McGinty, D.K., Droste, J.J., Fuson, K.S., Gitter, B.D., Hyslop, P.A., Johnstone, E.M., Li, W.Y., Little, S.P., Mabry, T.E., Miller, F.D. & Audia, J.E. 2001, "Functional gamma-secretase inhibitors reduce beta-amyloid peptide levels in brain", *Journal of neurochemistry,* vol. 76, no. 1, pp. 173-181.

Drechsel, D.N., Hyman, A.A., Cobb, M.H. & Kirschner, M.W. 1992, "Modulation of the dynamic instability of tubulin assembly by the microtubule-associated protein tau", *Molecular biology of the cell,* vol. 3, no. 10, pp. 1141-1154.

Ecobichon, D.J. 1996, "Toxic effects of pesticides" in *Casarett and Doull's Toxicology: The Basic Science of Poisons*, eds. C.D. Klaassen, M.O. Amdur & J. Doull, McGraw-Hill, New York, pp. 643-689.

Edbauer, D., Winkler, E., Haass, C. & Steiner, H. 2002, "Presenilin and nicastrin regulate each other and determine amyloid beta-peptide production via complex formation", *Proceedings of the National Academy of Sciences of the United States of America,* vol. 99, no. 13, pp. 8666-8671.

Edbauer, D., Winkler, E., Regula, J.T., Pesold, B., Steiner, H. & Haass, C. 2003, "Reconstitution of gamma-secretase activity", *Nature cell biology,* vol. 5, no. 5, pp. 486-488.

Edmondson, D.E., Mattevi, A., Binda, C., Li, M. & Hubalek, F. 2004, "Structure and mechanism of monoamine oxidase", *Current medicinal chemistry,* vol. 11, no. 15, pp. 1983-1993.

Egan, D., O'Kennedy, R., Moran, E., Cox, D., Prosser, E. & Thornes, R.D. 1990, "The pharmacology, metabolism, analysis, and applications of coumarin and coumarin-related compounds", *Drug metabolism reviews,* vol. 22, no. 5, pp. 503-529.

Egan, D.A. & O'Kennedy, R. 1992, "Rapid and sensitive determination of coumarin and 7-hydroxycoumarin and its glucuronide conjugate in urine and plasma by high-performance liquid chromatography", *Journal of chromatography,* vol. 582, no. 1-2, pp. 137-143.

Ehehalt, R., Keller, P., Haass, C., Thiele, C. & Simons, K. 2003, "Amyloidogenic processing of the Alzheimer beta-amyloid precursor protein depends on lipid rafts", *The Journal of cell biology,* vol. 160, no. 1, pp. 113-123.

Esler, W.P., Kimberly, W.T., Ostaszewski, B.L., Diehl, T.S., Moore, C.L., Tsai, J.Y., Rahmati, T., Xia, W., Selkoe, D.J. & Wolfe, M.S. 2000, "Transition-state analogue inhibitors of gamma-secretase bind directly to presenilin-1", *Nature cell biology,* vol. 2, no. 7, pp. 428-434.

Esler, W.P., Kimberly, W.T., Ostaszewski, B.L., Ye, W., Diehl, T.S., Selkoe, D.J. & Wolfe, M.S. 2002, "Activity-dependent isolation of the presenilin- gamma -secretase complex reveals nicastrin and a gamma substrate", *Proceedings of the National Academy of Sciences of the United States of America,* vol. 99, no. 5, pp. 2720-2725.

Fang, J.H., Wang, X.H., Xu, Z.R. & Jiang, F.G. 2010, "Neuroprotective effects of bis(7)-tacrine against glutamate-induced retinal ganglion cells damage", *BMC neuroscience,* vol. 11, pp. 31-2202-11-31.

Farris, W., Mansourian, S., Chang, Y., Lindsley, L., Eckman, E.A., Frosch, M.P., Eckman, C.B., Tanzi, R.E., Selkoe, D.J. & Guenette, S. 2003, "Insulin-degrading enzyme regulates the levels of insulin, amyloid beta-protein, and the beta-amyloid precursor protein intracellular domain in vivo", *Proceedings of the National Academy of Sciences of the United States of America,* vol. 100, no. 7, pp. 4162-4167.

Farzan, M., Schnitzler, C.E., Vasilieva, N., Leung, D. & Choe, H. 2000, "BACE2, a beta -secretase homolog, cleaves at the beta site and within the amyloid-beta region of the amyloid-beta precursor protein", *Proceedings of the National Academy of Sciences of the United States of America,* vol. 97, no. 17, pp. 9712-9717.

Fischer, A., Sananbenesi, F., Wang, X., Dobbin, M. & Tsai, L.H. 2007, "Recovery of learning and memory is associated with chromatin remodelling", *Nature,* vol. 447, no. 7141, pp. 178-182.

Francis, R., McGrath, G., Zhang, J., Ruddy, D.A., Sym, M., Apfeld, J., Nicoll, M., Maxwell, M., Hai, B., Ellis, M.C., Parks, A.L., Xu, W., Li, J., Gurney, M., Myers, R.L., Himes, C.S., Hiebsch, R., Ruble, C., Nye, J.S. & Curtis, D. 2002, "aph-1 and pen-2 are required for Notch pathway signaling, gamma-secretase cleavage of betaAPP, and presenilin protein accumulation", *Developmental cell,* vol. 3, no. 1, pp. 85-97.

Frederickson, C.J. 1989, "Neurobiology of zinc and zinc-containing neurons", *International review of neurobiology,* vol. 31, pp. 145-238.

Fu, H., Dou, J., Li, W., Cui, W., Mak, S., Hu, Q., Luo, J., Lam, C.S., Pang, Y., Youdim, M.B. & Han, Y. 2009, "Promising multifunctional anti-Alzheimer's dimer bis(7)-Cognitin acting as an activator of protein kinase C regulates activities of alpha-secretase and BACE-1 concurrently", *European journal of pharmacology,* vol. 623, no. 1-3, pp. 14-21.

Galimberti, D. & Scarpini, E. 2011, "Disease-modifying treatments for Alzheimer's disease", *Therapeutic advances in neurological disorders,* vol. 4, no. 4, pp. 203-216.

Gallo, M. & Lawryk, N. 1991, "Organic phosphorus pesticides." in *Handbook of PesticideToxicology.* , eds. W. Hayes & E. Laws, Academic Press, Chestnut Hill, Massachusetts, pp. 917-972.

Garino, C., Pietrancosta, N., Laras, Y., Moret, V., Rolland, A., Quelever, G. & Kraus, J.L. 2006, "BACE-1 inhibitory activities of new substituted phenyl-piperazine coupled to various heterocycles: chromene, coumarin and quinoline", *Bioorganic & medicinal chemistry letters,* vol. 16, no. 7, pp. 1995-1999.

Girisha, H.R., Narendra Sharath Chandra, J.N., Boppana, S., Malviya, M., Sadashiva, C.T. & Rangappa, K.S. 2009, "Active site directed docking studies: synthesis and pharmacological evaluation of cis-2,6-dimethyl piperidine sulfonamides as inhibitors of acetylcholinesterase", *European journal of medicinal chemistry,* vol. 44, no. 10, pp. 4057-4062.

Goedert, M. & Jakes, R. 2005, "Mutations causing neurodegenerative tauopathies", *Biochimica et biophysica acta,* vol. 1739, no. 2-3, pp. 240-250.

Gouras, G.K. & Beal, M.F. 2001, "Metal chelator decreases Alzheimer beta-amyloid plaques", *Neuron,* vol. 30, no. 3, pp. 641-642.

Greengard, P., Allen, P.B. & Nairn, A.C. 1999, "Beyond the dopamine receptor: the DARPP-32/protein phosphatase-1 cascade", *Neuron,* vol. 23, no. 3, pp. 435-447.

Grimsby, J., Lan, N.C., Neve, R., Chen, K. & Shih, J.C. 1990, "Tissue distribution of human monoamine oxidase A and B mRNA", *Journal of neurochemistry,* vol. 55, no. 4, pp. 1166-1169.

Guan, J.S., Haggarty, S.J., Giacometti, E., Dannenberg, J.H., Joseph, N., Gao, J., Nieland, T.J., Zhou, Y., Wang, X., Mazitschek, R., Bradner, J.E., DePinho, R.A., Jaenisch, R. & Tsai, L.H. 2009, "HDAC2 negatively regulates memory formation and synaptic plasticity", *Nature,* vol. 459, no. 7243, pp. 55-60.

Hama, E. & Saido, T.C. 2005, "Etiology of sporadic Alzheimer's disease: somatostatin, neprilysin, and amyloid beta peptide", *Medical hypotheses,* vol. 65, no. 3, pp. 498-500.

Han, S., Zhou, V., Pan, S., Liu, Y., Hornsby, M., McMullan, D., Klock, H.E., Haugen, J., Lesley, S.A., Gray, N., Caldwell, J. & Gu, X.J. 2005, "Identification of coumarin derivatives as a novel class of allosteric MEK1 inhibitors", *Bioorganic & medicinal chemistry letters,* vol. 15, no. 24, pp. 5467-5473.

Hebert, L.E., Weuve, J., Scherr, P.A. & Evans, D.A. 2013, "Alzheimer disease in the United States (2010-2050) estimated using the 2010 census", *Neurology,* vol. 80, no. 19, pp. 1778-1783.

Hoerr, R. & Noeldner, M. 2002, "Ensaculin (KA-672 HCl): a multitransmitter approach to dementia treatment", *CNS drug reviews,* vol. 8, no. 2, pp. 143-158.

Hofmann, M.A., Drury, S., Fu, C., Qu, W., Taguchi, A., Lu, Y., Avila, C., Kambham, N., Bierhaus, A., Nawroth, P., Neurath, M.F., Slattery, T., Beach, D., McClary, J., Nagashima, M., Morser, J., Stern, D. & Schmidt, A.M. 1999, "RAGE mediates a novel proinflammatory axis: a central cell surface receptor for S100/calgranulin polypeptides", *Cell,* vol. 97, no. 7, pp. 889-901.

Hori, O., Brett, J., Slattery, T., Cao, R., Zhang, J., Chen, J.X., Nagashima, M., Lundh, E.R., Vijay, S. & Nitecki, D. 1995, "The receptor for advanced glycation end products (RAGE) is a cellular binding site for amphoterin. Mediation of neurite outgrowth and co-expression of rage and amphoterin in the developing nervous system", *The Journal of biological chemistry,* vol. 270, no. 43, pp. 25752-25761.

Hornick, A., Lieb, A., Vo, N.P., Rollinger, J.M., Stuppner, H. & Prast, H. 2011, "The coumarin scopoletin potentiates acetylcholine release from synaptosomes, amplifies hippocampal long-term potentiation and ameliorates anticholinergic- and age-impaired memory", *Neuroscience,* vol. 197, pp. 280-292.

Hoult, J.R. & Paya, M. 1996, "Pharmacological and biochemical actions of simple coumarins: natural products with therapeutic potential", *General pharmacology,* vol. 27, no. 4, pp. 713-722.

Hu, Y., Ye, Y. & Fortini, M.E. 2002, "Nicastrin is required for gamma-secretase cleavage of the Drosophila Notch receptor", *Developmental cell,* vol. 2, no. 1, pp. 69-78.

Huang, E.J. & Reichardt, L.F. 2001, "Neurotrophins: roles in neuronal development and function", *Annual Review of Neuroscience,* vol. 24, pp. 677-736.

Huang, W.J., Chen, C.C., Chao, S.W., Yu, C.C., Yang, C.Y., Guh, J.H., Lin, Y.C., Kuo, C.I., Yang, P. & Chang, C.I. 2011, "Synthesis and evaluation of aliphatic-chain hydroxamates capped with osthole derivatives as histone deacetylase inhibitors", *European journal of medicinal chemistry,* vol. 46, no. 9, pp. 4042-4049.

Huang, X., Atwood, C.S., Hartshorn, M.A., Multhaup, G., Goldstein, L.E., Scarpa, R.C., Cuajungco, M.P., Gray, D.N., Lim, J., Moir, R.D., Tanzi, R.E. & Bush, A.I. 1999, "The A beta peptide of Alzheimer's disease directly produces hydrogen peroxide through metal ion reduction", *Biochemistry,* vol. 38, no. 24, pp. 7609-7616.

Huang, X., Atwood, C.S., Moir, R.D., Hartshorn, M.A., Vonsattel, J.P., Tanzi, R.E. & Bush, A.I. 1997, "Zinc-induced Alzheimer's Abeta1-40 aggregation is mediated by conformational factors", *The Journal of biological chemistry,* vol. 272, no. 42, pp. 26464-26470.

Huang, X., Cuajungco, M.P., Atwood, C.S., Hartshorn, M.A., Tyndall, J.D., Hanson, G.R., Stokes, K.C., Leopold, M., Multhaup, G., Goldstein, L.E., Scarpa, R.C., Saunders, A.J., Lim, J., Moir, R.D., Glabe, C., Bowden, E.F., Masters, C.L., Fairlie, D.P., Tanzi, R.E. & Bush, A.I. 1999, "Cu(II) potentiation of alzheimer abeta neurotoxicity. Correlation with cell-free hydrogen peroxide production and metal reduction", *The Journal of biological chemistry,* vol. 274, no. 52, pp. 37111-37116.

Huang, X., Cuajungco, M.P., Atwood, C.S., Moir, R.D., Tanzi, R.E. & Bush, A.I. 2000, "Alzheimer's disease, beta-amyloid protein and zinc", *The Journal of nutrition,* vol. 130, no. 5S Suppl, pp. 1488S-92S.

Huang, Y.T. & Blagg, B.S. 2007, "A library of noviosylated coumarin analogues", *The Journal of organic chemistry,* vol. 72, no. 10, pp. 3609-3613.

Hubalek, F., Binda, C., Khalil, A., Li, M., Mattevi, A., Castagnoli, N. & Edmondson, D.E. 2005, "Demonstration of isoleucine 199 as a structural determinant for the selective inhibition of human monoamine oxidase B by specific reversible inhibitors", *The Journal of biological chemistry,* vol. 280, no. 16, pp. 15761-15766.

Hung, A.Y., Koo, E.H., Haass, C. & Selkoe, D.J. 1992, "Increased expression of beta-amyloid precursor protein during neuronal differentiation is not accompanied by secretory cleavage", *Proceedings of the National Academy of Sciences of the United States of America,* vol. 89, no. 20, pp. 9439-9443.

Hussain, I., Powell, D., Howlett, D.R., Tew, D.G., Meek, T.D., Chapman, C., Gloger, I.S., Murphy, K.E., Southan, C.D., Ryan, D.M., Smith, T.S., Simmons, D.L., Walsh, F.S., Dingwall, C. & Christie, G. 1999, "Identification of a novel aspartic protease (Asp 2) as beta-secretase", *Molecular and cellular neurosciences,* vol. 14, no. 6, pp. 419-427.

Hyman, B.T., Van Hoesen, G.W., Damasio, A.R. & Barnes, C.L. 1984, "Alzheimer's disease: cell-specific pathology isolates the hippocampal formation", *Science (New York, N.Y.),* vol. 225, no. 4667, pp. 1168-1170.

Imahori, K. & Uchida, T. 1997, "Physiology and pathology of tau protein kinases in relation to Alzheimer's disease", *Journal of Biochemistry,* vol. 121, no. 2, pp. 179-188.

Inestrosa, N.C. & Alarcon, R. 1998, "Molecular interactions of acetylcholinesterase with senile plaques", *Journal of physiology, Paris,* vol. 92, no. 5-6, pp. 341-344.

Inestrosa, N.C., Alvarez, A. & Calderon, F. 1996, "Acetylcholinesterase is a senile plaque component that promotes assembly of amyloid beta-peptide into Alzheimer's filaments", *Molecular psychiatry,* vol. 1, no. 5, pp. 359-361.

Inestrosa, N.C., Roberts, W.L., Marshall, T.L. & Rosenberry, T.L. 1987, "Acetylcholinesterase from bovine caudate nucleus is attached to membranes by a novel subunit distinct from those of acetylcholinesterases in other tissues", *The Journal of biological chemistry,* vol. 262, no. 10, pp. 4441-4444.

Irizarry, M.C., Deng, A., Lleo, A., Berezovska, O., Von Arnim, C.A., Martin-Rehrmann, M., Manelli, A., LaDu, M.J., Hyman, B.T. & Rebeck, G.W. 2004, "Apolipoprotein E modulates gamma-secretase cleavage of the amyloid precursor protein", *Journal of neurochemistry,* vol. 90, no. 5, pp. 1132-1143.

Iuliano, L., Pacelli, A., Ciacciarelli, M., Zerbinati, C., Fagioli, S., Piras, F., Orfei, M.D., Bossu, P., Pazzelli, F., Serviddio, G., Caltagirone, C. & Spalletta, G. 2013, "Plasma fatty acid lipidomics in amnestic mild cognitive impairment and Alzheimer's disease", *Journal of Alzheimer's disease : JAD,* vol. 36, no. 3, pp. 545-553.

Ivanoiu, A., Adam, S., Van der Linden, M., Salmon, E., Juillerat, A.C., Mulligan, R. & Seron, X. 2005, "Memory evaluation with a new cued recall test in patients with mild cognitive impairment and Alzheimer's disease", *Journal of neurology,* vol. 252, no. 1, pp. 47-55.

Iwata, N., Higuchi, M. & Saido, T.C. 2005, "Metabolism of amyloid-beta peptide and Alzheimer's disease", *Pharmacology & therapeutics,* vol. 108, no. 2, pp. 129-148.

Iwata, N., Mizukami, H., Shirotani, K., Takaki, Y., Muramatsu, S., Lu, B., Gerard, N.P., Gerard, C., Ozawa, K. & Saido, T.C. 2004, "Presynaptic localization of neprilysin contributes to efficient clearance of amyloid-beta peptide in mouse brain", *The Journal of neuroscience : the official journal of the Society for Neuroscience,* vol. 24, no. 4, pp. 991-998.

Iwata, N., Tsubuki, S., Takaki, Y., Shirotani, K., Lu, B., Gerard, N.P., Gerard, C., Hama, E., Lee, H.J. & Saido, T.C. 2001, "Metabolic regulation of brain Abeta by neprilysin", *Science (New York, N.Y.),* vol. 292, no. 5521, pp. 1550-1552.

Iwatsubo, T. 2004, "The gamma-secretase complex: machinery for intramembrane proteolysis", *Current opinion in neurobiology,* vol. 14, no. 3, pp. 379-383.

Jahromi, M.M., Millward, B.A. & Demaine, A.G. 2000, "A polymorphism in the promoter region of the gene for interleukin-6 is associated with susceptibility to type 1 diabetes mellitus", *Journal of interferon & cytokine research : the official journal of the International Society for Interferon and Cytokine Research,* vol. 20, no. 10, pp. 885-888.

Jelic, V. & Kowalski, J. 2009, "Evidence-based evaluation of diagnostic accuracy of resting EEG in dementia and mild cognitive impairment", *Clinical EEG and neuroscience : official journal of the EEG and Clinical Neuroscience Society (ENCS),* vol. 40, no. 2, pp. 129-142.

Jenuwein, T. & Allis, C.D. 2001, "Translating the histone code", *Science (New York, N.Y.),* vol. 293, no. 5532, pp. 1074-1080.

Jeyachandran, V., Kumar, R.R., Ali, M.A. & Choon, T.S. 2013, "A one-pot domino synthesis and discovery of highly functionalized dihydrobenzo[b]thiophenes as AChE inhibitors", *Bioorganic & medicinal chemistry letters,* vol. 23, no. 7, pp. 2101-2105.

Ji, H.J., Hu, J.F., Wang, Y.H., Chen, X.Y., Zhou, R. & Chen, N.H. 2010, "Osthole improves chronic cerebral hypoperfusion induced cognitive deficits and neuronal damage in hippocampus", *European journal of pharmacology,* vol. 636, no. 1-3, pp. 96-101.

Joa, H., Vogl, S., Atanasov, A.G., Zehl, M., Nakel, T., Fakhrudin, N., Heiss, E.H., Picker, P., Urban, E., Wawrosch, C., Saukel, J., Reznicek, G., Kopp, B. & Dirsch, V.M. 2011, "Identification of ostruthin from Peucedanum ostruthium rhizomes as an inhibitor of vascular smooth muscle cell proliferation", *Journal of natural products,* vol. 74, no. 6, pp. 1513-1516.

Jones, M.R., Service, E.L., Thompson, J.R., Wang, M.C., Kimsey, I.J., DeToma, A.S., Ramamoorthy, A., Lim, M.H. & Storr, T. 2012, "Dual-function triazole-pyridine derivatives as inhibitors of metal-induced amyloid-beta aggregation", *Metallomics : integrated biometal science,* vol. 4, no. 9, pp. 910-920.

Kamal, A., Almenar-Queralt, A., LeBlanc, J.F., Roberts, E.A. & Goldstein, L.S. 2001, "Kinesin-mediated axonal transport of a membrane compartment containing beta-secretase and presenilin-1 requires APP", *Nature,* vol. 414, no. 6864, pp. 643-648.

Kancheva, V.D., Boranova, P.V., Nechev, J.T. & Manolov, I.I. 2010, "Structure-activity relationships of new 4-hydroxy bis-coumarins as radical scavengers and chain-breaking antioxidants", *Biochimie,* vol. 92, no. 9, pp. 1138-1146.

Kasa, P., Rakonczay, Z. & Gulya, K. 1997, "The cholinergic system in Alzheimer's disease", *Progress in neurobiology,* vol. 52, no. 6, pp. 511-535.

Kawas, C.H., Corrada, M.M., Brookmeyer, R., Morrison, A., Resnick, S.M., Zonderman, A.B. & Arenberg, D. 2003, "Visual memory predicts Alzheimer's disease more than a decade before diagnosis", *Neurology,* vol. 60, no. 7, pp. 1089-1093.

Keating, G. & O'Kennedy, R. 1997, "The Chemistry and Occurrence of Coumarins. Coumarins: Biology, Apllications and Mode of Action." in , ed. R. "O'Kennedy 'Thornes R.D.", John Wiley & Sons, Chichester, pp. 23-66.

Kim, S.H., Kang, K.A., Zhang, R., Piao, M.J., Ko, D.O., Wang, Z.H., Chae, S.W., Kang, S.S., Lee, K.H., Kang, H.K., Kang, H.W. & Hyun, J.W. 2008, "Protective effect of esculetin against oxidative stress-induced cell damage via scavenging reactive oxygen species", *Acta Pharmacologica Sinica,* vol. 29, no. 11, pp. 1319-1326.

Kislinger, T., Fu, C., Huber, B., Qu, W., Taguchi, A., Du Yan, S., Hofmann, M., Yan, S.F., Pischetsrieder, M., Stern, D. & Schmidt, A.M. 1999, "N(epsilon)-(carboxymethyl)lysine adducts of proteins are ligands for receptor for advanced glycation end products that activate cell signaling pathways and modulate gene expression", *The Journal of biological chemistry,* vol. 274, no. 44, pp. 31740-31749.

Kitazume, S., Tachida, Y., Oka, R., Shirotani, K., Saido, T.C. & Hashimoto, Y. 2001, "Alzheimer's beta-secretase, beta-site amyloid precursor protein-cleaving enzyme, is responsible for cleavage secretion of a Golgi-resident sialyltransferase", *Proceedings of the National Academy of Sciences of the United States of America,* vol. 98, no. 24, pp. 13554-13559.

Klajnert, B., Wasiak, T., Ionov, M., Fernandez-Villamarin, M., Sousa-Herves, A., Correa, J., Riguera, R. & Fernandez-Megia, E. 2012, "Dendrimers reduce toxicity of Abeta 1-28 peptide during aggregation and accelerate fibril formation", *Nanomedicine : nanotechnology, biology, and medicine,* vol. 8, no. 8, pp. 1372-1378.

Klinge, C.M., Wickramasinghe, N.S., Ivanova, M.M. & Dougherty, S.M. 2008, "Resveratrol stimulates nitric oxide production by increasing estrogen receptor alpha-Src-caveolin-1 interaction and phosphorylation in human umbilical vein endothelial cells", *FASEB journal : official publication of the Federation of American Societies for Experimental Biology,* vol. 22, no. 7, pp. 2185-2197.

Knowles, R.G. & Moncada, S. 1994, "Nitric oxide synthases in mammals", *The Biochemical journal,* vol. 298 (Pt 2), no. Pt 2, pp. 249-258.

Ko, J., Humbert, S., Bronson, R.T., Takahashi, S., Kulkarni, A.B., Li, E. & Tsai, L.H. 2001, "P35 and P39 are Essential for Cyclin-Dependent Kinase 5 Function during Neurodevelopment", *The Journal of neuroscience : the official journal of the Society for Neuroscience,* vol. 21, no. 17, pp. 6758-6771.

Kojro, E., Gimpl, G., Lammich, S., Marz, W. & Fahrenholz, F. 2001, "Low cholesterol stimulates the nonamyloidogenic pathway by its effect on the alpha -secretase ADAM 10", *Proceedings of the National Academy of Sciences of the United States of America,* vol. 98, no. 10, pp. 5815-5820.

Kontogiorgis, C.A. & Hadjipavlou-Litina, D.J. 2005, "Synthesis and antiinflammatory activity of coumarin derivatives", *Journal of medicinal chemistry,* vol. 48, no. 20, pp. 6400-6408.

Kontogiorgis, C.A., Xu, Y., Hadjipavlou-Litina, D. & Luo, Y. 2007, "Coumarin derivatives protection against ROS production in cellular models of Abeta toxicities", *Free radical research,* vol. 41, no. 10, pp. 1168-1180.

Koo, E.H. & Kopan, R. 2004, "Potential role of presenilin-regulated signaling pathways in sporadic neurodegeneration", *Nature medicine,* vol. 10 Suppl, pp. S26-33.

Korte, M., Carroll, P., Wolf, E., Brem, G., Thoenen, H. & Bonhoeffer, T. 1995, "Hippocampal long-term potentiation is impaired in mice lacking brain-derived neurotrophic factor", *Proceedings of the National Academy of Sciences of the United States of America,* vol. 92, no. 19, pp. 8856-8860.

Korzus, E., Rosenfeld, M.G. & Mayford, M. 2004, "CBP histone acetyltransferase activity is a critical component of memory consolidation", *Neuron,* vol. 42, no. 6, pp. 961-972.

Kouzarides, T. 2007, "Chromatin modifications and their function", *Cell,* vol. 128, no. 4, pp. 693-705.

Kramer, J.H., Reed, B.R., Mungas, D., Weiner, M.W. & Chui, H.C. 2002, "Executive dysfunction in subcortical ischaemic vascular disease", *Journal of neurology, neurosurgery, and psychiatry,* vol. 72, no. 2, pp. 217-220.

Krammer, A., Kirchhoff, P.D., Jiang, X., Venkatachalam, C.M. & Waldman, M. 2005, "LigScore: a novel scoring function for predicting binding affinities", *Journal of molecular graphics & modelling,* vol. 23, no. 5, pp. 395-407.

Krebs, C., Weinberg, J. & Akesson, E.J. 2011, *Neuroscience,* Wolters Kluwer/Lippincott Williams & Wilkins Health.

Kumar, R.S., Almansour, A.I., Arumugam, N., Osman, H., Ali, M.A., Basiri, A. & Kia, Y. 2013, "An Expedient Synthesis and Screening for Antiacetylcholinesterase Activity of Piperidine Embedded Novel Pentacyclic Cage Compounds", *Medicinal chemistry (Shariqah (United Arab Emirates)),* .

Kumar, Y.C., Malviya, M., Chandra, J.N., Sadashiva, C.T., Kumar, C.S., Prasad, S.B., Prasanna, D.S., Subhash, M.N. & Rangappa, K.S. 2008, "Effect of novel N-aryl sulfonamide substituted 3-morpholino arecoline derivatives as muscarinic receptor 1 agonists in Alzheimer's dementia models", *Bioorganic & medicinal chemistry,* vol. 16, no. 9, pp. 5157-5163.

Kurochkin, I.V. & Goto, S. 1994, "Alzheimer's beta-amyloid peptide specifically interacts with and is degraded by insulin degrading enzyme", *FEBS letters,* vol. 345, no. 1, pp. 33-37.

Kwon, Y.E., Park, J.Y., No, K.T., Shin, J.H., Lee, S.K., Eun, J.S., Yang, J.H., Shin, T.Y., Kim, D.K., Chae, B.S., Leem, J.Y. & Kim, K.H. 2007, "Synthesis, in vitro assay, and molecular modeling of new piperidine derivatives having dual inhibitory potency against acetylcholinesterase and Abeta1-42 aggregation for Alzheimer's disease therapeutics", *Bioorganic & medicinal chemistry,* vol. 15, no. 20, pp. 6596-6607.

LaDu, M.J., Falduto, M.T., Manelli, A.M., Reardon, C.A., Getz, G.S. & Frail, D.E. 1994, "Isoform-specific binding of apolipoprotein E to beta-amyloid", *The Journal of biological chemistry,* vol. 269, no. 38, pp. 23403-23406.

LaDu, M.J., Pederson, T.M., Frail, D.E., Reardon, C.A., Getz, G.S. & Falduto, M.T. 1995, "Purification of apolipoprotein E attenuates isoform-specific binding to beta-amyloid", *The Journal of biological chemistry,* vol. 270, no. 16, pp. 9039-9042.

Laird, F.M., Cai, H., Savonenko, A.V., Farah, M.H., He, K., Melnikova, T., Wen, H., Chiang, H.C., Xu, G., Koliatsos, V.E., Borchelt, D.R., Price, D.L., Lee, H.K. & Wong, P.C. 2005, "BACE1, a major determinant of selective vulnerability of the brain to amyloid-beta amyloidogenesis, is essential for cognitive, emotional, and synaptic functions", *The Journal of neuroscience : the official journal of the Society for Neuroscience,* vol. 25, no. 50, pp. 11693-11709.

Lange, K.L., Bondi, M.W., Salmon, D.P., Galasko, D., Delis, D.C., Thomas, R.G. & Thal, L.J. 2002, "Decline in verbal memory during preclinical Alzheimer's disease: examination of the effect of APOE genotype", *Journal of the International Neuropsychological Society : JINS,* vol. 8, no. 7, pp. 943-955.

Langston, J.W. 1990, "Selegiline as neuroprotective therapy in Parkinson's disease: concepts and controversies", *Neurology,* vol. 40, no. 10 Suppl 3, pp. suppl 61-6; discussion 67-9.

Lazarov, O., Lee, M., Peterson, D.A. & Sisodia, S.S. 2002, "Evidence that synaptically released beta-amyloid accumulates as extracellular deposits in the hippocampus of transgenic mice", *The Journal of neuroscience : the official journal of the Society for Neuroscience,* vol. 22, no. 22, pp. 9785-9793.

Leal, L.K., Ferreira, A.A., Bezerra, G.A., Matos, F.J. & Viana, G.S. 2000, "Antinociceptive, anti-inflammatory and bronchodilator activities of Brazilian medicinal plants containing coumarin: a comparative study", *Journal of ethnopharmacology,* vol. 70, no. 2, pp. 151-159.

Lee, S.F., Shah, S., Li, H., Yu, C., Han, W. & Yu, G. 2002, "Mammalian APH-1 interacts with presenilin and nicastrin and is required for intramembrane proteolysis of amyloid-beta precursor protein and Notch", *The Journal of biological chemistry,* vol. 277, no. 47, pp. 45013-45019.

Lee, S.J., Lee, U.S., Kim, W.J. & Moon, S.K. 2011, "Inhibitory effect of esculetin on migration, invasion and matrix metalloproteinase-9 expression in TNF-alpha-induced vascular smooth muscle cells", *Molecular medicine reports,* vol. 4, no. 2, pp. 337-341.

Lee, V.M., Goedert, M. & Trojanowski, J.Q. 2001, "Neurodegenerative tauopathies", *Annual Review of Neuroscience,* vol. 24, pp. 1121-1159.

Legoabe, L.J., Petzer, A. & Petzer, J.P. 2014, "alpha-Tetralone derivatives as inhibitors of monoamine oxidase", *Bioorganic & medicinal chemistry letters,* vol. 24, no. 12, pp. 2758-2763.

Levenson, J.M., O'Riordan, K.J., Brown, K.D., Trinh, M.A., Molfese, D.L. & Sweatt, J.D. 2004, "Regulation of histone acetylation during memory formation in the hippocampus", *The Journal of biological chemistry,* vol. 279, no. 39, pp. 40545-40559.

Li, H., Asberom, T., Bara, T.A., Clader, J.W., Greenlee, W.J., Josien, H.B., McBriar, M.D., Nomeir, A., Pissarnitski, D.A., Rajagopalan, M., Xu, R., Zhao, Z., Song, L. & Zhang, L. 2007, "Discovery of 2,4,6-trisubstituted N-arylsulfonyl piperidines as gamma-secretase inhibitors", *Bioorganic & medicinal chemistry letters,* vol. 17, no. 22, pp. 6290-6294.

Li, H. & Forstermann, U. 2009, "Resveratrol: a multifunctional compound improving endothelial function. Editorial to: "Resveratrol supplementation gender independently improves endothelial reactivity and suppresses superoxide production in healthy rats" by S. Soylemez et al", *Cardiovascular drugs and therapy / sponsored by the International Society of Cardiovascular Pharmacotherapy,* vol. 23, no. 6, pp. 425-429.

Li, H., Zhang, Y., Wang, H., Zheng, X. & Chen, X. 2012, "Nicousamide blocks the effects of advanced glycation end products on renal cells", *European journal of pharmacology,* vol. 674, no. 2-3, pp. 455-459.

Li, Q. & Sudhof, T.C. 2004, "Cleavage of amyloid-beta precursor protein and amyloid-beta precursor-like protein by BACE 1", *The Journal of biological chemistry,* vol. 279, no. 11, pp. 10542-10550.

Li, T., Ma, G., Cai, H., Price, D.L. & Wong, P.C. 2003, "Nicastrin is required for assembly of presenilin/gamma-secretase complexes to mediate Notch signaling and for processing and trafficking of beta-amyloid precursor protein in mammals", *The Journal of neuroscience : the official journal of the Society for Neuroscience,* vol. 23, no. 8, pp. 3272-3277.

Li, W., Mak, M., Jiang, H., Wang, Q., Pang, Y., Chen, K. & Han, Y. 2009, "Novel anti-Alzheimer's dimer Bis(7)-cognitin: cellular and molecular mechanisms of neuroprotection through multiple targets", *Neurotherapeutics : the journal of the American Society for Experimental NeuroTherapeutics,* vol. 6, no. 1, pp. 187-201.

Li, Y.M., Lai, M.T., Xu, M., Huang, Q., DiMuzio-Mower, J., Sardana, M.K., Shi, X.P., Yin, K.C., Shafer, J.A. & Gardell, S.J. 2000, "Presenilin 1 is linked with gamma-secretase activity in the detergent solubilized state", *Proceedings of the National Academy of Sciences of the United States of America,* vol. 97, no. 11, pp. 6138-6143.

Li, Y.M., Xu, M., Lai, M.T., Huang, Q., Castro, J.L., DiMuzio-Mower, J., Harrison, T., Lellis, C., Nadin, A., Neduvelil, J.G., Register, R.B., Sardana, M.K., Shearman, M.S., Smith, A.L., Shi, X.P., Yin, K.C., Shafer, J.A. & Gardell, S.J. 2000, "Photoactivated gamma-secretase inhibitors directed to the active site covalently label presenilin 1", *Nature,* vol. 405, no. 6787, pp. 689-694.

Lin, X., Koelsch, G., Wu, S., Downs, D., Dashti, A. & Tang, J. 2000, "Human aspartic protease memapsin 2 cleaves the beta-secretase site of beta-amyloid precursor protein", *Proceedings of the National Academy of Sciences of the United States of America,* vol. 97, no. 4, pp. 1456-1460.

Lleo, A., Berezovska, O., Herl, L., Raju, S., Deng, A., Bacskai, B.J., Frosch, M.P., Irizarry, M. & Hyman, B.T. 2004, "Nonsteroidal anti-inflammatory drugs lower Abeta42 and change presenilin 1 conformation", *Nature medicine,* vol. 10, no. 10, pp. 1065-1066.

Lovell, M.A., Xie, C. & Markesbery, W.R. 1999, "Protection against amyloid beta peptide toxicity by zinc", *Brain research,* vol. 823, no. 1-2, pp. 88-95.

Lu, X., Ji, H. & Silverman, R. 2002, "Flavins and Flavoproteins 2002. , editors. .; Berlin: 2002. p. 817-830." in *Flavins and Flavoproteins,* eds. S. Chapman, R. Perham & N. Scrutton, Agency for Scientific Publications, Berlin, pp. 817-830.

Lue, L.F., Kuo, Y.M., Roher, A.E., Brachova, L., Shen, Y., Sue, L., Beach, T., Kurth, J.H., Rydel, R.E. & Rogers, J. 1999, "Soluble amyloid beta peptide concentration as a predictor of synaptic change in Alzheimer's disease", *The American journal of pathology,* vol. 155, no. 3, pp. 853-862.

Luo, W., Dou, F., Rodina, A., Chip, S., Kim, J., Zhao, Q., Moulick, K., Aguirre, J., Wu, N., Greengard, P. & Chiosis, G. 2007, "Roles of heat-shock protein 90 in maintaining and facilitating the neurodegenerative phenotype in tauopathies", *Proceedings of the National Academy of Sciences of the United States of America,* vol. 104, no. 22, pp. 9511-9516.

Madhavan, G.R., Balraju, V., Mallesham, B., Chakrabarti, R. & Lohray, V.B. 2003, "Novel coumarin derivatives of heterocyclic compounds as lipid-lowering agents", *Bioorganic & medicinal chemistry letters,* vol. 13, no. 15, pp. 2547-2551.

Malviya, M., Kumar, Y.C., Mythri, R.B., Venkateshappa, C., Subhash, M.N. & Rangappa, K.S. 2009, "Muscarinic receptor 1 agonist activity of novel N-aryl carboxamide substituted 3-morpholino arecoline derivatives in Alzheimer's presenile dementia models", *Bioorganic & medicinal chemistry,* vol. 17, no. 15, pp. 5526-5534.

Mao, X., Yin, W., Liu, M., Ye, M., Liu, P., Liu, J., Lian, Q., Xu, S. & Pi, R. 2011, "Osthole, a natural coumarin, improves neurobehavioral functions and reduces infarct volume and matrix metalloproteinase-9 activity after transient focal cerebral ischemia in rats", *Brain research,* vol. 1385, pp. 275-280.

Maresca, A., Scozzafava, A. & Supuran, C.T. 2010, "7,8-disubstituted- but not 6,7-disubstituted coumarins selectively inhibit the transmembrane, tumor-associated carbonic anhydrase isoforms IX and XII over the cytosolic ones I and II in the low nanomolar/subnanomolar range", *Bioorganic & medicinal chemistry letters,* vol. 20, no. 24, pp. 7255-7258.

Maresca, A. & Supuran, C.T. 2010, "Coumarins incorporating hydroxy- and chloro-moieties selectively inhibit the transmembrane, tumor-associated carbonic anhydrase isoforms IX and XII over the cytosolic ones I and II", *Bioorganic & medicinal chemistry letters,* vol. 20, no. 15, pp. 4511-4514.

Maresca, A., Temperini, C., Pochet, L., Masereel, B., Scozzafava, A. & Supuran, C.T. 2010, "Deciphering the mechanism of carbonic anhydrase inhibition with coumarins and thiocoumarins", *Journal of medicinal chemistry,* vol. 53, no. 1, pp. 335-344.

Marr, R.A., Rockenstein, E., Mukherjee, A., Kindy, M.S., Hersh, L.B., Gage, F.H., Verma, I.M. & Masliah, E. 2003, "Neprilysin gene transfer reduces human amyloid pathology in transgenic mice", *The Journal of neuroscience : the official journal of the Society for Neuroscience,* vol. 23, no. 6, pp. 1992-1996.

Martinez, A., Alcantara, S., Borrell, V., Del Rio, J.A., Blasi, J., Otal, R., Campos, N., Boronat, A., Barbacid, M., Silos-Santiago, I. & Soriano, E. 1998, "TrkB and TrkC signaling are required for maturation and synaptogenesis of hippocampal connections", *The Journal of neuroscience : the official journal of the Society for Neuroscience,* vol. 18, no. 18, pp. 7336-7350.

Matos, M.J., Teran, C., Perez-Castillo, Y., Uriarte, E., Santana, L. & Vina, D. 2011, "Synthesis and study of a series of 3-arylcoumarins as potent and selective monoamine oxidase B inhibitors", *Journal of medicinal chemistry,* vol. 54, no. 20, pp. 7127-7137.

Maurice, T., Lockhart, B.P. & Privat, A. 1996, "Amnesia induced in mice by centrally administered beta-amyloid peptides involves cholinergic dysfunction", *Brain research,* vol. 706, no. 2, pp. 181-193.

Mayeux, R., Stern, Y., Ottman, R., Tatemichi, T.K., Tang, M.X., Maestre, G., Ngai, C., Tycko, B. & Ginsberg, H. 1993, "The apolipoprotein epsilon 4 allele in patients with Alzheimer's disease", *Annals of Neurology,* vol. 34, no. 5, pp. 752-754.

McBriar, M.D., Clader, J.W., Chu, I., Del Vecchio, R.A., Favreau, L., Greenlee, W.J., Hyde, L.A., Nomeir, A.A., Parker, E.M., Pissarnitski, D.A., Song, L., Zhang, L. & Zhao, Z. 2008, "Discovery of amide and heteroaryl isosteres as carbamate replacements in a series of orally active gamma-secretase inhibitors", *Bioorganic & medicinal chemistry letters,* vol. 18, no. 1, pp. 215-219.

McCall, K.A., Huang, C. & Fierke, C.A. 2000, "Function and mechanism of zinc metalloenzymes", *The Journal of nutrition,* vol. 130, no. 5S Suppl, pp. 1437S-46S.

McGeer, P.L., Rogers, J. & McGeer, E.G. 2006, "Inflammation, anti-inflammatory agents and Alzheimer disease: the last 12 years", *Journal of Alzheimer's disease : JAD,* vol. 9, no. 3 Suppl, pp. 271-276.

Meier-Ruge, W., Iwangoff, P., Reichlmeier, K. & Sandoz, P. 1980, "Neurochemical findings in the aging brain", *Advances in Biochemical Psychopharmacology,* vol. 23, pp. 323-338.

Melagraki, G., Afantitis, A., Igglessi-Markopoulou, O., Detsi, A., Koufaki, M., Kontogiorgis, C. & Hadjipavlou-Litina, D.J. 2009, "Synthesis and evaluation of the antioxidant and anti-inflammatory activity of novel coumarin-3-aminoamides and their alpha-lipoic acid adducts", *European journal of medicinal chemistry,* vol. 44, no. 7, pp. 3020-3026.

Meziane, H., Dodart, J.C., Mathis, C., Little, S., Clemens, J., Paul, S.M. & Ungerer, A. 1998, "Memory-enhancing effects of secreted forms of the beta-amyloid precursor protein in normal and amnestic mice", *Proceedings of the National Academy of Sciences of the United States of America,* vol. 95, no. 21, pp. 12683-12688.

Minichiello, L., Korte, M., Wolfer, D., Kuhn, R., Unsicker, K., Cestari, V., Rossi-Arnaud, C., Lipp, H.P., Bonhoeffer, T. & Klein, R. 1999, "Essential role for TrkB receptors in hippocampus-mediated learning", *Neuron,* vol. 24, no. 2, pp. 401-414.

Mladenovic, M., Mihailovic, M., Bogojevic, D., Vukovic, N., Sukdolak, S., Matic, S., Niciforovic, N., Mihailovic, V., Maskovic, P., Vrvic, M.M. & Solujic, S. 2012, "Biochemical and pharmacological evaluation of 4-hydroxychromen-2-ones bearing polar C-3 substituents as anticoagulants", *European journal of medicinal chemistry,* vol. 54, pp. 144-158.

Mohajeri, M.H., Kuehnle, K., Li, H., Poirier, R., Tracy, J. & Nitsch, R.M. 2004, "Anti-amyloid activity of neprilysin in plaque-bearing mouse models of Alzheimer's disease", *FEBS letters,* vol. 562, no. 1-3, pp. 16-21.

Moncada, S., Palmer, R.M. & Higgs, E.A. 1991, "Nitric oxide: physiology, pathophysiology, and pharmacology", *Pharmacological reviews,* vol. 43, no. 2, pp. 109-142.

Morgan, D., Diamond, D.M., Gottschall, P.E., Ugen, K.E., Dickey, C., Hardy, J., Duff, K., Jantzen, P., DiCarlo, G., Wilcock, D., Connor, K., Hatcher, J., Hope, C., Gordon, M. & Arendash, G.W. 2000, "A beta peptide vaccination prevents memory loss in an animal model of Alzheimer's disease", *Nature,* vol. 408, no. 6815, pp. 982-985.

Morris, J.C., Storandt, M., McKeel, D.W.,Jr, Rubin, E.H., Price, J.L., Grant, E.A. & Berg, L. 1996, "Cerebral amyloid deposition and diffuse plaques in "normal" aging: Evidence for presymptomatic and very mild Alzheimer's disease", *Neurology,* vol. 46, no. 3, pp. 707-719.

Motai, T. & Kitanaka, S. 2004, "Sesquiterpene coumarins from Ferula fukanensis and nitric oxide production inhibitory effects", *Chemical & pharmaceutical bulletin,* vol. 52, no. 10, pp. 1215-1218.

Muller-Thomsen, T., Arlt, S., Mann, U., Mass, R. & Ganzer, S. 2005, "Detecting depression in Alzheimer's disease: evaluation of four different scales", *Archives of clinical neuropsychology : the official journal of the National Academy of Neuropsychologists,* vol. 20, no. 2, pp. 271-276.

Murray, R.K.; Granner, D.K.; Mayes, P.A., Rodwell, Victor, W. 2003. Enzymes: Kinetics. (*In* Harper's Illustrated Biochemistry 26th eds). McGraw-Hill. pp. 60-71.

Murrell, J.R., Hake, A.M., Quaid, K.A., Farlow, M.R. & Ghetti, B. 2000, "Early-onset Alzheimer disease caused by a new mutation (V717L) in the amyloid precursor protein gene", *Archives of Neurology,* vol. 57, no. 6, pp. 885-887.

Nacmias, B., Latorraca, S., Piersanti, P., Forleo, P., Piacentini, S., Bracco, L., Amaducci, L. & Sorbi, S. 1995, "ApoE genotype and familial Alzheimer's disease: a possible influence on age of onset in APP717 Val-->Ile mutated families", *Neuroscience letters,* vol. 183, no. 1-2, pp. 1-3.

Nagahama, Y., Okina, T., Suzuki, N., Nabatame, H. & Matsuda, M. 2005, "The cerebral correlates of different types of perseveration in the Wisconsin Card Sorting Test", *Journal of neurology, neurosurgery, and psychiatry,* vol. 76, no. 2, pp. 169-175.

Nakamura, T., Kodama, N., Oda, M., Tsuchiya, S., Arai, Y., Kumamoto, T., Ishikawa, T., Ueno, K. & Yano, S. 2009, "The structure-activity relationship between oxycoumarin derivatives showing inhibitory effects on iNOS in mouse macrophage RAW264.7 cells", *Journal of natural medicines,* vol. 63, no. 1, pp. 15-20.

Natella, F., Lorrain, B., Prasad, A.K., Parmar, V.S., Saso, L. & Scaccini, C. 2010, "4-Methylcoumarins as Antioxidants: Scavenging of Peroxyl Radicals and Inhibition of Human Low-Density Lipoprotein Oxidation", *Biochimie,* vol. 92, no. 9, pp. 1147-1152.

Nikolic, M., Dudek, H., Kwon, Y.T., Ramos, Y.F. & Tsai, L.H. 1996, "The cdk5/p35 kinase is essential for neurite outgrowth during neuronal differentiation", *Genes & development,* vol. 10, no. 7, pp. 816-825.

Novaroli, L., Daina, A., Favre, E., Bravo, J., Carotti, A., Leonetti, F., Catto, M., Carrupt, P.A. & Reist, M. 2006, "Impact of species-dependent differences on screening, design, and development of MAO B inhibitors", *Journal of medicinal chemistry,* vol. 49, no. 21, pp. 6264-6272.

Novaroli, L., Reist, M., Favre, E., Carotti, A., Catto, M. & Carrupt, P.A. 2005, "Human recombinant monoamine oxidase B as reliable and efficient enzyme source for inhibitor screening", *Bioorganic & medicinal chemistry,* vol. 13, no. 22, pp. 6212-6217.

Nuchter, M., Ondruschka, B., Bonrath, W. & Gum, A. 2004, "Microwave assisted synthesis - a critical technology overview", *Green Chemistry,* vol. 6, no. 3, pp. 128-141.

O'Bryant, S.E., Humphreys, J.D., Smith, G.E., Ivnik, R.J., Graff-Radford, N.R., Petersen, R.C. & Lucas, J.A. 2008, "Detecting dementia with the mini-mental state examination in highly educated individuals", *Archives of Neurology,* vol. 65, no. 7, pp. 963-967.

Oda, T., Wals, P., Osterburg, H.H., Johnson, S.A., Pasinetti, G.M., Morgan, T.E., Rozovsky, I., Stine, W.B., Snyder, S.W. & Holzman, T.F. 1995, "Clusterin (apoJ) alters the aggregation of amyloid beta-peptide (A beta 1-42) and forms slowly sedimenting A beta complexes that cause oxidative stress", *Experimental neurology,* vol. 136, no. 1, pp. 22-31.

Oehlrich, D., Rombouts, F.J., Berthelot, D., Bischoff, F.P., De Cleyn, M.A., Jaroskova, L., Macdonald, G., Mercken, M., Surkyn, M., Trabanco, A.A., Tresadern, G., Van Brandt, S., Velter, A.I., Wu, T. & Gijsen, H.J. 2013, "Design and synthesis of bicyclic heterocycles as potent gamma-secretase modulators", *Bioorganic & medicinal chemistry letters,* vol. 23, no. 17, pp. 4794-4800.

Ohshima, T., Ward, J.M., Huh, C.G., Longenecker, G., Veeranna, Pant, H.C., Brady, R.O., Martin, L.J. & Kulkarni, A.B. 1996, "Targeted disruption of the cyclin-dependent kinase 5 gene results in abnormal corticogenesis, neuronal pathology and perinatal death", *Proceedings of the National Academy of Sciences of the United States of America,* vol. 93, no. 20, pp. 11173-11178.

Okada, Y. & Okada, M. 2013, "Protective effects of plant seed extracts against amyloid beta-induced neurotoxicity in cultured hippocampal neurons", *Journal of pharmacy & bioallied sciences,* vol. 5, no. 2, pp. 141-147.

Ooms, F., Frederick, R., Durant, F., Petzer, J.P., Castagnoli, N., Van der Schyf, C.J. & Wouters, J. 2003, "Rational approaches towards reversible inhibition of type B monoamine oxidase. Design and evaluation of a novel 5H-Indeno[1,2-c]pyridazin-5-one derivative", *Bioorganic & medicinal chemistry letters,* vol. 13, no. 1, pp. 69-73.

Oreland, L. & Gottfries, C.G. 1986, "Brain and brain monoamine oxidase in aging and in dementia of Alzheimer's type", *Progress in neuro-psychopharmacology & biological psychiatry,* vol. 10, no. 3-5, pp. 533-540.

Ott, A., Breteler, M.M., van Harskamp, F., Stijnen, T. & Hofman, A. 1998, "Incidence and risk of dementia. The Rotterdam Study", *American Journal of Epidemiology,* vol. 147, no. 6, pp. 574-580.

Otto, M., Wiltfang, J., Cepek, L., Neumann, M., Mollenhauer, B., Steinacker, P., Ciesielczyk, B., Schulz-Schaeffer, W., Kretzschmar, H.A. & Poser, S. 2002, "Tau protein and 14-3-3 protein in the differential diagnosis of Creutzfeldt-Jakob disease", *Neurology,* vol. 58, no. 2, pp. 192-197.

Pande, V. & Ramos, M.J. 2005, "NF-kappaB in human disease: current inhibitors and prospects for de novo structure based design of inhibitors", *Current medicinal chemistry,* vol. 12, no. 3, pp. 357-374.

Panegyres, P.K., Rogers, J.M., McCarthy, M., Campbell, A. & Wu, J.S. 2009, "Fluorodeoxyglucose-positron emission tomography in the differential diagnosis of early-onset dementia: a prospective, community-based study", *BMC neurology,* vol. 9, pp. 41-2377-9-41.

Pangalos, M.N., Jacobsen, S.J. & Reinhart, P.H. 2005, "Disease modifying strategies for the treatment of Alzheimer's disease targeted at modulating levels of the beta-amyloid peptide", *Biochemical Society transactions,* vol. 33, no. Pt 4, pp. 553-558.

Patrick, G.N., Zhou, P., Kwon, Y.T., Howley, P.M. & Tsai, L.H. 1998, "p35, the neuronal-specific activator of cyclin-dependent kinase 5 (Cdk5) is degraded by the ubiquitin-proteasome pathway", *The Journal of biological chemistry,* vol. 273, no. 37, pp. 24057-24064.

Patrick, G.N., Zukerberg, L., Nikolic, M., de la Monte, S., Dikkes, P. & Tsai, L.H. 1999, "Conversion of p35 to p25 deregulates Cdk5 activity and promotes neurodegeneration", *Nature,* vol. 402, no. 6762, pp. 615-622.

Patterson, S.L., Abel, T., Deuel, T.A., Martin, K.C., Rose, J.C. & Kandel, E.R. 1996, "Recombinant BDNF rescues deficits in basal synaptic transmission and hippocampal LTP in BDNF knockout mice", *Neuron,* vol. 16, no. 6, pp. 1137-1145.

Paya, M., Goodwin, P.A., De Las Heras, B. & Hoult, J.R. 1994, "Superoxide scavenging activity in leukocytes and absence of cellular toxicity of a series of coumarins", *Biochemical pharmacology,* vol. 48, no. 3, pp. 445-451.

Piazzi, L., Cavalli, A., Colizzi, F., Belluti, F., Bartolini, M., Mancini, F., Recanatini, M., Andrisano, V. & Rampa, A. 2008, "Multi-target-directed coumarin derivatives: hAChE and BACE1 inhibitors as potential anti-Alzheimer compounds", *Bioorganic & medicinal chemistry letters,* vol. 18, no. 1, pp. 423-426.

Piazzi, L., Rampa, A., Bisi, A., Gobbi, S., Belluti, F., Cavalli, A., Bartolini, M., Andrisano, V., Valenti, P. & Recanatini, M. 2003, "3-(4-[[Benzyl(methyl)amino]methyl]phenyl)-6,7-dimethoxy-2H-2-chromenone (AP2238) inhibits both acetylcholinesterase and acetylcholinesterase-induced beta-amyloid aggregation: a dual function lead for Alzheimer's disease therapy", *Journal of medicinal chemistry,* vol. 46, no. 12, pp. 2279-2282.

Pietsch, M. & Gutschow, M. 2005, "Synthesis of tricyclic 1,3-oxazin-4-ones and kinetic analysis of cholesterol esterase and acetylcholinesterase inhibition", *Journal of medicinal chemistry,* vol. 48, no. 26, pp. 8270-8288.

Qiu, W.Q., Walsh, D.M., Ye, Z., Vekrellis, K., Zhang, J., Podlisny, M.B., Rosner, M.R., Safavi, A., Hersh, L.B. & Selkoe, D.J. 1998, "Insulin-degrading enzyme regulates extracellular levels of amyloid beta-protein by degradation", *The Journal of biological chemistry,* vol. 273, no. 49, pp. 32730-32738.

Qiu, W.Q., Ye, Z., Kholodenko, D., Seubert, P. & Selkoe, D.J. 1997, "Degradation of amyloid beta-protein by a metalloprotease secreted by microglia and other neural and non-neural cells", *The Journal of biological chemistry,* vol. 272, no. 10, pp. 6641-6646.

Racchi, M. & Govoni, S. 1999, "Rationalizing a pharmacological intervention on the amyloid precursor protein metabolism", *Trends in pharmacological sciences,* vol. 20, no. 10, pp. 418-423.

Radanyi, C., Le Bras, G., Messaoudi, S., Bouclier, C., Peyrat, J.F., Brion, J.D., Marsaud, V., Renoir, J.M. & Alami, M. 2008, "Synthesis and biological activity of simplified denoviose-coumarins related to novobiocin as potent inhibitors of heat-shock protein 90 (hsp90)", *Bioorganic & medicinal chemistry letters,* vol. 18, no. 7, pp. 2495-2498.

Radic, Z., Pickering, N.A., Vellom, D.C., Camp, S. & Taylor, P. 1993, "Three distinct domains in the cholinesterase molecule confer selectivity for acetyl- and butyrylcholinesterase inhibitors", *Biochemistry,* vol. 32, no. 45, pp. 12074-12084.

Raj, H.G., Parmar, V.S., Jain, S.C., Goel, S., Poonam, Himanshu, Malhotra, S., Singh, A., Olsen, C.E. & Wengel, J. 1998, "Mechanism of biochemical action of substituted 4-methylbenzopyran-2-ones. Part I: Dioxygenated 4-methyl coumarins as superb antioxidant and radical scavenging agents", *Bioorganic & medicinal chemistry,* vol. 6, no. 6, pp. 833-839.

Rakonczay, Z. 2003, "Potencies and selectivities of inhibitors of acetylcholinesterase and its molecular forms in normal and Alzheimer's disease brain", *Acta Biologica Hungarica,* vol. 54, no. 2, pp. 183-189.

Reinke, A.A. & Gestwicki, J.E. 2007, "Structure-activity relationships of amyloid beta-aggregation inhibitors based on curcumin: influence of linker length and flexibility", *Chemical biology & drug design,* vol. 70, no. 3, pp. 206-215.

Reisberg, B., Doody, R., Stoffler, A., Schmitt, F., Ferris, S., Mobius, H.J. & Memantine Study Group 2003, "Memantine in moderate-to-severe Alzheimer's disease", *The New England journal of medicine,* vol. 348, no. 14, pp. 1333-1341.

Repsold, B.P. 2008, “Inhibition of monoamine oxidase B by substituted coumarin derivatives”, The North West University, pp 71.

Riederer, P., Danielczyk, W. & Grunblatt, E. 2004, "Monoamine oxidase-B inhibition in Alzheimer's disease", *Neurotoxicology,* vol. 25, no. 1-2, pp. 271-277.

Riederer, P., Sofic, E., Rausch, W.D., Schmidt, B., Reynolds, G.P., Jellinger, K. & Youdim, M.B. 1989, "Transition metals, ferritin, glutathione, and ascorbic acid in parkinsonian brains", *Journal of neurochemistry,* vol. 52, no. 2, pp. 515-520.

Riederer, P., Youdim, M.B., Rausch, W.D., Birkmayer, W., Jellinger, K. & Seemann, D. 1978, "On the mode of action of L-deprenyl in the human central nervous system", *Journal of neural transmission,* vol. 43, no. 3-4, pp. 217-226.

Riederer, P. & Jellinger, K. 1982, "Morphological and biochemical changes in the aging brain: pathophysiological and possible therapeutic consequences", *Experimental brain research,* vol. Suppl 5, pp. 158-166.

Ritchie, C.W., Bush, A.I., Mackinnon, A., Macfarlane, S., Mastwyk, M., MacGregor, L., Kiers, L., Cherny, R., Li, Q.X., Tammer, A., Carrington, D., Mavros, C., Volitakis, I., Xilinas, M., Ames, D., Davis, S., Beyreuther, K., Tanzi, R.E. & Masters, C.L. 2003, "Metal-protein attenuation with iodochlorhydroxyquin (clioquinol) targeting Abeta amyloid deposition and toxicity in Alzheimer disease: a pilot phase 2 clinical trial", *Archives of Neurology,* vol. 60, no. 12, pp. 1685-1691.

Roch, J.M., Masliah, E., Roch-Levecq, A.C., Sundsmo, M.P., Otero, D.A., Veinbergs, I. & Saitoh, T. 1994, "Increase of synaptic density and memory retention by a peptide representing the trophic domain of the amyloid beta/A4 protein precursor", *Proceedings of the National Academy of Sciences of the United States of America,* vol. 91, no. 16, pp. 7450-7454.

Rosler, N., Wichart, I. & Jellinger, K.A. 2001, "Intra vitam lumbar and post mortem ventricular cerebrospinal fluid immunoreactive interleukin-6 in Alzheimer's disease patients", *Acta Neurologica Scandinavica,* vol. 103, no. 2, pp. 126-130.

Rosser, B.G., Powers, S.P. & Gores, G.J. 1993, "Calpain activity increases in hepatocytes following addition of ATP. Demonstration by a novel fluorescent approach", *The Journal of biological chemistry,* vol. 268, no. 31, pp. 23593-23600.

Roussaki, M., Kontogiorgis, C.A., Hadjipavlou-Litina, D., Hamilakis, S. & Detsi, A. 2010, "A novel synthesis of 3-aryl coumarins and evaluation of their antioxidant and lipoxygenase inhibitory activity", *Bioorganic & medicinal chemistry letters,* vol. 20, no. 13, pp. 3889-3892.

Sabo, S.L., Ikin, A.F., Buxbaum, J.D. & Greengard, P. 2003, "The amyloid precursor protein and its regulatory protein, FE65, in growth cones and synapses in vitro and in vivo", *The Journal of neuroscience : the official journal of the Society for Neuroscience,* vol. 23, no. 13, pp. 5407-5415.

Sahara, N., Maeda, S., Yoshiike, Y., Mizoroki, T., Yamashita, S., Murayama, M., Park, J.M., Saito, Y., Murayama, S. & Takashima, A. 2007, "Molecular chaperone-mediated tau protein metabolism counteracts the formation of granular tau oligomers in human brain", *Journal of neuroscience research,* vol. 85, no. 14, pp. 3098-3108.

Saido, T.C. 2003, *Amyloid-Beta Metabolism and Alzheimer's Disease,* Eurekah.com/Landes Bioscience.

Saito, T., Iwata, N., Tsubuki, S., Takaki, Y., Takano, J., Huang, S.M., Suemoto, T., Higuchi, M. & Saido, T.C. 2005, "Somatostatin regulates brain amyloid beta peptide Abeta42 through modulation of proteolytic degradation", *Nature medicine,* vol. 11, no. 4, pp. 434-439.

Salmon, D.P., Thomas, R.G., Pay, M.M., Booth, A., Hofstetter, C.R., Thal, L.J. & Katzman, R. 2002, "Alzheimer's disease can be accurately diagnosed in very mildly impaired individuals", *Neurology,* vol. 59, no. 7, pp. 1022-1028.

Sandhya, B., Giles, D., Mathew, V., Basavarajaswamy, G. & Abraham, R. 2011, "Synthesis, pharmacological evaluation and docking studies of coumarin derivatives", *European journal of medicinal chemistry,* vol. 46, no. 9, pp. 4696-4701.

Sashidhara, K.V., Kumar, A., Bhatia, G., Khan, M.M., Khanna, A.K. & Saxena, J.K. 2009, "Antidyslipidemic and antioxidative activities of 8-hydroxyquinoline derived novel keto-enamine Schiffs bases", *European journal of medicinal chemistry,* vol. 44, no. 4, pp. 1813-1818.

Sashidhara, K.V., Kumar, M., Modukuri, R.K., Sonkar, R., Bhatia, G., Khanna, A.K., Rai, S. & Shukla, R. 2011, "Synthesis and anti-inflammatory activity of novel biscoumarin-chalcone hybrids", *Bioorganic & medicinal chemistry letters,* vol. 21, no. 15, pp. 4480-4484.

Saunders, A.M., Strittmatter, W.J., Schmechel, D., George-Hyslop, P.H., Pericak-Vance, M.A., Joo, S.H., Rosi, B.L., Gusella, J.F., Crapper-MacLachlan, D.R. & Alberts, M.J. 1993, "Association of apolipoprotein E allele epsilon 4 with late-onset familial and sporadic Alzheimer's disease", *Neurology,* vol. 43, no. 8, pp. 1467-1472.

Schalk, I., Ehret-Sabatier, L., Bouet, F., Goeldner, M. & Hirth, C. 1992, "Multidisciplinary Approaches to Cholinesterase Functions" in *Multidisciplinary Approaches to Cholinesterase Functions*, eds. A. Shafferman & B. Velan, Plenum Press, New York, pp. 117–120.

Scheltens, P. 2009, "Imaging in Alzheimer's disease", *Dialogues in clinical neuroscience,* vol. 11, no. 2, pp. 191-199.

Schenk, D., Barbour, R., Dunn, W., Gordon, G., Grajeda, H., Guido, T., Hu, K., Huang, J., Johnson-Wood, K., Khan, K., Kholodenko, D., Lee, M., Liao, Z., Lieberburg, I., Motter, R., Mutter, L., Soriano, F., Shopp, G., Vasquez, N., Vandevert, C., Walker, S., Wogulis, M., Yednock, T., Games, D. & Seubert, P. 1999, "Immunization with amyloid-beta attenuates Alzheimer-disease-like pathology in the PDAPP mouse", *Nature,* vol. 400, no. 6740, pp. 173-177.

Secci, D., Carradori, S., Bolasco, A., Chimenti, P., Yanez, M., Ortuso, F. & Alcaro, S. 2011, "Synthesis and selective human monoamine oxidase inhibition of 3-carbonyl, 3-acyl, and 3-carboxyhydrazido coumarin derivatives", *European journal of medicinal chemistry,* vol. 46, no. 10, pp. 4846-4852.

Seiffert, D., Bradley, J.D., Rominger, C.M., Rominger, D.H., Yang, F., Meredith, J.E.,Jr, Wang, Q., Roach, A.H., Thompson, L.A., Spitz, S.M., Higaki, J.N., Prakash, S.R., Combs, A.P., Copeland, R.A., Arneric, S.P., Hartig, P.R., Robertson, D.W., Cordell, B., Stern, A.M., Olson, R.E. & Zaczek, R. 2000, "Presenilin-1 and -2 are molecular targets for gamma-secretase inhibitors", *The Journal of biological chemistry,* vol. 275, no. 44, pp. 34086-34091.

Selkoe, D. & Kopan, R. 2003, "Notch and Presenilin: regulated intramembrane proteolysis links development and degeneration", *Annual Review of Neuroscience,* vol. 26, pp. 565-597.

Selkoe, D.J. 2002, "Alzheimer's disease is a synaptic failure", *Science (New York, N.Y.),* vol. 298, no. 5594, pp. 789-791.

Sheng, J.G., Price, D.L. & Koliatsos, V.E. 2003, "The beta-amyloid-related proteins presenilin 1 and BACE1 are axonally transported to nerve terminals in the brain", *Experimental neurology,* vol. 184, no. 2, pp. 1053-1057.

Sheng, J.G., Price, D.L. & Koliatsos, V.E. 2002, "Disruption of corticocortical connections ameliorates amyloid burden in terminal fields in a transgenic model of Abeta amyloidosis", *The Journal of neuroscience : the official journal of the Society for Neuroscience,* vol. 22, no. 22, pp. 9794-9799.

Sikkes, S.A., de Lange-de Klerk, E.S., Pijnenburg, Y.A., Scheltens, P. & Uitdehaag, B.M. 2009, "A systematic review of Instrumental Activities of Daily Living scales in dementia: room for improvement", *Journal of neurology, neurosurgery, and psychiatry,* vol. 80, no. 1, pp. 7-12.

Silverman, D.H. & Alavi, A. 2005, "PET imaging in the assessment of normal and impaired cognitive function", *Radiologic clinics of North America,* vol. 43, no. 1, pp. 67-77, x.

Simons, M., Keller, P., De Strooper, B., Beyreuther, K., Dotti, C.G. & Simons, K. 1998, "Cholesterol depletion inhibits the generation of beta-amyloid in hippocampal neurons", *Proceedings of the National Academy of Sciences of the United States of America,* vol. 95, no. 11, pp. 6460-6464.

Simon, S. & Massoulie, J. 1997, "Cloning and expression of acetylcholinesterase from Electrophorus. Splicing pattern of the 3' exons in vivo and in transfected mammalian cells", *The Journal of biological chemistry,* vol. 272, no. 52, pp. 33045-33055.

Sinha, S., Anderson, J.P., Barbour, R., Basi, G.S., Caccavello, R., Davis, D., Doan, M., Dovey, H.F., Frigon, N., Hong, J., Jacobson-Croak, K., Jewett, N., Keim, P., Knops, J., Lieberburg, I., Power, M., Tan, H., Tatsuno, G., Tung, J., Schenk, D., Seubert, P., Suomensaari, S.M., Wang, S., Walker, D., Zhao, J., McConlogue, L. & John, V. 1999, "Purification and cloning of amyloid precursor protein beta-secretase from human brain", *Nature,* vol. 402, no. 6761, pp. 537-540.

Sisodia, S.S., Kim, S.H. & Thinakaran, G. 1999, "Function and dysfunction of the presenilins", *American Journal of Human Genetics,* vol. 65, no. 1, pp. 7-12.

Smith, M.A., Hirai, K., Hsiao, K., Pappolla, M.A., Harris, P.L., Siedlak, S.L., Tabaton, M. & Perry, G. 1998, "Amyloid-beta deposition in Alzheimer transgenic mice is associated with oxidative stress", *Journal of neurochemistry,* vol. 70, no. 5, pp. 2212-2215.

Smith, M.A., Perry, G., Richey, P.L., Sayre, L.M., Anderson, V.E., Beal, M.F. & Kowall, N. 1996, "Oxidative damage in Alzheimer's", *Nature,* vol. 382, no. 6587, pp. 120-121.

Snyder, E.M., Nong, Y., Almeida, C.G., Paul, S., Moran, T., Choi, E.Y., Nairn, A.C., Salter, M.W., Lombroso, P.J., Gouras, G.K. & Greengard, P. 2005, "Regulation of NMDA receptor trafficking by amyloid-beta", *Nature neuroscience,* vol. 8, no. 8, pp. 1051-1058.

Sonsalla, P.K. & Golbe, L.I. 1988, "Deprenyl as prophylaxis against Parkinson's disease?", *Clinical neuropharmacology,* vol. 11, no. 6, pp. 500-511.

Soto-Ortega, D.D., Murphy, B.P., Gonzalez-Velasquez, F.J., Wilson, K.A., Xie, F., Wang, Q. & Moss, M.A. 2011, "Inhibition of amyloid-beta aggregation by coumarin analogs can be manipulated by functionalization of the aromatic center", *Bioorganic & medicinal chemistry,* vol. 19, no. 8, pp. 2596-2602.

Stern, D., Yan, S.D., Yan, S.F. & Schmidt, A.M. 2002, "Receptor for advanced glycation endproducts: a multiligand receptor magnifying cell stress in diverse pathologic settings", *Advanced Drug Delivery Reviews,* vol. 54, no. 12, pp. 1615-1625.

Strittmatter, W.J. & Roses, A.D. 1996, "Apolipoprotein E and Alzheimer's disease", *Annual Review of Neuroscience,* vol. 19, pp. 53-77.

Strittmatter, W.J., Saunders, A.M., Schmechel, D., Pericak-Vance, M., Enghild, J., Salvesen, G.S. & Roses, A.D. 1993, "Apolipoprotein E: high-avidity binding to beta-amyloid and increased frequency of type 4 allele in late-onset familial Alzheimer disease", *Proceedings of the National Academy of Sciences of the United States of America,* vol. 90, no. 5, pp. 1977-1981.

Strittmatter, W.J., Weisgraber, K.H., Huang, D.Y., Dong, L.M., Salvesen, G.S., Pericak-Vance, M., Schmechel, D., Saunders, A.M., Goldgaber, D. & Roses, A.D. 1993, "Binding of human apolipoprotein E to synthetic amyloid beta peptide: isoform-specific effects and implications for late-onset Alzheimer disease", *Proceedings of the National Academy of Sciences of the United States of America,* vol. 90, no. 17, pp. 8098-8102.

Su, B., Wang, X., Nunomura, A., Moreira, P.I., Lee, H.G., Perry, G., Smith, M.A. & Zhu, X. 2008, "Oxidative stress signaling in Alzheimer's disease", *Current Alzheimer research,* vol. 5, no. 6, pp. 525-532.

Suh, S.W., Chen, J.W., Motamedi, M., Bell, B., Listiak, K., Pons, N.F., Danscher, G. & Frederickson, C.J. 2000, "Evidence that synaptically-released zinc contributes to neuronal injury after traumatic brain injury", *Brain research,* vol. 852, no. 2, pp. 268-273.

Sullivan, J. & Blose, J. 1992, "Organophosphate and carbamate insecticides in *Hazardous Materials Toxicology-Clinical Principles of Environmental Health.* , eds. J. Sullivan & G. Krieger, Williams & Wilkins, Baltimore, pp. 1015-1026.

Suuronen, T., Kolehmainen, P. & Salminen, A. 2000, "Protective effect of L-deprenyl against apoptosis induced by okadaic acid in cultured neuronal cells", *Biochemical pharmacology,* vol. 59, no. 12, pp. 1589-1595.

Szegletes, T., Mallender, W.D. & Rosenberry, T.L. 1998, "Nonequilibrium analysis alters the mechanistic interpretation of inhibition of acetylcholinesterase by peripheral site ligands", *Biochemistry,* vol. 37, no. 12, pp. 4206-4216.

Tabner, B.J., Turnbull, S., El-Agnaf, O.M. & Allsop, D. 2002, "Formation of hydrogen peroxide and hydroxyl radicals from A(beta) and alpha-synuclein as a possible mechanism of cell death in Alzheimer's disease and Parkinson's disease", *Free radical biology & medicine,* vol. 32, no. 11, pp. 1076-1083.

Tanzi, R.E. 1999, "A genetic dichotomy model for the inheritance of Alzheimer's disease and common age-related disorders", *The Journal of clinical investigation,* vol. 104, no. 9, pp. 1175-1179.

Tareg, A. 2001, "Organophosphate and carbamate insecticides" in *Clinical environmental health and toxic exposures.* ed. G.R. Krieger, Lippincott Williams & Wilkins, Philadelphia, pp. 1046-1057.

Thinakaran, G. & Parent, A.T. 2004, "Identification of the role of presenilins beyond Alzheimer's disease", *Pharmacological research : the official journal of the Italian Pharmacological Society,* vol. 50, no. 4, pp. 411-418.

Timonen, J.M., Nieminen, R.M., Sareila, O., Goulas, A., Moilanen, L.J., Haukka, M., Vainiotalo, P., Moilanen, E. & Aulaskari, P.H. 2011, "Synthesis and anti-inflammatory effects of a series of novel 7-hydroxycoumarin derivatives", *European journal of medicinal chemistry,* vol. 46, no. 9, pp. 3845-3850.

Tomita, T., Watabiki, T., Takikawa, R., Morohashi, Y., Takasugi, N., Kopan, R., De Strooper, B. & Iwatsubo, T. 2001, "The first proline of PALP motif at the C terminus of presenilins is obligatory for stabilization, complex formation, and gamma-secretase activities of presenilins", *The Journal of biological chemistry,* vol. 276, no. 35, pp. 33273-33281.

Tong, L., Thornton, P.L., Balazs, R. & Cotman, C.W. 2001, "Beta -amyloid-(1-42) impairs activity-dependent cAMP-response element-binding protein signaling in neurons at concentrations in which cell survival Is not compromised", *The Journal of biological chemistry,* vol. 276, no. 20, pp. 17301-17306.

Town, T., Zolton, J., Shaffner, R., Schnell, B., Crescentini, R., Wu, Y., Zeng, J., DelleDonne, A., Obregon, D., Tan, J. & Mullan, M. 2002, "p35/Cdk5 pathway mediates soluble amyloid-beta peptide-induced tau phosphorylation in vitro", *Journal of neuroscience research,* vol. 69, no. 3, pp. 362-372.

Tully, T. 1997, "Regulation of gene expression and its role in long-term memory and synaptic plasticity", *Proceedings of the National Academy of Sciences of the United States of America,* vol. 94, no. 9, pp. 4239-4241.

Tyagi, Y.K., Kumar, A., Raj, H.G., Vohra, P., Gupta, G., Kumari, R., Kumar, P. & Gupta, R.K. 2005, "Synthesis of novel amino and acetyl amino-4-methylcoumarins and evaluation of their antioxidant activity", *European journal of medicinal chemistry,* vol. 40, no. 4, pp. 413-420.

Upadhyay, K., Bavishi, A., Thakrar, S., Radadiya, A., Vala, H., Parekh, S., Bhavsar, D., Savant, M., Parmar, M., Adlakha, P. & Shah, A. 2011, "Synthesis and biological evaluation of 4-styrylcoumarin derivatives as inhibitors of TNF-alpha and IL-6 with anti-tubercular activity", *Bioorganic & medicinal chemistry letters,* vol. 21, no. 8, pp. 2547-2549.

van der Stelt, M., Mazzola, C., Esposito, G., Matias, I., Petrosino, S., De Filippis, D., Micale, V., Steardo, L., Drago, F., Iuvone, T. & Di Marzo, V. 2006, "Endocannabinoids and beta-amyloid-induced neurotoxicity in vivo: effect of pharmacological elevation of endocannabinoid levels", *Cellular and molecular life sciences : CMLS,* vol. 63, no. 12, pp. 1410-1424.

Vance, J.E., Hayashi, H. & Karten, B. 2005, "Cholesterol homeostasis in neurons and glial cells", *Seminars in cell & developmental biology,* vol. 16, no. 2, pp. 193-212.

Vassar, R. 2004, "BACE1: the beta-secretase enzyme in Alzheimer's disease", *Journal of molecular neuroscience : MN,* vol. 23, no. 1-2, pp. 105-114.

Vassar, R., Bennett, B.D., Babu-Khan, S., Kahn, S., Mendiaz, E.A., Denis, P., Teplow, D.B., Ross, S., Amarante, P., Loeloff, R., Luo, Y., Fisher, S., Fuller, J., Edenson, S., Lile, J., Jarosinski, M.A., Biere, A.L., Curran, E., Burgess, T., Louis, J.C., Collins, F., Treanor, J., Rogers, G. & Citron, M. 1999, "Beta-secretase cleavage of Alzheimer's amyloid precursor protein by the transmembrane aspartic protease BACE", *Science (New York, N.Y.),* vol. 286, no. 5440, pp. 735-741.

Vecsey, C.G., Hawk, J.D., Lattal, K.M., Stein, J.M., Fabian, S.A., Attner, M.A., Cabrera, S.M., McDonough, C.B., Brindle, P.K., Abel, T. & Wood, M.A. 2007, "Histone deacetylase inhibitors enhance memory and synaptic plasticity via CREB:CBP-dependent transcriptional activation", *The Journal of neuroscience : the official journal of the Society for Neuroscience,* vol. 27, no. 23, pp. 6128-6140.

Vural, H., Sirin, B., Yilmaz, N., Eren, I. & Delibas, N. 2009, "The role of arginine-nitric oxide pathway in patients with Alzheimer disease", *Biological trace element research,* vol. 129, no. 1-3, pp. 58-64.

Waldemar, G., Dubois, B., Emre, M., Georges, J., McKeith, I.G., Rossor, M., Scheltens, P., Tariska, P., Winblad, B. & EFNS 2007, "Recommendations for the diagnosis and management of Alzheimer's disease and other disorders associated with dementia: EFNS guideline", *European journal of neurology : the official journal of the European Federation of Neurological Societies,* vol. 14, no. 1, pp. e1-26.

Wang, B., Hu, Q., Hearn, M.G., Shimizu, K., Ware, C.B., Liggitt, D.H., Jin, L.W., Cool, B.H., Storm, D.R. & Martin, G.M. 2004, "Isoform-specific knockout of FE65 leads to impaired learning and memory", *Journal of neuroscience research,* vol. 75, no. 1, pp. 12-24.

Wang, J., Brunkan, A.L., Hecimovic, S., Walker, E. & Goate, A. 2004, "Conserved "PAL" sequence in presenilins is essential for gamma-secretase activity, but not required for formation or stabilization of gamma-secretase complexes", *Neurobiology of disease,* vol. 15, no. 3, pp. 654-666.

Wattjes, M.P., Henneman, W.J., van der Flier, W.M., de Vries, O., Traber, F., Geurts, J.J., Scheltens, P., Vrenken, H. & Barkhof, F. 2009, "Diagnostic imaging of patients in a memory clinic: comparison of MR imaging and 64-detector row CT", *Radiology,* vol. 253, no. 1, pp. 174-183.

Web: http://www.rcsb.org/pdb/explore/explore.do?structureId=4EY7 [2014, Descember 28].

Web: http://www.rcsb.org/pdb/explore/explore.do?structureId=2V61 [2014, December 30].

Web: http://www.alz.org/downloads/facts_figures_2013.pdf [2013, October 16].

Web: (http://www.schrodinger.com/kb/1556). [2016, January 12]

Web: (http://www.worldalzreport2015.org/). [2016, August 15].

Weggen, S., Eriksen, J.L., Das, P., Sagi, S.A., Wang, R., Pietrzik, C.U., Findlay, K.A., Smith, T.E., Murphy, M.P., Bulter, T., Kang, D.E., Marquez-Sterling, N., Golde, T.E. & Koo, E.H. 2001, "A subset of NSAIDs lower amyloidogenic Abeta42 independently of cyclooxygenase activity", *Nature,* vol. 414, no. 6860, pp. 212-216.

Weingarten, M.D., Lockwood, A.H., Hwo, S.Y. & Kirschner, M.W. 1975, "A protein factor essential for microtubule assembly", *Proceedings of the National Academy of Sciences of the United States of America,* vol. 72, no. 5, pp. 1858-1862.

Weissbach, H., Smith, T.E., Daly, J.W., Witkop, B. & Udenfriend, S. 1960, "A rapid spectrophotometric assay of mono-amine oxidase based on the rate of disappearance of kynuramine", *The Journal of biological chemistry,* vol. 235, pp. 1160-1163.

Wiener, S.W. & Hoffman, R.S. 2004, "Nerve agents: a comprehensive review", *Journal of intensive care medicine,* vol. 19, no. 1, pp. 22-37.

Winblad, B. & Jelic, V. 2003, "Treating the full spectrum of dementia with memantine", *International journal of geriatric psychiatry,* vol. 18, no. Suppl 1, pp. S41-6.

Wong, P.C., Cai, H., Borchelt, D.R. & Price, D.L. 2002, "Genetically engineered mouse models of neurodegenerative diseases", *Nature neuroscience,* vol. 5, no. 7, pp. 633-639.

Wong, P.C., Price, D.L. & Cai, H. 2001, "The brain's susceptibility to amyloid plaques", *Science (New York, N.Y.),* vol. 293, no. 5534, pp. 1434.

Wood, M.A., Attner, M.A., Oliveira, A.M., Brindle, P.K. & Abel, T. 2006, "A transcription factor-binding domain of the coactivator CBP is essential for long-term memory and the expression of specific target genes", *Learning & memory (Cold Spring Harbor, N.Y.),* vol. 13, no. 5, pp. 609-617.

Wu, H.F., Chen, K. & Shih, J.C. 1993, "Site-directed mutagenesis of monoamine oxidase A and B: role of cysteines", *Molecular pharmacology,* vol. 43, no. 6, pp. 888-893.

Wu, J., Bie, B., Yang, H., Xu, J.J., Brown, D.L. & Naguib, M. 2013, "Activation of the CB2 receptor system reverses amyloid-induced memory deficiency", *Neurobiology of aging,* vol. 34, no. 3, pp. 791-804.

Xiao, C., Luo, X.Y., Li, D.J., Lu, H., Liu, Z.Q., Song, Z.G. & Jin, Y.H. 2012, "Synthesis of 4-methylcoumarin derivatives containing 4,5-dihydropyrazole moiety to scavenge radicals and to protect DNA", *European journal of medicinal chemistry,* vol. 53C, pp. 159-167.

Xiao, C., Song, Z.G. & Liu, Z.Q. 2010, "Synthesis of methyl-substituted xanthotoxol to clarify prooxidant effect of methyl on radical-induced oxidation of DNA", *European journal of medicinal chemistry,* vol. 45, no. 6, pp. 2559-2566.

Yan, R., Bienkowski, M.J., Shuck, M.E., Miao, H., Tory, M.C., Pauley, A.M., Brashier, J.R., Stratman, N.C., Mathews, W.R., Buhl, A.E., Carter, D.B., Tomasselli, A.G., Parodi, L.A., Heinrikson, R.L. & Gurney, M.E. 1999, "Membrane-anchored aspartyl protease with Alzheimer's disease beta-secretase activity", *Nature,* vol. 402, no. 6761, pp. 533-537.

Yan, R., Munzner, J.B., Shuck, M.E. & Bienkowski, M.J. 2001, "BACE2 functions as an alternative alpha-secretase in cells", *The Journal of biological chemistry,* vol. 276, no. 36, pp. 34019-34027.

Yan, S.D., Chen, X., Fu, J., Chen, M., Zhu, H., Roher, A., Slattery, T., Zhao, L., Nagashima, M., Morser, J., Migheli, A., Nawroth, P., Stern, D. & Schmidt, A.M. 1996, "RAGE and amyloid-beta peptide neurotoxicity in Alzheimer's disease", *Nature,* vol. 382, no. 6593, pp. 685-691.

Yang, E.B., Zhao, Y.N., Zhang, K. & Mack, P. 1999, "Daphnetin, one of coumarin derivatives, is a protein kinase inhibitor", *Biochemical and biophysical research communications,* vol. 260, no. 3, pp. 682-685.

Yasojima, K., Akiyama, H., McGeer, E.G. & McGeer, P.L. 2001, "Reduced neprilysin in high plaque areas of Alzheimer brain: a possible relationship to deficient degradation of beta-amyloid peptide", *Neuroscience letters,* vol. 297, no. 2, pp. 97-100.

Yin, J.C., Wallach, J.S., Del Vecchio, M., Wilder, E.L., Zhou, H., Quinn, W.G. & Tully, T. 1994, "Induction of a dominant negative CREB transgene specifically blocks long-term memory in Drosophila", *Cell,* vol. 79, no. 1, pp. 49-58.

Yu, X.M., Shen, G., Neckers, L., Blake, H., Holzbeierlein, J., Cronk, B. & Blagg, B.S. 2005, "Hsp90 inhibitors identified from a library of novobiocin analogues", *Journal of the American Chemical Society,* vol. 127, no. 37, pp. 12778-12779.

Yuce, B., Danis, O., Ogan, A., Sener, G., Bulut, M. & Yarat, A. 2009, "Antioxidative and lipid lowering effects of 7,8-dihydroxy-3- (4-methylphenyl) coumarin in hyperlipidemic rats", *Arzneimittel-Forschung,* vol. 59, no. 3, pp. 129-134.

Zhang, Y., Zou, B., Chen, Z., Pan, Y., Wang, H., Liang, H. & Yi, X. 2011, "Synthesis and antioxidant activities of novel 4-Schiff base-7-benzyloxy-coumarin derivatives", *Bioorganic & medicinal chemistry letters,* vol. 21, no. 22, pp. 6811-6815.

Zhou, X., Wang, X.B., Wang, T. & Kong, L.Y. 2008, "Design, synthesis, and acetylcholinesterase inhibitory activity of novel coumarin analogues", *Bioorganic & medicinal chemistry,* vol. 16, no. 17, pp. 8011-8021.